
## SYMPOSIUM ON SURFACE SCIENCE 2014

**St. Christoph am Arlberg, Austria**
**March 9 - 15, 2014**

# CONTRIBUTIONS

EDITORS
**Friedrich Aumayr, Ulrike Diebold, Christoph Lemell and Peter Varga**
TU Wien

# Scanning Probe Microscopy

## The new Fermi SPM

A "Cold-Tip SPM" - a new generation variable temperature SPM

- Compact design
- Temperature range: 15 K to 400 K
- Tip and sample cooled
- Low thermal drift
- STM, AFM & spectroscopy
- Sub pA STM
- Sensor exchange & 2D coarse

**10 K**
**achieved with flow cryostat**

For further information:
**omicron.nanoscience@oxinst.com**

**www.oxford-instruments.com**

OXFORD INSTRUMENTS
*The Business of Science®*

# **JT-SPM** System

JOULE-THOMSON SCANNING PROBE MICROSCOPE

## KEY FEATURES

- Base Temperature < 1.3 K
- Liquid He Holding Time > 4 days
- Maximum Temperature 400 K
- STM & AFM-heads
- Extreme Stability
- Optional Magnetic field up to 3T
- Nanonis Control System

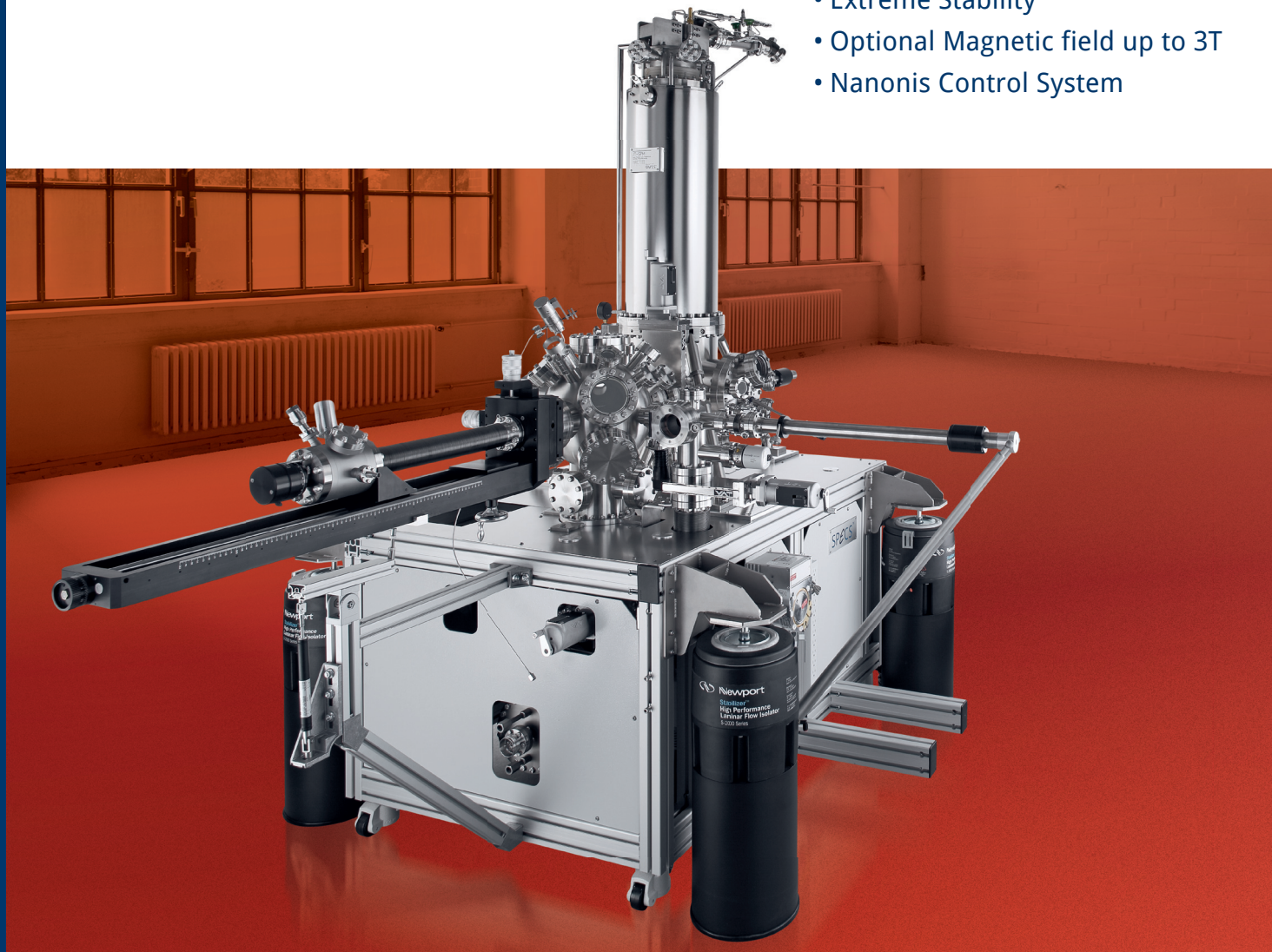


**SPECS** Surface Nano Analysis GmbH

T +49 30 46 78 24-0
E support@specs.com
H www.specs.com

SPECS™


## SYMPOSIUM ON SURFACE SCIENCE 2014

**St. Christoph am Arlberg, Austria**
**March 9 - 15, 2014**

# CONTRIBUTIONS

EDITORS
**Friedrich Aumayr, Ulrike Diebold, Christoph Lemell and Peter Varga**
TU Wien

This symposium is organized by

Friedrich Aumayr, Ulrike Diebold and Peter Varga
Institute of Applied Physics (IAP)
Vienna University of Technology (TU Wien)
Wiedner Hauptstr. 8-10/E134
1040 Vienna, Austria



Medieninhaber: F. Aumayr, U. Diebold und P. Varga, Institut für Angewandte Physik, Technische Universität Wien, Adresse: Wiedner Hauptstr. 8-10/E134, A-1040 Wien
Druck: R. & W. Smutny OEG, A-1110 Wien

## PREFACE

We welcome all participants and accompanying persons to the 27th Symposium on Surface Science (3S). The 3S was founded as a winter school by members of the Institute of Applied Physics of the Vienna University of Technology (TU Wien) in 1993. The conference seeks to promote the growth of scientific knowledge and its effective exchange among scientists in the field of surface physics and chemistry and related areas, including applied topics. Its format is similar to that of Gordon Conferences, with ample time for discussions and joint outdoor activities. The number of participants is kept below 100 in order to guarantee active communication between all attendees.

Initially the 3S was held exclusively in Austria and took place every other year. It became an annual event in 1990, and the site started to alternate between locations in France and Austria. In 1998 the 3S evolved into a truly global conference, with venues in the US, Canada, Bulgaria, Japan, Switzerland, Spain, France and Sweden, always returning to Austria in alternate years. This year we are again happy to host the 3S in Austria; for the 6th time in the Arlberg area.

We hope that all participants will experience a lively and successful meeting while enjoying the surroundings in this beautiful mountain region.

Fritz Aumayr Ulrike Diebold Peter Varga

Dates and locations of 3S conferences:

| | | | | | | | |
|---|---|---|---|---|---|---|---|
| 1983 | (31.01.-04.02.) | Obertraun | AT | 2002 | (03.03.-09.03.) | St.Christoph/Arlberg | AT |
| 1985 | (27.01.-02.02.) | Obertraun | AT | 2003 | (30.03.-05.04.) | La Plagne | FR |
| 1988 | (22.05.-28.05.) | Kaprun | AT | 2004 | (29.02.-06.03.) | St.Christoph/Arlberg | AT |
| 1990 | (11.03.-17.03.) | La Plagne | FR | 2005 | (13.03.-19.03.) | Les Arcs 1800 | FR |
| 1991 | (10.02.-16.02.) | Obertraun | AT | 2006 | (05.03.-11.03.) | St. Christoph/Arlberg | AT |
| 1992 | (15.03.-21.03.) | La Plagne | FR | 2007 | (11.03.-17.03.) | Les Arcs 2000 | FR |
| 1993 | (09.05.-15.05.) | Kaprun | AT | 2008 | (02.03.-08.03.) | St. Christoph/Arlberg | AT |
| 1994 | (06.03.-12.03.) | Les Arcs | FR | 2009 | (08.03.-14.03.) | St. Moritz | CH |
| 1995 | (23.04.-29.04.) | Kaprun | AT | 2010 | (07.03.-13.03.) | St. Christoph/Arlberg | AT |
| 1997 | (26.01.-31.01.) | Aussois | FR | 2011 | (06.03.-12.03.) | Baqueira Beret | ES |
| 1998 | (29.03.-04.04.) | Park City | US | 2012 | (11.03.-17.03.) | St. Christoph/Arlberg | AT |
| 1999 | (21.02.-27.02) | Pamporova | BG | 2013 | (03.03.-09.03.) | Åre | SE |
| 2000 | (15.02.-18.02.) | Kananaskis | CA | 2014 | (09.03.-15.03.) | St. Christoph/Arlberg | AT |
| 2001 | (07.01.-13.01.) | Furano | JP | | | | |


# SYMPOSIUM ON SURFACE SCIENCE 2014

## St. Christoph am Arlberg, Austria
## March 9 - 15, 2014

# Time Schedule

### Sunday, 9 March 2014

| | |
|---|---|
| 16:00 – 18:30 | **Registration** |
| 20:00 – 20:20 | **Opening** |
| | *Chair: P. Varga* |
| 20:25 – 20:45 | **U. Heinzmann**<br>*Spin-, angle-, phase- and time-resolved photoemission* |
| 20:45 – 21:05 | **T. Michely**<br>*The backside of graphene: manipulation of adsorption by intercalation* |
| 21:05 – 21:25 | **H. Brune**<br>*Distinction of nuclear spin states with the STM* |

## Monday, 10 March 2014

*Chair: U. Diebold*

08:00 – 08:20 **W.-D. Schneider**
*Coulomb charge rings and quantum-size effects in metal islands on dielectric supports*

08:20 – 08:40 **M. Setvin**
*Small and large polarons in $TiO_2$ rutile and anatase*

*Chair: M. Altman*

16:40 – 17:00 **H. Ibach**
*Surface, interface and standing spin waves of 3d metal films*

17:00 – 17:20 **H.Pfnür**
*Highly correlated charges and spins in Pb/Si(557)*

17:20 – 17:40 **J. H. Dil**
*Spin texture of $Bi_2Se_3$ thin films in the quantum tunneling limit*

17:40 – 18:00 **A. P. Protogenov**
*Universal edge state transport in topological insulators*

18:00 – 18:20 **N. Müller**
*Spin effects in ultrafast charge transfer measurements on Ar/Co interfaces using a TOF-Mott-polarimeter*

*Chair: B. Hendriksen*

19:30 – 19:50 **F. J. Giessibl**
*Evidence for atom by atom transformation of graphene into diamond induced by the tip of a force microscope*

19:50 – 20:10 **W. Steurer**
*Au adatoms on NaCl: charge tristability and detailed adsorption site analysis by LT-STM/AFM*

20:10 – 20:30 **D. W. van Baarle**
*Can we see atoms in nano-scale friction? A bottom-up analysis of friction, based on damping*

20:30 – 20:50 **S. Müller**
*Electromechanical coupling coefficients of sp-bonded metals from first principles*

## Tuesday, 11 March 2014

*Chair: K. H. Ernst*

08:00 – 08:20 **K. Reuter**
*When atomic-scale resolution is not enough: Heat and mass transfer effects in in-situ model catalyst studies*

08:20 – 08:40 **J. Gustafson**
*High-energy surface X-ray diffraction and surface faceting during catalytic reaction*

*Chair: E. Taglauer*

16:40 – 17:00 **J. Enrique Ortega**
*Donor-to-acceptor core-level shifts in monolayer blends contacting noble metal surfaces*

17:00 – 17:20 **T. Koshikawa**
*Perpendicular magnetization of $[CoNi_x]_y$ multi-layers with high brightness and high spin-polarized LEEM and simulation based on LLG equation*

17:20 – 17:40 **J. Åhlund**
*Ground-breaking instrumentation development for photoelectron spectroscopy – New capabilities and applications*

17:40 – 18:00 **T. U. Kampen**
*Joule-Thomson scanning probe microscope*

18:00 – 18:20 **M. Maier**
*FERMI Cold Tip SPM: A new generation of variable temperature SPM for spectroscopy*

*Chair: G. Thornton*

19:30 – 19:50 **S. Förster**
*Surface-driven topological oxide quasicrystals*

19:50 – 20:10 **F. Mittendorfer**
*How reactive is a perovskite surface? The surface chemistry of $Sr_3Ru_2O_7$*

20:10 – 20:30 **J. Yuhara**
*Structural analysis of ultra-thin zinc oxide film on Rh(100)*

20:30 – 20:50 **H. Oberhofer**
*A theoretical description of water splitting on metal decorated oxide surfaces*

## Wednesday, 12 March 2014

*Chair: F. Aumayr*

08:00 – 08:20 **K. Morgenstern**
*Short-range and long-range interaction during thermal and laser-driven diffusion on metal surfaces*

08:20 – 08:40 **T. Greber**
*Nanoscale lateral segregation on h-BN/PtRh(111)*

*Chair: P. Bauer*

16:30 – 16:50 **J. Seifert**
*Surface structure of alanine on Cu(110) studied by grazing scattering of fast atoms*

16:50 – 17:10 **R. Schuch**
*Transmission of highly charged ions through mica nanocapillaries of various cross sections*

*Chair: A. P. Seitsonen*

17:10 – 18:30 **Posterintroduction**

**M. S. Altman**
*Probing buried magnetic interfaces with spin-polarized low energy electrons*

**P. Bauer**
*Electronic stopping of slow light ions in insulators*

**B. Berger**
*Interaction of nitrogen ions with tungsten and nitrogen saturated tungsten surfaces*

**R. Bliem**
*Cluster nucleation and growth from a highly super-saturated 2D phase: Ag/$Fe_3O_4$(001)*

**K. N. Eltsov**
*Gold intercalation under grapheme monolayer on Ni(111)*

**K.-H. Ernst**
*A metal surface with chiral memory*

**R. Fasel**
*Bottom-up fabrication of graphene nanoribbons: From molecules to devices?*

**S. Gerhold**
*Water adsorption at the tetrahedral titania surface layer of $SrTiO_3$(110)-(4x1): An STM and photoemission study*

**W. Heckel**
*Ab-initio based investigations of aliphatic and aromatic acids on $TiO_2$-surfaces: a precursor for hybrid materials design*

**A. Klimov**
*Effect of film boundaries on the quasi-ballistic transport of charge carriers in PbSnTe films in strong electric and magnetic fields*

**S. Yu. Krylov**
*Friction remembers*

**C. Lemell**
*Classical simulations for surface-streaking experiments*

**E. Lundgren**
*Aluminum oxide formation and stability*

**L. R. Merte**
*Ultra-thin FeO films grown on Ag(100)*

**R. V. Mom**
*Surface stress induced by agglomerated impurities: the case of a Mo-Au alloy*

**P. Müller**
*Combining low-energy electron microscopy and scanning probe microscopy techniques for surface science*

**D. Roth**
*Electronic stopping of slow light ions in transition metals*

**A. P. Seitsonen**
*On the electronic structure of Au(111), studied with density functional theory*

**V. Smejkal**
*Interaction of slow highly charged ions with carbon nano membranes*

**Y. Suchorski**
*Laterally-resolved reaction kinetics in CO oxidation on Pd: powder versus plane Pd(hkl) surfaces*

**A. S. Terekhov**
*Work function - mediated oxygen adsorption and oxidation of p-GaAs(Cs,O) – surfaces*

**G. Thornton**
*Support-morphology induced modification of adsorbate bonding to nanoparticles*

**P. Varga**
*Ion beam induced crystallographic and magnetic transformation of Fe films on Cu(100)*

**C. Virojanadara**
*Effects of Al on epitaxial graphene grown on 6HSiC(0001)*

19:30 – 21:30 **Postersession**

## Thursday, 13 March 2014

*Chair: R. Fasel*

08:00 – 08:20 **H. Marbach**
*Electron beam induced surface activation for the lithographic fabrication of clean nanostructures*

08:20 – 08:40 **T.Šikola**
*Selective deposition of metallic and semiconductor nanostructures at prepatterned surfaces*

*Chair: G. Renaud*

16:40 – 17:00 **J. V. Barth**
*Pathways to surface-confined complex networks*

17:00 – 17:20 **M. Buck**
*Molecular self-assembly on Ag and Cu modified Au surfaces: Intermolecular vs. molecule-substrate interactions*

17:20 – 17:40 **A. Winkler**
*New aspects of the nucleation of organic thin films*

17:40 – 18:00 **M. McEntee**
*Insights involving the catalytically active $Au/TiO_2$ interfacial sites for oxidation reactions using infrared spectroscopy*

18:00 – 18:20 **M. H. Farstad**
*The growth of $TiO_x$ on Pd(111) and Pd(100) by chemical vapor deposition*

*Chair: P. M. Echenique*

19:30 – 19:50 **U. Starke**
*Intercalation in epitaxial graphene on SiC: From quasifree standing graphene to superlattices*

19:50 – 20:10 **V. M. Silkin**
*Low-energy plasmonic structure of doped free-standing graphene*

20:10 – 20:30 **L. I. Johansson**
*The electron band structure of multilayer graphene on C-face SiC studied by Angle Resolved Photoemission (ARPES)*

20:30 – 20:50 **D. Menzel**
*Ultrafast charge transfer at graphene monolayers: hybridisation, final state dimensionality, and slow-down*

## Friday, 14 March 2014

*Chair: C. Lemell*

08:00 – 08:20 **J. Libuda**
*Surface science and model catalytic studies of liquid organic hydrogen carriers*

08:20 – 08:40 **G. Rupprechter**
*Model studies of Ni(Pd)-$ZrO_2$-$Pt_3(Pd_3)Zr$ solid oxide fuel cell (SOFC) anodes: preparation, stability, water and CO adsorption*

*Chair: Y. Suchorski*

16:30 – 16:50 **L. Hammer**
*Structure of adsorption phases of oxygen on Ir(100)*

16:50 – 17:10 **M. Ignacio**
*Role of strain in the stability of hetero-epitaxial island on a nanopillar*

17:10 – 17:30 **F. Cheynis**
*Surface diffusion of reactive solid nano-islands*

17:30 – 17:50 **W. Eberhardt**
*Morphology and electronic properties of Cu-Phthalocyanine:$C_{60}$ bulk heterojunction blends for photovoltaic applications*

17:50 – 18:10 **S. N. Filimonov**
*Dynamics of steps at the sidewalls of nanowires*

*Chair: P. Müller*

18:30 – 18:50 **C. Teichert**
*Surface science differently: What holds paper fibers together*

18:50 – 19:10 **M. E. Messing**
*Determination of nanoparticle surface area for improved nanotoxicology studies*

19:10 – 19:35 **Giant Slalom Race Award Ceremony**

20:00 **Conference Dinner**

# *CONTRIBUTIONS*

# Content

# *Sunday*

# Spin-, angle-, phase- and time-resolved photoemission

U. Heinzmann

*Molecular and Surface Physics, Faculty of Physics, Bielefeld University, Germany*
*(e-mail: uheinzm@physik.uni-bielefeld.de)*

The talk reviews the cross-linking of these types of photoemission experiments on solids and adsorbates. In particular new and recently obtained results of electron spin-polarization in photoemission with $[Mn_6^{III}Cr^{III}]$- and $[Fe_6^{III}Cr^{III}]$-single-molecule magnets (SMMs) adsorbed on solid surfaces measured in the paramagnetic phase at room temperature without magnetic fields are quantitatively compared with XMCD asymmetries measured at 2K at high magnetic fields in the ferromagnetic phase [1]. $[Mn_6^{III}Cr^{III}]$-SMMs adsorbed as a monolayer on HOPG shows a four-fold symmetry in its crystallographic order. The lateral dimension period matches the size of the molecule whereas the layer height resembles the height of the SMMs, as detected by means of molecular-resolved nc-AFM and Kelvin-probe-FM in UHV [2].

Furthermore, new measurements of attosecond time-resolved photoemission on a van-der Waals crystal performed with a 300 as short XUV pulse in the presence of a 5fs phase stabilized infrared pulse as the “clock” by use of the streaking method have been performed [3]. The layered structure of the investigated crystal yields element specific photoelectrons emitted from different depth and thus helps resolving the physical origin of temporal delays in photoemission as studied for the first time by Cavalieri et al [4], that the photoemission from W(110) 4f core-level states is delayed by about 100 as with respect to the electron emission from the valence band. The physical origin of this delay was not completely understood and controversial theoretical models co-exist. The talk also discusses the relationship of these as-delays of photoelectron wave packets with phase-shifts measured by means of the dynamical spin-polarization of photoelectrons in a cw photoemission experiment [5].

[1] A. Helmstedt, N. Dohmeier et al to be published (2014) and A. Helmstedt, N. Müller, A. Gryzia, N. Dohmeier, , A. Brechling, M. Sacher, U. Heinzmann, V. Hoeke, E. Krickemeyer, T. Glaser, S. Bouvron, M. Fonin and M. Neumann), J. Phys.: Condens. Matter 23, 266001 (2011)

[2] A. Gryzia, T. Volkmann et al to be published (2014) and A. Gryzia, H. Predatsch, A. Brechling, V. Höke, E. Krickemeyer, C. Derks, M. Neumann, T. Glaser and U. Heinzmann, Nanoscale Res. Lett. 6, 486 (2011)

[3] S. Neb, F. Merschjohann, P. Bartz, M. Hensen, C. Strüber, N. Müller, W. Pfeiffer and U. Heinzmann, to be published (2014)

[4] A.L. Cavalieri, N. Müller, Th. Uphues, V.S. Yakovlev, A. Baltuska, B. Horvath, B. Schmidt, L. Blümel, R. Holzwarth, S. Hendel, M. Drescher, U. Kleineberg, P. M. Echenique, R. Kienberger, F. Krausz and U. Heinzmann, Nature 449, 1029 (2007)

[5] U. Heinzmann and J.H. Dil, topical review, J. Phys. Condens. Matter 24, 173001 (2012)

# The backside of graphene: manipulation of adsorption by intercalation

T. Michely, S. Schumacher, F. Huttmann, A. Martinez-Galera, S. Runte, D.F. Förster, C. Busse, M. Petrovic[1], M. Kralj[1], S. Blügel[2], N. Atodiresei[2], V. Caciuc[2], P. Lazic[3], T.O. Wehling[4]

*II. Physikalisches Institut, Universität zu Köln, 50937 Köln, Germany*
*(corresponding author: T. Michely, e-mail: michely@ph2.uni-koeln.de)*

[1] *Institut za fiziku, Bijenčka 46, 10000 Zagreb, Croatia*

[2] *Peter Grünberg Institut (PGI) and Institute for Advanced Simulation (IAS), Forschungszentrum Jülich and JARA, 52425 Jülich, Germany*

[3] *Ruđer Bošković Institute, Bijenička 54, 10000 Zagreb, Croatia*

[4] *Institut für Theoretische Physik, Universität Bremen, Otto-Hahn-Allee 1, 28359 Bremen, Germany*

The ease by which graphene is affected through contact with other materials is one of its unique features and defines an integral part of its potential for applications. Intercalation, the insertion of atomic layers in between the backside of graphene and the supporting substrate, is an efficient tool to change its interaction with the environment on the frontside. By partial intercalation of graphene (Gr) on Ir(111) with Eu or Cs we induce strongly n-doped graphene patches through the contact with these intercalants. They coexist with nonintercalated, slightly p-doped Gr patches. We employ these backside doping patterns [1] to directly visualize doping induced binding energy differences of ionic adsorbates and organic molecules through low-temperature scanning tunneling microscopy (STM) [2].

In detail, we find that Eu adsorbed at 300 K to Gr preferentially binds to the slightly p-doped areas of Gr/Ir(111) with a Dirac point position with respect to the Fermi level of $E_D \approx 0.1$ eV. Binding of Eu to the strongly n-doped Gr/Eu/Ir(111) areas with $E_D \approx -1.4$ eV is not observed. The adsorbed Eu is highly mobile at 300 K. Thereby, it is enabled to move to areas of higher binding energy, where it forms clusters as well as extended monolayer islands. Cs deposition at 300 K onto Gr/Ir(111) causes the coexistence of extended Cs intercalation islands with a doping level of $E_D \approx -1.1$ eV and a dilute Cs adatom gas on the non-intercalated areas [3]. Though the ionized Cs adatoms adsorbed to Gr repel by Coulomb interaction, not a single adatom is found on Gr/Cs/Ir(111), underlining the preferred binding to the slightly p-doped Gr/Ir(111).

The weaker binding of adatoms, adatom clusters, and extended islands of cationic adsorbates to Gr areas with strong n-doping is linked to work function changes resulting from the doping.

The lowering of the kinetic energy upon delocalization of the electron donated by the ion to the substrate system is diminished in the n-doped areas just by the work function difference of graphene between n-doped and p-doped areas. The Coulomb penalty associated with charge redistribution upon adsorption, including screening, reduces the binding energy differences substantially below those estimated from work function differences. We confirmed these inferences not only by density functional theory (DFT) calculations for the systems under concern, but also by DFT calculations for doped, free standing graphene.

Not only ionic binding to Gr is affected by doping, but also van der Waals binding of organic molecules. As examples, we analyzed binding of benzene ($C_6H_6$) and naphthalene ($C_{10}H_8$) to Gr/Ir(111) and Gr/Eu/Ir(111). After low temperature adsorption followed by an annealing step enabling molecular mobility and accumulation in the stronger binding areas, we find molecular islands invariably bound to the strongly n-doped, intercalated patches. Thermal desorption spectroscopy confirms quantitatively these binding energy differences of the molecules to Gr/Ir(111) and Gr/Eu/Ir(111). We attribute stronger binding of the organic molecules to n-doped Gr to the larger polarizability of graphene with a partially filled $\pi^*$-band.

We speculate that also covalent bonds, that is, the interaction of radicals with Gr, will be substantially influenced by the Gr doping level. By using a doping pattern, the latter would allow one to imprint a chemical pattern to Gr. This might have far reaching practical consequences for Gr lithography.

Financial support from Deutsche Forschungsgemeinschaft through SFB608, project MI581/17-2, and INST 2156/514-1, the Ministry of Science of the Republic of Croatia and Deutscher Akademischer Austauschdienst via the project “Electrons in two dimensions”, and the Ministry of Science of the Republic of Croatia via project No. 035-0352828-2840 is acknowledged. We thank A. Rosch for critical reading of the manuscript and I. Šrut for experimental assistance.

[1] S. Schumacher, D.F. Förster, M. Rösner, T.O. Wehling, and T. Michely, Phys. Rev. Lett. 110, 086111 (2013)

[2] S. Schumacher, T.O. Wehling, P. Lazič, S. Runte, D.F. Förster, C. Busse, M. Petrović, M. Kralj, S. Blügel, N. Atodiresei, V. Caciuc, and T. Michely, Nano Lett. 13, 5013 (2013)

[3] M. Petrović, I. Šrut Rakić, S. Runte, C. Busse, J. T. Sadowski, P. Lazić, I. Pletikosić, Z.-H. Pan, M. Milun, P. Pervan, N. Atodiresei, R. Brako, D. Šokčević, T. Valla, T. Michely and M. Kralj, Nature Comm. 4, 2772 (2013)

# Distinction of Nuclear Spin States with the STM

Fabian Donat Natterer[1,2], François Patthey[1], and Harald Brune[1]
[1] *Ecole Polytechnique Fédérale de Lausanne (EPFL), CH-1015 Lausanne, Switzerland*
[2] *Present address: National Institute of Standards and Technology (NIST), Gaithersburg, MD 20899-6202, USA*
harald.brune@epfl.ch

**Abstract:** Inelastic electron tunneling spectroscopy is a powerful tool to determine the chemical identity of adsorbates by their vibrational energies, or to characterize their magnetic properties by spin-excitations. With STM these studies can be performed with atomic resolution. Here we demonstrate the spectroscopy of the rotational eigenvalues with the STM and illustrate its potential for physisorbed hydrogen and its isotopes. The observed excitation energies show the expected scaling with mass, and they are very close to the gas phase values indicating that the adsorbed molecules behave as quasi free rigid rotors in three dimensions. Since these energies are characteristic for the molecular nuclear spin states, we are able to identify the *para* and *ortho* species of hydrogen and deuterium, respectively. We thereby demonstrate nuclear spin sensitivity with unprecedented spatial resolution.

The nucleons of $H_2$ are fermions and therefore the molecular wave function is anti-symmetric with respect to proton permutation. Since the vibrational and the electronic $(^1\Sigma_g^+)$ ground states are symmetric, either the rotational or the nuclear wave functions have to be anti-symmetric. Therefore the antisymmetric nuclear singlet state (para) requires a symmetric rotational wave function (even rotational quantum number $J$), whereas the symmetric nuclear triplet state (ortho) implies an antisymmetric rotational wave function (odd $J$). Without inhomogeneous magnetic fields, one nuclear spin state can not be transformed into the other. Therefore each of the two nuclear spin isomers remains in its rotational subspace, with characteristic energies for the first rotational excitations $J = 0 \rightarrow 2$, respectively, $J = 1 \rightarrow 3$. The existence of nuclear disparate forms of $H_2$ with room temperature equilibrium abundance of 1:3 for para:ortho, has been predicted by Heisenberg [1]. The first preparation of pure para $H_2$ enabled the confirmation of this prediction by emission spectra and heat conductivity measurements in the gas phase [2].

The interaction of $H_2$ with solid surfaces is either strong, where it leads to the dissociation and the subsequent chemisorption of single H atoms, or it is weak, where the molecules are bound by van der Waals forces in a physisorbed state that is stable at low temperature. The latter case is of interest for the detection of the two nuclear spin isomers for surface adsorbed $H_2$. This has been achieved with neutron diffraction [3, 4], nuclear magnetic resonance [5, 6], and high-resolution electron energy loss spectroscopy (HREELS) [7, 8, 9]. HREELS detected the $J = 0 \rightarrow 2$ transition of para $H_2$ by an electron energy loss of 46 – 49 meV, a very weak loss peak at 70 meV has been attributed to the $J = 1 \rightarrow 3$ of ortho $H_2$ [8]. The respective gas phase values are 43.9 and 72.8 meV [10, 11]. The weak ortho $H_2$ signal decayed after a few minutes [8], which has been interpreted as ortho to para-$H_2$ conversion by short range magnetic interactions with the surface [12]. Evidence for rotational excitations has also been seen for the lowest energy $J = 0 \rightarrow 1$ of HD by high-resolution inelastic He atom scattering [13]. Also this technique is potentially able to discern the nuclear isomers. However, the molecules were adsorbed on NaCl(100) where they are only bound by 40 meV and therefore the primary energy of the He atoms was chosen below 35 meV and thus too low to excite rotations in either one of the $H_2$ isomers [13].

So far, rotational excitations of surface adsorbed molecules have only been observed with spatially integrating techniques. STM was shown to excite hindered or vibrationally assisted rotations in molecules [14]. However, the eigen energies of molecular rotations have been determined only very recently with the STM using inelastic electron tunneling spectroscopy (IETS). We report our results on STM rotational excitation spectroscopy (STM-RES) for $H_2$ and its isotopes adsorbed on a hexagonal boron nitride ($h$-BN) layer grown on a Ni(111) surface [15]. Similar work has been performed in parallel to ours, albeit with much weaker RES features since the molecules were directly adsorbed onto a metal surface [16].

The principle of IETS is that the excitation of an inelastic process in the tunnel junction creates an additional conductance channel and thus leads to a step of the differential conductance at the characteristic energy of the process. This has been demonstrated for vibrations of individual molecules [17], for phonons [18], for magnetic excitations of individual atoms [19], and for magnons [20].

The STM image in Fig. 1 shows a hexagonally close-packed monolayer of physisorbed $H_2$ molecules that forms a commensurate $(\sqrt{3} \times \sqrt{3})\mathrm{R}30^\circ$ structure with respect to the underlying $h$-BN. The $dI/dV$ spectra on $H_2$, $D_2$, and HD monolayers are shown in the middle of Fig. 1. Each curve reveals two pairs of conductance steps. Their threshold energies are symmetric around zero bias, as expected for IETS. Each step shows up as a clear peak ($V_\mathrm{t} > 0$) or dip ($V_\mathrm{t} < 0$) in the numerical derivatives $d^2I/dV^2$ shown on the right hand side of Fig. 1. The low energy excitations are phonon gaps of the commensurate molecular layers [15] and of less interest in the present context. We focus on the high energy excitations that are located

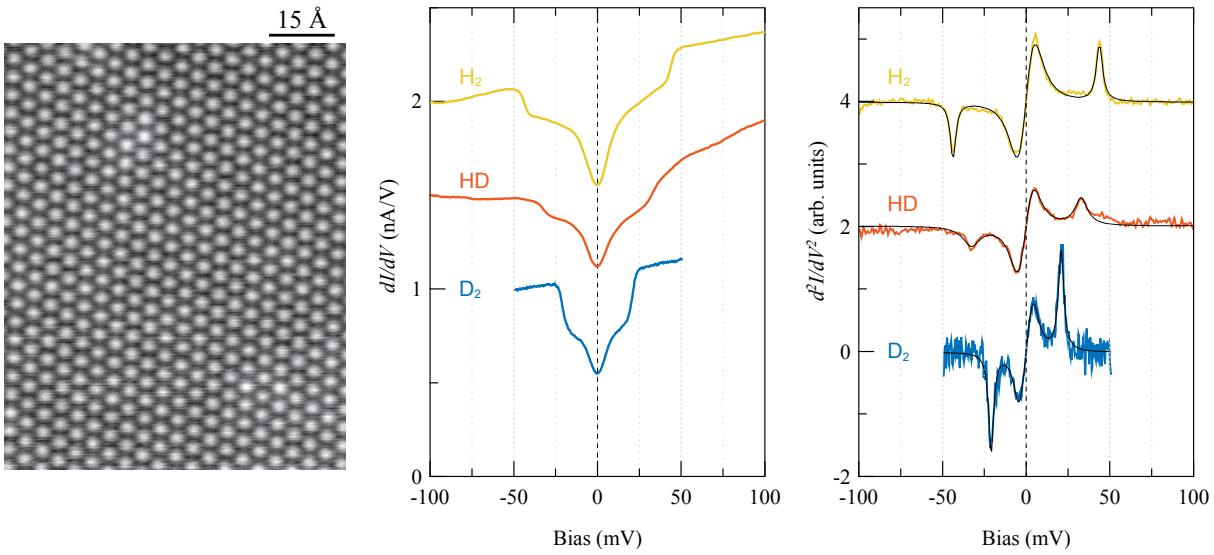


Figure 1: left: STM image of full $(\sqrt{3}\times\sqrt{3})$R30° $H_2$ monolayer on $h$-BN/Ni(111) (100 L $H_2$, $V_t = -20$ mV, $I_t = 20$ pA, $T = 4.7$ K). middle: $dI/dV$ of $H_2$ (◯), HD (△), and $D_2$ (□). The conductance steps at 43.7, 32.8, and 20.9 meV represent rotational $J = 0 \rightarrow 2$ transitions. The low-energy steps close to $E_F$ are attributed to phonon gaps of the commensurate molecular layer. Spectra are averages of 615 (◯), 1100 (△), and 75 (□) $dI/dV$-curves. The spectra were vertically offset by 0.5 nA/V for clarity (bias modulation 2 mV peak-to-peak at 397 Hz). right: Numerical derivative $d^2I/dV^2$. The black full lines show fits with a multi peak Lorentzian function.

at $(43.75 \pm 0.07)$, $(32.8 \pm 0.4)$, and $(20.89 \pm 0.07)$ meV, for $H_2$, HD, and $D_2$, respectively. Their ratios unambiguously identify them as rotational transitions since the energy of a rotational quantum state $J$ of a linear molecule is with $E_J^{\mathrm{rot}} = J(J+1)\hbar^2/2I$ inversely proportional to its moment of inertia $I$. In addition, the absolute excitation energies of all three molecules match the reported gas-phase values discussed above. Most importantly, the spectra identify $H_2$ in its para, and $D_2$ in its ortho nuclear spin configuration. As in previous HREELS work, we only find the lowest energy $J = 0$ nuclear spin isomer of both molecules.

For molecules directly adsorbed onto Ni(111), we observe no rotational excitation by the tunnel electrons, in agreement with former low-$T$ STM studies [21, 22, 23, 24, 25] and with the fact that such features are very weak for molecules being temporarily trapped between an STM tip and a Au(110) surface [16]. Seeking evidence for the respective other spin isomer of $H_2$ and $D_2$, we have performed experiments on $h$-BN/Rh(111)-$(12 \times 12)$ and on graphene/Ru(0001)-$(23 \times 23)$ [26]. In both cases, we detect pronounced conductance steps corresponding again to the $J = 0 \rightarrow 2$ transition of the respective nuclear spin isomer with ground state $J = 0$. For diatomic and polyatomic molecules with undistinguishable nucleons, such as $H_2$, $N_2$, $O_2$, $NH_3$, $H_2O$, and $CH_4$, the nuclear spin states can now be inspected with unprecedented spatial resolution. We gratefully acknowledge discussions with G. Ertl and funding from the Swiss National Science Foundation.

**References**

[1] W. Heisenberg, Z. Phys. **41**, 239 (1927).
[2] K. F. Bonhoeffer and P. Harteck, Z. Phys. Chem. B **4**, 113 (1929).
[3] M. Nielsen *et al.*, J. Phys. Colloques **38**, C4 (1977).
[4] V. L. P. Frank *et al.*, Phys. Rev. Lett. **61**, 436 (1988).
[5] P. R. Kubik *et al.*, C. J. Phys. **63**, 605 (1985).
[6] K. Kim and N. S. Sullivan, Phys. Rev. B **55**, R664 (1997).
[7] S. Andersson and J. Harris, Phys. Rev. Lett. **48**, 545 (1982).
[8] P. Avouris *et al.*h, Phys. Rev. Lett. **48**, 199 (1982).
[9] R. Palmer and R. Willis, Surf. Sci. **179**, L1 (1987).
[10] I. F. Silvera, Rev. Mod. Phys. **52**, 393 (1980).
[11] P. C. Souers *Hydrogen Properties for Fusion Energy* (University of California Press, Berkeley, 1986).
[12] E. Ilisca, Prog. Surf. Sci. **41**, 217 (1992).
[13] F. Traeger and J. P. Toennies, J. Phys. Chem. B **108**, 14710 (2004).
[14] B. C. Stipe *et al.*, Science **279**, 1907 (1998).
[15] F. D. Natterer *et al.*, Phys. Rev. Lett. **111**, 175303 (2013).
[16] S. Li *et al.*, Phys. Rev. Lett. **111**, 146102 (2013).
[17] B. C. Stipe *et al.*, Science **280**, 1732 (1998).
[18] H. Gawronski *et al.*, Science **319**, 930 (2008).
[19] A. J. Heinrich *et al.*, Science **306**, 466 (2004)
[20] T. Balashov *et al.*, Phys. Rev. Lett. **97**, 187201 (2006).
[21] J. A. Gupta *et al.*, Phys. Rev. B **71**, 115416 (2005).
[22] R. Temirov *et al.*, New J. Phys. **10**, 053012 (2008).
[23] M. Sicot *et al.*, Surf. Sci. **602**, 3667 (2008).
[24] C. Weiss *et al.*, Phys. Rev. Lett. **105**, 086103 (2010).
[25] C. Lotze *et al.*, Science **338**, 779 (2012).
[26] F. D. Natterer *et al.*, in preparation.

# *Monday*

# Coulomb charge rings and quantum-size effects in metal islands on dielectric supports

W.-D. Schneider[1,2]

[1]*Institut de Physique de la Matière Condensée, Ecole Polytechnique Fédérale de Lausanne (EPFL), CH-1015 Lausanne, Switzerland*
[2]*Fritz-Haber-Institute of the Max-Planck-Society, D-14195 Berlin, Germany*
*( e-mail: wolf-dieter.schneider@epfl.ch)*

A detailed knowledge of the electron transport properties and the electronic structure of metallic nanostructures on dielectric supports is not only important for the development of a future nanoscale electronics but also for the selection and the improvement of nanoscale catalysts in heterogeneous catalysis. However, the accurate characterization and understanding of such systems at the nanoscale is an experimentally challenging task. In the past, we investigated with low-temperature scanning probe techniques [1] nanoscale Pb-islands on different supports and elucidated their size-dependent supraconducting properties [2], electron confinement [3], and dynamical Coulomb blockade phenomena [4].

Here, we study the transport properties and the electronic structure of individual nanosized double-barrier tunnel junctions consisting of a tip, flat metallic Pb islands, and a supporting dielectric ultrathin NaCl film on Ag(111). The observed differential conductance spectra display the presence of Coulomb blockade phenomena [5] characteristic for single-electron tunneling processes, which are well described within the semi-classical orthodox theory. Under specific tunneling conditions in the Coulomb staircase regime, very striking concentric lines which follow the island contours, are visible in topographic images as well as in dI/dV maps. These Coulomb charge rings reflect the influence of the tip-island junction on the fractional residual charge $Q_0$ on the nanoisland [5].

Moreover, electron quantization in arbitrarily shaped gold islands, containing between 50 and 200 atoms, supported on MgO thin films on Ag(001) is observed and analyzed within simple particle-in-a-box models and via a density functional tight-binding approach. We find a correlation between the island geometry and the gap between the highest occupied (HOMO) and the lowest unoccupied molecular orbital (LUMO) in the finite-sized islands. The linear excentricity is identified as suitable descriptor for this relationship, as it combines information on both island size and shape. These results may help to elucidate the interplay between electronic and chemical properties of oxide-supported clusters as encountered in heterogeneous catalysis [6,7].

Support from the Swisss National Science Foundation and the DFG Excellence-Initiative 'Unicat' is gratefully acknowledged.

[1] R. Gaisch, J.K. Gimzewski, B. Reihl, R.R. Schlittler, M. Tschudy, and W.-D. Schneider, Ultramicroscopy **42-44**, 1621 (1992).

[2] C. Brun, I.-P. Hong, F. Patthey, I. Yu. Sklyadneva, R. Heid, P. M. Echenique, K. P. Bohnen, E. V. Chulkov, and W.-D. Schneider, Phys. Rev. Lett. **102**, 207002 (2009).

[3] I.-P. Hong, C. Brun, F. Patthey, I. Yu. Sklyadneva, X. Zubizarreta, R. Heid, V. M. Silkin, P. M. Echenique, K. P. Bohnen, E. V. Chulkov, and W.-D. Schneider, Phys. Rev. B **80**, 081409(R) (2009).

[4] C. Brun, K.-H. Müller, I. P. Hong, F. Patthey, C. Flindt, and W.-D. Schneider, Phys. Rev. Lett. **108**, 126802 (2012).

[5] I. P. Hong, C. Brun, M. Pivetta, F. Patthey, and W.-D. Schneider, Front. Physics **1**, 13 (2013).

[6] X. Shao, Y. Cui, W.-D. Schneider, N. Nilius, and H.-J. Freund, J. Phys. Chem. C **116,** 17980 (2012).

[7] C. Stiehler, Y. Pan, W.-D. Schneider, P. Koskinen, H. Häkkinen, N. Nilius, and H.-J. Freund, Phys. Rev. B **88**, 115415 (2013).

# Small and Large Polarons in $TiO_2$ Rutile and Anatase

M. Setvin,[1] C. Franchini,[2] X. Hao,[1] B. Daniel,[1] M. Schmid,[1] G. Kresse,[2] and U. Diebold[1]

[1] *Institut für Angewandte Physik, Technische Universität Wien, A-1040 Wien, Austria*
*(corresponding author: M. Setvin, e-mail: setvin@iap.tuwien.ac.at)*

[2] *Faculty of Physics and Center for Computational Materials Science, Universität Wien, Sensengasse 8/12, A-1090 Wien, Austria*

$TiO_2$ is a prototypical metal oxide used in photocatalysis [1], photoelectrochemical (Grätzel) solar cells [2], transparent optical conductors [3] or memristors [4]. Industrially two forms of $TiO_2$ are used, rutile and anatase. The behavior of charge carriers is of key importance in virtually all applications of these materials. When excess electrons are added to the conduction band of an oxide, the electron-phonon interaction may result in electron trapping – the formation of either localized (small) or delocalized (large) polarons [5].

We used a combination of STM, STS and DFT+*U* to investigate the nature of electron polarons in rutile and anatase. The excess electrons in rutile can localize at any lattice Ti atom, forming a small polaron. The polarons in rutile can easily hop to neighboring sites. Electrons in a perfect anatase lattice prefer a delocalized (band-like) solution, while small polarons can only be formed at defects. Large polarons were observed in Nb-doped anatase in vicinity of subsurface Nb dopants.

We further discuss the impact of the different behavior of excess electrons (localized *vs.* delocalized) on applications. For example, Nb-doped anatase is a transparent optical conductor, while Nb-doped rutile is a bad electrical conductor with semiconductor-like transport properties [6]. Another example is related to photocatalysis: Rutile (110) surface can trap electrons at any lattice site, while anatase (101) surface allows charge trapping only at the step edges.

Work supported by the Advanced ERC grant “OxideSurfaces”.

[1] M. A. Henderson, Surf. Sci. Rep. **66**, 185 (2011).
[2] M. Grätzel, Nature **414**, 338 (2001).
[3] Y. Furubayashi *et al*., Appl. Phys. Lett. **86**, 252101 (2005).
[4] K. Szot *et al.*, *Nanotechnology* **22**, 1 (2011).
[5] I. G. Austin, N. F. Mott, Adv. Phys. **50**, 757 (2001).
[6] S. X. Zhang *et al.,* J Appl. Phys. **102**, 013701 (2007).

# Surface, interface and standing spin waves of 3d metal films

Harald Ibach, Eugen Michel and Jayaraman Rajeswari

*Peter Grünberg Institut, Research Center Jülich, 52425 Jülich, Germany*
*Jülich Aachen Research Alliance, Germany*

h.ibach@fz-juelich.de

Wave packets of spin waves offer the unique capability to transport a quantum bit, the spin, without the transport of charge or mass. In this context, large wave-vector / high-energy spin waves are of particular interest as they permit a spin confinement within a few nanometers. Stimulated by the development of advanced electron energy loss spectrometers [1-3] a considerable number of experimental studies concerning large wave-vector / high-energy surface spin waves of 3d-metal films have emerged lately. These studies were accompanied, partly even anticipated, by considerable effort in theory aiming at the understanding of localized spin waves in thin films of itinerant magnets and at the description of inelastic electron scattering from such excitations

In this talk I will show that the power of electron energy loss spectroscopy (EELS) reaches beyond studies of surface spin waves. By virtue of the finite penetration depth of low energy electrons, spin waves localized at interfaces between a substrate and a thin capping layer may be studied yielding information about the exchange coupling between atoms at the interface.

Furthermore, the quantization of spin waves with wave vectors perpendicular the film gives rise to standing modes to which EELS has likewise access. Such studies, when carried out as function of the film thickness, yield information on the layer dependence of the exchange coupling [4]. With the help of a further advanced spectrometer we have investigated the dispersion of standing modes in fcc and hcp cobalt films (Fig. 1). A comparison of experimental data on the dispersion of the lowest standing wave to predictions of two theoretical studies of Costa et al. and Bergqvist et al [5, 6] shows that neither theory fits the data as such (Fig. 2). However the model of Bergvist et al can be brought to agreement with experiment by a uniform reduction of the exchange constants. This shows that the larger interlayer coupling between the surface layer and the next layer underneath in the model of Bergqvist et al. is an essential ingredient in the correct interpretation of the experimental data.

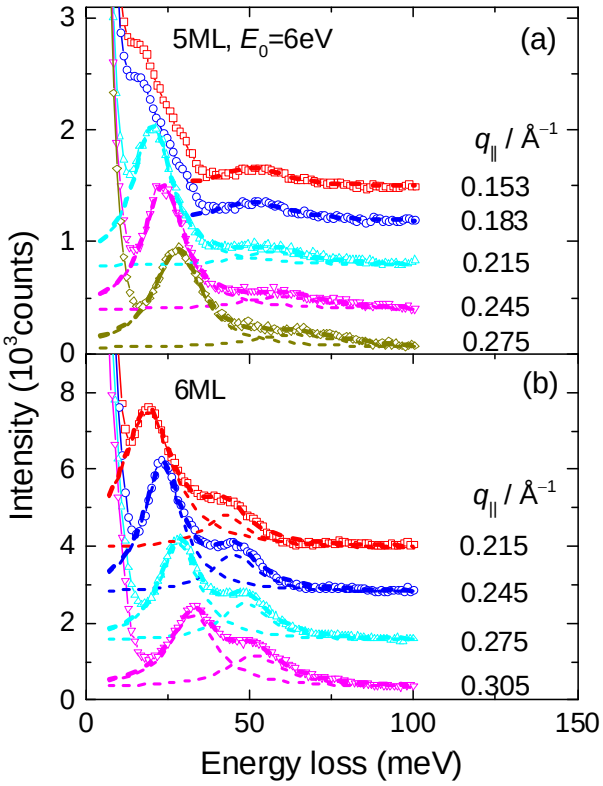


Fig. 1: surface and standing spin wave in fcc cobalt layers

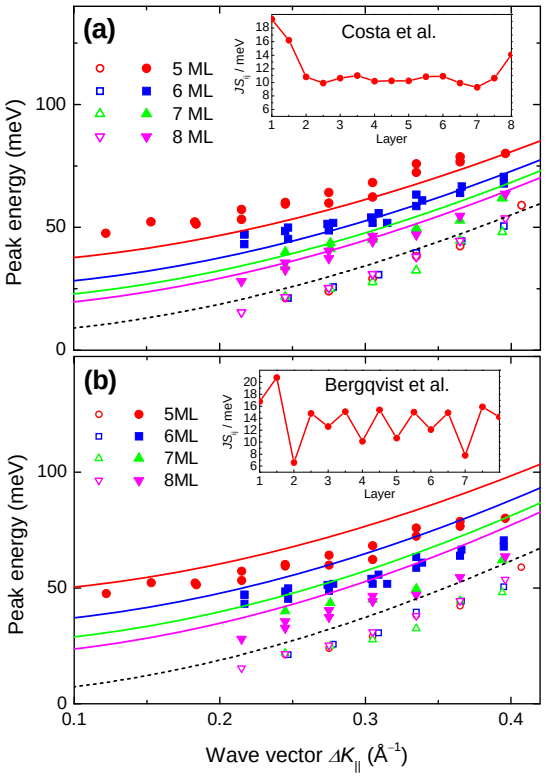


Fig. 2: Dispersion of surface and standing spin waves in 5-8ML cobalt films with comparison to theory

An unresolved issue is the energy dependence of the probability of inelastic scattering by spin waves. This probability shows a resonance peak at low energies and and levels off to immeasurably low values at higher electron energies, more than an order of magnitude lower than cacluated in the only theoretical study of Gokhale and Mills [7]. In view of the fact that all experimental data on surface spin waves are obtained with impact energies in the low energy resonance range the absence of a working theory is rather unsatisfactory.

[1] H. Ibach, D. Bruchmann, R. Vollmer, M. Etzkorn, P. S. A. Kumar, J. Kirschner, Rev. Sci. Instrum. 74 (2003) 4089.
[2] H. Ibach, J. Rajeswari, C. M. Schneider, Rev. Sci. Instrum. 82 (2011) 123904.
[3] H. Ibach, J. Rajeswari, J. Electr. Spectros. Rel. Phenom. 185 (2012) 61.
[4] J. Rajeswari, H. Ibach, C. M. Schneider, A. T. Costa, D. L. R. Santos, D. L. Mills, Phys. Rev. B 86 (2012) 165436
[5] A. T. Costa, R. B. Muniz, D. L. Mills, Phys. Rev. B 70 (2004) 054406.
[6] L. Bergqvist, A. Taroni, A. Bergman, C. Etz, O. Eriksson, Phys. Rev. B 87 (2013) 144401.
[7] M. P. Gokhale, A. Ormeci, D. L. Mills, Phys. Rev. B 46 (1992) 8978.

# Highly correlated charges and spins in Pb/Si(557)

C. Tegenkamp, D. Lükermann, H. Dil[1], H. Pfnür

*Institut für Festkörperphysik, Leibniz-Universität Hannover, 30167 Hannover, Germany*
*(corresponding author: H. Pfnür, e-mail: pfnuer@ifkp.uni-hannover.de)*

[1] *École Polytechnique Fédérale de Lausanne, Physics Section, CH-1015 Lausanne, Switzerland*

Two- or three-dimensional interactions strongly modify and stabilize the properties of wire arrays, and can lead to special one-dimensional behavior not predicted by standard theories either in 1D or 2D. Pb/Si(557) is an impressive example of how semiconducting surfaces can be functionalized simply by adsorption of a physical monolayer of a metal. Adsorbate induced reconstructions on mesoscopic length scales, causing strong modifications of the surface band structure, electronic stabilization of new facet orientations and strong anisotropic Rashba splitting result in a unique and physically very rich system with intriguing spectroscopic and transport phenomena, as we will demonstrate.

The adsorption of 1.3 ML Pb at low temperatures on Si(557) followed by annealing to 640K leads to the formation of Pb-chains with an average interchain spacing of d=1.5nm. The Pb film on the micro-Si(111) facets has a 10-fold periodicity due to the formation of five $\sqrt{3}x\sqrt{3}$ units separated by $\sqrt{7}x\sqrt{3}$ domain walls. Interestingly, the Pb-chains reorganize the structure of the Si(557) substrate forming at low temperatures a long-range ordered (223) facet structure.

The electronic stabilization of this phase is obvious from ARPES measurements, which show that a mini gap, around 20meV in size, opens only perpendicular to the steps. Close to the Fermi energy the interchain distance, *d,* is seen by Umklapp structures with a spacing in reciprocal space of $g=2\pi/d$ [1,2].

The delicate interplay between the atomic structure and the spin-polarized band structure results in unique electrical properties: macroscopic dc-conductivity measurements below 78K show that electronic transport occurs only along the chain direction, while an insulating behavior is found in the perpendicular direction due to perfect Fermi nesting ($g = 2k_F$) [1,2]. The transport properties can be changed by temperature, excess Pb coverage and external magnetic fields. Above 78K, the system undergoes a refacetting transition and the system switches into a 2d- transport regime.

Strong anisotropic magneto-transport was found for Pb-wetting layers close to completion of the physical monolayer caused by an enhanced elastic scattering rate in the direction perpendicular to the step direction. Furthermore, anti-localization is found for all monolayer structures due to strong spin-orbit coupling.

Recently, spin resolved ARPES measurements have been performed. As expected, the surface states reveal Rashba-splitting with the spin polarization strictly along the wires. In fact, the coherent superposition of both Rashba channels is manifested by an extraordinarily large Rashba splitting of $\Delta K = 0.2$ Å$^{-1}$. This splitting corresponds exactly to g/2, i.e. the Rashba splitting is commensurate with the Umklapp structure so that nesting between surface bands of the same spin polarization can occur at $2k_{Rashba}=g$ [3]. This means that the spin texture close to the Fermi surface is alternating between adjacent terraces, giving rise to spin-polarized charge-density waves in the direction across the wires.

This additional spin order is responsible for anomalies on magnetoconductance at 1.31 ML Pb

coverage. Carrying out magnetoconductance experiments close to 1.31 ML Pb coverage, the spin-orbit scattering time increases by two orders of magnitude [4], a consequence of the fact that backscattering on a spin-polarized terrace is only allowed if the spin is conserved.

New superstructures are formed by an excess Pb coverage up to 0.1ML due to ordered step decoration indicating strong electron-electron correlation across steps. This leads to new long range ordered states and formation of a sequence of 1D charge density waves up to a concentration of 1.5 ML, but also, as very recent angular and spin resolved photoemission studies show, to new ordered spin states, which will be discussed.

[1] C. Tegenkamp, T. Ohta, J.L. McChesney, H. Dil, E. Rotenberg, H. Pfnür, K. Horn, Phys. Rev. Lett. **100,** 076802 (2008).
[2] C. Tegenkamp, Z. Kallassy, H. Pfnür, H.-L. Günter, V. Zielasek, M. Henzler, Phys. Rev. Lett. **95,** 176804(2005).
[3] D. Lükermann, M. Gauch, M. Czubanowski, H. Pfnür, C. Tegenkamp, Phys. Rev. B **81**, 125429 (2010).
[4] C. Tegenkamp, D. Lükermann, H. Pfnür, B. Slomski, G. Landolt H. Dil, Phys. Rev. Lett. **109**, 266401 (2012).

# Spin texture of $Bi_2Se_3$ thin films in the quantum tunneling limit.

G. Landolt[1,2], S. Schreyeck[3], S. V. Eremeev[4,5], B. Slomski[1,2], S. Muff[1,2,6], J. Osterwalder[1], E. V. Chulkov[5,7], C. Gould[3], G. Karczewski[3,8], K. Brunner[3], H. Buhmann[3], L. W. Molenkamp[3], and J. H. Dil[1,2,6]

[1]*Physik-Institut, Universität Zürich, 8057 Zürich, Switzerland*
*(corresponding author: Hugo Dil, jan-hugo.dil@psi.ch)*
[2]*Swiss Light Source, Paul Scherrer Institute, 5232 Villigen, Switzerland*
[3]*Physikalisches Institut, Experimentelle Physik III, Universität Würzburg, D-97074, Germany*
[4]*Institute of Strength Physics and Materials Science, Russian Academy of Sciences, Siberian Branch, Tomsk, 634021 Russia*
[5]*Tomsk State University, Tomsk, 634050 Russia*
[6]*Institut de Physique de la Matière Condensée, Ecole Polytechnique Fédérale de Lausanne, CH-1015 Lausanne, Switzerland*
[7]*Donostia International Physics Center (DIPS) and CFM, Centro Mixto CSIC-UPV/EHU, Departamento de Fisica de Materiales, UPV/EHU, 20080 San Sebastian, Spain*
[8]*Institute of Physics, Polish Academy of Sciences, 02-668 Warsaw, Poland*

Topological insulators have gained a lot of attention recently because of their unique spin-polarized surface states. For any practical use or for the realization of exotic new physical phenomena these surface states should be separated from the bulk states and lie in a well defined bulk band gap. In a variety of ARPES studies this situation has been attempted to be realized by chemically doping the system. However, in a recent study combining bulk sensitive Seebeck measurements and surface sensitive ARPES we have found that the surface induced band bending can be as large or larger as the band gap [1]. This directly renders it improbable that such materials will find practical use. One way around this inherent difficulty of semiconducting materials is to use systems where the band gap is by definition at the Fermi level. An example of this are Kondo insulators and recently we identified $SmB_6$ as a topological Kondo insulator [2].

Another possibility, which does not rely on low temperatures, is to use thin films where band bending effects are expected to play less of a role because of the reduced bulk to surface ratio. On the other hand, quantum tunneling between states at opposite surfaces can open up a gap in the topological state and apparently lift the topological protection and influence the spin texture. It has been argued that in this case the electronic structure can be described by a Rashba-type spin splitting [3], but it is still unclear how the topological surface states exactly emerge from these Rashba-split states at the topological

phase transition. Our work shows how the spin texture develops across a topological phase transition and provides the groundwork for realization of two-dimensional spintronic devices based on topological semiconductors.

By means of spin- and angle-resolved photoelectron spectroscopy [4] we studied the spin structure of hight quality thin films of the topological insulator $Bi_2Se_3$ grown by MBE on InP(111). For thicknesses below six quintuple layers the spin-polarized metallic topological surface states interact with each other via quantum tunneling and a gap opens up in the Dirac cone. Our measurements show that the resulting surface states can be described by massive Dirac cones which are split in a Rashba-like manner due to the substrate induced inversion asymmetry. The inner and the outer Rashba branches have distinct localization in the top and the bottom part of the film, whereas the band apices are delocalized throughout the entire film. Supported by density functional theory calculations our results [5] not only explain how the states behave across the topological transition but can for example also be used to determine the direction of charge transfer between two semiconductors.

[1] S. Muff et al. Phys. Rev. B **88**, 035407 (2013).

[2] N. Xu et al. Phys. Rev. B **88**, 121102(R) (2013).

[3] Y. Zhang et al. Nat Phys **6**, 584 (2010).

[4] J. H. Dil, J. Phys.: Condens. Matter **21**, 403001 (2009).

[5] G. Landolt et al. Physical Review Letters.....

# Universal Edge State Transport in Topological Insulators

Alexander P. Protogenov,[1,2] Valery A. Verbus,[3] and Evgueni V. Chulkov[4,5,6,7]

[1] *Institute of Applied Physics of the RAS, Nizhny Novgorod 603950, Russia; alprot@appl.sci-nnov.ru*
[2] *Donostia International Physics Center (DIPC), 20018 San Sebastián/Donostia, Spain*
[3] *Institute for Microstructures of the RAS, Nizhny Novgorod 603950, Russia*
[4] *Departamento de Física de Materiales, Facultad de Ciencias Químicas, Uviversidad del País Vasco, Apartado 1072, 20080 San Sebastián/Donostia, Spain*
[5] *Donostia International Physics Center (DIPC), 20018 San Sebastián/Donostia, Spain*
[6] *Centro de Física de Materiales CFM-Materials Physics Center MPC, Centro Mixto CSIC-UPV/EHU, 20018 San Sebastián/Donostia, Spain*
[7] *Tomsk State University, Tomsk 634050, Russia*

A topological insulator is a quantum phase of matter with gapless electron states on the surface and gapped ones, in the bulk. In two-dimensional systems, conducting electron states propagate along the edge of the topological insulator. These states have a linear Dirac dispersion and spin locked to the momentum [1–3]. In the talk, we will consider the universality of the transport characteristics in two-dimensional topological insulators.

It is convenient to use the ballistic Landauer-Bütticker approach [4] writing the current $I_i$, injected through the terminal $i$ into a sample as

$$I_i = \frac{e^2}{h}\sum_{j=1}^{N}(T_{ji}V_i - T_{ij}V_j)\ . \tag{1}$$

Here, $V_j$ is the voltage on the terminal $j$, $e$ is the electron charge, $h$ is the Planck constant, and $h/e^2$ is the resistance unit. We will equate it further to unity. $T_{ij}$ is the matrix element of transmission from the terminal $i$ to the terminal $j$, and $N$ is the total number of terminals. It plays a role of the tuning parameter. The edge electron modes in topological insulators propagate in two directions. We will put that the transmission coefficients between neighboring terminals are equal to unity: $T_{i+1,i} = T_{i,i+1} = 1$ and other probabilities are equal to zero. The $N$-terminal scheme implies the use of the periodic boundary conditions $T_{N+1,N} = T_{1,N}$, $T_{N,N+1} = T_{N,1}$ in the both directions of the edge state propagation. The labels of terminals, whose voltages we will measure, will contain information about the influence of the edge state current between the terminals, through which the current flows about the voltage distribution on other terminals.

Let the current $I_{1N}$ flows through terminals 1 and $N$ (see Fig. 1) and the voltage be measured on all other terminals. In this case, the equation which determines the voltage on the contacts, has the form

$$A\,V = I\ , \tag{2}$$

where the matrix $A$ equals $A_{ij} = 2\delta_{ij} - \delta_{i,j+1} - \delta_{i,j-1} - \delta_{i,1}\,\delta_{j,N} - \delta_{i,N}\,\delta_{j,1}$, $\delta_{ij}$ is the Kronecker delta, $1 \le i,j \le N$, $V = (V_1, V_2, \dots V_{N-1}, V_N)$, and $I = I_{1N}(1, 0, \dots 0, -1)$. We are interested in the difference between the voltage on terminals. Since the vector $V$ is invariant with respect to the constant value shift, we may assume that $V_N = 0$.

For arbitrary $N$, the solution of Eq.(2) has the form $V_i = I_{1N}\left(1 - \frac{i}{N}\right)$. Therefore, the resistance $(V_1 - V_N)/I_{1N}$ between terminals 1 and $N$ equals $R_{1N,1N} = (N-1)/N$. The nonlocal resistance $R_{kl,ij=}(V_i - V_j)/I_{kl}$ at $k = 1, l = N$ when measuring the voltage between the terminals $i$ and $j$ is

$$R_{1N,ij} = \frac{j-i}{N}\ . \tag{3}$$

To find the voltage distribution in the situation, when the current flows from the terminal 1 to the terminal $k$, in the right-hand side of Eq.(2,) we have to use the equation for the current in the form of $I = I_{1k}(1, 0, \cdots -1, \dots 0)$. Here, $-1$ is located in the $k$ place. The exact solution of Eq.(2) in this general case has the form

$$V_i = I_{1k}\left(1 - \frac{i}{N}(1 - k + N)\right)\ , \tag{4}$$

if $1 \le i \le k$, and

$$V_i = I_{1k}(1 - \frac{i}{N})(1 - k)\ , \tag{5}$$

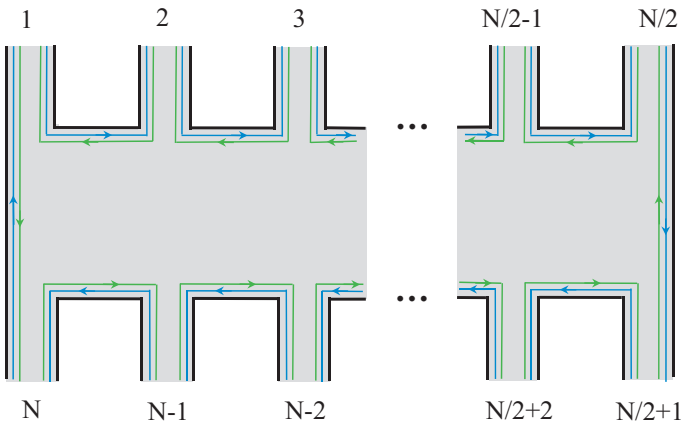


FIG. 1: Distribution of edge states in a two-dimensional $N$-terminal insulator.

if $k \le i \le N$. These assignments of the current and voltage terminals determine the following values of the resistance

$$R_{1k,ij} = \begin{cases} \frac{j-i}{N}\,(1-k+N)\,, & 1 \le i,j \le k, \\ \frac{j-i}{N}\,(1-k)\,, & k \le i,j \le N, \\ \frac{j-i}{N}\,(1-k)+(k-i), & 1 \le i \le k,\ k \le j \le N\ . \end{cases} \tag{6}$$

One can easy verify that after the interchange of the current $(1k)$ and voltage $(ij)$ probe indices and the shifts $k \to j-i+1, j \to k-i+1, i \to N-i+2$ these equations satisfy the Onsager-Casimir symmetry relations $R_{mn,kl} = R_{kl,mn}$ [5] for the nonlocal resistances $R_{mn,kl}$. We would also like to mention the fact that topological universality of the ballistic transport due to the edge states under ideal conditions is determined by the topological properties of the electron quantum bulk states. Therefore, the considered phenomenon in a trivial insulator is absent.

We focused on the universal exhibition of topological order in the transport properties of ideal two-dimensional topological insulators in the most representative form. The study of the transport characteristics of the topological insulator $SmB_6$ revealed [6] that in the three-dimensional case the transport properties significantly depend on the geometry of samples and terminal assignments. A deviation from the universal behavior takes place also in two-dimensional systems. It occurs due to metal droplets inside real contacts. This phenomenon can be described in terms of an additional terminal. The effect of this and other factors such as a finite width of the terminal, reflections from the internal interfaces, and other conditions on amplitudes of the transitions between current and voltage terminals has been studied in Refs. [7–10].

To conclude, we have described the universal distribution of the resistances studying the edge state transport in the two-dimensional topological insulators in the ballistic transport regime.

The authors are grateful to C. L. Kane, M. Büttiker and S. V. Eremeev for useful discussions. This work was supported in part by the RFBR Grant Nos. 13-02-12110 and 14-02-00174.

[1] M. Z. Hasan and C. L. Kane, Rev. Mod. Phys. **82**, 3045 (2010).
[2] X.-L. Qi and S.-C. Zhang, Rev. Mod. Phys. **83**, 1057 (2011).
[3] J. E. Moore, Nature **464**, 194 (2010).
[4] M. Büttiker, Phys. Rev. B **38**, 9375 (1988).
[5] M. Büttiker, IBM J. Res. Dev. **32**, 317 (1988).
[6] J. Botimer, D.J. Kim, S. Thomas, T. Grant, Z. Fisk, and Jing Xia, Robust Surface Hall Effect and Nonlocal Transport in $SmB_6$: Indication for an Ideal Topological Insulator, arXiv:1211.6769.
[7] A. Roth, C. Brüne, H. Buhmann, L. W. Molenkamp, J. Maciejko, X.-L. Qi, and S.-C. Zhang, Science **325**, 294 (2009).
[8] J. Wang, B. Lian, H. Zhang, S.-C. Zhang, Anomalous Edge Transport in the Quantum Anomalous Hall State, arXiv: 1306.1817
[9] C. Brüne, A. Roth, H. Buhmann, E. M. Hankiewicz, L. W. Molenkamp, J. Maciejko, X.-L. Qi and S.-C. Zhang, Nature Physics **8**, 485 (2012) and the Supplementary Information.
[10] C. Brüne, A. Roth, E. G. Novil, M. König, H. Buhmann, E. M. Hankiewicz, W. Hanke, J. Sinova and L. W. Molenkamp, Nature Physics **6**, 448 (2010) and the Supplementary Information.

# Spin Effects in Ultrafast Charge Transfer Measurements on Ar/Co Interfaces using a TOF-Mott-Polarimeter

T. Sundermann[1], N. Müller[1], U. Heinzmann[1], W. Wurth[2], J. Bauer[3], R. Han[3], P. Feulner[3]

[1] *Fak. für Physik, Molekül- und Oberflächenphysik, Universität Bielefeld, 33615 Bielefeld, Germany (corresponding author: N. Müller, e-mail: nmueller@physik.uni-bielefeld.de)*

[2] *Institut für Experimentalphysik, Universität Hamburg, 22761 Hamburg, Germany*

[3] *Physik-Department E20, Technische Universität München, 85747 Garching, Germany*

The schema of the core hole clock method [1,2] and the technique of spin resolved time of flight electron spectroscopy [3] are combined to study spin transfer effects from resonantly $2p_{3/2} \rightarrow 4s$ excited Ar atoms to emitted electrons. Thereby the Ar atoms are physisorbed on top of an in plane magnetized Co adlayer on W(110). In this adsorbate system the charge transfer into the empty minority conduction band of Co is preferred for excited electrons with minority spin state [4]. Correspondingly the mean orientation of the persistent Ar atoms can be changed and the Ar atoms ionized by the charge transfer can be oriented.

For exciting the Ar $2p_{3/2} \rightarrow 4s$ resonance circularly as well as linearly polarized synchrotron radiation of energy $h\nu = 244.6$ eV is used (BESSY beamline UE56/II PGM2, single bunch mode). Emitted electrons are energy and spin analyzed by means of a TOF spectrometer followed by a spherical Mott polarimeter operated in retarding mode at a scattering energy of 45 keV [3]. Depending on the partial transfer of the primarily excited 4s electron into the empty minority conduction band of Co, electron emission spectra following the decay of the excited Ar $2p_{3/2}$ hole states show significant peaks corresponding to autoionization (spectator) processes and normal Auger decays.

If circularly polarized radiation is applied the excited Ar 4s electrons are spin polarized and the $2p_{3/2}$ core holes oriented due to the relativistic selection rules. As with measurements at free Ar atoms [5] the emitted electrons are strongly spin polarized with a degree of electron spin polarization up to about 80%. Changing the alignment of helicity and magnetization from parallel to antiparallel shifts the spin polarization measured in autoionization peaks, the spin direction parallel to the helicity is more preferred. With excitation by linearly polarized radiation, spin polarization effects up to about 20% appear for autoionization emission channels. These effects prove the spin dependent charge transfer from excited unpolarized Ar 4s states to empty minority conduction band states of Co.

The results show that our method opens a way to study spin dependent charge transfer processes also for low Z adsorbates when spin polarized excited states can not be prepared by optical pumping.

We acknowledge travel funding and the provision of beamtime at beamline UE56/2-PGM2 of BESSY II by the Helmholtz-Zentrum Berlin, and we thank W. Mahler and B. Zada for assistance during the experiments.

[1] D. Menzel, Chem. Soc. Rev., **37,** 2212 (2008)
[2] P. A. Brühwiler, O. Karis, N. Martensson, Rev. Mod. Phys., **74**, 706 (2002)
[3] G. Snell, M. Drescher, N. Müller, U. Heinzmann, U. Hergenhahn, J. Viefhaus, F. Heiser, U. Becker, N. B. Brookes, Phys. Rev. Lett. **76**, 3923 (1996)
[4] F.Blobner, R. Han, A. Kim, W. Wurth, P. Feulner, to be published
[5] B. Lohmann, B. Langer, G. Snell, U. Kleiman, S. Canton, M. Martins, U. Becker, N. Berrah, Phys.Rev. **A71,** 20701 (2005)

# Evidence for atom by atom transformation of graphene into diamond induced by the tip of a force microscope

T. Hofmann, A. J. Weymouth, A. Donarini[1], F. J. Giessibl

*Institute of Experimental and Applied Physics, University of Regensburg, D-93053 Regensburg, Germany, franz.giessibl@ur.de*

[1]*Institute of Theoretical Physics, University of Regensburg, D-93053 Regensburg, Germany*

In 2009, Gross *et al*. proposed to use carbon-monoxide terminated tips to image pentacene, an organic molecule [1]. This approach has enabled submolecular spatial resolution on many other organic molecules as well as atomic resolution of graphene [2].

Here, we perform simultaneous STM and AFM on epitaxial graphene, grown by the Seyller group (U Erlangen-Nürnberg, now Chemnitz) on the carbon side of SiC. We use a qPlus sensor with a tungsten tip that is terminated by a CO molecule that oscillates at a constant amplitude of 50 pm. We record a series of seven physical observables that are used to create images and to analyze the interaction in detail: 1. A tunneling current $I$ (averaged over the oscillation cycle of the cantilever), 2. a frequency shift $\Delta f = f_0 \langle k_{ts} \rangle / (2k)$, where $\langle k_{ts} \rangle$ is the tip-sample force gradient (averaged over the oscillation), 3.-6. higher harmonics $a_n$ of order n from 2 to 5, where the deflection $q$ of the force sensor is expressed $q(t)=\sum a_n \cos(n 2\pi f t)$ with $a_1=A=50$ pm and $f = f_0+\Delta f$. The higher harmonics are usually below the detection limit (in this experiment about 100 fm), their rise above the noise marks the presence of sharp force transients [3,4]. Figure 1 shows the evolution of three ($I$, $\Delta f$, $a_3$) of these seven channels with decreasing distance. The five data sets cover a distance range of merely 60 pm with a distance decrement of 12 pm. The tunnelling current, shown in the left column, is inversed with respect to the atomic lattice of graphene, due to the $p_x/p_y$ symmetry of the front orbitals in the CO terminated tip (C.J.Chens derivative rule), but it does not change significantly with distance.

The frequency shift shows a truthful image of graphene for $z$-values from 60 to 36 pm, showing the known sharpening effects due to lateral CO bending [1], and the third harmonic shows only noise in that distance regime (the other orders remain below the detection noise for all distances). For $z$ values below 36 pm, the contrast starts to invert, and the third harmonic starts to emerge from its noise floor, starting at the hollow site of the graphene lattice and developing rings with increasing diameters with reduced $z$-values.

We have developed a model that explains the contrast reversal in $\Delta f$ as a consequence of the lateral bending of the CO tip – the CO molecule cannot bend laterally when trapped in a hollow site, however it can bend easily when located on a ridge or an atom site of the graphene lattice. We also find compelling evidence that the rise of $a_3$ is related to a rehybridization of the sp2 bonds to sp3 bonds, where the graphene surface layer and the

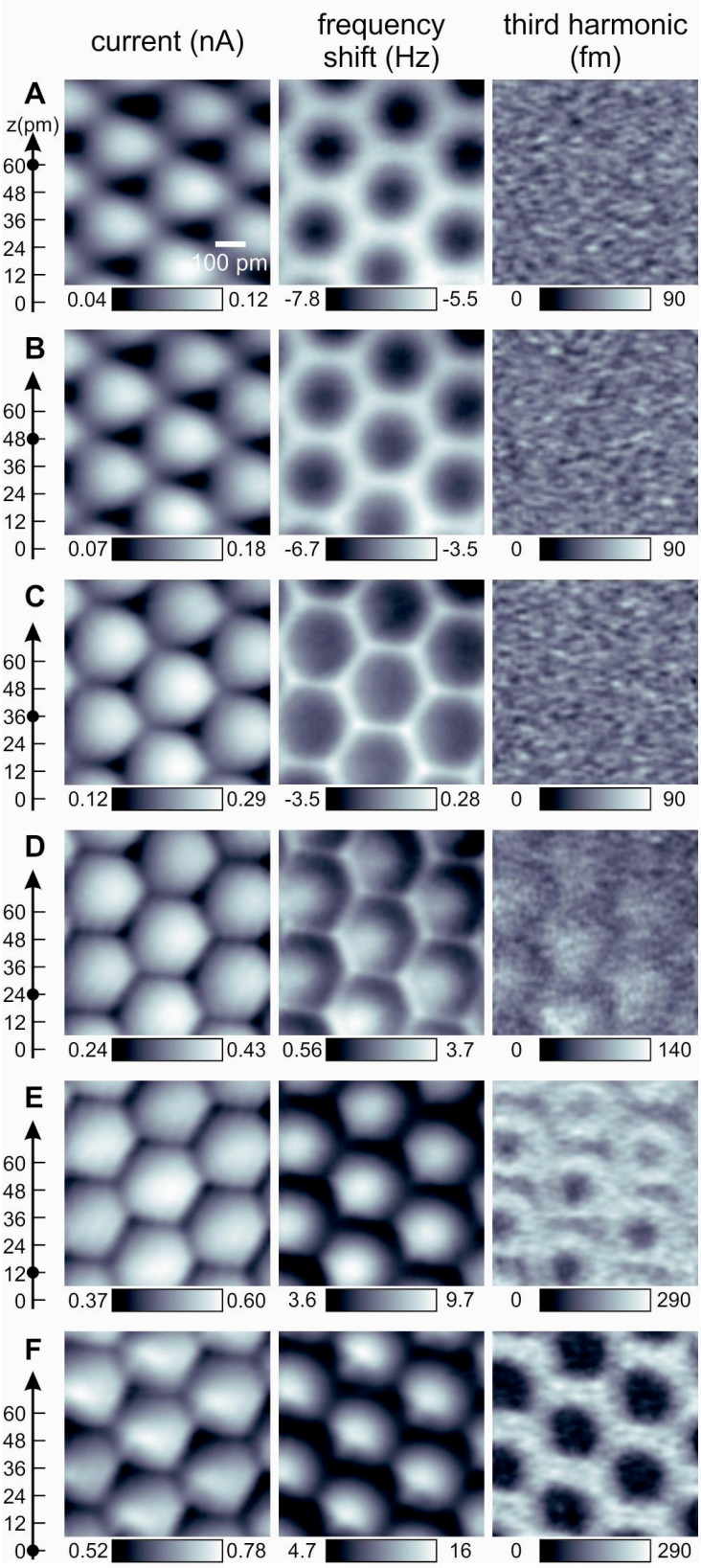


[3] U. Dürig, N. J. Phys. **2**, 5 (2000).

[4] S. Hembacher et al., *Science* **305**, 380 (2004).

carbon buffer layer are induced to locally rehybridize. It has been known since a long time that graphite can be transformed to diamond at pressures of a few Gigapascals and elevated temperatures. In our experiment, we find that the higher harmonics arise at a repulsive forces that, when divided by the area of a unit cell, correspond to similar pressures as the known pressure of laboratory diamond creation.

We have also looked into other possible reasons for higher harmonic creation, such as a buckling of the CO molecule or a penetration of the CO molecule into the hollow site of graphene. However, considering control experiments we performed on graphene grown on Cu and highy oriented pyrolytic graphite, we conclude that induced rehybridization is the origin of the higher harmonics.

The experiments show, that higher harmonic force microscopy can be used to observe transient phenomena that are beyond the intrinsic temporal resolution of AFM.

[1] L. Gross, F. Mohn, N. Moll, P. Liljeroth, G. Meyer, *Science* **325**, 1110 (2009).

[2] M. P. Boneschanscher, J. van der Lit, Zh. Sun, I. Swart, P. Liljeroth, and D. Vanmaekelbergh, *ACS Nano* **6**, 10216 (2012).

# Au adatoms on NaCl: charge tristability and detailed adsorption site analysis by LT-STM/AFM

W. Steurer[1], B. Schuler[1], N. Pavlicek[1], L. Gross[1], J. Repp[2], I. Scivetti[3], M. Persson[3,4], G. Meyer[1]

[1] *IBM Research-Zurich, 8803 Rüschlikon, Switzerland (corresponding author: W. Steurer, e-mail: wst@zurich.ibm.com)*

[2] *Institute of Experimental and Applied Physics, University of Regensburg, 93053 Regensburg, Germany*

[3] *Surface Science Research Centre and Department of Chemistry, University of Liverpool, Liverpool L69 3BX, UK*

[4] *Department of Applied Physics, Chalmers University of Technology, SE-412 96 Göteborg, Sweden*

Bilayer NaCl films on metal supports have proven expedient for controlling the charge state of individual atoms and molecules [1–4] and for electronically decoupling molecules from the underlying substrate [5–7]. The physical mechanism behind the charge stability are large ionic relaxations within the NaCl film, leading to an energy barrier between the charged and the neutral state. As the charge stability depends strongly on the electronic level alignment with respect to the Fermi level of the substrate system, the number of stable charge states may vary even for similar materials. For example, two and three stable charge states have been reported for Au [1,3] and Ag adatoms [2], respectively.

Interest in these studies comes from the prospect of implementing charge state control based functionality in the framework of molecular electronics. However, with regard to possible future applications, it would be desirable to achieve charge state stability irrespective of the exact level alignment. This requirement is naturally fulfilled on bulk-like insulator films where charges cannot drain off. A promising system in this respect is thick insulating NaCl films grown on metal substrates. As a first step toward the application of thick NaCl films for charge stability experiments, we present a detailed study of Au adatoms adsorbed on 2–10 monolayer thick NaCl films grown on Cu(111) and Cu(100).

We show that Au adatoms on NaCl exhibit charge tristability (neutral, negatively charged, and positively charged) independent of the layer thickness. Atomically-resolved STM and AFM images reveal that the inherent adsorption positions on NaCl films, which are 3 ML or thicker, are on top of a chlorine atom for the neutral Au adatom, and in bridge position for the negative and positive charge states, respectively. On bilayer NaCl, the adsorption positions are identical to the ones on thick films except for the Au anion, which adsorbs on-top Cl on the

Cu(100) substrate, and on both bridge position as well as on-top Cl for NaCl on the Cu(111) substrate.

Using a simplified density-functional theory (DFT) approach to handle charged adsorbates [8], we show that small changes in the lattice constant of NaCl are responsible for the different adsorption positions of the negatively charged Au adatom on bilayer NaCl. With decreasing lattice constant, the adsorption position changes from bridge position to on-top Cl. On Cu(100), NaCl grows in a commensurate fashion, resulting in a slightly compressed bilayer NaCl film compared to three and more layers. On Cu(111), the growth of NaCl is incommensurate, giving rise to the formation of a Moiré pattern with locally varying lattice spacing, an effect which is most pronounced for bilayer NaCl.

For the Au cation, we find a bistable adsorption position close to the bridge position, which can be reversibly switched by the STM tip in a controlled manner. The positively charged Au adatom sits slightly off-center and pushes the neighboring chlorine atoms significantly out of their normal position. DFT calculations corroborate this interpretation.

Support by ERC Advanced Grant `CEMAS' is gratefully acknowledged.

[1] J. Repp, G. Meyer, F. E. Olsson, and M. Persson, Science 305, 493 (2004).

[2] F. E. Olsson, S. Paavilainen, M. Persson, J. Repp, and G. Meyer, Phys. Rev. Lett. 98, 176803 (2007).

[3] L. Gross, F. Mohn, P. Liljeroth, J. Repp, F. J. Giessibl, and G. Meyer, Science 324, 1428 (2009).

[4] I. Swart, T. Sonnleitner, and J. Repp, Nano Lett. 11, 1580 (2011).

[5] J. Repp, G. Meyer, S. M. Stojkovic, A. Gourdon, and C. Joachim, Phys. Rev. Lett. 94, 026803 (2005).

[6] T. Leoni, O. Guillermet, H. Walch, V. Langlais, A.Scheuermann, J. Bonvoisin, and S. Gauthier, Phys. Rev. Lett. 106, 216103 (2011)

[7] J. Repp, G. Meyer, S. Paavilainen, F. E. Olsson, and M. Persson, Science 312, 1196 (2006).

[8] I. Scivetti and M. Persson, arXiv:1310.8476 [cond-mat.mtrl-sci]

# Can we see atoms in nano-scale friction? A bottom-up analysis of friction, based on damping

D.W. van Baarle, S.Yu. Krylov[1], M.E.S. Beck, J.W.M Frenken

*Kamerlingh Onnes Laboratory, Leiden University, P.O. Box 9504, 2300RA Leiden, The Netherlands*
*(corresponding author: D.W. van Baarle, e-mail: baarled@physics.leidenuniv.nl)*

[1] *Institute of Physical Chemistry and Electrochemistry, Russian Academy of Sciences, Leninsky prospect 31, 119071 Moscow, Russia*

After the invention of the scanning tunneling microscope, several scanning probe techniques have been developed which routinely result in atomic resolution. One variant of such a microscope is the friction force microscope (FFM) which records the lateral friction force between a scanning tip and a substrate surface. As friction is still not a well understood phenomenon, this system is very suitable to study friction. Here, we will use the typical experimental results of the FFM and knowledge from atomic energy dissipation to build a consistent picture of friction between nano-scale surfaces. Our straight forward analysis not only yields a more fundamental insight into the friction mechanism, but also sets some constraints to typical parameters (e.g. contact size) in order either to get high friction or to enter a different friction regime like superlubricity.

In order to study friction at the nano-scale, quite some FFM's have been developed all over the world which routinely result in 2-dimensional lateral force maps showing atomic resolution (or maybe better: atomic periodicities), e.g. see [1-2]. These maps show a so called stick-slip (SS) behaviour of the tip touching the substrate. During the 'stick' the system stores potential energy which is released and dissipated during the 'slip' by the friction between tip and substrate. So the mere fact that an atomic pattern is observed in an FFM image gives us quantitative information about the energy dissipation rate of the contact.

We will show that a comparison of this system with knowledge from theory and experiments on energy dissipation of atoms on surfaces yields striking results concerning the behaviour of the friction contact. A both qualitative and quantitative analysis shows that we are forced to draw tight conclusions about the contact size and the effective mass involved in order to explain the experimental results. As a natural consequence the interpretation of the 2-dimensional force maps of the FFM will be improved.

The research presented also elucidates the more general friction mechanism of single-asperity contacts. Using our results one might be able to make predictions about the friction behaviour of these contacts and hence might predict which friction regime (e.g. stick-slip or superlubricity) will be applicable to a specific contact. So this is not only a step forward to understand friction, but also to control friction.

Supports of the European Commission (Grant ERC-2010-AdG_20100224) and the Foundation for Fundamental Research on Matter (FOM, The Netherlands) are gratefully acknowledged.

[1] M. Dienwiebel, J.W.M. Frenken et al, Rev. Sci. Instrum. **76,** 043704 (2005).
[2] A. Schirmeisen, L. Jansen, and H. Fuchs, Phys. Rev. B **71,** 245403 (2005).

# Electromechanical coupling coefficients of sp-bonded metals from first principles

Anja Michl[1,2], Sandra Hoppe[1], Jörg Weissmüller[1,3], and Stefan Müller[1]

[1] *Institute of Advanced Ceramics, Hamburg University of Technology, D-21073 Hamburg*
[2] *Institute of Materials Research, Materials Mechanics, Helmholtz-Zentrum Geesthacht, D-21502 Geesthacht*
[3] *Institue of Materials Physics and Technology, Hamburg University of Technology, D-21073 Hamburg*
*(corresponding author: S. Müller, e-mail: stefan.mueller@tuhh.de)*

The response of the surface stress $f$ of a metallic surface to a variation in the superficial charge density $q$ defines an electrocapillary coupling parameter, $\varsigma = \delta f/\delta q$. The surface-induced stresses in the bulk of a solid electrode result in an elastic deformation, thus allowing to determine $\varsigma$ from the bending of cantilevers [1, 2] or from porous metal expansion [3] in reaction to electric charging in electrolyte. This electrocapillary coupling strength is appreciable for nanoscale metal structures with a high surface-to-volume ratio suggesting their use as actuators with large stroke and strain energy density [3, 4]. Investigations of electrocapillary coupling are mainly based on a thermodynamic Maxwell relation, $\varsigma = \mathrm{d}f/\mathrm{d}q|_e = \mathrm{d}U/\mathrm{d}e|_q$ [5], that links the surface stress charge response at equilibrium to the response of the electrode potential $U$ to tangential strain $e$. Since the variation of the potential of zero charge of an electrode surface in electrolyte is closely linked to the variation of the work function $W$ in vacuum [6, 7], it is possible to investigate electrocapillary coupling using the concepts and methods of theoretical surface science without explicit consideration of the electrolyte solution [8].

Using density functional theory, we have calculated such strain response parameters $\mathrm{d}W/\mathrm{d}e$ for sp-bonded metals. Surprisingly, for Al, we find an abnormal positive sign for the coupling coefficient [9], while all other investigated metals show the usual negative response parameter (in their natural crystal structure). This finding holds for all investigated surface orientations (100), (110), and (111). A comparison of the three surface orientations is shown in Fig. 1, where the work function for relaxed layers is plotted as a function of the in-plane strain. The response for the (100) surface is the largest one ($\mathrm{d}W/\mathrm{d}e_{100} = 1.02$ eV), whereas the magnitude is similar for the other two orientations ($\mathrm{d}W/\mathrm{d}e_{111} = 0.63$ eV and $\mathrm{d}W/\mathrm{d}e_{110} = 0.58$ eV).

It is possible to decompose the work function into an orientation-dependent surface quantity, the dipole barrier $V_{\mathrm{dip}}$, which arises from the redistribution of the electronic charge at the metallic surface and a volume dependent quantity, the Fermi energy $E_{\mathrm{f}}$. It turns out that in contrast to the resulting strain response of the work function, the contributions have negative sign and are considerably larger in magnitude, especially for the static cases without transverse contraction. The positive coupling coefficient of the work function is thus the difference of larger negative surface and volume contributions, which only nearly cancel.

Analyzing the dependence of the strain response on the electron density within the framework of the jellium model, our study links the unusual positive sign of the response of the work function to tangential strain for aluminium to its high electron density. Yet, the pronounced variation of the response with surface orientation also shows that the response behaviour cannot be understood based on the electron density alone.

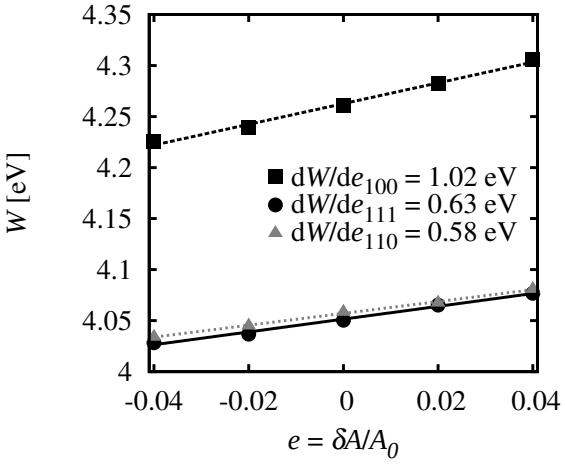


Figure 1: Work function $W$ vs. in-plane strain $e$ for (100), (111) and (110) surfaces of aluminum with relaxed interlayer distances. For all three orientations the response parameters have a positive sign with the largest coefficient obtained for the (100) surface.

Based on such results for Al, we will analyze trends of the coupling coefficients with respect to valence electron density, crystal structure, and work function of other sp-metal surfaces and discuss identified correlations.

# References

[1] H. Ibach, Surf. Sci. Rep. **29**, 195–263 (1997).

[2] W. Haiss, Rep. Prog. Phys. **64**, 591 (2001).

[3] J. Weissmüller, R.N. Viswanath, D. Kramer, P. Zimmer, R. Würschum, and H. Gleiter, Science **300**, 312 (2003).

[4] H. J. Jin, X.L. Wang, S. Parida, K. Wang, M. Seo, and J. Weissmüller, Nano Lett. **10**, 187 (2010).

[5] A. Y. Gokhshtein, Doklady Akademii Nauk SSSR **187**, 601 (1969).

[6] S. Trassatti, J. Electroanal. Chem. **33**, 351 (1971).

[7] D. Rath D and D. Kolb, Surf. Sci. **109** 641 (1981).

[8] Y. Umeno, C. Elsässer, B. Meyer, P. Gumbsch, M. Nothacker M, J. Weissmüller, F. Evers, Europhys. Lett. **78**, 13001 (2007).

[9] A. Michl, J. Weissmüller, and S. Müller, J. Phys.: Condens. Matter **25**, 445012 (2013).

# *Tuesday*

# When atomic-scale resolution is not enough: Heat and mass transfer effects in *in-situ* model catalyst studies

S. Matera and K. Reuter

*Lehrstuhl für Theoretische Chemie, Technische Universität München, D-85747 Garching, Germany*
*(corresponding author: K. Reuter, e-mail: karsten.reuter@ch.tum.de)*

A central goal in *in-situ* studies of defined model catalysts has been to obtain (at best) as resolved spectro- or microscopic information as has been established in UHV surface science. With this focus possible heat and mass transport limitations in the ambient environments have not received much attention. In parts they may even be unavoidable, considering the often significant constraints that *in-situ* techniques impose on the design of the reactor chamber. We investigate such effects with our newly developed first-principles based multi-scale modeling approach integrating kinetic Monte Carlo simulations into a fluid dynamical treatment [1]. Apart from the conceptual discussion in idealized reactor geometries [2], it is in particular the recent integration of our scheme into the general purpose Catalytic Foam solver [3] that now enables us to also explicitly address the complex flow profiles in actual *in-situ* reactor chambers.

Our simulations generally demonstrate the crucial role of heat and mass transfer limitations in the emerging field of *in-situ* model catalyst studies, in particular for the unselective and therefore high turnover CO oxidation that is prominently used as allegedly simple test reaction. For lateral flows over the model catalyst as e.g. in reactor STM realizations the observed substantial variation in the gas-phase pressures and temperature between inlet and catalyst surface extends even to the lateral position at the active surface, i.e. the transport limitations lead to pronounced lateral changes in surface composition across the catalyst surface [4]. The transport limitations also clearly affect recent *in-situ* X-ray photoelectron spectroscopy measurements [5] and can actually be visualized e.g. through planar laser induced fluorescence (PLIF) [6]. On top of this, our latest time-resolved simulations even predict the formation of Rayleigh-Bénard type convection instabilities. These complexities prevent the aspired direct relation between measured activity and defined catalyst structure, and therewith underscore the importance of carefully designed reactor geometries in *in-situ* studies.

Support by the Deutsche Forschungsgemeinschaft is gratefully acknowledged.

[1] S. Matera and K. Reuter, Catal. Lett. 133, 156 (2009).
[2] S. Matera and K. Reuter, Phys. Rev. B 82, 085446 (2010).

[3] M. Maestri and A. Cuoci, CatalyticFOAM, www.catalyticfoam.polimi.it
[4] S. Matera and K. Reuter, J. Catal. 295, 261 (2012).
[5] S. Blomberg, M.J. Hoffmann, J. Gustafson, N.M. Martin, V.R. Fernandes, A. Borg, Z. Liu, R. Chang, S. Matera, K. Reuter, and E. Lundgren, Phys. Rev. Lett. 110, 117601 (2013).
[6] S. Matera, J. Zetterberg, S. Blomberg *et al*., to be published.

# High-energy surface X-ray diffraction and surface faceting during catalytic reaction

J. Gustafson, M. Shipilin, C. Zhang, A. Stierle[1,2], U. Hejral[1,2], U. Ruett[1], O. Gutowski[1], P.-A. Carlsson[3], M. Skoglundh[3], E. Lundgren

*Synchrotron Radiation Research, Lund University, Box 118, 221 00 Lund, Sweden.*

[1] *Deutsches Elektronen-Synchrotron (DESY), 22603 Hamburg, Germany.*

[2] *Fachbereich Physik Universität Hamburg, Jungiusstr. 9, 20355 Hamburg, Germany.*

[3] *Competence Centre for Catalysis, Chalmers University of Technology, 412 96, Göteborg, Sweden*

Surface X-ray diffraction (SXRD) is one of few methods available for surface structure determination under ambient conditions. Due to the broken periodicity at the surface, the reciprocal lattice will, in addition to Bragg reflections originating from the bulk, include so-called crystal truncation rods (CTRs), which connect the Bragg reflections *perpendicular* to the surface. In case the in-plane periodicity at the surface differs from that of the underlying bulk, additional superstructure rods arise in reciprocal space, and the shapes, positions and directions of these CTRs and superstructure rods hold detailed information about the atomic surface structure.

A serious drawback of conventional SXRD, with X-rays in the range of 10-30 keV and a point or small two-dimensional (2D) detector, is the limited amount of data that can be acquired in a reasonable time frame. Exploring 2D maps from a substantial part of reciprocal space is extremely time-consuming, and mapping of the 3D reciprocal space with high resolution is currently impossible even with synchrotron radiation. As a result, the probed surface structure has to be known qualitatively from other measurements, and an unexpected structure may easily be left unnoticed, especially under harsh conditions. Furthermore, obtaining a quantitative data set (from an already qualitatively known structure) takes in the order of 10 hours with traditional use of SXRD.

In this contribution we demonstrate how the use of high-energy X-rays (85 keV) in combination with a large 2D detector accelerates the data collection by several orders of magnitude and enables full surface-structure determination by 3D mapping of reciprocal space on a time scale suitable for in situ studies. In addition, the small diffraction angles, resulting from the high photon energy, and the large detector result in data that are easily presented in a more intuitive way, since each detector image contains the projection of a full plane in reciprocal space and straight lines in reciprocal space correspond to straight lines on the detector.

We also present (HE)SXRD results from Rh(553) and Pd(553) during CO oxidation. It has previously been shown that these surfaces undergo significant rearrangements upon exposure to $O_2$. On Rh(553) the result is a coexistence of (331), exposing a 1D oxide, and (111) facets under mildly oxidizing conditions, and equivalent (111) and (11-1) facets covered by surface oxide at higher $O_2$ pressures [1]. On Pd(553) a surface oxide has been found with (332) orientation [2]. We show that during CO oxidation, similar rearrangements occur, and the ratio between CO and $O_2$ in the feed gas corresponds to the $O_2$ pressure in the previous results. In addition, CO rich conditions results in (110) facets formation.

As an example, Fig. 1 shows HESXRD data from Pd(553) during CO oxidation in 2.1 mbar $O_2$ and 4 mbar CO at a sample temperature of about 300°C. The 2.2° angle between the CTRs and the vertical (553) direction directly reveals the formation of (332) facets, which coexist with (111) facets.

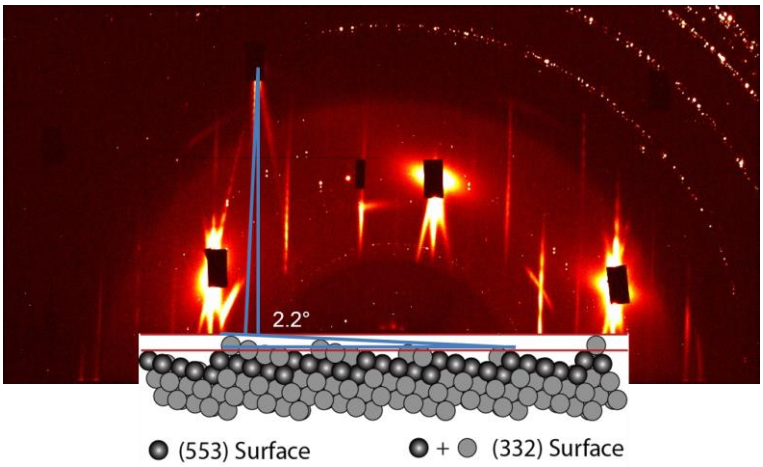


**Figure 1** HESXRD data from Pd(553) during CO oxidation. The 2.2° angle between the CTRs and the vertical (553) direction directly reveals the formation of (332) facets, which coexist with (111) facets.

This work is done within the Röntgen-Ångström collaboration. The authors would like to thank the Swedish Research Council, the Swedish Foundation for Strategic Research, the Crafoord Foundation, the Knut and Alice Wallenberg Foundation, the Anna and Edwin Berger Foundation and the BMBF (project 05K10PS1 NanoXcat) for financial support.

[1] J. Gustafson, A. Resta, A. Mikkelsen, R. Westerstrom, J. N. Andersen, E. Lundren, Physical Review B 74, 035401 (2006)

[2] R. Westerström, J. Gustafson, A. Resta, A. Mikkelsen, J. N. Andersen, and E. Lundgren, Phys. Rev. B 76, 155410 (2007)

# Donor-to-acceptor core-level shifts in monolayer blends contacting noble metal surfaces

A. El-Sayed[1,2], P. Borghetti[2], E. Goiri[3], C. Rogero[2], L. Floreano[4], Y. Wakayama[5], J. L. Cabellos[3], D. Mowbray[3], A. Rubio[2], D. G. De Oteyza[2,5], and J. Enrique Ortega[1,2,3]

[1] *Departamento de Fisica Aplicada I, UPV/EHU, San Sebastián, Spain.*
[2] *Centro de Física de Materiales (CFM), (CSIC-UPV/EHU), San Sebastián, Spain.*
[3] *Donostia International Physics Center (DIPC), San Sebastián, Spain.*
[4] *CNR-IOM, Laboratorio Nazionale TASC, Trieste, Italy*
[5] *National Institute for Materials Science (NIMS), 1-1 Namiki, Tsukuba, Japan.*

The active interface in charge injection devices can be generally defined by a monolayer-thick blend of donor and/or acceptor molecules in contact with a metal surface. At such interface, energy barriers for electron and hole injection are determined by the offset from HOMO and LUMO molecular levels with respect to the Fermi level of the metal electrode. However, the HOMO and LUMO alignment is not easy to elucidate in complex multi-component, molecule/metal systems from valence band photoemission measurements. We have explored the use of core-level photoemission as a way to straightforwardly and transparently assess molecular level alignment in donor-acceptor/metal interfaces [1]. We have performed systematic experiments combining acceptor-like fluorinated phthalocyanine ($F_{16}$CuPc) and perfluoropentacene (PFP) with pentacene (PEN) and copper phthalocyanine (CuPc), respectively, on Au(111), Ag(111) and Cu(111) surfaces. We observe a qualitatively similar binding energy shift in core-levels as a function of molecular donor/acceptor ratio in all systems, i.e., irrespectively of the molecule or the metal. I will show that a left-to-right, donor-to-acceptor core-level shift can be defined, which roughly mimics a stoichiometry-dependent level alignment at the molecule/metal interface. Finally, I will discuss the limits and exceptions to such general behavior.

This work was supported by the Spanish MICINN (MAT2010-21156-C03-01 and -C03-03), the Basque Government (IT-621-13 and -578-13), European Research Council Advanced Grant DYNamo (ERC-2010-AdG Proposal No. 267374), and Spanish Grants FIS2010-21282-C02-01 and PIB2010US-00652. J.L.C. acknowledges financial support from the Mexican CONACyT program, D.J.M. from the Spanish “Juan de la Cierva” program (JCI-2010-08156), and D.G.O. from the European Union under FP7-PEOPLE-2010-IOF-271909.

[1] A. El-Sayed, E. Goiri, P. Borghetti, C. Rogero, L. Floreano, D. Mowbray, J.L. Cabellos-Quiroz, Y. Wakayama, A. Rubio, J.E. Ortega, and D.G. de Oteyza, ACS Nano **7**, 6914−6920 (2013).

# Perpendicular magnetization of $[CoNi_x]_y$ multi-layers with high brightness and high spin-polarized LEEM and simulation based on LLG equation

Takanori Koshikawa[1], Masahiko Suzuki[1], Kazue Kudo[2], Kazuki Kojima[3], Tsuneo Yasue[1], Noriko Akutsu[1], Agerico Dino[3], Hideaki Kasai[3] and Ernst Bauer[4]

1) Osaka Electro-Communication University, Osaka, Japan,
2) Ochanomizu University, Tokyo, Japan,
3) Osaka University, Osaka, Japan,
4) Arizona State University, Tempe, USA

Current induced domain wall motion is a key phenomenon to realize novel spintronics devices such as a race-track memory (IBM) and a domain wall motion magneto-resistive random access memory (NEC). It has been indicated that domain walls in nanowires with perpendicular magnetic anisotropy can move with lower current density than those with in-plane magnetic anisotropy. Multilayer $[CoNi_X]$ multi-layer is known to exhibit perpendicular magnetic anisotropy and is expected as a material for the devices with low operation current]. We investigated magnetic property during growth of the $[CoNi_x]y$ multi-layer with our high brightness and highly spin-polarized SPLEEM [1-3]. We will also reproduce the magnetic domain pattern formation of the surface of Co/Ni multilayers by numerical simulations based on the Landau-Lifshitz-Gilbert (LLG) equation, which describes the dynamics of local magnetization. Fig. 1 shows experimental and simulation results of magnetic domain images of multilayers of pairs of $[CoNi_2]$ on W(110) [4]. The numerical simulations well reproduce the magnetic domain patterns observed in the experiments.

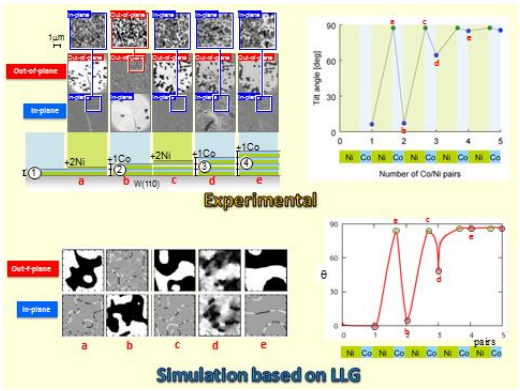


Fig.1 Magnetic domains of Co/Ni multi-layers

[1] N.Yamamoto *et al.*, J. Appl. Phys. **103**, 064905 (2008).
[2] X.G. Jin *et al.*, Appl. Phys. Express **1**, 045602 (2008).
[3] M.Suzuki *et al.*, Appl. Phys. Express **3**, 026601 (2010).
[4] M.Suzuki et.al., J.Phys.Condens.Matter. **25**, 406001 (2013). (Short news on the web of IOP and IOPselect)
[5] K.Kudo et.al., J.Phys.Condens.Matter. **25**, 395005 (2013).

# Ground-breaking Instrumentation Development for Photoelectron Spectroscopy – New Capabilities and Applications

J. Åhlund

*VG Scienta, Vallongatan 1, SE-752 28 Uppsala, Sweden*
*(corresponding author: J. Åhlund, e-mail: john.ahlund@vgscienta.com)*

Photoelectron spectroscopy (PES) is an excellent tool in surface science due to the possibility to probe electronic and geometric structure. During the past decades PES has gone through a remarkable evolution due to the improvement of instrumentation, e.g. development of parallel angular detection, increase in kinetic energy range detection and the possibility to record spectra from samples in a gas atmosphere of several mbar [1]. Here we will discuss the evolution of PES in terms of hemispherical analyzer development with focus on angular resolved PES (ARPES) and ambient pressure PES (APPES).

The instrumental performance has greatly increased over the years in terms of stability and resolution [2]. Today it is possible to record x-ray PES (XPS) spectra in a home laboratory with an instrumental resolution in the 200 meV range [3] and to obtain a binding energy accuracy in the order of ±0.05 eV [4], to measure in the 10 keV range in hard x-ray PES (HAXPES) [5] and at very low kinetic energies using laser excited PES. The best achieved resolution today is measured using laser PES and the instrumental resolution is here reported to be in micro eV's [6].

Angle resolved PES (ARPES) made a quantum leap in the 1990's when VG Scienta revolutionized ARPES with the introduction of parallel angle-resolving analysers, thereby allowing for simultaneous measurements of electrons with different emission angles (along the slit axis) without having to tilt the sample [7]. Although the lens of a hemispherical analyser is circularly symmetric, different emission angles can only be simultaneously recorded along one axis. Currently, a new type of hemispherical deflector type analyzer is being developed. This patent-pending novel analyser, Scienta DA30, represents yet another breakthrough in ARPES instrumentation, since it enables ARPES measurements in a full cone without changing sample position. Here we will demonstrate the capabilities of this analyser and show some initial results.

The bulk of the PES experiments are done under normal surface science conditions (Ultra High Vacuum). However, for some applications, e.g. catalysis, the UHV requirement limits the use of PES due to the pressure gap problem. This motivates the study of systems at higher pressures (HP). For this purpose recent analyzer development has also been focused on APPES [8] with the goal of constructing a high transmission lens able to reach 25 mbar

pressure and beyond around the sample. The Scienta HiPP-2 analyzer is capable of measuring within these pressures. Here we will demonstrate the capabilities of this analyser and show some initial results.

The HiPP-2 analyzer development is supported by VINNOVA.

[1] C. S. Fadley, NIMA 601, 8 (2009)

[2] F. Reinert, G. Nicolay, S.Schmidt, D. Ehm and S. Hüfner, PRB 63, 115415 (2001)

[3] F. Mangolini, J. Åhlund, G. E. Wabiszewski, V. P. Adiga, P. Egberts, F. Streller, K. Backlund, P. G. Karlsson, B. Wannberg and R. W. Carpick, RSI, 83, 093112 (2012)

[4] F. Mangolini, F. Rose, J. Hilbert and R. W. Carpick, APL 103, 161605 (2013)

[5] K. Kobayashi, NIMA, 601, 32 (2009)

[6] K. Okazakii, Y. Ota, Y. Kotani, W. Malaeb, Y. Ishida, T. Shimojima, T. Kiss, S. Watanabe, C.-T. Chen, K. Kihou, C. H. Lee, A. Iyo, H. Eisaki, T. Saito, H. Fukazawa, Y. Kohori, K. Hashimoto, T. Shibauchi, Y. Matsuda, H. Ikeda, H. Miyahara, R. Arita, A. Chaninani and S. Shin, Science 337, 1314 (2012)

[7] N. Mårtensson, P. Baltzer, P. A. Brühwiler, J. O. Forsell, A. Nilsson, A. Stenborg and B. Wannberg, Journal of Electron Spectroscopy and Related Phenomena 70 (2), 117-128 (1994)

[8] D. E. Starr, Z. Liu, M. Hävecker, A. Knop-Gericke and H. Bluhm, Chem Soc Rev, 42, 5833 (2013)

# Joule-Thomson Scanning Probe Microscope

T. U. Kampen

*SPECS Surface Nano Analysis GmbH, Voltastrasse 5, 13355 Berlin, Germany*
*(e-mail: thorsten.kampen@specs.com)*

The JT-SPM marks SPECS' latest significant achievement in state-of-the-art low temperature STM and AFM technology for advanced research in microscopy, spectroscopy, and atomic manipulation.

The cryostat concept is based on a Joule-Thomson stage attached to a liquid He bath cryostat with vapour-cooled shields and a surrounding $LN_2$ vessel, all in a UHV environment. The Joule-Thomson stage cools the STM down to approximately 1 K using $^4$He. The handling of the gas flow through the Joule-Thomson stage is very simple. Helium gas from a cylinder is pre-cooled to 4 K and expanded in a long capillary to a pressure of a few millibars. Liquefied helium is collected in the Joule-Thomson vessel.

The Joule-Thomson stage can also be operated with $^3$He in a closed cycle. This option can be installed without modifying the UHV system. With $^3$He the temperature can be reduced to 650 mK. The STM has an extreme mechanical stability at all temperatures and allows positioning of the tip above an atom for extended periods.

A superconducting magnet can be installed upon request or added later to apply magnetic fields up to 3 Tesla normal to the sample. The split coil magnet is mounted in UHV on the 4 K radiation shield. A precision power supply ensures automated and safe operation. Magnet operation does not increase helium consumption since the magnet is powered through high-TC superconducting supply leads.

The JT-STM can be upgraded with the proven KolibriSensor™ technology for non-contact AFM at sub-angstrom amplitudes. The KolibriSensor™ features a separately contacted metallic tip for STM mode scanning or electrical tip access in nc-AFM mode. The Nanonis control system exploits both techniques, i.e. STM and AFM, to the fullest, and is therefore especially suited to all kinds of scanning probe experiments.

# FERMI Cold Tip SPM: A new generation of variable temperature SPM for spectroscopy

C. Troeppner, M. Atabak, J. Koeble, B. Guenther, B. Uder, M. Maier

*Oxford Instruments Omicron NanoScience, 65232 Taunusstein, Germany*
*(corresponding author: M. Maier, e-mail: Markus.Maier@oxinst.com)*

We present design and first results of a new generation of variable temperature scanning probe microscope (SPM) that has been developed to enhance the performance in tunnelling spectroscopy at lower and variable temperatures. The new microscope for ultra high vacuum is based on a new stage design using a flow cryostat compatible for cooling with liquid nitrogen or helium. In contrast to earlier established designs of variable temperature SPM's where only the sample is cooled, this new SPM also cools the scanner with tip. This is realized by a new developed compact microscope stage with thermal shields and a cooling management system. With the new design we achieve lower temperatures and improve drift by more than an order of magnitude compared to previous variable temperature stages. Sample temperatures down to 10 K (with helium) and 95 K (with nitrogen) have been achieved. The temperature stability is better than 5mK / min and the measured thermal drift is below 1 pm/s. During cooling the mechanical z stability is better than 3 pm. These conditions enhance spectroscopy measurement capability. "Loop off" times of up to 10 s per single spectroscopy curve have been measured. The new flow cryostat also allows for changing between nitrogen cooling and helium cooling in less than 90 min during a running experiment. Pre-cooling with nitrogen during the starting phase of an experiment also reduces running costs for liquid helium. This new SPM is configured for imaging in STM as well as AFM with a non-optical sensor in a temperature range between 10- 400 K. Switching between the 2 modes can be accomplished without breaking vacuum.

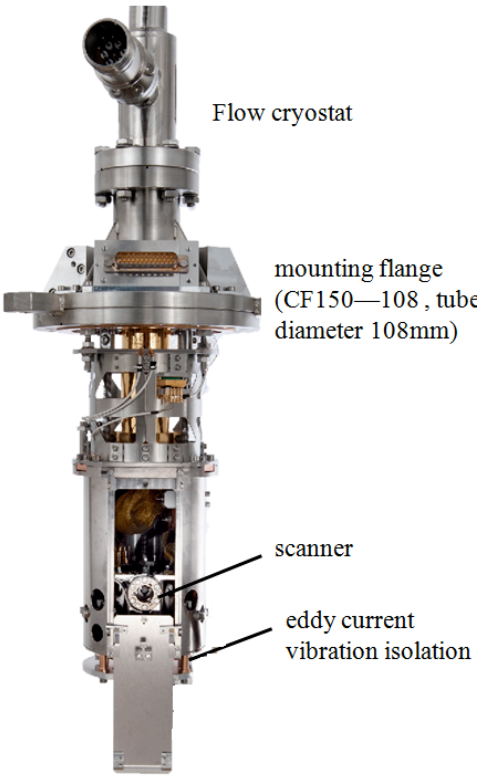

A new concept for cooling has been realized. The concept includes cooling the scanner and introduces an optimized heat management system. Similar to previous variable temperature setups a flow cryostat is used. This cryostat can be operated with liquid helium or liquid nitrogen. The new microscope stage consists of a scanner (that carries the tip) mounted to the inner shielded stage. Sample and scanner are both separately connected via flexible cooling connections to the cold finger of the flow cryostat.

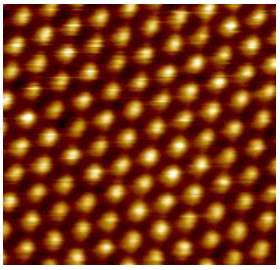

STM on Au(111) at 95K using nitrogen, z stability < 3pm

The temperature of the cold finger is stabilized using a heater element and a temperature sensor close to the cold finger. Sample and scanner are connected to individual heater elements and temperature sensors for individual temperature stabilization. The outer thermal shield is pre-cooled by a connection to the exhaust gas line of the flow cryostat. All heater elements with temperature sensors are controlled individually with a temperature controller. This concept allows independent regulation of sample and scanner temperature at different low temperature settings to achieve best thermal drift values.

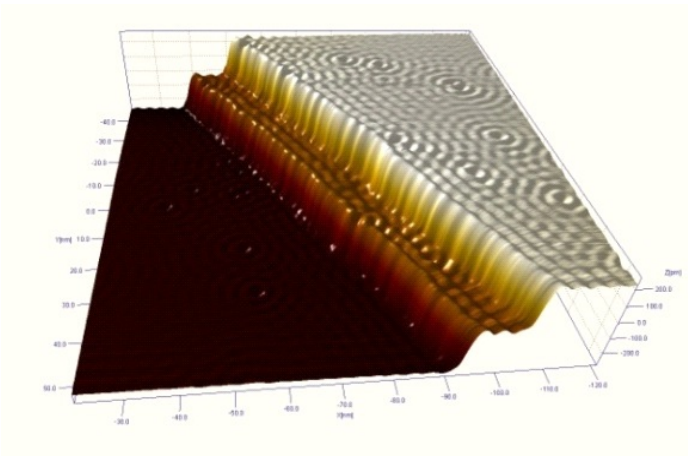

STM on Ag(111) at 10K showing electron standing waves

# Surface-driven topological oxide quasicrystals

S. Förster[1], K. Meinel[1], R. Hammer[1], M. Trautmann[1], and W. Widdra [1,2]

[1] *Institute of Physics, Martin-Luther-Universität Halle-Wittenberg, Halle, Germany*
*(corresponding author: S. Förster, e-mail: stefan.foerster@physik.uni-halle.de)*

[2] *Max-Planck-Institut für Mikrostrukturphysik, Halle, Germany*

Perovskite oxides represent a versatile class of materials with a simple cubic or pseudo-cubic crystal structure. The family of perovskite oxides contains insulators, metals, semiconductors, and superconductors with nearly identical lattice parameters. Some are magnetically ordered in various structures and many are catalytically active. By substitution of ions, by application of strain, or incorporation of defects in individual perovskites their properties can be altered in a controlled fashion. In addition, due to the structural equivalence perovskites with different properties can be combined in multilayer systems to produce functional materials with unique properties [1].

We report here on the formation of a quasicrystal (QC) thin film on a Pt(111) surface. This QC film is derived from the classical perovskite oxide $BaTiO_3$. It is the most studied ferroelectric perovskite oxide which has an easily accessible ferroelectric to paraelectric phase transition at 400 K. Due to matching lattice conditions $BaTiO_3$ can be grown epitaxially on selected metal substrates. On Pt(001) and on Pt(111) periodic thin films of either $BaTiO_3$(100) or $BaTiO_3$(111) have been grown depending on substrate orientation and preparation conditions [2-4]. As we demonstrate here, astonishingly also a two-dimensional dodecagonal quasicrystalline structure can be formed by annealing an initially 1.4 nm thick $BaTiO_3$ film on Pt(111) [5]. It develops at a temperature of 1250 K from a wetting layer spreading between a few thicker $BaTiO_3$(111) islands.

Quasiperiodic structures are characterized by a lack of translational order within the material. Instead a bond orientational order is found which produces a distinct diffraction pattern of non-crystallographic symmetry. In contrast to the two-, three-, four-, and six-fold symmetries of periodic structures five-, eight-, ten, and twelve-fold (dodecagonal) symmetries are observed in quasicrystals. Low-energy electron diffraction (LEED) measurements of the quasicrystalline wetting layer derived from $BaTiO_3$ on Pt(111) as presented here shows a bright and sharp pattern with dodecagonal symmetry.

High-resolution scanning tunneling microscopy (STM) images taken at room temperature as well as at low temperatures (80 K) resolve the individual surface atoms which form quadratic, triangular, and rhombic building blocks with an edge length of 6.9 Å. All three types of

building blocks are grouped in the dodecagonal Gähler tiling [6]. One of these dodecagons is shown in Fig. 1.

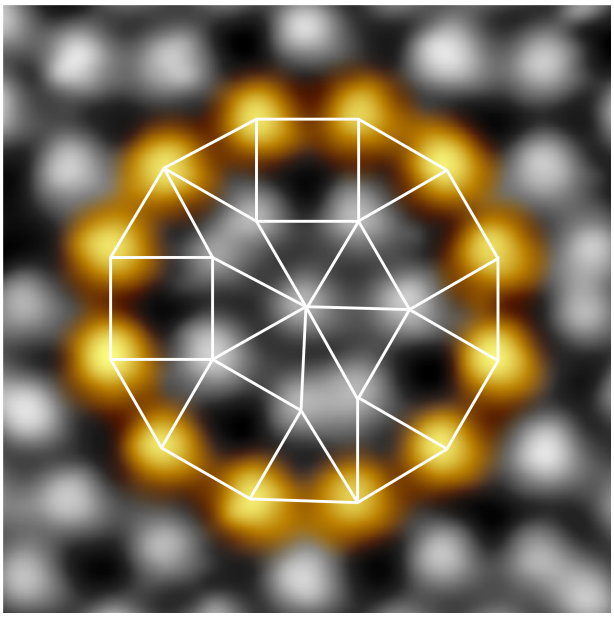

*Figure 1: Atomically resolved STM image of the typical dodecagonal motif of the quasicrystalline thin film on Pt(111). 4x4 nm², I= 30 pA, U = 0.1 V.*

In addition to this dodecagonal atomic arrangement, the same structural building blocks are found on $(2 + \sqrt{3})$ and $(2 + \sqrt{3})^2$ larger scales indicating the characteristic self-similarity of an long-range ordered quasicrystal.

The observed interface-driven formation of a two-dimensional quasicrystal from a perovskite oxide potentially extends the quasicrystal concept to a broader range of materials. It demonstrates that frustration at the interface between two periodic materials can drive a thin film into a topological, aperiodic quasicrystalline phase, as proposed previously [7]. Such structures might also be applicable as ultrathin buffer layers for the accommodation of large lattice mismatches in conventional epitaxy [8].

Support by the DFG via SFB 762 „Functionality of Oxide Interfaces“ is gratefully acknowledged.

[1] I. Vrejoiu, M. Alexe, D. Hesse, and U. Gösele, Adv. Funct. Mater. **18** (2008), 3892.
[2] S. Förster and W. Widdra, Surface Science **604** (2010), 2163.
[3] S. Förster, M. Huth, K.-M. Schindler, and W. Widdra, J. Chem. Phys. **135** (2011), 104701.
[4] S. Förster, K. Meinel, K.-M. Schindler, and W. Widdra, Surf. & Interf. Anal. **44** (2012), 628.
[5] S. Förster, K. Meinel, R. Hammer, M. Trautmann, and W. Widdra, Nature **502** (2013), 215.
[6] F. Gähler in Quasicrystalline Materials, Ch. Janot and J.M. Dubois (eds.), World Scientific 1988
[7] A. R. Smith, K.-J. Chao, Q. Niu, and C.-K. Shih, Science **273**,(1996), 226.
[8] K. J. Franke, P. Gille, K.-H. Rieder, and W. Theis, Phys. Rev. Lett. **99** (2007), 036103

# How reactive is a perovskite surface? The surface chemistry of $Sr_3Ru_2O_7$

F. Mittendorfer[1,2], B. Stöger[1], M. Hieckel[1,2], J. Redinger[1,2], Z. Wang[1], M. Schmid[1], and U. Diebold[1]

[1] *Institute of Applied Physics, Vienna University of Technology, A-1040 Vienna, Austria (corresponding author: F. Mittendorfer, e-mail: Florian.Mittendorfer@tuwien.ac.at)*

[2] *Center for Computational Materials Science, Vienna University of Technology, A-1050 Vienna, Austria*

In the recent years, complex transition metal oxide surfaces have received enormous attention, both due to the fundamental properties as well as their potential for applications in the field of energy storage and conversion. While there is a wealth of studies investigating the physical properties of ternary perovskite oxides, such as multiferroicity or superconductivity, only little is known about the chemistry of these materials. In this talk, I will present a combined theoretical and experimental study on the surface chemistry of $Sr_3Ru_2O_7$. On the basis of density functional theory (DFT) calculations [1,2] and scanning tunneling microscopy (STM) measurements, I will discuss how the electronic and catalytic properties of the oxide are modified under realistic conditions.

$Sr_3Ru_2O_7$ is a member of the ruthenate Ruddlesden-Popper series, consisting of double layers of the $SrRuO_3$ perovskite. In agreement with the experimental observations, the crystal has only a low cleavage energy of 0.6 eV/unt cell due to its layered structure, allowing for the easy creation of well-defined surfaces. In contrast to the bulk $SrRuO_3$ structures, where the RuO octahedra are both rotated and tilted, only a rotation of the octahedral is predicted for the $Sr_3Ru_2O_7$ surface.

Surprisingly, the STM measurements show a high chemical activity of the $Sr_3Ru_2O_7$ surface [3]. On the basis of the DFT calculations, we conclude that these observations are not related to imperfections at the surface, such as vacancies or Ca substitutional atoms, but rather to the facile adsorption of carbon monoxide (CO). By explicitly mapping the reaction pathway we could identify the crucial steps for the incorporation of the CO molecule: While the process is preceded by a precursor where the CO molecule is adsorbed via a surface oxygen atom (Fig. 1a), it can easily be converted to a carboxylate-like COO species at the surface (Fig. 1b). With an adsorption energy of -2.2 eV, the latter structure shows a high chemical stability and leads to characteristic pattern at the surface, which can be readily observed experimentally.

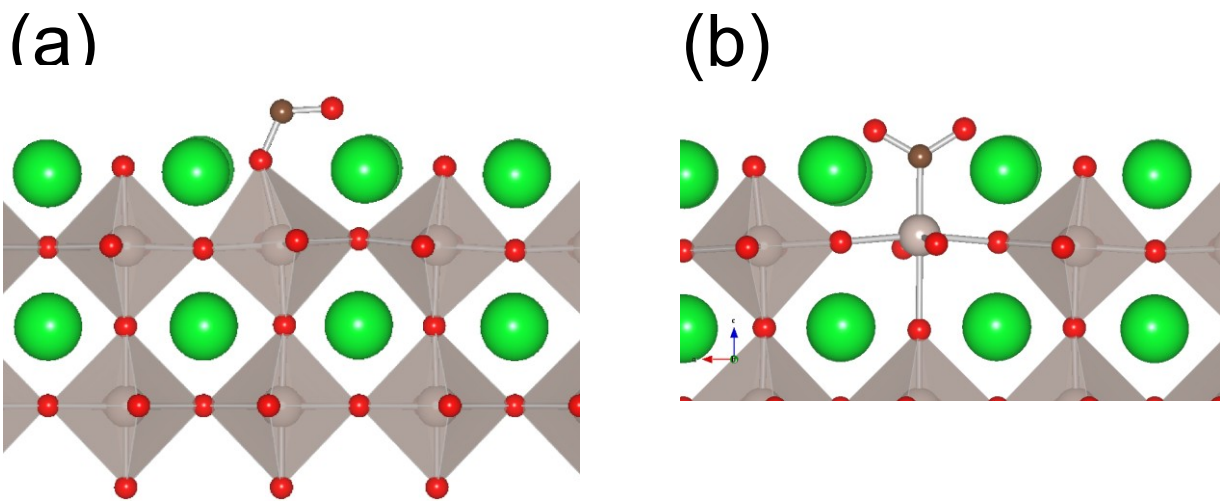


**Fig. 1 Structural models for the adsorption of CO on $Sr_3Ru_2O_7$: (a) precursor structure (b) chemisorbed (carboxylate-like) configuration.**

Support by the Austrian Science Fund (FWF) under the SFB *Functional Oxide Surfaces and Interfaces* (project F45) and computing time at the Vienna Scientific Cluster (VSC-2) is gratefully acknowledged.

[1] G. Kresse and J. Furthmüller, Comput. Mater. Sci. 6, 15 (1996), G. Kresse and J. Hafner, Phys. Rev. B 47, 558 (1993).

[2] P. E. Blöchl, Phys. Rev. B 50, 17953 (1994),G. Kresse and D. Joubert, Phys. Rev. B 59, 1758 (1999).

[3] B. Stöger, M. Hieckel, F. Mittendorfer, et al. „High chemical activity of a perovskite surface: Reaction of Co on Sr3Ru2O7“, in submission (2013)

# Structural analysis of ultra-thin zinc oxide film on Rh(100)

J. Yuhara, D. Kato, T. Matsui, S. Mizuno[1]

*School of Engineering, Nagoya University, Furo-cho, Chikusa-ku, Nagoya, Japan*
*(corresponding author: J. Yuhara, e-mail: j-yuhara@nagoya-u.jp)*

[1]*Department of Molecular and Material Science, Kyushu University, Kasuga-koen, Fukuoka, Japan*

The thin oxide film on metal supports is of fundamental importance, since the structure of the thin films is generally characterized by the atomic arrangement and chemical reactivity of the substrate. Consequently, atomic structures and depolarization mechanisms are expected to be distinctly different from those of the bulk. Recently, the growth of the zinc oxide film on Ag(111) [1,2] and Pd(111) [3,4] has been explored quite extensively. ZnO(0001) films on Ag(111) have been identified to form a planar sheet like in the hexagonal boron-nitride (h-BN) prototype structure [1]. Periodic *ab initio* density functional calculations reveal that local density of states of the h-BN ZnO/Ag(111) is similar to that of bulk ZnO [2]. The h-BN ZnO structure is also reported on Pd(111), yielding free-standing like structure rather than reconstructed structure influenced by the oxide film and metal support interface [3,4]. The functional calculations demonstrate that the h-BN structure is thermodynamically more stable than the wurtzite structure for self-supporting thin films [5,6].

To this end, we have carried out a low-energy electron diffraction (LEED) and scanning tunneling microscopy (STM) study of single atomic layer ZnO films deposited on Rh(100), which belongs to not threefold but fourfold symmetry. The ZnO films exhibited c(16×2) superstructure at the coverage of 0.8 ML. Although the STM image showed single and double dotted spots arranged periodically with keeping c(16×2) fourfold symmetry, the first order spots originating from the zinc oxide film exhibited a hexagonal LEED pattern, indicating a ZnO(0001) threefold film on Rh(100) [7].

In this paper, we present a combined experimental and theoretical study on the detailed structure of the zinc oxide thin film on Rh(100) by means of Dynamic LEED *I-V* curve analysis and *ab initio* DFT total energy calculations. Two optimized models 1 and 2 are determined from experiments and calculations, as shown in Fig.1. The overall Pendry R-factor of 0.14 has been achieved for both models (Fig.2). Th simulated STM images clearly indicate that the model 1 is dominant and the model 2 is locally formed (Fig.3). In summary, it is concluded that the zinc oxide thin film forms modified *h*-BN structure, reflecting an atomic periodicity of Rh(100).

[1] C. Tusche, H. L. Meyerheim, and J. Kirschner, Phys. Rev. Lett. **99**, 026102 (2007).
[2] G. Barcaro; I. O. Thomas, and A. Fortunelli, J. Chem. Phys. **132**, 124703 (2010).
[3] H. Gabasch, A. Knop-Gericke, R. Schlögl, S. Penner, B. Jenewein K. Hayek, and B. Klötzer, J. Phys. Chem. B **110**, 11391 (2006).

[4] G. Weirum, G. Barcaro, A. Fortunelli, F. Weber, R. Schennach, S. Surnev, and F.P. Netzer, J. Phys. Chem. C **132**, 15432 (2010).
[5] C.L. Freeman, F. Claeyssens, N.L. Allan, and J.H. Harding, Phys. Rev. Lett. **96**, 066102 (2006).
[6] F. Claeyssens, C.L. Freeman, N.L. Allan, Y. Sun, M.N.R. Ashfold, and J.H. Harding, J. Mater. Chem. **15**, 139 (2005).
[7] D. Kato, T. Matsui, and J. Yuhara, Surf. Sci. **604**, 1283 (2010).

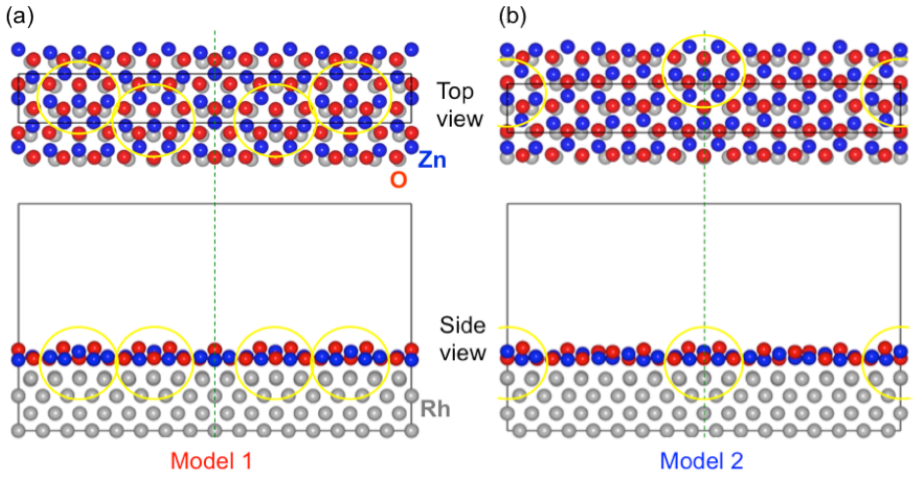


Fig.1 Two structural models of zinc oxide film on Rh(100) as determined by *ab initio* calculations and quantitative LEED in a top and side view. c(16×2) unit cells are indicated.

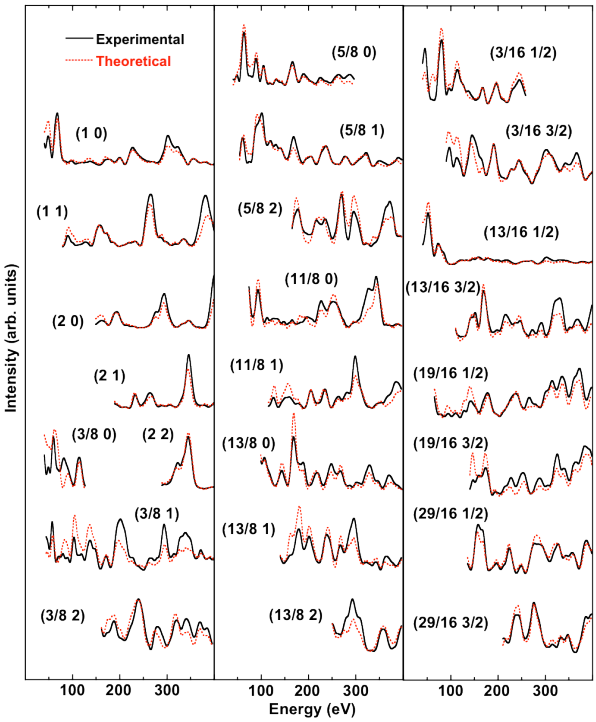


Fig.2 Comparison between experimental (full line/black) and calculated (broken line/red) LEED *I-V* spectra of the best fit model of the zinc oxide film on Rh(100). ($R_{Pe}$=0.14)

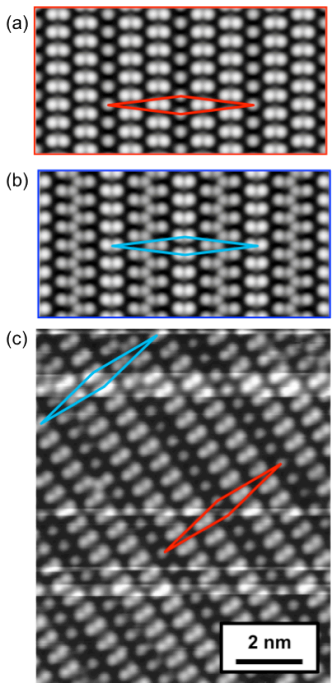


Fig.3 (a)-(b) The simulated STM images of the c(16×2) structural models 1 and 2. The c(16×2) cells are indicated. (c) The experimental STM image.

# A theoretical description of water splitting on metal decorated oxide surfaces

Harald Oberhofer,* Daniel Berger, Markus Sinstein, Ran Jia, and Karsten Reuter
*Theoretische Chemie, Technische Universität München*

Efficient, sustainable production of molecular hydrogen—a promising alternative to batteries in terms of energy storage—is still an unsolved problem. Implementation of direct water splitting using only sunlight and suitable metal-oxide photo-catalysts so far has been hampered by poor photon absorption properties of the materials and low reaction efficiencies. In order to understand the microscopic processes involved in photo-catalytic hydrogen production we implemented an implicit solvent model and a solid state QM/MM embedding scheme based on ChemShell into the all electron DFT and beyond code FHI-aims.[1] This allows us to study defects and charged systems—as occurring in electron-hole driven water splitting—without any spurious interaction between periodic images, while at the same time yielding the correct electrostatic potential and solvent screening in the QM region.

In order to overcome the limitations of current water splitting setups we study the use of small metal clusters nano-patterned on an oxide surface which is often used in experimental setups. Yet, the microscopic effect of such so-called co-catalysts is still not fully understood in literature.

We develop an enhanced version of the computational hydrogen electrode approach pioneered by Nørskov and Rossmeisl,[2] of water oxidation reactions on metal clusters in the non-scalable size regime (less than 55 atoms) and compare with the bare extended oxide surface.[3] On top of these results we discuss the influence of solvent on the reaction as well as the stabilisation of electron holes necessary for the reaction.

Support by the Alexander von Humboldt foundation and the TUM international graduate school of science and engineering is gratefully acknowledged.

[1] V. Blum *et al.*, Comp. Phys. Commun. **180**, 2175 (2009)
[2] A. Valdes *et al.*, J. Phys. Chem. C **112**, 9872 (2008)
[3] H. Oberhofer, K. Reuter, J. Chem. Phys. **139**, 44710 (2013)

* harald.oberhofer@tum.de

# *Wednesday*

# Short-range and long-range interaction during thermal and laser-driven diffusion on metal surfaces

Ch. Zaum[1], K. Morgenstern

*Lehrstuhl für physikalische Chemie I, Ruhr-Universität Bochum, Universitätsstr. 150, D-44801 Bochum, Germany*
*(corresponding author: K. Morgenstern, e-mail: karina.morgenstern@rub.de)*

[1] *Abteilung für atomare und molekulare Strukturen, Institut für Festkörperphysik, Leibniz Universität Hannover, Appelstr. 2, D-30171 Hannover, Germany*

As part of reactions, the motion of adparticles on surfaces is a particular active area of research, because a variety of basic physical and chemical processes start with the transport of objects on a surface [1]. For instance in heterogeneous catalysis, the reactants have to diffuse to the active sites, at which the actual reaction proceeds. The mobility of the objects frequently limits the overall reaction rate [2]. Adsorbate diffusion has therefore been studied intensively, however, mostly at dilute coverage [1]. For a realistic, i.e. high, adsorbate coverage, adsorbate interactions have to be considered. Apart from short-range interaction, which might influence the mobility of molecules that approach to fractions of a nanometer, long-range interaction as mediated by surface states have to be considered.

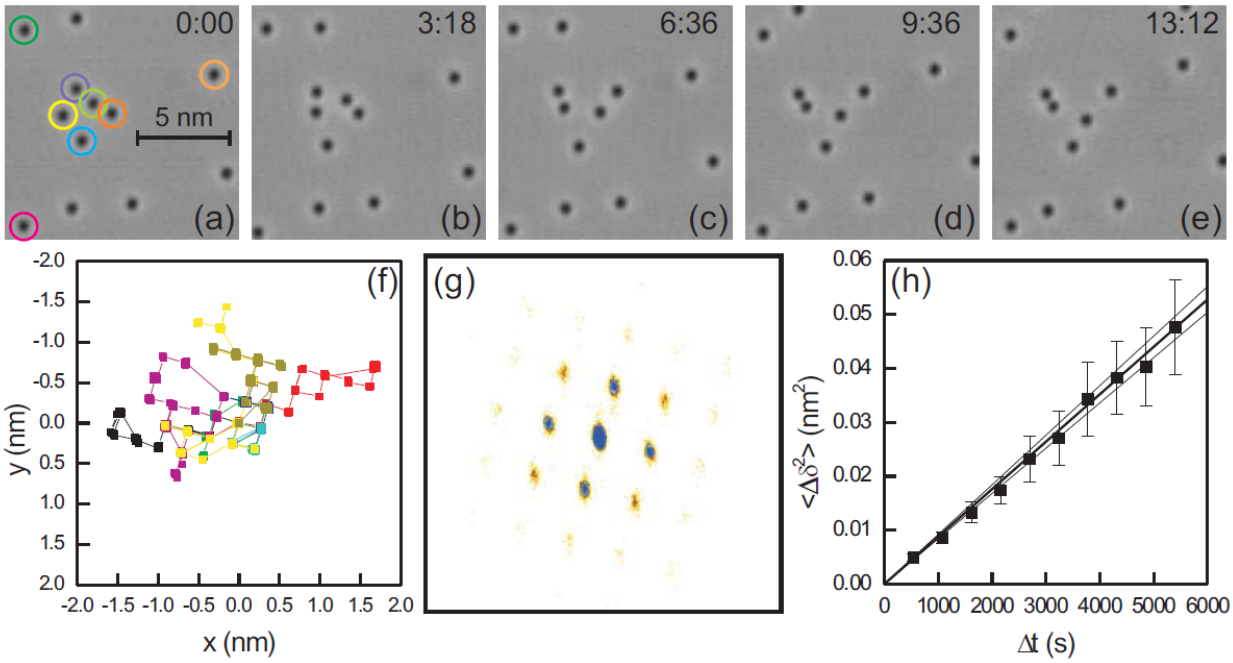


We discuss these two types of interactions for the diffusion of CO molecules on Ag(100) and on Cu(111). The Figure demonstrates the principle of the measurement. The diffusion is followed in time-lapse series over extended time spans recorded by s canning tunneling

microscopy in the temperature range of 15 K to 23 K and of 30 K and 38 K, respectively. A few snapshot of an image series recorded for CO on Ag(100) at 21.8 K are displayed in (a) to (d). The motion of individual molecules is followed throughout the series as shown in (f). From all series recorded, the diffusion lattice is determined as shown in (g), here quadratic between on-top sites. The diffusivity at a certain temperature is then determined through the Einstein relation (slope in (h)). By recording and analyzing 100.000s of molecule positions, we are able to extract energies and prefactors of diffusion from the Arrhenius dependence of the diffusivity with temperature for both systems with very small error bars.

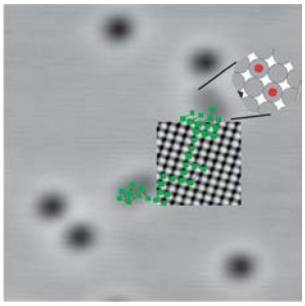

For diffusion on Ag(100) the short range attraction of the CO molecules leads to a dimerization (see left) that is accompanied by a drastically increased diffusivity due to a severely reduced activation energy in spite of a reduced prefactor. The latter decrease by t wo orders of magnitude is explained quantitatively based on transition state theory as an additional degree of rotational freedom in the ground state.

For diffusion on Cu(111), we present experimental evidence for surface state mediated interaction between two and between three adsorbates. In the course of our analysis, we resolve a former discrepancy between predicted and measured interaction energies [3]. Furthermore, an influence of the coverage on the surface state mediated pair interaction is revealed.

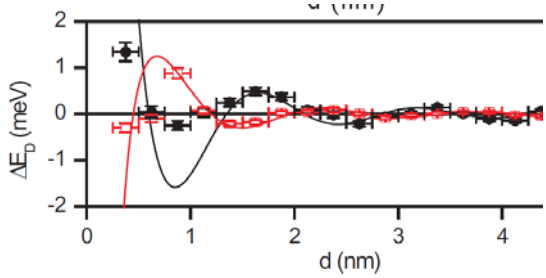


For the latter case, we compare the thermal-diffusion induced adsorbate distribution to one induced by metal-absorbed femto-second laser pulses. Both, thermal and laser-driven diffusion show an oscillatory energy dependence on distance. Surprisingly, the phase is inverted, i.e. at distances at which thermal diffusion is most difficult, it is easiest for laser-driven diffusion and vice versa. Possible reasons for this phase shift are discussed.

Support by the German Science foundation and the German-Israeli Foundation is gratefully acknowledged.

[1] G. Antczak, G. Ehrlich, Surface Diffusion (Cambridge University Press, New York, 2010).

[2] P. Jensen, Rev. Mod. Phys. 1999, 71, 1695.

[3] P. Hyldgaard, M. Persson, J. Phys. Condens. Matter 12, L13 (2000); P. Hyldgaard, T.L. Einstein, Europhys. Lett. 59, 265 (2002); E. Wahlström, I. Ekvall, H. Olin, L. Walldén, Appl. Phys. A 66, S1107 (1998); J. Repp, F. Moresco, G. Meyer, K.-H. Rieder, P. Hyldgaard, M. Persson, Phys. Rev. Lett. 85, 2981 (2000); N. Knorr, H. Brune, M. Epple, A. Hirstein, M.A. Schneider, K. Kern, Phys. Rev. B 65, 115420; (2002); K. Morgenstern, K.-F. Braun, K.-H. Rieder, Phys. Rev. Lett. 93, 056102 (2004); K. Morgenstern, K.-H. Rieder, New J. Phys. 7, 139 (2005); M. Mehlhorn, V. Simic-Milosevic, S. Jaksch, P. Scheier, K. Morgenstern, Surf. Sci. 604, 1698 (2010).

# Nanoscale lateral segregation on *h*-BN/PtRh(111)

Roland Stania,[1] Irakli Kalichava,[2] Bernd Schönfeld,[3] Jürg Osterwalder,[1] Wolfgang Heckel,[4] Tobias Kerscher,[4] Stefan Müller,[4] Philip R. Willmott,[2] and Thomas Greber[1]

[1]Physik-Insitut, Universität Zürich, CH-8057 Zürich, Switzerland
[2]Paul Scherrer Institut, CH-5232 Villigen PSI, Switzerland
[3]Federal Institute of Technology Zürich, CH-8093 Zürich, Switzerland
[4]Hamburg University of Technology, Institute of Advanced Ceramics, D-21073 Hamburg, Germany
*(corresponding author: T. Greber, e-mail: greber@physik.uzh.ch)*

Surface segregation, i.e. the deviation from the bulk composition of a multicomponent system at the surface, is a well-known phenomenon. For intermetallic compounds it has implications in e.g. hydrogen storage [1] or nano-catalysis [2].
The driving forces for segregation are strain release and different surface energies [3]. Today's computational power allows to tackle the particularly large problem of surface segregation, by a concerted effort of density functional theory, cluster expansion and Monte-Carlo simulations. The comparison to existing experiments [4] shows excellent agreement [5]. For example, for carbon on $Pt_{25}Rh_{75}$ that is of interest for the growth of epitaxial graphene carbon induced segregation [4] was recently confirmed theoretically [6].
In systems with more than one adsorbate, chemical waves may be generated, which lead to lateral segregation on the micrometer scale [7]. Here we report on lateral segregation in the top layer of a PtRh (111) surface on the nanometer scale. This is obtained during the growth of a single layer of hexagonal boron nitride, which also imposes the formation of a 2.8 nm Pt super-honeycomb.
On Rh(111) epitaxially grown hexagonal boron nitride (*h*-BN) forms a corrugated monolayer with a 13 on 12 super-honeycomb-structure known as the h-BN nanomesh [8]. In contrast *h*-BN on Pt(111) forms a flat layer with an approximate 10 on 9 superstructure being weaker bond than the nanomesh [9]. The investigation of *h*-BN/PtRh(111) reveals a corrugated nanomesh-like 11 on 10 superstructure. Lateral segregation occurs in the topmost layer of the substrate during growth of *h*-BN, where Rh atoms form islands under the pores of the nanomesh, which are surrounded by Pt atoms under the wires.

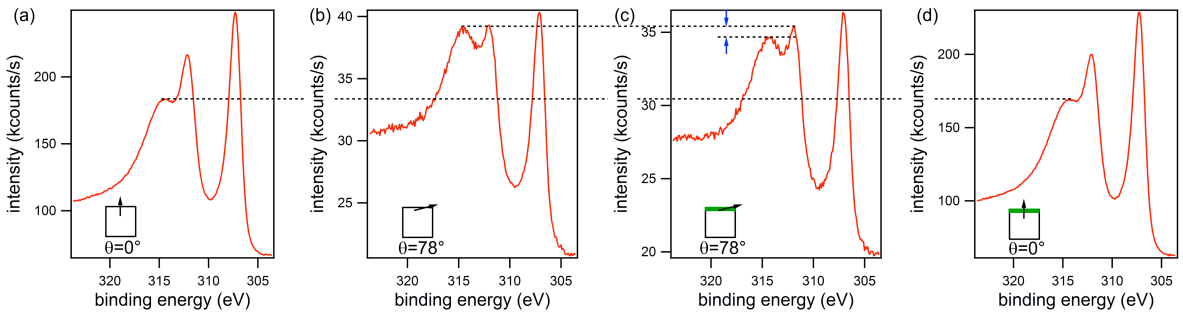


*Fig. 1: Angle resolved Mg Kα x-ray photoelectron spectroscopy (XPS) for clean and h-BN covered PtRh(111). The spectral region of the Rh 3d ($E_B$=307 and 312 eV) peaks and the Pt 3d$_{5/2}$ ($E_B$=315 eV) peak is shown for the two systems and two emission angles θ. a) Clean PtRh, normal emission θ =0°. b) Clean PtRh, grazing emission θ =78°. c) h-BN/PtRh, normal emission θ =0°. d) h-BN/PtRh, grazing emission θ =78°.*

The unit cell size is obtained by surface x-ray diffraction, while angular resolved photoemission indicates a “nanomesh” structure and the lateral segregation.

Figure 1 shows photoemission data of Pt and Rh core levels. Comparison of Figure a) and b) confirms a significant relative increase of Pt emission in grazing emission, which is in line with the known vertical surface segregation of platinum. Over all, Pt segregation into the top layer persists after the growth of a single layer of *h*-BN on top of the crystal (compare d) with c)). Though, at grazing emission the Pt:Rh ratio, which reflects at these electron kinetic energies and emission angle mainly emission from the top PtRh layer, is larger for the bare surface than for the *h*-BN covered one (compare b) with c)). Since this *h*-BN induced Rh segregation into the top-layer must be related to the local interaction strength of the *h*-BN with the metal, which is strong in the nanomesh pores, and weak in the nanomesh wire regions, we conclude Rh segregation to the pore regions in the first substrate layer.

This picture of lateral segregation at the nanometer scale is perfectly confirmed by density functional theory within a cluster expansion approach.

In conclusion we have shown that lateral segregation on the nanometer scale may be induced by the growth of *h*-BN superstructures. The resulting regular structure is expected to display properties different from random alloy surfaces.

Financial support by the Schweizerischen Nationalfonds (SNF) and the Deutschen Forschungsgemeinschaft (DFG) is gratefully acknowledged.

[1] Siegmann, Schlapbach and Brundle, Phys. Rev. Lett. 40 (1978) 972.

[2] Mayrhofer et al. Angew. Chem. Int. Ed. 48 (2009) 3529.

[3] Abraham, Phys. Rev. Lett. 40 (1980) 972.

[4] Platzgummer et al. Surf. Sci. 419 (1999) 236.

[5] Welker, Wieckhorst, Kerscher, and Müller, J. Phys. Condens. Matter 22 (2010) 384203.

[6] Kerscher, Landgraf, Podloucky, and Müller, Phys. Rev. B 86 (2012) 195420.

[7] Esch et al. Surf. Sci. 443 (1999) 245.

[8] Corso et al. Science, 303 (2004) 217.

[9] Cavar et al. Surface Science, 602 (2008) 1722.

# Surface structure of alanine on Cu(110) studied by grazing scattering of fast atoms

J. Seifert, E. Meyer, M. Busch, and H. Winter

*Institut für Physik, Humboldt-Universität zu Berlin, D-12489, Germany*
*(corresponding author: J. Seifert, e-mail: jan.seifert@physik.hu-berlin.de)*

We have studied the adsorption and the atomic structure of the amino acid alanine on Cu(110) by means of low energy electron diffraction (LEED) and grazing scattering of atoms with energies of some keV.

Alanine is the smallest amino acid which is intrinsically chiral, i.e. it is incongruent to its mirror image and thus exists in two forms with different molecular handedness. Well ordered adsorbate films with monolayer coverage were prepared by exposing a Cu(110) surface to enantiopure alanine (R or S alanine) or to racemic alanine (equal mixture of R and S) and annealing at temperatures up to $T_a$ = 520 K. Recording the specular intensity of scattered He atoms allowed us to control the adsorption process in-situ where a maximum indicates a coverage of one monolayer. For different annealing temperatures various superstructure phases can be observed [1, 2]. The phase IV ($T_a \approx 450$ K) of enantiopure and racemic alanine/ Cu(110) with a (3×2) unit cell was investigated in detail [3, 4], but also the phase III ($T_a \approx 400$ K) with an assembly of molecules in chiral clusters was studied.

In the regime of axial surface channeling, for sufficiently small projectile energies and polar incident angles, diffraction phenomena of scattered atoms and molecules can be observed by means of a position-sensitive channelplate detector (fast atom diffraction - FAD) [5-7]. From the splitting of diffraction spots the unit cell size and symmetry, and from relative intensities, atomic positions in the topmost layer can be deduced [8-10]. For the system of alanine/Cu(110) we have demonstrated the first application of FAD to thin films of organic molecules [3]. The splitting of diffraction spots are consistent with a *c*(3×2) unit cell which is different from the *pg*(3×2) unit cell, assumed so far for this phase. Since with this method the topmost part of the surface is tested, deviations from LEED measurements can occur [10, 11]. However, also the LEED pattern can be explained by a *c*(3×2) unit cell when multiple diffraction is taken into account.

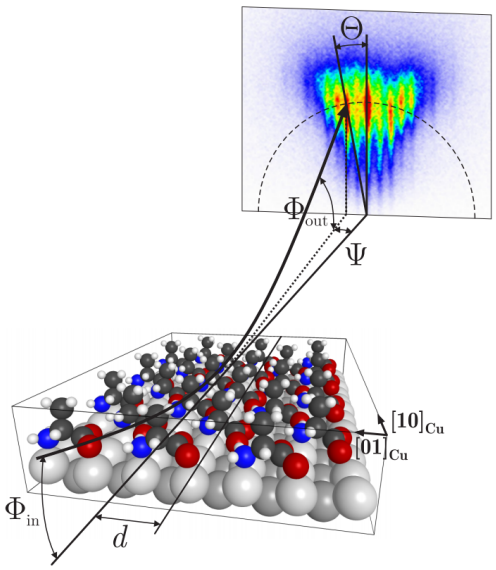


Figure 1. Sketch of scattering geometry for FAD

For the enantiopure phase IV and racemic phase IVa (low temperature annealing), using FAD, we reveal an elongation of the unit cell in $[10]_{Cu} = [\bar{1}10]$ direction by about 5%. We conclude an arrangement of the sticking out methyl groups at the corners of a $c(n\times2)$ unit cell with $n = 3.16 \pm 0.04$. This provides an explanation for the displacement of diffraction spots in LEED patterns observed in former and the present studies. The enhanced unit cell size results in a reduced coverage $\Theta = 1/n$ for these phases. This explains the temperature induced transition of the "undistorted" phase IVb to the "distorted" IVa by gradual desorption and the transition from IVa to IVb for dosing additional amounts of alanine.

The enhanced length of the unit cell in one direction also leads to a slight azimuthal rotation of the diagonal of a $p(3\times2)$ unit cell, which is the direction of the basis vector of a $c(3\times2)$ adsorbate unit cell. The change of the azimuthal direction of an axial channel by about 1.5° results in a significant modification of the scattering geometry which can be observed in the angular distributions of scattered atoms or molecules. When for a stepwise azimuthal rotation of the target the intensity of specularly reflected particles is evaluated, the resulting triangulation curves exhibit dips, whenever the projectile beam is aligned along axial channels. For the transition from phase IVb to IVa of racemic alanine upon annealing, a shift of the channel and therefore the enhanced unit cell size $c(3.16\times2)$ can be clearly observed.

A uniformly spaced arrangement of molecules which is incommensurate to the substrate includes bridge sites of the binding oxygen and nitrogen atoms. This seems to be unlikely, when close to on-top positions are preferred as described in literature. Also a significant reconstruction of the substrate can be ruled out from the results of ion beam triangulation (IBT). Instead, the binding atoms (i.e. the adsorption footprint) have local $p(3\times2)$ symmetry but different deformations of neighboring molecules lead to an arrangement of methyl groups in a stretched unit cell $c(3.16\times2)$.

Supported by the Deutsche Forschungsgemeinschaft under contract Wi 1336.

[1] S. Barlow, S. Louafi, D. Le Roux, J. Williams, C. Muryn, S. Haq, and R. Raval, Surf. Sci. 590, 243 (2005)
[2] S. Haq, A. Massey, N. Moslemzadeh, A. Robin, S. M. Barlow, and R. Raval, Langmuir 23, 10694 (2007)
[3] J. Seifert, M. Busch, E. Meyer, and H. Winter, Phys. Rev. Lett. 111, 137601 (2013)
[4] J. Seifert, M. Busch, E. Meyer, and H. Winter, submitted to Phys. Rev. B
[5] A. Schüller, S. Wethekam, and H. Winter, Phys. Rev. Lett. 98, 016103 (2007)
[6] P. Rousseau, H. Khemliche, A. G. Borisov, and P. Roncin, Phys. Rev. Lett. 98, 016104 (2007)
[7] H. Winter and A. Schüller, Prog. Surf. Sci. 86, 169 (2011)
[8] J. Seifert, A. Schüller, H. Winter, R. Wlodarczyk, J. Sauer, and M. Sierka, Phys. Rev. B 82, 035436 (2010)
[9] A. Schüller, D. Blauth, J. Seifert, M. Busch, H. Winter, K. Gärtner, R. Wlodarczyk, J. Sauer, and M. Sierka, Surf. Sci. 606, 161 (2012)
[10] J. Seifert and H. Winter, Phys. Rev. Lett. 108, 065503 (2012)
[11] J. Seifert and H. Winter, Nucl. Instrum. Methods Phys. Res. B 315, 9 (2013)

# Transmission of highly charged ions through mica nanocapillaries of various cross sections

HQ. Zhang[*], N. Akram[**], I. L. Soroka[†], C. Trautmann[1] and R. Schuch

*Physics Department, Stockholm University, S-106 91 Stockholm, Sweden*
*(corresponding author: R. Schuch, e-mail: schuch@fysik.su.se)*

[1] *GSI Helmholtzzentrum f˙ur Schwerionenforschung, D-64291 Darmstadt, Germany*

Studies of the transmission of slow highly charged ions (HCIs) through nanocapillaries in various insulating materials were performed over ten years [1-3]. It started with the discovery of the new phenomenon[1] that the majority of the transmitted ions retain their initial charge state and kinetic energy, even when the capillaries are tilted by an angle larger than the angle allowed geometrically by the aspect ratio. This so-called guiding effect is attributed to a self-organized formation of charge patches on the inner walls due to initial ion impact [1-3]. Focusing and tailoring of ion beams is of interest for new beam optics.

All previous studies on guiding HCIs through insulating nanocapillaries have utilized capillaries of circular cross sections. There the shape of the angular distribution of transmitted ions is only determined by the aspect ratio and the tilt angle of the capillaries with respect to the beam. However, when breaking this rotational symmetry by using capillaries of rhombic and rectangular cross-sections in mica, strong influences from the geometrical shape of the guiding channels on the ion transmission profile were revealed [4]. It was found that capillaries of rhombic cross section produce rectangular shaped ion transmission profiles and, vice versa, capillaries of rectangular geometry give a rhombic beam shape [4,5] (see Fig. below). The dominant of role of the image force in this shaping effect was revealed by the immediate onset of the shaped profiles and by trajectory simulations.

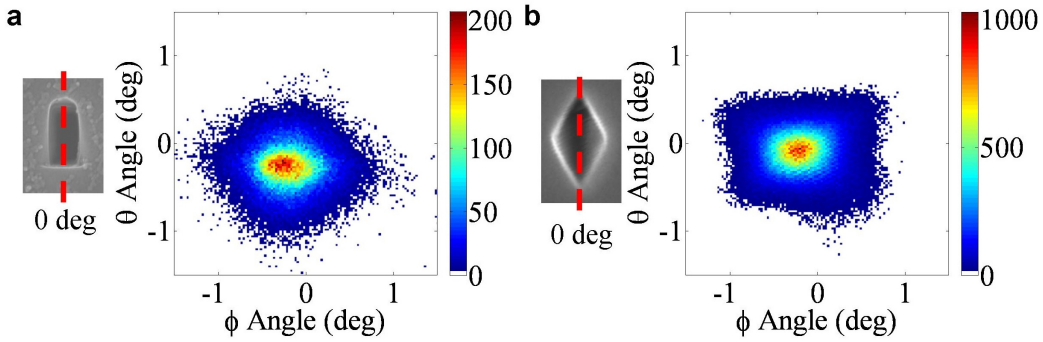


Figure: Two-dimensional angular distributions for 7-keV $Ne^{7+}$ transmitted through mica capillaries of rectangular (a) and rhombic (b) cross-section with the corresponding orientations of the long sides of the rectangles and the long axes of the rhombi in a plane perpendicular to the beam (as indicated on the left panel).

In this report, we show characteristics of the beam shaping effect from measurements of HCIs transmitted through rhombic and rectangular nanocapillaries. We disantangle the role of the image charge and the deposited charge by measuring the time evolution of the transmitted angular distributions during charge-up. This time evolution measurements reveal that the characteristic shaping of the transmitted angular distributions starts immediately with uncharged capillaries, and remains during the charging-up process while the center position shifts towards larger deflection angles away from the beam direction. By varying capillary tilt angles we find that the shape of transmitted ions gets distorted for tilt angles larger than the aspect ratio. The beam shaping effect is demonstrated to occur for incident energies up to almost 100 keV. A simulation, based on a static distribution of the deposited charge as well as the induced image charge, is performed to quantitatively explain the observations. The simulation shows clear evidence that the transmission profiles are shaped by the image force while the deposited charge deflects the transmitted ions.

Support by Swedish Research Council (VR) .

* Present address: School of Nuclear Science and Technology, Lanzhou University, Lanzhou 730000, China

** Present address: Physics Department, COMSATS Institute of Information Technology, Lahore, Pakistan

† Present address: School of Chemical Science and Engineering, Nuclear Chemistry, Royal Institute of Technology, SE-100 44 Stockholm, Sweden

.

[1] N. Stolterfoht et al., Phys. Rev. Lett. **88** (2002) 133201

[2] C. Lemell, J. Burgdörfer, F. Aumayr, Prog. Surf. Science 88, (2013) 237

[3] P. Skog, HQ. Zhang, R. Schuch, Phys. Rev. Lett. **101** (2008) 223202

[4] Y. Yamazaki, Nucl. Instr. Meth. B **258** (2007) 139

[5] HQ. Zhang et al., Phys. Rev. Lett., **108** (2012) 193202

[6] HQ. Zhang et al., Phys. Rev. A **86** (2012) 022901

# *Postersession*

# Probing buried magnetic interfaces with spin-polarized low energy electrons

Q. Wu[1], C. Ji[1], R. Zdyb[2], E. Bauer[3], M.S. Altman[1]

[1] *Department of Physics, Hong Kong University of Science and Technology, Kowloon, Hong Kong (corresponding author: M.S. Altman, e-mail: phaltman@ust.hk)*

[2] *Institute of Physics, Marie Curie-Skłodowska University, Lublin, Poland*

[3] *Department of Physics, Arizona State University, Tempe, Arizona, U.S.A.*

Many intriguing magnetic phenomena can occur in nanometer-scale structures due to their small dimensions. Among various possible nanostructures, ultrathin films have attracted significant attention because their magnetic properties can be strongly influenced by the interaction with the supporting substrate [1]. This may occur via various possible mechanisms that act on the bulk, e.g. elastic strain, or that are confined to the interface, e.g. exchange biasing or interface magnetic anisotropy. Application of magnetic-sensitive experimental techniques that can probe variably from film surface to buried interface is desirable for the identification and understanding of interfacial effects on magnetic thin films. This may be achieved by exploiting elastic scattering of spin-polarized low energy electrons because of the well-known energy dependence of the electron inelastic mean free path (IMFP) and its strong spin-dependence in magnetic materials [2,3]. Using spin polarized low energy electron microscopy (SPLEEM) [4] to investigate Fe films on W(110) surface modified by the presence of single or bi-layer noble metal films, we utilize these key IMFP characteristics of low energy electrons to probe buried magnetic interfaces and to establish spin-resolved depth profiling capability.

SPLEEM image intensity for Fe films on a W(110) surface pre-covered with a 1 ML Cu film exhibits spin-dependent oscillations as functions of incident electron energy and Fe film thickness due to the spin-dependent quantum size effect (QSE) (Fig. 1) [5]. The oscillation amplitude depends upon the incident spin polarization direction due to the spin-dependence of the IMFP. Although this QSE in electron reflectivity also becomes weaker with increasing thickness due to inelastic scattering, it remains substantial up to the maximum film thickness studied, 9 ML. The dispersion of intensity peaks that are associated with quantum well resonances above the vacuum level is consistent with the spin-dependent unoccupied band structure of bulk Fe in the ΓN direction. Comparison to results for Fe/W(110) films without a Cu buffer layer [6] indicates that the Cu layer extends the substrate interface that imposes the quantum confinement in subsequent film layers. This comparison also reveals that a +1.1 eV band offset is induced by the presence of the interfacial Cu layer.

SPLEEM observations of 3 ML Fe films on a W(110) surface precovered with a 2 ML Au film reveal complex in-plane magnetic domain structure. Domain magnetization directions that are separated by a few degrees are identified from the dependence of magnetic contrast on the spin polarization direction of the incident electron beam relative to the magnetization hard axis (Fig. 2). However, magnetic depth profiling that exploits the energy dependence of the spin-dependent IMFP [2,3] demonstrates that apparent domain magnetization directions converge with decreasing IMFP at higher electron energy. This unusual observation is accounted for by a layered non-collinear spin configuration in the Fe film, which is decoupled from the W substrate by the Au buffer layer.

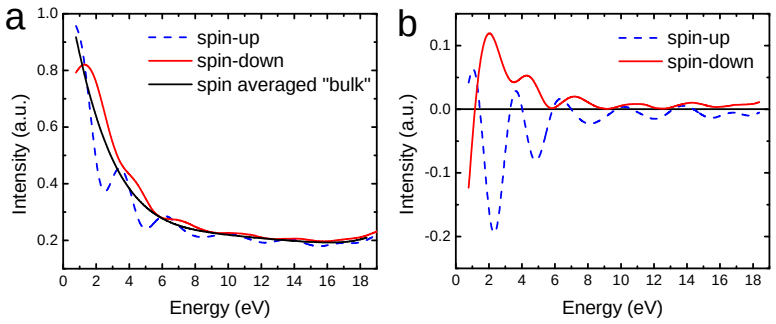


**Figure 1**. (a) Raw experimental spin-up and spin-down I(V) curves for Fe(6 ML)/Cu(1ML)/W(110) and the spin averaged I(V) curve. (b) Experimental QSE intensity oscillations after correction for the incomplete spin polarization of the electron beam and subtraction of the spin averaged curve. The energy zero is the vacuum level.

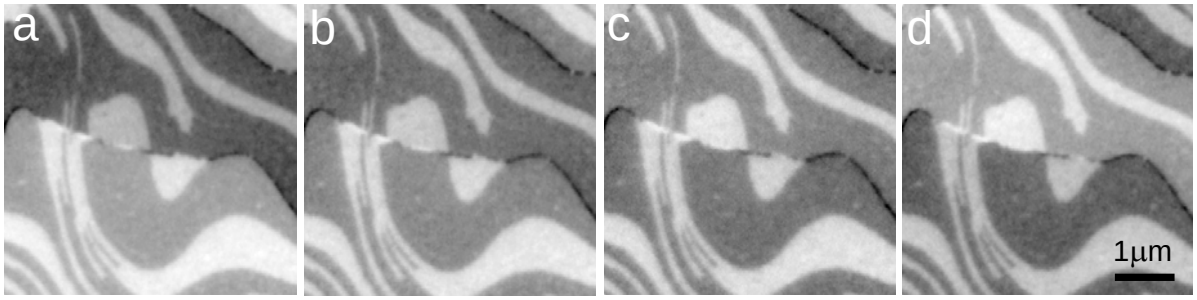


**Figure 2**. SPLEEM images of Fe (3ML)/Au(2ML)/W(110) acquired with incident in-plane spin polarization aligned close to the magnetization hard axis direction ($\phi$ = 0). The deviations of the in-plane polarization azimuthal angle $\phi$ from the nominal hard axis are (a) -2.7º ,(b) -0.9º , (c) +0.9º , (d) +2.7º.

Financial support from the Hong Kong Research Grants Council under Grant Nos. HKUST600110 and HKUST600111 is gratefully acknowledged.

[1] C.A.F. Vaz, J.A.C. Bland and G. Lauhoff, Rep. Prog. Phys. **71**, 056501 (2008).
[2] J. Hong and D. Mills, Phys. Rev. B **62**, 5589 (2000).
[3] R. Zdyb, E. Bauer, J. Phys.: Condensed Matt. **25**, 272201 (2013).
[4] E. Bauer, Rep. Prog. Phys. **57**, 895 (1994).
[5] Q. Wu and M.S. Altman, Ultramicroscopy **130**, 109 (2013).
[6] R. Zdyb and E. Bauer, Phys. Rev. Lett. **88**, 166403 (2002).

# Electronic stopping of slow light ions in insulators

D. Roth, D. Goebl, and P. Bauer

*Institut für Experimentalphysik, Abteilung für Atom- und Oberflächenphysik,*
*Johannes Kepler Universität Linz, A-4040 Linz, Austria*
*(corresponding author: P. Bauer, e-mail: peter.bauer@jku.at)*

The study of energy loss of ions when propagating in a solid has a long history. By convention, one distinguishes between *nuclear stopping* due to repulsive Coulomb interaction with the nuclei and *electronic stopping* due to transfer of energy to the electronic system. The resulting deceleration is described by the *stopping power* $S = -dE/dx$. Alternatively, one introduces the *stopping cross section* $\varepsilon$ related to $S$ via $\varepsilon = (1/n)\cdot S$, where $n$ denotes the atomic density of the target. While for high ion velocities electronic stopping is well understood [1, 2], the prevailing mechanisms are still unresolved in the regime of low ion velocities.

For projectile velocities $v << v_F$, where $v_F$ denotes the Fermi velocity of the target electrons, only weakly bound conduction and valence electrons can be excited. For a free electron gas (FEG), $dE/dx = Q(Z_1, r_s)v$, where $Q(Z_1, r_s)$ denotes the friction coefficient which depends on the atomic charge of the projectile $Z_1$ and the Wigner-Seitz radius $r_s$. Experimentally, deviations from velocity proportionality were observed for materials with finite excitations thresholds, e.g. for the *d*-band in noble metals or the band gap energy $E_g$ in insulators. For instance, for transition and noble metals changes in the slope of $\varepsilon$ were observed in the velocity range 0.2 a.u. $< v <$ 0.5 a.u. [3, 4]. In insulators, electronic stopping has been found to vanish for ion velocities lower than a certain threshold velocity, $v_{th}$ [5, 6]. Surprisingly, even for LiF ($E_g$ = 14 eV) the threshold velocity is below 0.1 a.u., i.e., nonlinearities in the metals occur at considerably higher velocities even if their excitation thresholds are much lower.
In this contribution we present an analysis of electronic stopping of H and He ions in LiF and $SiO_2$ adopting the charge exchange model developed to describe the observations in grazing surface scattering [7]. The key point of this charge exchange model is that in an insulator H and He move as neutral projectiles, which in the Madelung potential of the ionic crystal can capture an electron from an anion, e.g. $F^-$; when the negative projectile moves on, it will either transfer an electron to the conduction band very efficiently or an exciton will be formed on the expense of the kinetic energy of the ion [8]. A quantitative comparison of TD-DFT calculations [9] to experimental data shows that only with inclusion of the charge exchange channel a satisfactory agreement is obtained in the threshold regime of electronic stopping.

Support by the Fonds zur Förderung der Wissenschaftlichen Forschung (FWF-Project P22587-N20) and provision of the TiN samples by Ion-TOF are gratefully acknowledged.

[1] C. P. Race, D. R. Mason, M. W. Finnis, W. M. C. Foulkes, A. P. Horsfield, and A. P. Sutton, Rep. Prog. Phys. **73**, 116501 (2010).

[2] P. Sigmund, Particle Penetration and Radiation Effects: General Aspects and Stopping of Swift Point Charges (Springer, Berlin, New York, 2008).

[3] S. N. Markin, D. Primetzhofer, S. Prusa, M. Brunmayr, G. Kowarik, F. Aumayr, and P. Bauer, Phys. Rev. B 78, 195122 (2008).

[4] S. N. Markin, D. Primetzhofer, M. Spitz, and P. Bauer, Phys. Rev. B 80, 205105 (2009).

[5] S. N. Markin, D. Primetzhofer, and P. Bauer, Phys. Rev. Lett. 103, 11, 113201 (2009).

[6] D. Primetzhofer, S.N. Markin, and P. Bauer, Nucl. Instr. Meth. B 269, 19, 2063-2066 (2011).

[7] H. Winter, Phys. Rep. 367, 387 (2002) and references therein.

[8] H. Winter, C. Auth, and A.G. Borisov, Nucl. Instr. Meth. B115, 133 (1996).

[9] M.A. Zeb, J. Kohanoff, D. Sanchez-Portal, and E. Artacho, Nucl. Instr. Meth. B303, 59 (2013).

# Interaction of nitrogen ions with tungsten and nitrogen saturated tungsten surfaces

Katharina Dobes, Bernhard Berger, Valerie Smejkal, and Friedrich Aumayr

*Institute of Applied Physics, TU Wien, Association EURATOM-ÖAW*
*Wiedner Hauptstr. 8-10/E134, 1040 Vienna Austria, EU*

In a fusion reactor, where nitrogen is used as a seeding gas to mitigate the heat load to the plasma facing components [1], it is expected that mixed tungsten-nitride surfaces will build up during operation. For fusion research it is of major concern to investigate the influence of such mixed material layers on physical properties of the plasma facing components such as e.g. their sputtering yield or their melting point. As the incorporation of nitrogen reduces the electrical conductivity of the tungsten surface, the resulting tungsten nitride layers might also be prone to potential sputtering - a phenomenon which has been observed for various non-conducting materials in the past [2].

Sputtering of nitrogen saturated tungsten surfaces under the impact of seeding gas ions (N, Ne, Ar) was therefore investigated under controlled laboratory conditions using a quartz crystal microbalance technique [3, 4]. In the presented investigations, particular emphasis was put on testing any charge state dependency of the sputtering yield.

The observed sputtering yields were found to be independent of the charge state of the projectiles for both surfaces (W and N-saturated W). From this, no enhancement of wall erosion rates in fusion machines due to potential sputtering of N saturated W surfaces has to be expected. In previous studies [5] it was however found that for W-nitride surfaces the electrical conductivity, which is a determining factor in the occurrence of potential sputtering, depends on the deposition conditions. The absence of potential sputtering might therefore still be influenced by parameters like the wall temperature, the N impact energy and generally the actual N content in mixed, N containing W surfaces in a future fusion reactor.

Erosion of W-nitride surfaces was found to be smaller for Ne impact than for Ar impact, as can be expected from the purely kinetic nature of the sputtering process. Additionally the total sputtering yield of W-nitride surfaces is found to be comparable to the sputtering yield on pure W, with N erosion apparently balancing the reduction of the partial W sputtering yield. This on the other hand means that the release of W from W-nitride is decreased compared to erosion of pure W surfaces, which is in agreement with the results reported in [6].

This work was supported by the European Communities under the Contract of Association between EURATOM and the Austrian Academy of Science. It was carried out within the framework of the European Fusion Development Agreement as part of the work program EFDA Task Force on Plasma Wall Interactions.

[1] A. Kallenbach, et al., Plasma Phys. Control. Fusion 52 (2010) 055002
[2] F. Aumayr, and HP. Winter, Philos. Trans. R. Soc. London 362 (2004) 77
[3] G. Hayderer, M. Schmid, P. Varga, HP. Winter, and F. Aumayr, Rev Sci. Instrum. 70 (1999) 3696
[4] A. Golczewski, K. Dobes, G. Wachter, M. Schmid, and F. Aumayr, Nucl. Instr. Meth. B 267 (2009) 695
[5] J. Lin, A. Tsukune, T. Suzuki, and M. Yamada, J. Vac. Sci. Technol. A 17 (1999) 936
[6] K. Schmid, A. Manhard, Ch. Linsmeier, A. Wiltner, T. Schwarz-Selinger, W. Jacob, S. Mändl, Nucl. Fusion 50 (2010) 025006

# Cluster Nucleation and Growth from a Highly Supersaturated 2D Phase: Ag/$Fe_3O_4$(001)

Roland Bliem,[1] Lukas Perneczky,[1] Zbynek Novotny,[1] David Fobes,[2]
Zhiqiang Mao,[2] Michael Schmid,[1] Ulrike Diebold,[1] and Gareth S. Parkinson[1]

[1]*Institute of Applied Physics, Vienna University of Technology, Vienna, Austria*[*]

[2]*Tulane University, New Orleans, Louisiana 70118, USA*

## Abstract

The nucleation and growth of Ag clusters at the $(\sqrt{2} \times \sqrt{2})$R45°-$Fe_3O_4$(001) surface was studied using scanning tunneling microscopy (STM). This surface functions as a robust adsorption template, stabilizing a complete array of Ag adatoms with a nearest-neighbor distance of 0.84 nm to temperatures as high as 670 K, which indicates that in this system nucleation is not thermally induced. This stable arrangement of adatoms provides a well-defined initial state for the study of growth and nucleation processes at the surface. As the local coverage exceeds 1 ML, the number of Ag adatoms exceeds the number of available adsorption sites and the system enters a supersaturated state. Cluster nucleation occurs spontaneously at room temperature; with mild annealing, the nuclei grow at the expense of the surrounding material. This behavior cannot be reconciled with any of the established growth modes.

The observation in STM movies that Ag adatom mobility is constrained to 1D motion allows the conclusion that the 1D denuded zones, or "vacancy trails", associated with each cluster are created by Ag mobility. An analysis of the vacancy trails after annealing to different temperatures shows that clusters grow via three distinct processes occurring at different temperatures and rates. The four STM images of different coverages of Ag at different temperatures in Figure 1 show stable adatoms (a) compared to the three growth processes occurring in the presence of clusters (b-d): Cluster nuclei are mobile and diffuse to step edges, capturing otherwise stable Ag adatoms encountered along their path (b). With the clusters immobilized, adatom diffusion and capture takes over as the dominant process (c). Above 720 K, the $(\sqrt{2} \times \sqrt{2})$R45° reconstruction is lifted, adatoms are no longer stabilized, and the system evolves rapidly to large (>10 nm) nanoparticles (d), consistent with the thermodynamic preference for 3D crystallites.

[*] bliem@iap.tuwien.ac.at

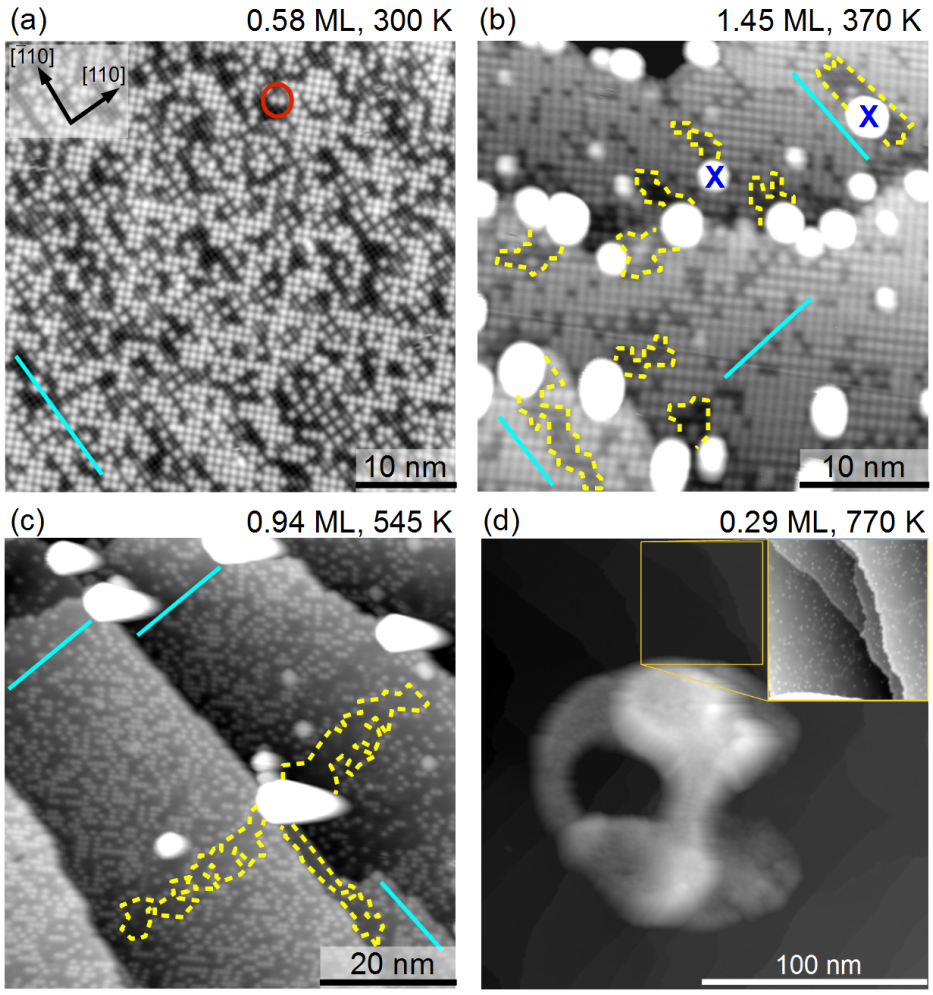


FIG. 1. (a) STM image of 0.58 ML Ag adatoms (two in the red circle) on $Fe_3O_4(001)$ as deposited at room temperature ($U_{sample}$ = +1.2 V, $I_t$ = 0.3 nA, 46 x 46 $nm^2$) (b) STM image ($U_{sample}$ = +1.2 V, $I_t$ = 0.3 nA, 36 x 36 $nm^2$, initially 1.45 ML Ag, flash-annealed at 370 K) exhibiting coexistence between Ag clusters and adatoms. Vacancy trails (yellow dashed lines) extend away from the clusters in the local Fe row direction (cyan lines). These arise when the clusters capture Ag atoms while diffusing on the surface. (c) STM image ($U_{sample}$ = +1.45 V, $I_t$ = 0.3 nA, 67 x 67 $nm^2$) showing initially 0.94 ML Ag, flash-annealed at 545 K. Ag adatoms coexist with large Ag clusters immobilized at step edges. Vacancy trails extend away from the clusters in equal distances on different terraces. This is consistent with adatom diffusion taking over as the primary cause of cluster growth. The cyan lines indicate the local Fe row directions. (d) After annealing to 770 K most adatoms have been incorporated in large clusters. Owing to the height of the cluster, the shape corresponds to an image of the STM tip.

# Gold intercalation under graphene monolayer on Ni(111)

S.L. Kovalenko, B.V. Andryushechkin, and K.N. Eltsov

*A.M. Prokhorov General Physical Institute RAS, 119991 Moscow, Ulitsa Vavilova 38, Russia*
*(corresponding author: K.N. Eltsov, e-mail: eltsov@kapella.gpi.ru)*

In the wake of impressive experiments performed at 'the Manchester group' on a single atomic sheet of graphite transferred on silicon oxide by means of 'Scotch Tape technology' [1,2], the academic community has struggled to create an intelligent technique for graphene layers production on a solid state surface. This issue has not been appropriately addressed so far. Both methods viewed as most promising - high-temperature annealing of hexagonal silicon carbide and cracking of hydrocarbons on surfaces of some metals (Ni, Ru, Re, etc.) – require gold intercalation under graphene to create a quasi-free graphene layer (the Dirac cone waist being at the Fermi level) [3,4]. Also, the graphene electronic structure (the Dirac cone energy position, the formation of a energy band gap, etc.) varies depending on the intercalated metal (Ag, Cu, Si, Cs, etc.). The conditions under which metal intercalation under graphene is possible have been found empirically, while the intercalate atomic structure and the process explaining how alien atoms settle under a graphene layer have remained unknown.

This paper presents the results of a study of the gold intercalation process in the "graphene monolayer on Ni(111) surface" system. The study was performed in ultra-high vacuum using low-energy electron diffraction (LEED), Auger electronic spectroscopy (AES), and scanning tunneling microscopy (STM). The graphene on a Ni(111) surface was formed by a sequence of "propylene adsorption at 300°C / annealing at 500°C" cycles, in which gold was first deposited on a graphene layer at 300°C, and then the entire Au/Gr/Ni(111) system was annealed at 500 °C.

We have found that this technique of carbon deposition creates a nearly ideal epitaxial graphene monolayer on the Ni(111) surface. Its lattice orientation is the same as that of the substrate (without any rotation), which is proven by STM and LEED observations. STM images taken at room temperature show that as gold deposits on Gr/Ni(111) as a series of rather large detached 3D islands. As the surface of the Au/Gr/Ni(111) system is then annealed at 500°C, however, the gold morphology changes dramatically. The large islands "melt down" into 2D "pools" retaining a core of the initial island. Structurally, the "pools" represent a network of triangular dislocation loops (see Fig. 1) characteristic of a "gold monolayer on Ni(111) surface" system [5].

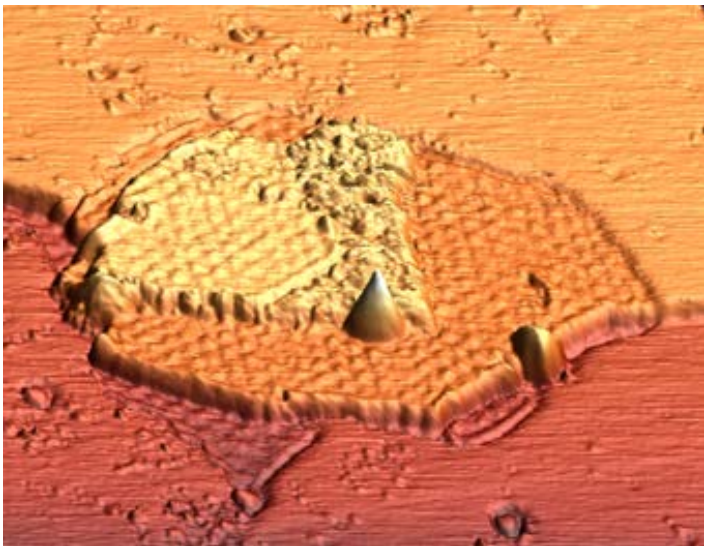

Fig. 1 An STM image (83*83 nm) of the Au/Gr/Ni(111) surface annealed at 500°C for one hour. The "pool" (a 2D periodically structured area) is clearly seen on three terraces, while two residual gold islands remain on the top and bottom terraces.

This is a clear sign that gold has settled under the graphene layer. At the same time, STM also very clearly demonstrates a graphene monolayer on top of the remainders of the gold islands, which suggests carbon atoms diffusion through a volume or along the surface of a gold island, rather than metal atoms diffusion through a graphene layer. As the system is heated up, the "pools" expand until they cover the entire sample surface.

In the paper, we discuss how the intercalated layer forms and what we think its atomic structure is.

Support by the BMBF (project No 05K12OD3) is gratefully acknowledged.

[1] K.S. Novoselov, A.K. Geim, S.V. Morozov, D. Jiang, Y. Zhang, S.V. Dubonos,I.V. Grigorieva, A.A. Firsov, Science 306 (2004) 666.
[2] K.S. Novoselov, E. McCann, S.V. Morosov, V.I. Falko, M.I. Katsnelson, U. Zeitler, D. Jiang, F. Schedin, A.K. Geim, Nat. Phys. 2 (2006) 177.
[3] M. N. Nair, M. Cranney, F. Vonau, D. Aubel, P. Le F`evre, A. Tejeda, F. Bertran, A. Taleb-Ibrahimi, and L. Simon, PHYS. REV. B **85** (2012) 245421.
[4] A. M. Shikin, A. G. Rybkin, D. Marchenko, A. A. Rybkina, M. R. Scholz, O. Rader and A. Varykhalov, New Journal of Physics 15 (2013) 013016.
[5] J. Jacobsen, L. P. Nielsen, F. Besenbacher, I. Stensgaard, E. Lægsgaard, T. Rasmussen, K. W. Jacobsen, and J. K. Nørskov, Phys. Rev. Lett. **75** (1995) 489.

# A metal surface with chiral memory

C. Karageorgaki[1] and K.-H. Ernst[1,2]

[1]*Empa, Swiss Federal Laboratories for Materials Research and Technology*
*(corresponding author: K.-H. Ernst, e-mail: karl-heinz.ernst@empa.ch)*

[2] *Department of Chemistry, University Zurich, Zürich, Switzerland*

Chiral and achiral butanedioic acids have been studied in order to better understand self-assembly at the molecular level and the molecules' interactions with metal surfaces. Here we present LEED, STM, RAIRS and TPD results of achiral and chiral members of the $C_4$ dicarboxylic acid family, namely, maleic acid (MAL) [1], fumaric acid (FUA) [2], malic acid (MA) [3] and dimethyl succinic acid (DMSU) on a Cu(110) surface (Fig. 1). The molecules show often coverage dependent "surface explosion" decomposition processes and identical LEED structures. These, observed as the superposition of two mirror domains, suggest that the chirality transfer derives from the substrate, when the molecule has no functional groups that can form hydrogen bonds. Interestingly enough, the same LEED structures have been observed for other $C_4$ dicarboxylic acids, in particular succinic acid [5] and racemic malic acid [6]. STM results show that the substrate is etched by the molecules, leading to a reconstruction of the surface, something that was first reported for malic acid [3] and recently also for tartaric acid [7]. After careful prolonged annealing the autocatalytic decomposition reaction is initiated, but the reconstructed metal surface prevails. This leads to a chiral metal surface without the molecules originally causing the reconstruction present (Fig. 2).

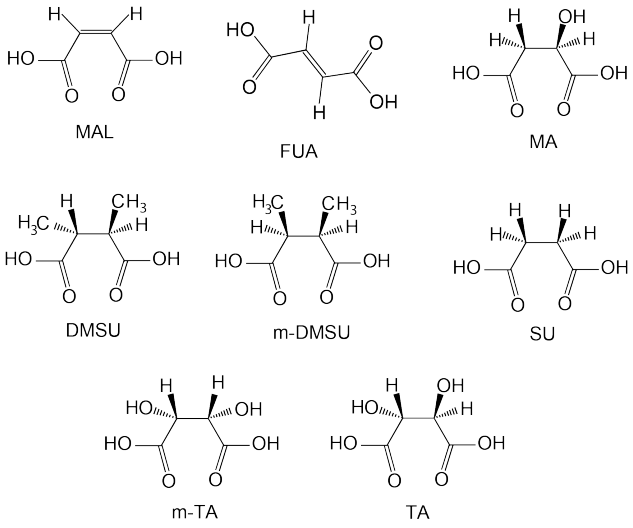


**Fig. 1.** Structural formulas of various $C_4$ dicarboxylic acids: maleic acid (MAL), fumaric acid (FUA), malic acid (MA), dimethyl succinic acid (DMSU), *meso*-dimethyl succinic acid (*m*-DMSU), succinic acid (SU), tartaric acid (TA), and *meso*-tartaric acid (*m*-TA).

The exact mechanism for this chiral restructuring remains still unclear, but it opens interesting application pathways, since the exposed Cu adatom rows could potentially act as active chiral sites for enantioselective processes.

Support by the Swiss National Science Foundation (SNSF) is gratefully acknowledged.

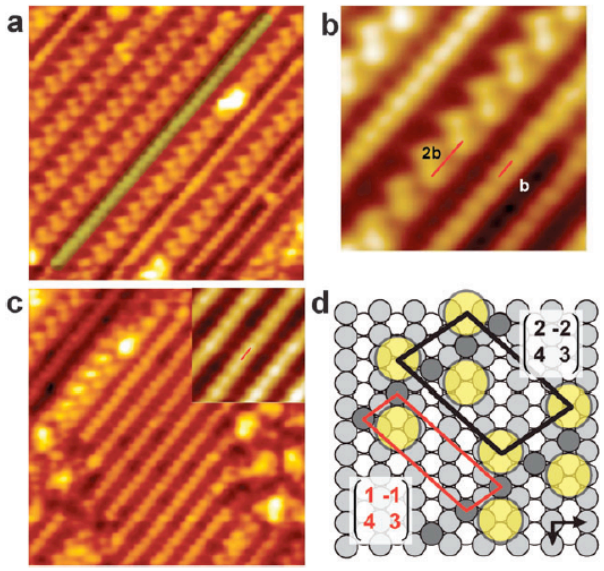


Fig. 2. STM images and tentative model for a (1 1, –5 2) structure of maleic acid on Cu(110). (a) STM image of the (1 –1, 4 3) domain [= mirror domain of (1 1, –5 2)]. A zigzag row of molecules is the basic motif. The green semi-transparent line marks a row of Cu adatoms (17 nm × 17 nm, I = 680 pA , U = 464 mV). (b) STM image highlighting the doubled periodicity of the molecular unit cell with respect to the adatom row periodicity (4.8 nm × 4.8 nm I = 780 pA, U = 464 mV, filtered). (c) STM image of chiral metal area without molecules (17 nm × 17 nm, I = 780 pA, U = 464 mV, inset: 4.8 nm × 4.8 nm, filtered). (d) Tentative model for a reconstructed Cu(110) surface with Cu adatom rows stabilized by MAL molecules. The molecular adlattice unit cell and the adatom lattice unit cell are indicated.

[1] C. Karageorgaki, K.-H. Ernst, *Chem. Comm.* (in press)
[2] C. Karageorgaki, D. Passerone, K.-H. Ernst, *Surf. Science* (in press)
[3] C. Roth, D. Passerone, L. Merz, M. Parschau, K.-H. Ernst *J. Phys. Chem. C* **2011**, 115 *1240*
[4] C. Karageorgaki, K.-H. Ernst, *J. Phys. Chem. C* **2014** (submitted)
[5] M. Parschau, S. Romer and K.-H. Ernst, *J. Am. Chem. Soc.* **2004**, 126 15398-15399.
[6] C. Roth, M. Parschau, and K.-H. Ernst, ChemPhysChem **2011**, 12, 1572–1577.
[7] T. J. Lawton, V. Pushkarev, D. Wei, F. R. Lucci, D. S. Sholl, A. J. Gellman, E. C. H. Sykes, *J. Phys. Chem. C* **2013**, 117, 22290–22297

# Bottom-up fabrication of graphene nanoribbons: From molecules to devices?

Jinming Cai, Hajo Söde, Leopold Talirz, Ivan Shorubalko, Reinhard Berger[1], Xinliang Feng[1], Klaus Müllen[1], Liangbo Liang[2], Vincent Meunier[2], Carlo A. Pignedoli, Pascal Ruffieux, and Roman Fasel

*Empa, Swiss Federal Laboratories for Materials Science and Technology, 8600 Dübendorf, Switzerland*
*(corresponding author: R. Fasel, e-mail: roman.fasel@empa.ch)*

[1] *Max Planck Institute for Polymer Research, Ackermannweg 10, 55124 Mainz, Germany*
[2] *Department of Physics, Rensselaer Polytechnic Institute, Troy, NY 12180, United States of America*

Graphene nanoribbons (GNRs) – narrow stripes of graphene – are predicted to be semiconductors with an electronic band gap that sensitively depends on the ribbon width. For armchair GNRs (AGNRs) the band gap is inversely proportional to the ribbon width, with an additional quantum confinement-related periodic modulation which becomes dominant for AGNRs narrower than ~3 nm. This allows, in principle, for the design of GNR-based structures with specific and widely tunable electronic properties, but requires structuring with atomic precision. The inability to produce graphene nanostructures with the needed precision has so far hampered the experimental investigation of the electronic structure of narrow GNRs and their exploration in device configurations, which is in contrast to an impressive number of GNR-related computational studies.

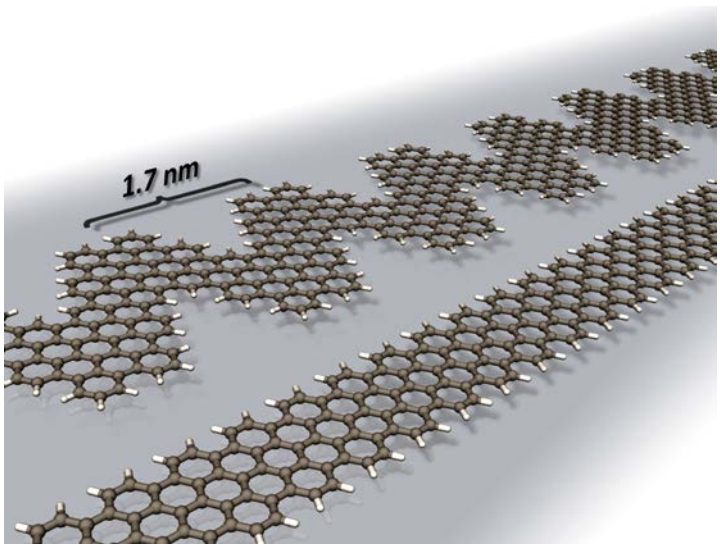


In this presentation, I will review a recently developed bottom-up approach to the fabrication of atomically precise GNRs [1]. It is based on a surface-assisted synthetic route using specifically designed precursor monomers, and has made available ultra-narrow GNRs and related graphene nanostructures for experimental investigations of their structural, electronic and optical properties [1-8]. For the case of AGNRs of width $N$=7 (7-AGNR), the electronic band gap and band dispersion have been determined

with high precision [7,8]. Optical characterization has revealed important excitonic effects [8], which are in good agreement with expectations for quasi-one-dimensional graphene systems. The versatility of the bottom-up approach also allows for the fabrication of substitutionally doped GNRs and heterostructures. I will present examples for both type I and type II heterojunctions with band shifts up to 0.5 eV. First attempts of field effect transistor fabrication and characterization will be presented, revealing serious challenges in patterning and contact fabrication that are related to the nanoscale dimensions of individual AGNRs.

[1] J. Cai et al., *Nature,* **466** (2010) 470.
[2] M. Bieri et al., *Chem. Commun*., (2009) 6919.
[3] M. Bieri et al., *J. Am. Chem. Soc*., **132** (2010) 16669.
[4] M. Treier et al., *Nature Chemistry*, **3** (2011) 61.
[5] S. Blankenburg et al., *ACS Nano,* **6** (2012) 2020.
[6] P. Ruffieux et al., *ACS Nano,* **6** (2012) 6930.
[7] L. Talirz et al., *J. Am. Chem. Soc*. **135** (2013) 2060.
[8] J. Cai et al. ; R. Denk et al., H. Söde et al., in preparation.

# Water Adsorption at the Tetrahedral Titania Surface Layer of $SrTiO_3$(110)-(4x1): An STM and Photoemission Study.

Zhiming Wang,[†] Xianfeng Hao,[†] Stefan Gerhold,[†] Zbynek Novotny,[†] Cesare Franchini,[‡] Eamon McDermott,[§] Karina Schulte,[⊥] Michael Schmid,[†] and Ulrike Diebold[†]

[†]Institute of Applied Physics, Vienna University of Technology, Vienna, Austria
[‡]Faculty of Physics & Center for Computational Material Science, University of Vienna, Vienna, Austria,
[§]Institute of Materials Chemistry, Vienna University of Technology, Vienna, Austria,
[⊥]MAX IV Laboratory, Lund University, Lund, Sweden.

The interaction of water with the (4 × 1) surface of $SrTiO_3$(110) was investigated theoretically by density functional theory (DFT) and experimentally by scanning tunneling microscopy (STM) and photoemission spectroscopy (PES). A striking inertness toward water adsorption was found on this surface consisting of an overlayer of $TiO_4$ tetrahedra. STM, core-level and valence band PES studies show that water dissociates at oxygen vacancies, while it neither adsorbs nor dissociates on the stoichiometric surface. This is in agreement with DFT calculations. By comparison with the tetrahedrally coordinated surface of anatase $TiO_2$(001)-(1 × 4), our study suggests that two-dimensional tetrahedrally coordinated $TiO_4$ overlayers provide a remarkably hydrophobic surface. In addition, enhanced reactivity due to deposited Sr adatoms is discussed.

# Ab-initio based investigations of aliphatic and aromatic acids on $TiO_2$-surfaces: a precursor for hybrid materials design

Wolfgang Heckel, Beatrix A. M. Elsner, and Stefan Müller

*Hamburg University of Technology,*
*Institute of Advanced Ceramics,*
*Denickestr. 15, D-21075 Hamburg*
∗ *e-mail: wolfgang.heckel@tuhh.de*

For a couple of years, the effort to create hierarchically structured multicomponent materials has been increased continuously. For the design of such called hybrid materials with desired mechanical (e.g. hardness, stiffness, ductility) and electronic (e.g. conductivity) properties, a detailed knowledge of the structure and stability at the interface between individual types of materials plays a crucial role. Indeed, the interaction of the different composite ingredients, such as hard inorganic materials, ductile metals or soft polymers, controls the mechanical properties.

Our research focuses on the first hierarchical level. Density functional theory has been applied in order to study the crystallographic and electronic atomic structure and the energetic stability. For this, the biggest challenge is to find the ground state structure of hybrid materials in order to create a model system being still small enough to allow for its application on state-of-the-art computer systems.

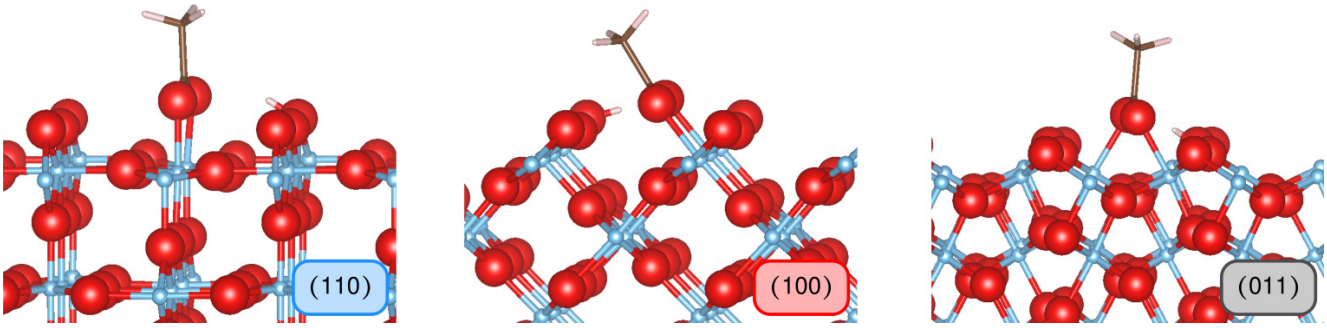


Figure 1: Energetically most favorable adsorption sites for acetic acid on $TiO_2$ (110), (100), and (011) surfaces.

As the starting point for further calculations, we performed a detailed analysis for the quite well-known interface of small carboxylic acids (CA) and $TiO_2$ rutile facets (Figure 1).[1] In terms of adsorption geometries and binding energies, our results fully agree with theoretical as well as with experimental literature values. More precisely, on all considered $TiO_2$ surfaces, the rather high adsorption energy of about 1 eV per molecule is confirmed. Being covered by CA, the (011) surface favors the bulk-like structure over the vacuum $(2 \times 1)$ reconstruction [2], as it is predicted for $H_2O$ in ref. [3]. Additionally, the investigation of the density of states reveals only a very slight increase of binding energy in presence of pre-adsorbed hydrogen. On all three surfaces, a high,

dense coverage can appear as long as the CA side chains are small. Therefore, CA is broadly used for linking strongly ceramics and polymer.

Current thermal desorption measurements [4] give rise to the assumption, that CA with an aromatic side chain can still improve the binding energy compared to CA with simple aliphatic ones. In case of aromatic side chains, the main desorption peak shifts up to a 0.15 eV higher desorption energy compared to CA with aliphatic side chains, which is apparently due to attractive interaction of neighbored benzene rings.

In order to verify this strong suspicion, we have investigated benzoic acids on $TiO_2$ surfaces with density functional theory. Our results show clearly the requirement of applying an exchange correlation functional with van der Waals correction, to describe properly the attractive interaction of adsorbing molecules among each other (Figure 2). The resulting binding energies increase up to about 0.18 eV per molecule compared to CA with aliphatic side chains. The crucial points for the optimal inter-molecular distances and subsequently strengthened binding are, firstly, the substrate periodicity, and, secondly, the adsorbate inclination.

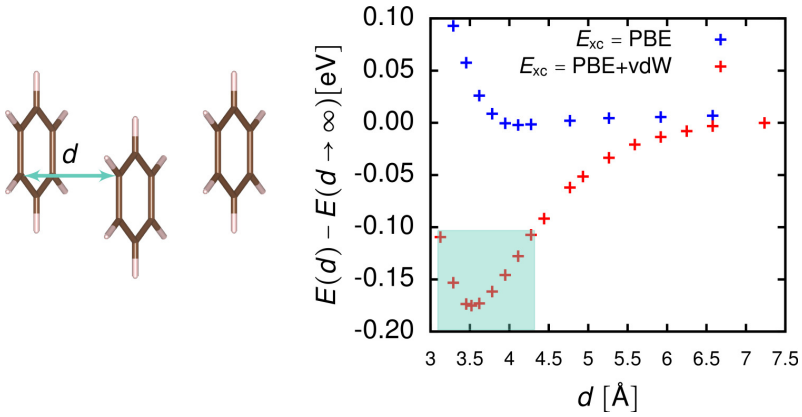


Figure 2: Interaction of neighbored benzene rings: In DFT calculations, attraction is only observed in case of applying an exchange correlation functional with van der Waals correction.

Supported by DFG, SFB 986, project A4.

# References

[1] W. Heckel, B. Elsner, C. Schulz and S. Müller, submitted.

[2] X. Gong, N. Khorshidi, A. Stierle, V. Vonk, C. Ellinger, H. Dosch, H. Cheng, A. Selloni, Y. He, O. Dulub, and U. Diebold, Surf. Sci. **603**, 138 (2009).

[3] U. Aschauer, and A. Selloni, Phys. Rev. Lett. **106**, 166102 (2011).

[4] A. Dreyer, and G. Schneider, unpublished.

# Effect of film boundaries on the quasi-ballistic transport of charge carriers in PbSnTe films in strong electric and magnetic fields

A. Klimov, V. Epov, N. Paschin, V. Shumsky

*Institute of Semiconductor Physics, SB RAS, 630090 Novosibirsk, Russia*
*(corresponding author: A. Klimov, e-mail: klimov@isp.nsc.ru)*

Possible occurrence of quasi-ballistic transport of free charge carriers in $Pb_{1-x}Sn_xTe$ films is a consequence of a unique combination of properties of solid solution $Pb_{1-x}Sn_xTe$ in the range of compositions $x\approx0.24$-$0.28$ [1-3]. Such compositions refer to band-gap energy values $E_g\approx0.06$-$0.04$ eV. Like in other narrow-gap semiconductors, the specific resistivity of undoped $Pb_{1-x}Sn_xTe$ samples with $x\approx0.24$-$0.28$ remains rather low down to temperature T=4.2 K, at which in the present study measurements were performed. Investigation into the transport of charge carriers in strong electric fields in such samples is almost impossible because of the strong ohmic heating of the samples. However, the doping of the material with indium to a concentration of 1-3 at.% induces the so-called metal-dielectric transition in it [4,5], at which the specific resistance shows a considerable growth and reaches, at T=4.2 K, values in excess of $10^{10}$ Ω·cm. In the latter case, a strong electric field can be applied to a $Pb_{1-x}Sn_xTe$ film of micrometer thickness without a notable heating of the sample. Unlike in ordinary insulators, the mobility of free charge carriers in $Pb_{1-x}Sn_xTe$:In reaches values $\mu\approx10^4$-$10^5$ $cm^2V^{-1}s^{-1}$, their effective mass being close to $m^*\approx0.01m_0$, where $m_0$ is the free-electron mass. As a result, the drift velocity $v_E$ of charge carriers in a field $E\approx10^3$ V/cm can reach a value of $10^8$ cm/s, and their kinetic energy $m^*v_E^2/2$ may become several times greater than the mean thermal kinetic energy. It is those conditions that correspond to a quasi-ballistic transport of charge carriers that resembles the motion of free electrons in vacuum. Simultaneously, in the case of ohmic conductivity in $Pb_{1-x}Sn_xTe$ films of micrometer thickness with the values of ρ and μ indicated above even in fields $E\leq10^3$ V/cm the electric current remains too low to measure. Situation changes if, for the indicated field strengths E, the conduction turns out to be dominated, instead of ohmic current, by a space-charge-limited current in the presence of traps [6]. The cause for such domination in $Pb_{1-x}Sn_xTe$:In is, first, a low value of the band-gap energy of the material which facilitates injection of charge carriers out of contacts and, second, the high magnitude of the static dielectric constant, typical of $A^4B^6$ compounds and reaching, in the case of interest, $\varepsilon_0\approx2000$-$3000$ [7]. As a result, the capacitance of $Pb_{1-x}Sn_xTe$:In planar structures of micrometer thickness with typical inter-electrode separation 30 μm appears to be high, together with the density of the space charge injected out of contacts, which factor, together with the high mobility of injected charge carriers, ensures an easily measurable current value in the micro- and milli-ampere range in fields $E\leq1$-$3\cdot10^3$ V/cm without a notable

heating of the sample. In the regime of space-charge-limited injection currents, trap recharging processes turn out to be essential. The characteristic time of such processes in $Pb_{1-x}Sn_xTe$:In films observed upon a rapid change of bias voltage, or the magnitude or direction of magnetic field **B**, reaches several seconds and over.

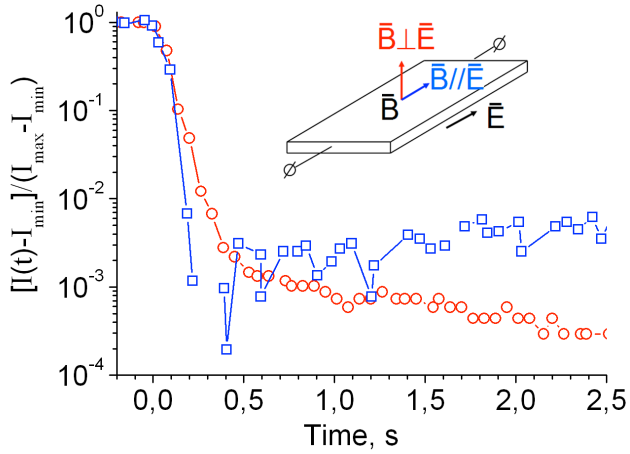


*Normalized current versus time after switching-on (red circles, **B⊥E**) and switching-out (blue squares, **B//E**) of a magnetic field of strength **B**=2T.*

In $Pb_{1-x}Sn_xTe$ samples examined in the present study the kinetics of current relaxation proved to be different for different orientations of **B** (see the figure). Earlier in [8], the curves of the current versus smoothly varied orientation of field **B** were found to be dependent on whether the charge carriers are deflected in the magnetic field towards the free surface of the film or towards the film/substrate interface. In the present publication, we discuss a model for the observed phenomena involving the consideration of both the trap recharging processes and the interaction of free charge carriers with film boundaries in the regime of quasi-ballistic transport. In the latter regime with **B⊥E**, the trajectory of charged particles looks like a cycloid rather than a circle while in the case of **B||E** a spiral motion in the direction of field **E** becomes essential. In addition, we consider the effect which the discussed transport phenomena have on the observed properties of $Pb_{1-x}Sn_xTe$:In as a topological insulator material [9,10].

[1] G. Nimtz, B. Schlicht, Narrow-gap lead salts. In "Narrow Gap Semiconductors Springer Tracts in Modern Physics" 98, 1 (1983)

[2] B.A.Volkov, L.I.Ryabova, D.R.Khokhlov, Physics-Uspekhi 45, 819 (2002)

[3] D.V. Shamshur, R.V. Parfen'ev, A.V. Chernyaev, S.A. Nemov, Physics of the Solid State 52, 1815 (2010)

[4] K. Morigaki and F. Yonezawa, Suppl. Progr. Theor. Phys. 57, 146 (1975)

[5] B.A. Akimov, N.B. Brandt, S.A.Bogoslovskii, L.I.Ryabova, S.M. Chudinov, JETP Letters 29, 9 (1979)

[6] M.A. Lampert, P. Mark, Current Injection in Solids. N.-Y. Academic Press, 1970, 351p

[7] A.E. Klimov, V.N. Shumsky, Ferroelectrics – Physical Effects, ed. by M. Lallart, Chapter 23, InTech, Rijeka, Croatia, 2011, p.527

[8] A. Klimov, V. Shumsky, and V. Epov, Surface Sciences Symposium, March 11-17, 2012, St. Christoph am Arlberg, Austria, p. 75 (2012)

[9] Su-Yang Xu, Chang Liu, N. Alidoust et. al., Nat. Commun. 3, 1192 (2012)

[10] S. Safaei, P. Kacman, and R. Buczko, Phys. Rev. B 88, 045305 (2013)

# Friction remembers

S.Yu. Krylov [1], D.W. van Baarle, and J.W.M. Frenken

*Kamerlingh Onnes Laboratory, Leiden University, P.O. Box 9504, 2300 RA Leiden, The Netherlands*
*(corresponding author: S.Yu.Krylov, e-mail: krylov@physics.LeidenUniv.nl)*

[1] *Institute of Physical Chemistry and Electrochemistry, Russian Academy of Sciences, Leninsky prospect 31, 119071 Moscow, Russia*

Atomic resolution obtained in friction force microscopy (FFM) experiments (see, e.g., [1]) is based on regular stick-slip motion of a sharp tip with respect to the surface lattice periodicity. The traditional description of atomic-scale friction in terms of mechanical stick-slip instabilities appears so successful, that it obscures the actual mechanisms of energy dissipation. Recently we have shown [2,3] that the mere fact that atomic stick-slip patterns are readily observed in experiments implies that the inherent dissipation rate is close to the characteristic frequency of the measuring system (nearly critical damping). This observation seems to defy common sense, since the inherent dissipation rate is dominated by the characteristic frequency of the macroscopic system, i.e. by the flexibility and mass of the measuring system, rather than by the microscopic properties of the tip-substrate contact.

We propose that the observed paradox stems from the essential role of memory effects in the dissipation process. Traditionally, one assumes that the dissipative force is simply linear in velocity $\dot{x}$, with constant damping factor $\eta$ (the dissipation rate),

$$F_{\text{diss}} = -M\eta\dot{x} \qquad (1)$$

(mass $M$ of the moving object is introduced in (1) by formal reasons to provide $\eta$ with the convenient dimensionality of frequency). This implies that thermal noise is white (δ-correlated) and memory effects can be neglected. To our knowledge, however, the applicability of this approximation to atomic scale friction has never been properly justified. Indirect indications for the possibly pronounced role of memory effects have been found in a model system of a particle coupled to a large system of oscillators, see [4] and references therein.

If there is no clear separation between the system relaxation time and the noise correlation time, nonequilibrium statistical mechanics dictates (see, e.g., [4]) that the dissipative force can be non-linear in velocity and can depend on its values in previous moments of time,

$$F_{\text{diss}}(t) = -M\int_{-\infty}^{t}\hat{\eta}(t-\tau)\dot{x}(\tau)d\tau \qquad (2)$$

The memory function $\hat{\eta}(t-\tau)$ is related with the noise correlation function via the fluctuation-dissipation theorem. If memory effects are important, the usage of the linear form of (1) implies that the description is coarsened, i.e. averaged over a sufficiently long time

interval. For an oscillator (the FFM tip) interacting with a solid surface, the characteristic time interval is related with the period of its vibration. Replacing the velocity $\dot{x}$ by its mean value during half a period, we retrieve the familiar form of the dissipative force (1) from the general form (2), but with $\eta$ replaced by the mean dissipation rate characteristic for the specific type of motion considered. In this way, the damping factor in the approximation of Eq. (1) directly acquires a dependence on the characteristic frequency. This dependence results from the coarsening that is inherent in (1), and it provides a clue to understanding the nearly critical damping.

We propose an atomistic model of frictional energy dissipation that allows to elucidate the origin of memory. Our approach is based on the concept of a dynamical deformation pattern (DDP). When an object (the tip apex) is in contact with the surface, there is local deformation of the substrate lattice. This deformation pattern follows the object upon its motion along the surface. Dynamical deformation of the lattice is an essentially dissipative process, as it is accompanied by the creation of phonons, with their subsequent thermalization. In this picture, energy dissipates not due to motion of the object with respect to the surface but due to the motion of the object together with the dynamical deformation pattern with respect to ideal non-deformed lattice. In other words, the dissipation is related with damping of the induced motion of solid atoms which are currently involved into the DDP.

At first glance, the effective size of DDP can seem very small, since the (static) deformation of the substrate lattice rapidly decays with distance $n$ from the contact (in units of atomic spacing $a$), typically as $n^{-2}$ (when $n$ is large compared to the contact size). However, the number of solid atoms at distance $n$ from the contact scales as $n^2$, and these two trends compensate each other. Consequently, DDP can be—in principal—infinitely large, and its actual effective size should be determined by some more subtle effects. Apparently, this is the system history that determines which atoms of the solid have already been involved into collective motion with the object and which not. This physics is at the origin of the velocity dependent memory function $\hat{\eta}(t-\tau)$ in the general expression (2).

For an oscillator (the FFM tip), the effective DDP includes atoms which have been involved in concerted motion during half the period of its vibration. As a consequence, calculations show that the mean dissipation rate turns out to be close to the characteristic frequency, thus giving a natural explanation to the paradox of nearly critical damping.

Supports of the European Commission (Grant ERC-2010-AdG_20100224) and the Foundation for Fundamental Research on Matter (FOM, The Netherlands) are gratefully acknowledged.

[1] R. W. Carpick and M. Salmeron, Chem. Rev. 97, 1163 (1997)

[2] S. Yu. Krylov and J. W. M. Frenken, Colloid Journal 74, 569 (2012)

[3] S.Yu. Krylov, D.W. van Baarle, and J.W.M. Frenken, in J. Gustafson and E. Lundgren (eds), 3S'13, Int. Symposium on Surface Science 2013, Contributions, p. 25-26 (Lund University, 2013)

[4] P. Hänggi, P. Talkner, and M. Borkovec, Rev. Mod. Phys. 62, 251 (1990).

# Classical simulations for surface-streaking experiments

C. Lemell, K. Tökesi[1], and J. Burgdörfer

*Institute for Theoretical Physics, Vienna University of Technology, Vienna, Austria*
*(corresponding author: C. Lemell, e-mail: lemell@concord.itp.tuwien.ac.at)*

[1] *Institute of Nuclear Research of the Hungarian Academy of Sciences (ATOMKI), 4001 Debrecen, Hungary*

The development of experimental timing techniques working on the attosecond time scale have given access to the time-resolved observation of the photoelectric effect with intention to measure the intrinsic duration of the photoexcitation process in experiments using targets from single atoms to solids. Current experimental setups are based on the idea that an electron excited by an XUV pump pulse "feels" the electric field of an IR probe pulse starting from the moment of emission. Under this assumption a direct mapping of final energy (momentum) and emission time can be established.

In the case of atoms, the measured (apparent) time delay between different photoemission lines could be shown to be predominantly composed of a quantum mechanical part (Wigner-Smith-Eisenbud phase shift) and a transport related (classical) part due to the motion of the particle in the combined fields of the probing laser pulse and the ionic core left behind. Depending on the energy of the released electron apparent time delays of tens of attoseconds were measured and simulated [1].

Detailed analysis of the observed relative time delay of photoemission from solid surfaces is prohibitively complicated due to the size of the system (number of particles involved) and the different origin of the emitted electrons (core vs. valence band electrons). Additionally, large relative delays of about 100 as have been reported for the emission of tungsten core and valence band states [2]. In agreement with most recent experimental results [3] our simulations explain the measured delay essentially as transport phenomena within the target material [4].

Central to our simulation method is the ballistic transport of electrons after excitation. The velocity of the electrons is usually deduced from the free-particle dispersion relation (in atomic units) but could be easily changed to reflect the true band structure of the crystal where available. This, however, is so far not the case for the investigated systems at electron energies between 50 and 100 eV. Therefore, deviations of the simulated data from the experimental results may serve as an indicator for a more complex band structure in this high-energy regime and may serve as an indirect way to measure the dispersion relation by varying the XUV energy of the pump pulse.

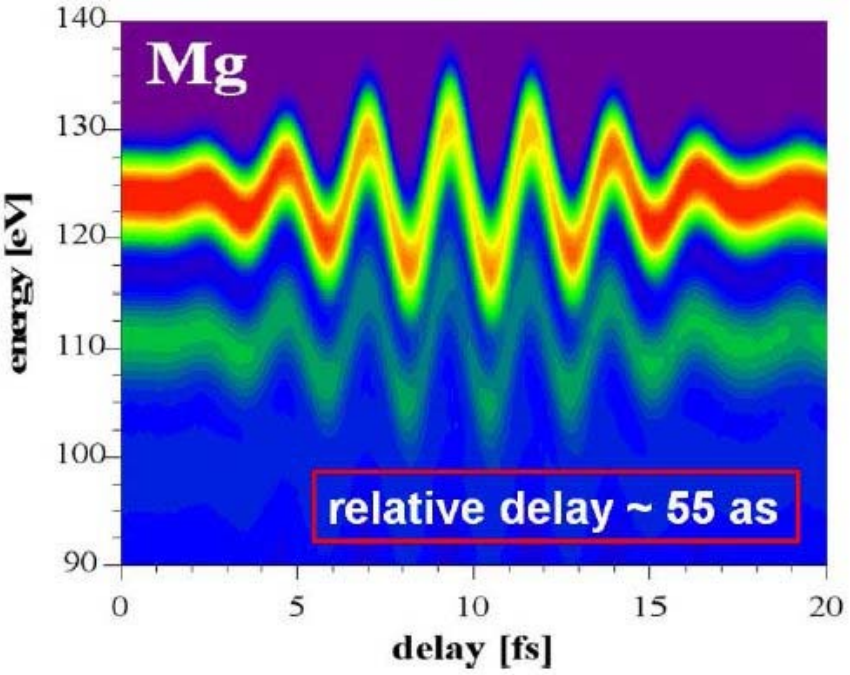


Streaking spectrum of bulk Mg. Two well separated lines from excited conduction band electrons can be observed. Top line: no energy loss; bottom line: electrons have excited a plasmon in the electron gas. The relative delay is about 55 as.

In our recent simulations we have concentrated on the following model systems: single monolayer oxygen on tungsten, single crystal Mg, and Mg covered tungsten surfaces with coverages from 1 to 4 monolayers [5]. Significant relative delays between the emission of core and valence band states allow for a test of our model. In my presentation I will discuss details of our simulation method, show simulation results, and present suggestions for future experiments.

This work was supported by the Austrian Fonds zur Förderung der wissenschaftlichen Forschung under Grants No. FWF-SFB016 “ADLIS” and No. 17449, the European ITS-LEIF network under Grant No. RII3#026015, and the TeT under Grant No. AT-7/2007. One of us (K.T.) was also partially supported by the grant “Bolyai” from the Hungarian Academy of Sciences and the Hungarian National Office for Research and Technology. We thank the group of R. Kienberger MPQ Garching for making their latest data available to us prior to publication.

[1] S. Nagele, R Pazourek, J Feist, K Doblhoff-Dier, C Lemell, K Tőkési and J Burgdörfer, J. Phys. B. **44**, 081001 (2011).

[2] A. L. Cavalieri, N. Müller, Th. Uphues, V. S. Yakovlev, A. Baltuka, B. Horvath, B. Schmidt, L. Blümel, R. Holzwarth, S. Hendel, M. Drescher, U. Kleineberg, P. M. Echenique, R. Kienberger, F. Krausz and U. Heinzmann, Nature **449**, 1029 (2007).

[3] S. Neppl, R. Ernstorfer, E. M. Bothschafter, A. L. Cavalieri, D. Menzel, J. V. Barth, F. Krausz, R. Kienberger, and P. Feulner, Phys. Rev. Lett. **109**, 087401 (2012).

[4] C. Lemell, B. Solleder, K. Tőkési, and J. Burgdörfer, Phys. Rev. A **79**, 062901 (2009).

[5] S. Neppl, PhD thesis, http://mediatum.ub.tum.de/doc/1093402/, (2012).

# Aluminum oxide formation and stability

F. Bertram [(1)], L. Rulik [(1)], F. Zhang [(2)], J. Evertsson [(1)], A. Mikkelsen[(1)], E. Lundgren[(1)], F. Carla [(3)], J. Pan [(2)]

*(corresponding author: E. Lundgren, e-mail: edvin.lundgren@sljus.lu.se)*

*[(1)] Div. of Synchrotron Radiation Research, Institute of Physics, Lund University, Sweden*
*[(2)] KTH, Department of Chemistry, Division of Surface and Corrosion Science, 10044 Stockholm, Sweden*
*[(3)] ESRF, B. P. 220, 38043 Grenoble, France*

Aluminum and aluminum alloys are used in a broad range of everyday commercial products as well as of interest in future microelectronics. As a result of the attractive properties of Al, extensive research on Al has been made for a long time, focusing both on applied as well as on basic research, with the ultimate aim on improved Al products. For instance, it has since long been realized that the corrosion resistance of Al is dependent upon a naturally protective oxide film [1] formed in air at room temperature. The oxide film is naturally self-renewing and accidental abrasion or other mechanical damage of the surface film is rapidly self-repaired by re-oxidation. The detailed properties of this oxide film are crucial for the corrosion protection, in particular in aggressive environments, and the oxide film formation has therefore received enormous attention [2]. Surface science studies have provided detailed information on the initial formation of the low temperature protective oxide using highly controlled ultra high vacuum conditions and well-prepared single crystal surfaces [3-7] as well by using theoretical means [8].

However, many applications for Al require increased corrosion protection for better durability. This can be obtained by increasing the thickness of the protective oxide by electrochemical means using anodization. Anodization is the electrochemical growth of an oxide by applying a potential to the aluminum in an electrolyte. Much less is known about the atomic scale structures and chemical processes occurring on Al surfaces under these conditions, since it is necessary to perform measurements during the electrochemical reaction and the process of forming a thick anodic oxide.

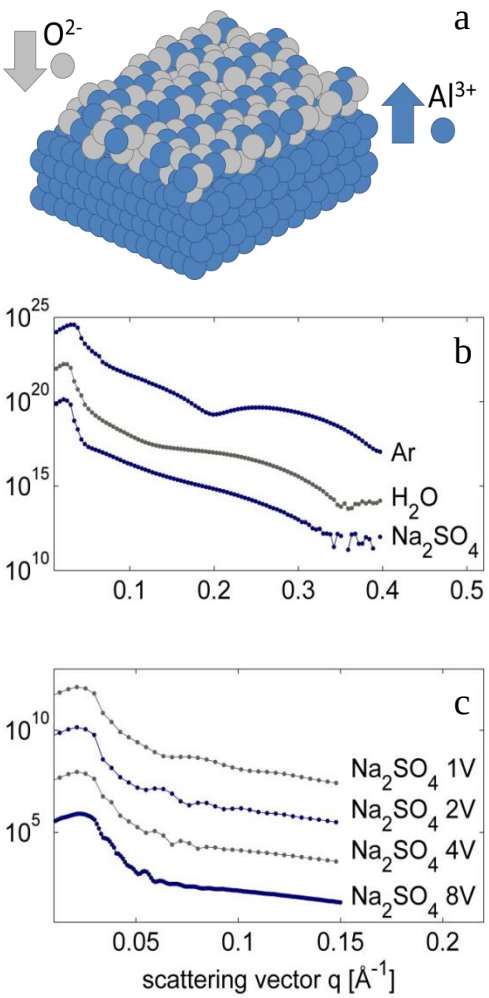


**Figure 1:** a) Illustration of the anodization process. By applying a voltage Al ions are dissolved from the Al surface and reacting with oxygen ions from the electrolyte. b) XRR measurements of an Al single crystal with native oxide in argon, water, and sodium sulphate. c) XRR measurements performed during anodization of the single crystal. The thickness increases from ~3nm (native oxide) up to ~80nm (at 8V).

On the other hand, the protective alumina film may be a great challenge in important processing stages of aluminum products. For instance in the brazing process of aluminum, which is extremely important for aluminum based heat exchangers, the oxide barrier is instead an obstacle for a perfect result. Therefore, to improve on the brazing of aluminum requires the detailed understanding of oxide morphologies and how the oxide breaks up/melts during heating to mimic the liquid braze melt formed in the process of generating solid metallic joints.

In this contribution, we will present recent results from in situ reflectivity measurements from aluminum single crystals and industrial aluminum polycrystalline alloys during anodization (see Fig. 1). Our measurements show that we can extract structural information while growing alumina film in the electrochemical cell. We will also present a combined XPS/PEEM study while heating commercial aluminum alloys to study the segregation properties and ultimate oxide break-up/melting on the microscopic scale.

**References**

[1] N. Cabrera and N. F. Mott, Rep. Prog. Phys. **12** 163 (1948).
[2] F. P. Fehlner and N. F. Mott. Oxid. Met. **2** 59 (1970).
[3] C. F. McConville, D. L. Seymour, D. P. Woodruff, and S. Bao, Surf. Sci. **188**, 1, (1987)
[4] H. Brune, J. Wintterlin, R. J. Behm, and G. Ertl, Phys. Rev. Lett. **68**, 624 (1992).
[5] C. Berg, S. Raaen, A. Borg, J. N. Andersen, E. Lundgren, and R. Nyholm, Phys. Rev. B. **47**, 13063 (1993).
[6] N. Cai and G. Zhou, K. Muller and D. E. Starr, PRL **107**, 035502 (2011)
[7] N. Cai and G. Zhou, K. Muller and D. E. Starr, Phys. Rev. B **84**, 125445 (2011)
[8] A. Hasnaoui, O. Politano, J. M. Salazar, and G. Aral Phys. Rev. B **73**, 035427 (2006).

# Ultra-thin FeO films grown on Ag(100)

L.R. Merte, S. Ataran, M. Shipilin, S. Blomberg, J. Gustafson and E. Lundgren

*Div. of Synchrotron Radiation Research, Lund University, SE-22100 Lund, Sweden*
*(Corresponding author: L.R. Merte, email: lindsay.merte@sljus.lu.se)*

Monolayer-thick FeO films are intriguing materials from the perspective of surface chemistry and catalysis. In particular, due to structural flexibility and charge transfer between the films and the underlying metallic surfaces, both electropositive and electronegative species may be stably adsorbed, the latter case involving a local inversion of the film's polarity, with Fe ions reversibly flipping their positions [1]. Incorporation of excess oxygen into the film, without dewetting, is possible by formation of an O-Fe-O trilayer phase [2] as well as oxygen-rich 1D dislocation defects [3], and such oxygen-enriched FeO films have been implicated as a highly active phase in oxidation catalysis [4].

Previous studies on a variety of substrates have shown that FeO grows preferentially with a hexagonal (111)-like orientation, even on square Pt(100) surfaces [5], and despite the initial expectation that a polar rock-salt (111) termination should be less stable than a nonpolar (100) termination. This common structure is stabilized in a polar state by charge transfer from the film to the surface [6, 7], and hence the films' electronic and chemical properties should be tunable to some extent by changing the metal substrate. Even more significant effects should be expected upon changing from 3-fold triangular to 4-fold square coordination, as in the case of a FeO(100)-like monolayer film, though such a film has not, to our knowledge, been reported to date.

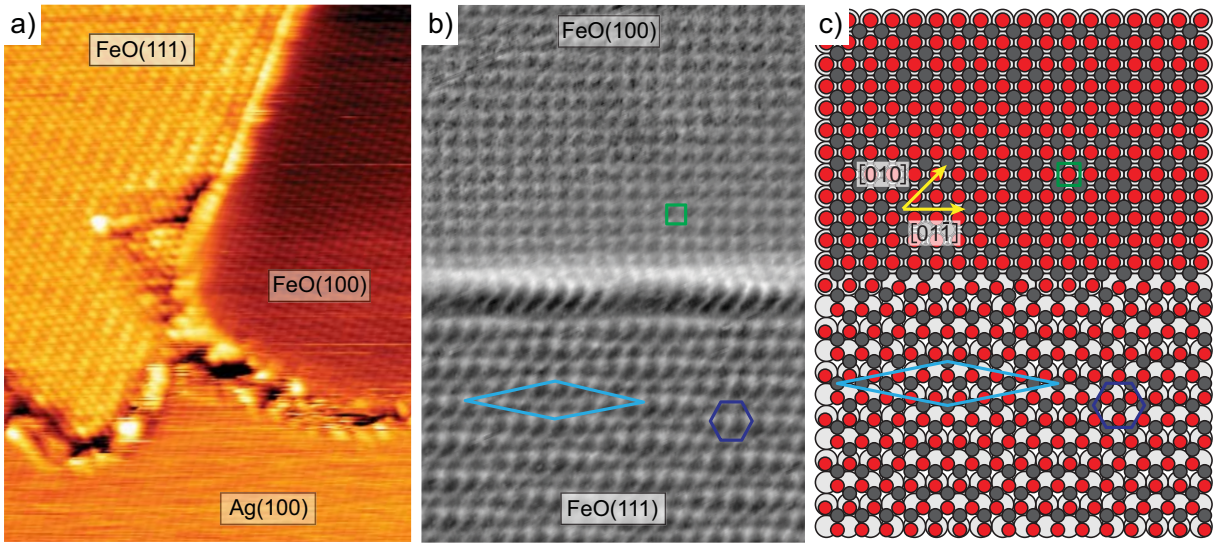


Figure 1. a) STM i mage (1.5 V, 1.0 nA) of square "(100)" and hexagonal "(111)" FeO layers on Ag(100). b) STM image (1.5 V, 1.0 nA, differentiated contrast) of a djacent square and he xagonal FeO dom ains. (1×1) (green) and c(2×10) (light blue) unit cells are indicated, along with the hexagonal basis of the latter structure (dark blue). c) Schematic model corresponding to b).

With the aim of elucidating the effects of the substrate on the chemical properties of ultra-thin FeO films, we have investigated the growth of FeO on Ag(100). This surface exhibits a) a significantly smaller work function compared to the most heavily-studied Pt(111), which should lead to significant differences in chemical properties for a (111)-like film, and b) a small lattice mismatch with bulk FeO, potentially enabling production of (100)-like films of monolayer thickness.

Figure 1(a,b) show STM images of FeO grown on Ag(100) by reactive deposition of Fe in an $O_2$ ambient. We observe coexisting quasi-hexagonal c(2×10) and pseudomorphic (1×1) phases, assigned tentatively to FeO(111) and FeO(100) films, respectively. The domains are typically joined by atomically smooth domain boundaries parallel to close-packed rows of the hexagonal phase, such that FeO(100) grains are rectangular, and are terminated along polar {011} directions (see Fig. 1c) , in contrast to e.g. MgO(100)/Ag(100), where only nonpolar {001} edges are observed. Differences in apparent height between the two phases are attributed to electronic effects, suggesting the development of a band gap in the FeO(100) phase in contrast to the metallic FeO(111) structure [6].

References

[1] J. Goniakowski *et al.*, Phys. Rev. B **80**, 125403 (2009).
[2] L. Giordano *et al.*, J. Phys. Chem. C **114**, 21504 (2010).
[3] H. Zeuthen *et al.*, J. Phys. Chem. C **117**, 15155 (2013).
[4] Y.-N. Sun *et al.*, Angew. Chem. Int. Ed. **49**, 4418 (2010).
[5] G. H. Vurens *et al.*, Surf. Sci. **268**, 170 (1992).
[6] L. Giordano *et al.*, Phys. Rev. B **76**, 75416 (2007).
[7] J. Goniakowski, and C. Noguera, Phys. Rev. B **79**, 155433 (2009).

# Surface stress induced by agglomerated impurities: the case of a Mo-Au alloy

R.V. Mom, M.J. Rost, J.W.M. Frenken, I.M.N. Groot

*Leiden Institute of Physics, Niels Bohrweg 2, 2300RA Leiden, The Netherlands*
*(corresponding author: R.V. Mom, e-mail:mom@physics.leidenuniv.nl)*

In an effort to bridge the materials gap, surface science is moving towards ever more complex systems. Besides the variety of structures in „real world“ materials, impurities may also play a key role in determining their properties. Since impurities in metals often tend to segregate, their surface properties are particularly affected.

To study the influence of agglomerated impurities on surface stress, an Au(111) crystal polluted with Mo was used. Although molybdenum dissolves poorly in bulk gold, a surface alloy can easily be formed [1]. At elevated temperatures, the bulk of the Au(111) crystal can also be contaminated [2]. Segregation of Mo from the bulk leads to molydenum nanorods encapsulated in gold just under the surface, as displayed in figure 1.

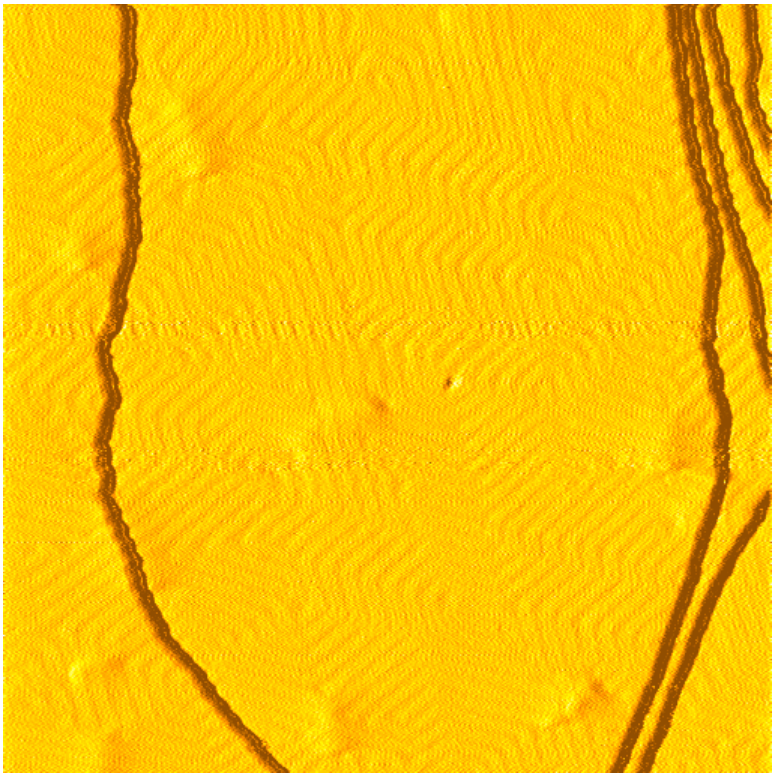

Figure 1: Differentiated STM image of Mo nanorods encapsulated in the Au(111) substrate. Size: 240x240nm

It has been shown that the herringbone reconstruction in Au(111) is very sensitive to factors like stress and chemical environment [3,4,5]. The reconstruction can respond to these by altering its periodicity [5] and/or its preferential direction [4]. For the case presented here, there is a clear influence on the directions observed in the herringbone.

We will discuss the nature of the perturbations in the herringbone, the length scales involved and the interplay with the orientation of the Mo nanorods.

This project is financially supported by a Dutch SmartMix grant and the NIMIC partner organizations through NIMIC, a public-private partnership.

[1] M.M. Biener, J. Biener, R. Schalek, C.M. Friend, Surface Science 594, 221 (2005)

[2] J.L. Murray, L.H. Bennett, H. Baker, Binary Alloy Phase Diagrams 1, 283 (1986)

[3] M.M. Biener, J. Biener, C.M. Friend, Surface Science 601, 1659 (2007)

[4] O. Schaff, A. K. Schmid, N. C. Bartelt, J. de la Figuera, R. Q. Hwang, Mat. Sci. and En. A319–321, 914 (2001)

[5] U. Tartaglino, E. Tosatti, D. Passerone, F. Ercolessi, Physical Review B 65, 241406 (2002)

# Combining Low-Energy Electron Microscopy and Scanning Probe Microscopy techniques for Surface Science

F. Cheynis, F. Leroy, A. Ranguis, B. Detailleur, P. Bindzi, P. Müller

Aix-Marseille Université, Centre Interdisciplinaire de Nanosciences de Marseille (CINaM), UMR 7325, Case 913, Campus de Luminy, 13288 Marseille Cedex 9, France

The recent interest for materials such as graphene, an ideal 2D material, has brought forward a clear need for complementary surface microscopies in the name of Low-Energy Electron Microscopy / Photo-Emitted Electron Microscopy (LEEM/PEEM) and Scanning Probe Microscopy (SPM) techniques. LEEM/PEEM allows to characterise in real time a crystalline surface at a mesoscopic lateral scale $2 - 150\,\mu m$. SPM gives access to a 3D quantitative topography at a lateral scale of a few 10 nm and for an acquisition time of typically 10-15min. To the best of our knowledge only three setups, combining under ultra-high vacuum (UHV), LEEM/PEEM and SPM exist around the world: I06 beamline at Diamond Light Source, UK [1], Univ. California, Davis, USA [2] and Univ. Montreal, Canada [3].

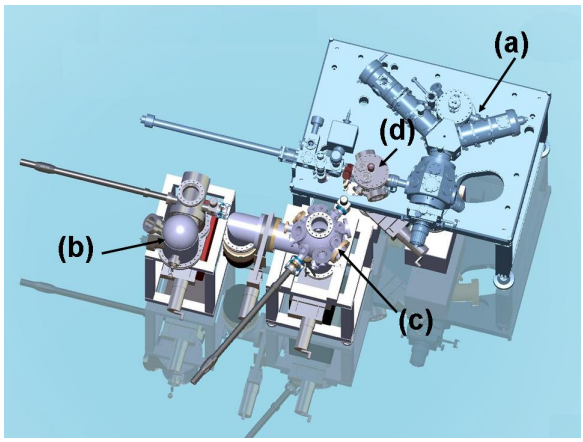


Figure 1: *Experimental setup*

In this poster we present the new setup recently installed at CINaM. It is composed of three main chambers including a Low-Energy ElectronMicroscope / Photo- Emitted Electron Microscopy (LEEM/PEEM, label a in Fig. 1), a variable-temperature Scanning Probe Microscope (vt-SPM, label b) and a sample surface preparation chamber (label c). Up to four sampleholders can be stored in a dedicated UHV chamber (label d). The samples can be outgassed by radiative heating up to typically 850K using a furnace. The samples can be introduced under UHV conditions using one of the two loadlocks located on a straight axis towards either the LEEM/PEEM or the vt-SPM techniques.

Our innovative approach has been to design a sampleholder preserving the optimal functionalities of both microscopes. More specifically, the sample is fixed on a Omicron SPM plate using spot-welded Ta wires or a spot-welded windowed Ta foil. This plate is in turn mounted on a modified Elmitec cartridge base made of Ti including a receptacle for the Omicron sample plate.

Demonstrations of the capabilities of the system is made by characterising a same sample surface with both available microscopy techniques. For instance on top of Fig.2 is shown a LEEM image of graphene on 6H-SiC(0001) (FOV=10 $\mu m$ and electron energy 20 eV). In Fig 2

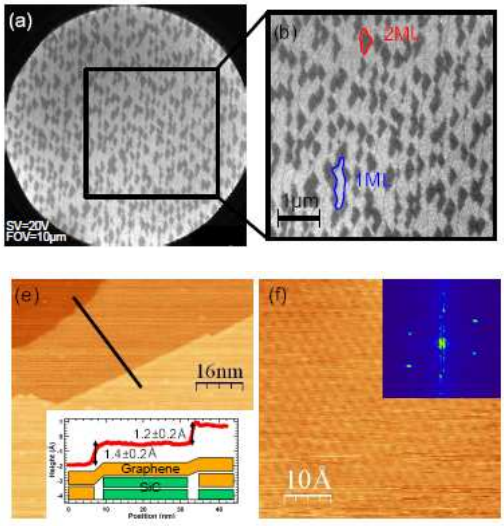


Figure 2: *LEEM and STM images of the same surface of graphene/SiC: on top LEEM images of graphene on 6H-SiC(001) obtained with a field of view of 10 µm and electron energy of 20 eV. Bottom: STM images of the same graphene surface. The inset shows the height profile along the black line and an interpretation of the local layer stacking matching the measured height steps.*

we also report a zoom exhibiting two distinctive domain contrasts. Bottom of Fig.2 corresponds to STM images of the same graphene surface (left: 80×80 $nm^2$ , V=4.1V, I=0.8 nA, z=0.9 nm; right: 5×5 $nm^2$ , V=1.7V, I=5.0 nA, z=0.2 nm). The inset shows the height profile along the black line and an interpretation of the local layer stacking matching the measured height steps. A 2D FFT of the image is also shown in the right inset.

## References

[1] [1] S. S. Dhesi, S. A. Cavill, A. Potenza, H. Marchetto, R. A. Mott, P. Steadman, A. Peach, E. L. Shepherd, X. Ren, U. H. Wagner, R. Reininger, AIP Conf. Proc. 1234 (2010) 311, online; accessed 8-October-2013.

[2] [2] C. L. H. Devlin, D. N. Futuba, A. Loui, J. D. Shine, S. Chiang, Mater. Sci Eng. B 96 (2002) 215–220.

[3] [3] Online; accessed 8-October-2013.

# Electronic stopping of slow light ions in transition metals

D. Roth, D. Goebl, and P. Bauer

*Institut für Experimentalphysik, Abteilung für Atom- und Oberflächenphysik,*
*Johannes Kepler Universität Linz, A-4040 Linz, Austria*
*(corresponding author: D. Roth, e-mail: dietmar.roth@jku.at)*

The energy loss of ions propagating in a solid has been under close investigation for many decades. The aim in this field of research is to achieve a profound understanding of ion-target interactions useful for a variety of applications, e.g. surface and thin film characterization by ion beam techniques, plasma-wall interactions relevant for nuclear fusion reactors or radiation therapy in medicine.

By convention, one distinguishes between two distinct energy-loss mechanisms due to which kinetic energy of the projectile is transferred to the target: either by repulsive Coulomb interaction with the nuclei (nuclear stopping) or by excitation of the electrons (electronic stopping). The resulting deceleration force $-\mathrm{d}E/\mathrm{d}x$ is called stopping power $S$; to overcome the density dependence of $S$, one usually introduces the electronic stopping cross section $\varepsilon$ related to $S$ via $\varepsilon = (1/n)\cdot S$, where $n$ denotes the atomic density of the target. While for high ion velocities electronic stopping is well understood [1, 2], unanswered questions still persist in the regime of low ion velocities.

For projectile velocities $v << v_F$, where $v_F$ denotes the Fermi velocity of the target electrons, only weakly bound conduction and valence electrons can be excited. Distinct effects in the electronic stopping power due to the electronic band structure have been observed. For metals without specific features in the band structure electrons can be described as free electron gas (FEG). Here, $S = Q(Z_1,r_s)\cdot v$, where $Q(Z_1,r_s)$ denotes the friction coefficient which depends on the atomic charge of the projectile $Z_1$ and the electron density described by the Wigner-Seitz radius $r_s$, respectively. $S$ exhibits deviations from velocity proportionality in materials with finite excitations thresholds due to their electronic structure, e.g. for the $d$-band in noble metals or the band gap in insulators. Experimentally, changes in the slope of $S$ were observed for transition and noble metals [3, 4]; in insulators, electronic stopping vanishes for velocities below a certain threshold velocity, $v_{th}$ [5, 6]. For He ions, additional energy loss mechanisms to electron-hole pair excitation, e.g. charge exchange cycles in Al [7], may contribute to the total electronic stopping cross section.

Recently, the role of $d$-electrons in electronic stopping of H and He in metals has been explored more closely by comparison of experimental Q values to DFT calculations [9,10]. For H ions in Cu, Au and Ag [11] which feature d-band offsets of 2 eV (Cu, Au) and 4 eV (Ag) with respect to the Fermi energy $E_F$, deviations from velocity proportionality of $S$ can be

explained as follows: at very low ion velocities $v < 0.2$ a.u., predominantly *s*- and *p*- electrons contribute efficiently to electronic stopping and $S$ is proportional to $v$. When $v > 0.2$ a.u., subsequent excitation of *d*-electrons leads to the experimentally observed changes in the slope of $S$. In order to get a more complete picture of electronic stopping in metals, in a next step it would be interesting to investigate electronic stopping in transition metals where $E_F$ is situated inside the *d*-band.

In this contribution we present electronic stopping of H and He ions in Pt and TiN deduced from experiments employing time-of-flight Low Energy Ion Scattering (LEIS) [12]. Both, Pt and TiN feature partially populated *d*-bands with a high density of states at the Fermi level and represent therefore suitable probes to investigate electronic energy loss in metals, where the *d*-electrons dominate the stopping process at low ion velocities.

Support by the Fonds zur Förderung der Wissenschaftlichen Forschung (FWF-Project P22587-N20) and provision of the TiN samples by Ion-TOF are gratefully acknowledged.

[1] C. P. Race, D. R. Mason, M. W. Finnis, W. M. C. Foulkes, A. P. Horsfield, and A. P. Sutton, Rep. Prog. Phys. **73**, 116501 (2010).

[2] P. Sigmund, Particle Penetration and Radiation Effects: General Aspects and Stopping of Swift Point Charges (Springer, Berlin, New York, 2008).

[3] S. N. Markin, D. Primetzhofer, S. Prusa, M. Brunmayr, G. Kowarik, F. Aumayr, and P. Bauer, Phys. Rev. B 78, 195122 (2008).

[4] S. N. Markin, D. Primetzhofer, M. Spitz, and P. Bauer, Phys. Rev. B 80, 205105 (2009).

[5] S. N. Markin, D. Primetzhofer, and P. Bauer, Phys. Rev. Lett. 103, 11, 113201 (2009).

[6] D. Primetzhofer, S.N. Markin, and P. Bauer, Nucl. Instr. Meth. B 269, 19, 2063-2066 (2011).

[7] D. Primetzhofer, S. Rund, D. Roth, D. Goebl, and P. Bauer, Phys. Rev. Lett. 107, 163201 (2011).

[9] P. M. Echenique, R. M. Nieminen, J. C. Ashley, and R. H. Ritchie, Phys. Rev. A 33, 897 (1986).

[10] J. I. Juaristi, M. Alducin, R. Díez Muiño, H. F. Busnengo, and A. Salin, Phys. Rev. Lett. 100, 116102 (2008).

[11] D. Goebl. D. Roth, and P. Bauer, Phys. Rev. A 87, 062903 (2013).

[12] H.H. Brongersma, M. Draxler, M. de Ridder, and P. Bauer, Surf. Sci. Rep. 62, 3: 63-109 (2007).

# On the electronic structure of Au(111), studied with density functional theory

Ari Paavo Seitsonen

*Institut für Chemie, Universität Zürich, Winterthurerstrasse 190, CH-8057 Zürich, Switzerland*

*(corresponding author: Ari P Seitsonen, e-mail: Ari.P.Seitsonen@iki.fi*

One of the basic properties of surfaces is their band structure, that may contain surface states, which are characteristic for the surface termination. They are sensitive to atomic and electronic modifications, and can be thus act as a probe for example to the surface reactivity.

On coinage metals Cu, Ag and Au there is a prominent surface state at and closeby the $\Gamma$ point of the Brillouin zone. This state is often detected in scanning tunnelling microscope images, even through adsorbed molecular or full layers of for example NaCl.

As the atomic geometry of the Herringbone reconstruction of Au(111) has already been studied using the Density Functional Theory (DFT) recently [1,2], we concentrate here on the electronic structure of the surface, and in particular the surface state. We have therefore performed DFT calculation both for the unreconstructed and reconstructed. Further we studied the influence of stacking faults, surface termination with hydrogen and capping with an insulating layer, for example *h*-BN.

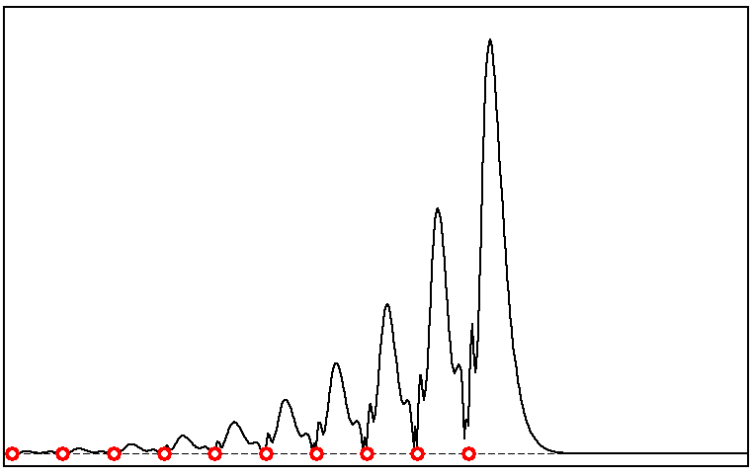

[1] "Simulation of the Au(111)-$(22 \times \sqrt{3})$ surface reconstruction", Yun Wang, Noel S Hush and Jeffrey R Reimers, *Phys. Rev. B*, **2007**, 75, 233416.

[2] "Structure and local reactivity of the Au(111) surface reconstruction", Felix Hanke and Jonas Björk, *Phys. Rev. B* 87, 235422 (2013)

# Interaction of slow highly charged ions with carbon nano membranes

Elisabeth Gruber, Richard A. Wilhelm*, Rene Heller*, Valerie Smejkal, Robert Ritter, Stefan Facsko* and Friedrich Aumayr

*Institute of Applied Physics, TU Wien – Vienna University of Technology, 1040 Vienna, Austria EU*
** Helmholtz-Zentrum Dresden-Rossendorf, 01328 Dresden, Germany, EU*

The ability of highly charged ions to induce various kinds of nanostructures at solid surfaces was intensively investigated within recent years [1 - 6]. Whether these nanostructures were hillocks, craters or of blister type they all had one thing in common: a pronounced dependency of their size on the projectiles potential energy and to a minor extend on their velocity. Thus by tuning the incident ions charge state the size of nanostructures can be precisely adjusted.

The mechanisms of nano-structuring by HCI impact were intensely investigated and especially for insulating surfaces of alkali and earth alkali crystals plausible models could be derived from extensive experimental results [1 - 4]. Thereby it turned out that the confinement of initial excitations by the relaxing projectile as well as the coupling of electronic excitations to the phononic system of the target play a major role in the formation of nanostructures [5]. However, a strong local confinement of electronic excitation is not exclusively present in insulators, but also by reducing dimensions of the interaction volume. This is literally achieved when going to 2D-materials.

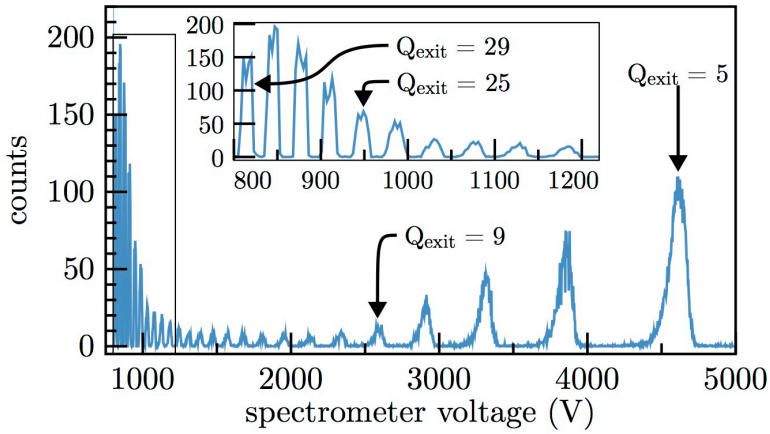


Figure 1: Charge state and energy loss spectrum of $Xe^{30+}$ ions after passing a CNM.

In the present contribution we therefore will show recent results of investigations on the nano structure formation by HCIs on 1nm thick freestanding carbon nano membranes (CNMs). We could successfully demonstrate the ability of HCI to create nano pores into CNMs with a diameter of a few nm, which is controllable by the projectile's charge state [6].

Beside these findings the use of a 2D material as a target offers another unique opportunity that was not available in all previous investigations on bulk materials: the ability to have a look onto the projectile after interaction with the surface.

We could access the HCIs charge and energy transfer to the surface during interaction by observing its energy and charge state distribution by means of an electrostatic analyzer (Fig.1). As a result of these investigations we will present energy loss and charge spectra of low energy (4keV…135keV) Xenon ions of various charge states (q=5+…40+) when passing through CNMs. Mechanisms to explain the experimental findings with special emphasis on the non-equilibrium charge state dependent energy loss of HCIs will be discussed.

Support by the Fonds zur Förderung der Wissenschaftlichen Forschung (projects I1114-N20) is gratefully acknowledged.

[1] A.S. El-Said, et al., Phys. Rev. Lett. 100, 237601 (2008)

[2] R. Heller, et al., Phys. Rev. Lett. 101, 096102 (2008)

[3] A.S. El-Said, et al., Phys. Rev. B 82, 033403 (2010)

[4] A.S. El-Said, et al., Phys. Rev. Lett. 109, 117602 (2012)

[5] F. Aumayr, et al., J.Phys.:Cond.Mat. 23, 393001 (2011)

[6] R. Ritter, et al., Appl. Phys. Lett. 102, 063112 (2013)

# Laterally-resolved reaction kinetics in CO oxidation on Pd: powder *versus* plane Pd(hkl) surfaces

Y Suchorski[1], M. Datler[1], I. Bespalov[1], R. Schlögl[2], G. Rupprechter[1]

[1]*Institute of Materials Chemistry, Vienna University of Technology, A-1210 Vienna, Austria*

[2]*Fritz-Haber-Institut der Max-Planck-Gesellschaft, D-14195 Berlin, Germany*

*(corresponding author: Y. Suchorski, e-mail: yuri.suchorski@imc.tuwien.ac.at)*

To answer the question whether the results obtained under "idealised" condition (UHV, single crystal surfaces) are applicable for the commercial catalysts (supported powder particles, ambient pressure) the manifold comparison of the catalytic behaviour of the powder and single crystal samples is necessary. A severe problem in such a comparison is the difficulty to create exactly the same conditions for both kinds of samples during the experiments. Another problem lies in the necessity to perform the laterally-resolved studies of reaction kinetics, since, in contrary to the single crystal studies, it is hardly possible to create a catalytic powder sample with spatially homogeneous properties.
We have demonstrated recently, that it is possible to provide exactly the same conditions and to obtain the laterally-resolved kinetic data (on a μm-scale) in CO oxidation on individual domains of a Pt or Pd foil by analysis of the local PEEM intensities during the reaction [1, 2]. The approach is based on the fact that the local photoemission yield during the reaction is related (via the local work function) to the CO or oxygen coverage. The mentioned coverage governs also directly the rate of the CO oxidation reaction [3]. Thus the analysis of the local photoemission yield (i.e. local PEEM intensity) might provide the local kinetic data. Simultaneously, the global kinetics can be monitored by mass-spectrometry (MS, Fig.1).

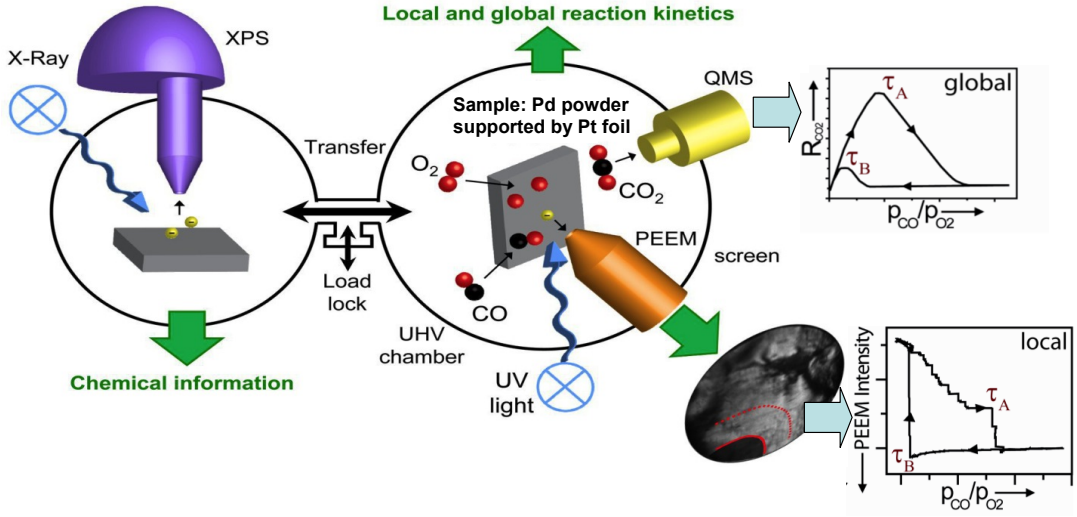


Fig.1. Experimental approach.

In present contribution, we apply this approach to Pd powder samples in order to compare the reaction behaviour of Pd powder with that of different Pd(hkl) domains of a polycrystalline Pd foil. To avoid the influence of the oxidic support and to reduce the materials gap problem to the question of the sole morphologic complexity, i.e. existence

of different kinds of active sites, the Pd powder was supported by Pt foil. The analysis of the local intensity of video-PEEM images recorded *in situ* during the catalytic CO oxidation in the $10^{-5}$ mbar pressure range yielded the local kinetic transitions between the high- and low-activity steady states on the individual domains of the Pt-support and on the Pd-powder agglomerates. Local kinetic transitions are accompanied by the reaction fronts which were observed for the first time in the CO oxidation on Pd-powder, as is illustrated by an oxygen front in Fig.2.

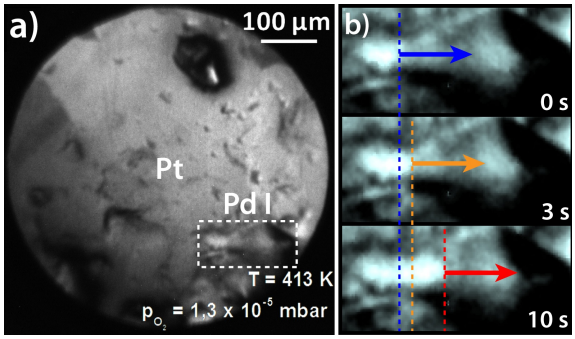


**Fig.2.** Oxygen front on a Pd powder agglomerate supported by a Pt foil.
a) An *in situ* PEEM-snapshot of the field of view during the CO oxidation.
b) PEEM-videoframes from a rectangular area marked in (a). Dashed lines mark the reaction front propagation.

Since the reaction behaviour of the Pd-powder appeared to be independent from the Pt-support, the local kinetic phase diagrams could be obtained separately for the Pd-powder and for the Pt(hkl)-domains at exactly the same experimental conditions (since in one experiment on one combined sample). The kinetic phase diagrams for the Pd-powder, obtained in this way, are compared with those of individual Pd(hkl)-domains of a polycrystalline Pd foil measured in independent experiments [2].
To study the role of defects, the kinetic phase diagrams for the Pd-powder are compared with the corresponding diagrams for the Pd(hkl) domains with artificially created surface defects (by $Ar^+$-sputtering of the annealed surface, [4]).

Support by the Fonds zur Förderung der Wissenschaftlichen Forschung (SFB-F45-04 FOXSI) is gratefully acknowledged. Authors also thank Johannes Frank (IMC, TU Vienna) for his technical support.

[1] Y. Suchorski, Ch. Spiel, D. Vogel, W. Drachsel, R. Schlögl, G. Rupprechter, Chem.Phys.Chem. 11 (2010) 3231
[2] D.Vogel, C. Spiel, Y. Suchorski, A. Trinchero, R. Schlögl, H. Grönbeck, G. Rupprechter, Angew. Chem. Int. Ed. 51 (2012) 10041
[3] G. Ertl, Science 254 (1991) 1750
[4] D. Vogel, C. Spiel, M. Schmid, M. Stöger-Pollach, R. Schlögl, Y. Suchorski, G. Rupprechter, J. Phys. Chem. C 117 (2013) 12054.

# Work function - mediated oxygen adsorption and oxidation of p-GaAs(Cs,O) – surfaces.

K.V. Toropetsky, H.E. Scheibler and A.S. Terekhov

*Rzhanov Institute of Semiconductor Physics Siberian Branch of Russian Academy of Sciences, 630090, Novosibirsk, Russia*

*(corresponding author: A.S. Terekhov, e-mail: terek@isp.nsc.ru)*

Cesium (Cs) – promoted oxygen adsorption on semiconductors surfaces was discovered long ago [1] and attracted considerable attention because of two reasons. At first, it enabled one to understand deeper the fundamental features of adsorption [1]. At second, it was practically used for the controllable low temperature oxidation of silicon and for the preparation of p-GaAs(Cs,O) – photocathodes with effective negative electron affinity. To describe the Cs – promoted dissociative oxygen adsorption, both local [2] and non – local [3] mechanisms of electron transfer from semiconductor surface to the antibonding $2\pi^*$ orbital of $O_2$ were proposed. The local mechanism assumes the direct transfer of electron from the Cs – atom to the oxygen molecular and its subsequent dissociation [2]. In this case the amount of adsorbed oxygen should be proportional to the Cs – coverage ($\theta_{Cs}$) [2]. The non-local nature of Cs-promoted oxygen adsorption dominates when electrons are transferred to the oxygen molecular via semiconductor surface band states [3]. In this case the work function $\mathbf{\Phi}$ mediates the amount of adsorbed oxygen [3]. The local nature of Cs-promoted oxygen adsorption on silicon was revealed experimentally [4]. The character of Cs – promoted oxygen adsorption on p-GaAs (Cs,O) – surface is not established up to now. Our previous experimental studies [5] of this topic demonstrated the influence of $\mathbf{\Phi}$ of the p-GaAs (Cs,O) – surface on the probability of oxygen adsorption, because the sticking coefficient of oxygen adsorption $\mathbf{S_{Ox}}$ decreased considerably, when $\mathbf{\Phi}$ p-GaAs (Cs,O) – surface exceeded some critical value $\mathbf{\Phi^*}\approx 3$ eV along with the increase of oxygen expose $\mathbf{D_{Ox}}$. On the other side, the latter observation was seemed to be in contrary with the well known Cs-promoted catalytic oxidation of p-GaAs(Cs,O) – surface, which was observed experimentally up to the very large $\mathbf{D_{Ox}}$.

In the present work we continued our study of Cs-promoted oxygen adsorption on p-GaAs and the catalytic oxidation of this surface and have found, that both these phenomena are basically controlled by the macroscopic work – function of p-GaAs(Cs,O) – surface. Therefore, the non – local character of both phenomena on p-GaAs(Cs,O) – surface was revealed. Experiments were performed by use of epitaxial p-GaAs - samples with (111) A,B – orientations, so that both As-terminated and Ga-terminated surfaces were studied. After removal of oxide layers by HCl – isopropanol solution under pure nitrogen atmosphere, GaAs - samples were transferred into XHV- chamber without contact with air. The base pressure in

this chamber was within ~ $4x10^{-9}$ Pa – range and was dominated by hydrogen. Both Cs and $O_2$ were produced by carefully outgassed and computer controlled dispensers. To evaluate cesium coverage $\theta_{Cs}$, the driven current of Cs dispenser was stabilized at the value, which provided the maximum of photocurrent from p-GaAs (Cs) - surface at the ~ 30 minute of operation. The $\mathbf{D_{Ox}}$ was calculated from measured $O_2$ – pressure. The amount of adsorbed oxygen was evaluated by the measurement of the variation of $\mathbf{\Phi}$ of p-GaAs(Cs,O) – surface after the $O_2$ – expose. The contribution of physically adsorbed oxygen was minimized by the measurement of $\mathbf{\Phi}(t)$ after the end of $O_2$ – expose. The $S_{Ox}$ was calculated from the equation $\Delta\mathbf{\Phi} = \mathbf{S_{Ox}}\times\mathbf{D_{Ox}}\times\mathbf{d_{Ox}}$, were $d_{Ox}$ – is the dipole moment of the adsorbed oxygen [6]. To determine $\mathbf{\Phi}$ of p-GaAs(Cs,O) – surface, the computer controlled UV-LED ($\hbar\omega = 280$ nm) illuminated the ~ 2 mm diameter spot at the center of GaAs and the energy distribution of emitted photoelectrons was measured by the retarding field technique. The $\mathbf{\Phi}$ was assumed to coincide with the energy position of low energy threshold of this distribution.

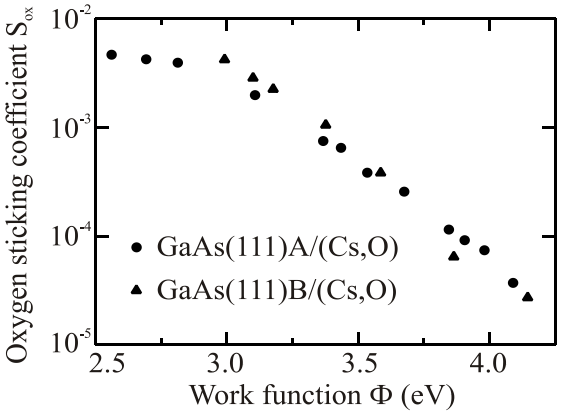


Figure 1

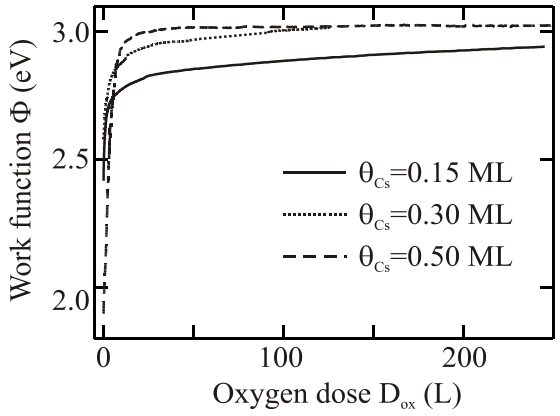


Figure 2

Fig. 1 demonstrates the $\mathbf{S_{Ox}(\Phi)}$ – curves, which were measured at p-GaAs(Cs,O) – surfaces with different stoichiometry. One can see, that $\mathbf{S_{Ox}}$ exponentially depends on $\mathbf{\Phi}$ and is not sensitive to the surface stoichiometry. These findings agree well with non – local character of Cs – promoted $O_2$ – adsorption at p-GaAs(Cs,O) – surfaces. Fig. 2 presents time evolutions of $\mathbf{\Phi}$ for three p-GaAs – samples with different $\theta_{Cs}$. One can see, that if $\theta_{Cs} < 0.5$ ML, $\mathbf{\Phi}$ is increased along with $\mathbf{D_{Ox}}$, while if $\theta_{Cs} = 0.5$ ML, $\mathbf{\Phi}$ does not depend on $D_{Ox}$. It means, that if $\mathbf{D_{Ox}}$ exceeded 40 L, the surface structure of (Cs,O) – layer is not varied along with growth of $\mathbf{D_{Ox}}$ and catalytic oxidation of GaAs occurs.

This work was supported by The Russian Foundation for Basic Research (grant № 12-02-00418-a).

[1] W. E. Spicer, I, Lindau, C.Y.Su, P.W. Chye, and P. Pianetta, Appl. Phys. Letters, 33, 934 (1978)
[2] J. E. Ortega, E. M. Oelling, J.Ferron, and R. Miranda, Phys. Rev. B 36, 6213(1987)
[3] H. I. Starnberg, P. Soukiassian and Z.Hurych, Phys. Rev. B 39, 12775 (1989)
[4] S. Nishigaki, T. Sasaki, S. Matsuda, N. Kawanishi, H. Takeda and K. Yamada, Surf. Sci. 242, 358 (1991)
[5] K.V. Toropetsky, O.E. Tereshchenko, A.S. Terekhov, JETP Letters 88, 520 (2008)
[6] T.U. Kampen, M. Eyckeler, W. Monch, Appl.Surf.Sci. 123/124, 28 (1998)

# Support-morphology induced modification of adsorbate bonding to nanoparticles

Oliver Yim[1], Chi Pang[1], Diego R. Hermoso[2], Ruben Perez[2], Geoff Thornton[1]

*1. London Centre for Nanotechnology*
*University College London*

*2. Departamento de Fisica Teorica de la Materia Condensada*
*Universidad Autonoma de Madrid*

Supported metal nanoparticles are frequently used as models of heterogeneous catalysts, with behaviour thought to be dependent on the nanoparticle size. Above a certain size it has generally been assumed that the nanoparticle behaves in the same way towards adsorbates as would a semi-infinite crystal. In this work, we examine this proposition using CO adsorption on Pd nanoparticles supported on $TiO_2$(110) using scanning tunnelling microscopy. The results show that the CO lateral registry differs from the single crystal. This phenomenon arises from a curvature of the nanoparticle that is caused by the underlying substrate step-edges. At a CO coverage of half a monolayer, two types of CO adlayer form in addition to those observed on the native Pd(111) surface. Density functional theory calculations suggest that their formation is driven by curvature-related strain.

# Ion Beam Induced Crystallographic and Magnetic Transformation of Fe Films on Cu(100)

Jonas Gloss[2], S.Shah Zaman[1], Zbynek Novotny[1], Michael Schmid[1], M. Urbanek[2],

Peter Varga[1,2]

[1] *Institute of Applied Physics (IAP),Vienna University of Technology (VUT), Vienna, Austria*

[2] *Central European Institute of Technology (CEITEC) at Brno University of Technology (BUT), Brno, Czech Republic*

It has been show before by LEED and also STM that 8ML Fe films grown on Cu(100) have an fcc structure[1,2,3] and it was known also that such a film is nonmagnetic at room temperature[3]. We could show by high resolution STM and also by LEED that in such a film bcc structured needles are formed by ion bombardment and that the number of this needles increases with ion dose[4] .

It could also be unambiguous confirmed by SMOKE [4] that this crystallographic transition is related also to a transition from paramagnetic to ferromagnetic structure. The influence of the ion energy was determined and experiments with $Kr^+$, $Xe^+$ (which showed transformation at much lower energy and dose as for using $Ar^+$ ion beams) and $He^+$ ions (which could not transform the fcc Fe into bcc at all) gave us the possibility to understand the mechanism. The best explanation could be given by applying the „thermal spike“ model[5] which assumes that the iron melts in a small volume along the ion trajectory and a certain (very low) probability exists that the molten Fe re-crystallize in bcc structure.

To produce nanostructures by ion beams we could make use of an ion beam lithography machine (CHARPAN)[6], which has been developed by Ion Micro Systems [IMS Nanofabrication AG , www.ims.co.at]. After irradiating the film in CHARPAN the resulting magnetic nanostructure was measured by using a Magnetic Force Microscope (MFM). By that we were able to produce structures of about 50 nm [4]. It was still not clear what limits the size of the structure because on the one hand the focusing of the ion beam seems to be not good enough and on the other hand the resolution of the magnetic force microscope may also be on the limit.

To find out if the transformation is limited by the irradiated area we performed an experiment in situ of the STM by using a nanostructured SiN mask (produced by the group of H.P.Oepen, University Hamburg) and irradiated with a parallel 2kev $Ar^+$ ion beam with a diameter of about 100mm. This SiN mask consits of several arrays of 80-nm diameter holes in 1mm distance. STM images showed that the transformation is mainly within the irradiated area [Fig. 1].

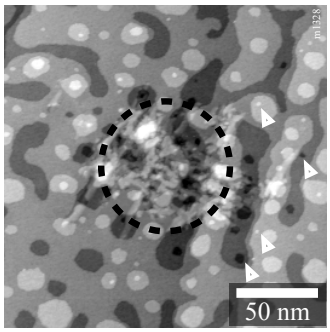


Fig.1 STM image of transformed fcc Fe in the area of one the 80 nm hole in the SiN mask (dotted circle) by 2keV $Ar^+$ ion beam (the bright needles are bcc and protrude only slightly out of the irradiated area)

Furthermore we grew much thicker fcc Fe films (up to 44 monolayers) by co-evaporation of Ni and/or using slightly increased CO pressure[7]. If the concentration of Ni and/or CO was too high, the film grew in a very stable fcc non magnetic structure and could not be transformed by ion bombardment any more. If the concentration of Ni and/or CO was too low the film grew from the beginning on in ferromagnetic bcc structure[7,8]. In Fig.3 a phase diagram is given which shows the possible combination of CO pressure and Ni concentrations for growing metastable nonmagnetic fcc Fe films which can be transformed by ion bombardment into ferromagnetic bcc structure.

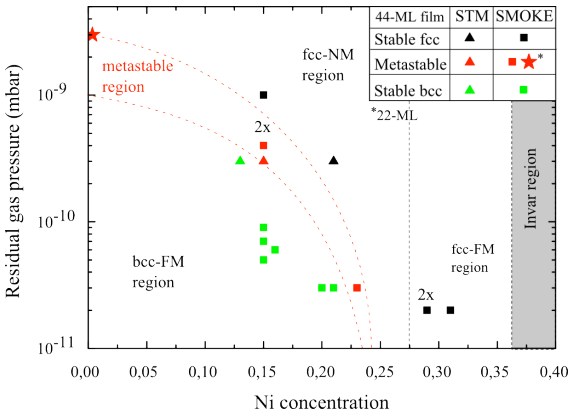


Fig.3 Experimentally determined phase diagram of the dependence of the structural and magnetic phases of $Fe_xNi_{1-x}$ films on Ni concentration and on the residual gas pressure during deposition. The data are combined from the experiments done in the SMOKE and STM UHV setups. The only CO stabilized 22-ML thick film is marked by an asterisk. Red dotted lines show approximately Ni concentration dependence of the boundaries of the metastable region. At Ni concentrations above 28% the films are fcc ferromagnetic (black dotted line).

Sameena Shah Zaman is thankful to Higher Education Commission (HEC) of Pakistan for financial support. This work was also funded by the Austrian Fonds zur Förderung der wissenschaftlichen Forschung (FWF). Michal Urbanek and Peter Varga acknowledge support by the European Regional Development Fund at CEITEC BUT (CEITEC – CZ.1.05/1.1.00/02.0068) and the Grant Agency of the Czech Republic (project no. P102/12/P443).

[1] A.Biedermann, M.Schmid, P.Varga, Phys. Rev. Lett.86 (2001) 464-467
[2] A.Biedermann, R.Tscheließnig, M.Schmid and P.Varga, Phys. Rev. Lett. 87 (2001)
[3] J.Thomassen, F.May, B.Feldmann, M.Wuttig and H.Ibach, Phys.Rev.Lett 69 (1992) 3831
[4] W. Rupp, A. Biedermann, B. Kamenik, R. Ritter, Ch. Klein, E. Platzgummer, M. Schmid, P. Varga, Appl. Phys.Lett. 93 (2008) 063102
[5] W. Schilling and H. Ullmaier, in Materials, Science, and Technology, Chemie, Weinheim, 1993,Vol. 10, pp. 180–241.
[6] E. Platzgummer, H. Loeschner, and G. Gross, Proc. SPIE 6730, 673033 2007.
[7] S. Shah Zaman, P. Dvorak, R. Ritter, A. Buchsbaum, D. Stickler, H.P. Oepen, M. Schmid, P. Varga J. Appl. Phys. 110 (2011) 024309
[8] J. Gloss, S. Shah Zaman, J. Jonner, Z. Novotny, M. Schmid, P. Varga, and M. Urbanek Appl. Phys.Lett 103(2013) 262405

# Effects of Al on epitaxial graphene grown on 6H-SiC(0001)

C. Xia , L. I. Johansson, A.A. Zakharov[1], L. Hultman, and C. Virojanadara

*Department of Physics, Chemistry, and Biology (IFM), Linköping University, S-581 83 Linköping, Sweden*
*(corresponding author: C. Virojanadara, email: chavi@ifm.liu.se)*

[1]*MAX-lab, Lund University, S-22100 Lund, Sweden*

Graphene, one single layer of graphite, is one of the most promising candidate materials for future electronic devices [1,2]. Especially epitaxial graphene grown on Si-terminated silicon carbide (SiC) substrates by thermal graphitization is considered one of the most convenient methods to obtain single layer graphene suitable for device operation at high temperature, high voltage environments. However, the choice of metal to be used as a contact material for graphene-based electronic devices is still an open question.

Aluminum (Al) is one of the common metals used in SiC-based electronics. It has been reported that Al-6H-SiC provides good rectification characteristics with low reverse leakage current [3]. Al is also easy to use, abundant in nature and inexpensive. It has, however, not yet been revealed if Al provides a good choice of contact material for graphene-based electronic devices. Al can form ternary compounds such as $Al_4SiC_4$ and $Al_4Si_2C_5$, having desirable ceramic properties [4]. Al can also change the electric field at the graphene/SiC interface and affect the surface band bending, which is crucial for rectifying devices. Single layer, i.e., single π-band, electronics or bi-layer graphene, two π-bands, electronics are typically carefully selected for specific devices. However, if this property can change just by varying the temperature by a few hundred degrees the device may be unreliable. Moreover, formation of different compounds at the graphene/SiC interface or on the graphene surface may change the intrinsic doping level and affect device properties. No detailed studies of the chemical composition, the surface morphology, the electronic structure and atomic structure before and after Al deposition on epitaxial graphene and after subsequent heating have been reported earlier. We therefore performed studies for the question if Al may provide a good choice of contact material for graphene-based devices.

Aluminum was deposited on epitaxial monolayer-grown graphene on SiC(0001) and the effects of annealing up to 1200 °C on the surface and interface morphology, chemical composition, and electron band structure were analyzed *in situ* by synchrotron-based techniques at the MAX Laboratory.

Monolayer graphene electronic properties were found to remain stable from room temperature up to ca. 300°C. Bilayer graphene properties were however detected after annealing at ca. 400°C. The Dirac point was found to shift slightly upwards towards the Fermi level upon heating. At higher temperatures, i.e. around 700-800°C, additional chemical reactions were observed to occur. The surface morphology and chemical composition in the surface region were investigated step-by-step using the low energy electron microscopy (LEEM) and photoemission electron microscopy

(PEEM) techniques. Selected area low energy electron diffraction (LEED) was used to collect the diffraction pattern from small selected areas. These results indicated different ordered phases on the surface and phase transition to occur at different annealing temperatures. These findings will be presented and discussed.

The authors gratefully acknowledge support from the Swedish Research Council #621-2011-4252 and Linnaeus Grant.

[1] A. K. Geim Graphene, Science 324, 1530 (2009)
[2] C. Berger, Z. Song, X. Li, X. Wu, N. Brown, C. Naud, D. Mayou, T. Li, J. Hass, A. N. Marchenkov, E. H. Conrad, P. N. First and W. De Heer, Science 312, 1191 (2006)
[3] K. Yasuda, T. Hayakawa and M. Saji, IEEE Trans. Electron Devices 34, 2002 (1987)
[4] A. Hussain, S. Aryal, P. Rulis, M. Choudhry and W. Ching, Phys. Rev. B 78, 195102 (2008)

# *Thursday*

# Electron beam induced surface activation for the lithographic fabrication of clean nanostructures

Florian Vollnhals[1], Tom Woolcot[2], Marie-Madeleine Walz[1], Martin Drost[1], Fan Tu[1], Esther Carrasco Burgos[1], Hans-Peter Steinrück[1], Geoff Thornton[2] and Hubertus Marbach[1]

[1] *Lehrstuhl für Physikalische Chemie II, Universität Erlangen-Nürnberg, Egerlandstr. 3, 91058 Erlangen, Germany,*
*(corresponding author: H. Marbach, e-mail: hubertus.marbach@fau.de)*

[2] *London Centre for Nanotechnology and Department of Chemistry, University College London, 17-19 Gordon Street, London WC1H 0AH, UK*

The extremely small spot size of modern focused electron beams does not only enable high resolution microscopy (SEM, TEM) but also make them ideal tools for the modification or generation of nanostructures. Focused electron beam induced processing (FEBIP) is for example the basis for state of the art mask repair tools in semiconductor industry or prototype circuit editing. The most prominent FEBIP technique is electron beam induced deposition (EBID) in which adsorbed precursor molecules are locally dissociated by the impact of the electron beam leaving a deposit of the non-volatile dissociation products on the surface [1]. A common problem in EBID is the unintended codeposition from residual gases or the precursor itself and thus the contamination of the deposit. With our distinct "surface science approach" to FEBIP we were able to overcome this problem and fabricate, e.g. , pure iron structures from the precursor ironpentacarbonyl, $Fe(CO)_5$ [2] It turned out that not only the reduction of residual gases in UHV is crucial but also the condition of the surface and the signature of the precursor in QMS determine the chemical composition of the deposit. For example on clean Rh(110) $Fe(CO)_5$ decomposes catalytically and continues to grow autocatalytically already at room temperature [2b].

Based on these findings we recently explored focused electron beam induced surface activation (FEBIA), a novel FEBIP technique [3-5]. Thereby, in a first step, the chemical properties of the surface are modified via the e-beam such that it becomes active towards the decomposition of certain precursor molecules. In a second step the surface is exposed to the precursor which decomposes at the preirradiated area and eventually continues to grow autocatalytically. We demonstrate the feasibility of FEBIA with $Fe(CO)_5$ for different oxide surfaces, e.g. $TiO_2$(110) [4] (Fig 1)and silica [3] and expand it to porphyrin layers on Ag(111) [5]. For the oxides the activation mechanism was identified as due to electron induced oxygen desorption and thus the generation of reactive oxygen vacancies [3,4]. For the organic layers it appears that reactive C species are formed. Interestingly we observe that FEBIA is much more efficient on porphyrin multilayers than on the respective monolayer (Fig. 2). This can be

related to the quenching of electron induced effects (like electron attachment) in the monolayer case due to the close proximity of the porphyrins to the Ag surface [5]. The underlying physical/chemical processes and potential applications of FEBIA will be discussed.

Support by the DFG through grant MA 4246/1-2, MA 4246/2-1/ research Unit funCOS, the Excellence Cluster "Engineering of Advanced Materials" and COST Action CM1301 (CELINA) is gratefully acknowledged.

[1] van Dorp, W. F.; Hagen, C. W., J. Appl. Phys. 104, 081301 (2008); Utke, I.; Hoffmann, P.; Melngailis, J., JVST B, 26, 1197 (2008); I. Utke, A. Gölzhäuser, Ang. Chem. Int. Ed., 49, 9328 (2010)

[2] Lukasczyk, T., M. Schirmer, H.P. Steinrück, and H. Marbach, a) SMALL, 4, 841 (2008) and b)Langmuir, 25, 11930 (2009)

[3] M.-M. Walz, M. Schirmer, F. Vollnhals, T. Lukasczyk, H.P. Steinrück, and H. Marbach, Ang. Chem. Int. Ed., 49, 4669 (2010) and PCCP, 13, 17333 (2011), M.-M. Walz, F. Vollnhals, F. Rietzler, M. Schirmer, H.P. Steinrück and H. Marbach, App. Phys. Lett., 100, 053118 (2012).

[4] F. Vollnhals, T. Woolcot, M.-M. Walz, S. Seiler, H.P. Steinrück G. Thornton and H. Marbach, J. Phys. Chem. C, 117, 17674 (2013)

[5] F. Vollnhals, P. Wintrich, M.-M. Walz, H.P. Steinrück and H. Marbach, Langmuir, 29, 12290 (2013)

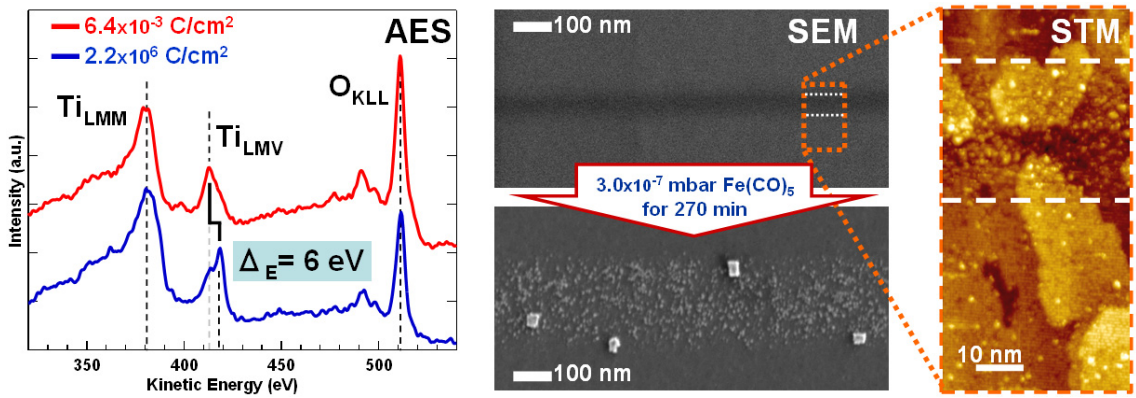


**Figure 1:** *EBISA on TiO2(110). Left: Auger electron spectra of the TiO2 surface after irradiation with a low and a high electron dose revealing the electron stimulated oxygen loss and the Ti signal shift from the oxidic to the metallic state. Center: SE micrographs of a line scan before (top) and after precursor dosage, demonstrating the growth of iron clusters and crystallites. Right: STM image of an electron irradiated line (dashed lines), showing the disorder and defects introduced by the focussed electron beam.*

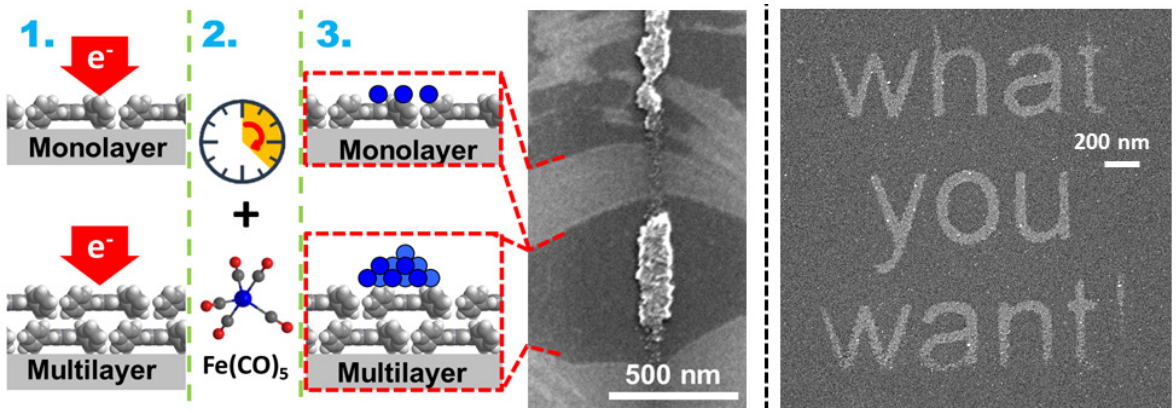


**Figure 2:** Left side: *Scheme and SEM image of FEBIA on porphyrin layers on Ag(111). The process is much more effective on the bilayer than on the monolayer as evidenced by the massive Fe deposits on the multilayer in the SEM micrograph. Right side: Fe deposits on an oxide surface fabricated with FEBIA demonstrating the ability to draw nanostructures with lithographic control.*

# Selective Deposition of Metallic and Semiconductor Nanostructures at Pre-patterned Surfaces

J. Mach, M. Kolíbal, T. Šamořil, J. Hulva, P. Mareš, M. Konečný, F. Ligmajer, R. Kalousek, T. Vystavěl[1], J. Spousta, P. Varga, and T. Šikola

*Inst. of Physical Engineering., Brno University of Technology, Technická 2, 616 69 Brno, Czech Rep. (corresponding author: T. Šikola, e-mail: sikola@fme.vutbr.cz)*

*CEITEC BUT, Brno University of Technology, Technická 10, 61669 Brno, Czech Republic*

*[1]FEI Company, Podnikatelská 6, 612 00 Brno, Czech Republic*

In our group we have been interested in fabrication of various functional nanostructures for plasmonics and spintronics. One of the useful techniques in this field is the selective growth of nanostructures making it possible to grow nanoparticles just at specific sites of our interest. This finds its application for instance in fabrication of ordered arrays of nanostructures, or in accurate placing of a nanoparticle into the vicinity of another one (e.g. SERS, Plasmon enhanced luminescence, etc.). To do it, a lot of surface science phenomena (e.g. adatom adsorption and desorption, surface tension, surface diffusion, nucleation, modification of surface termination groups,….) has to be properly exploited.

The selective growth generally represents a hybrid technique combining top down and bottom up approaches. The top down step is used for the pre-patterning of substrates in order to create nucleation centers for formation of nanostructures. The bottom up approach provides delivery of atoms to the pre-patterned substrates (usually by UHV evaporation). In our previous works we studied the selective growth carried out on Si samples pre-patterned either by AFM local anodic oxidation (Ga nanodroplet arrays, [1]) or focused ion beam modification (Co nanoparticles and nanowires, [2]).

In the contribution we will report on our recent results on the selective deposition of GaN nanocrystals and formation of Au nanoparticles.

As for the growth of GaN nanocrystals, the patterning of a native silicon oxide was performed by a Ga focused ion beam (FIB) to create nucleation centers in form of an array of pits and grooves. To synthesize GaN nanocrystals at the nucleation sites,, a sequential deposition of Ga thermal atoms and hyperthermal nitrogen ions (< 50 eV) was carried out under UHV conditions at 300°C using a special atom-ion beam source developed in our group [3]. The chemical composition of the nanocrystals was monitored in situ by XPS. The morphology of these crystals was studied by SEM and AFM related techniques. Using scanning confocal micro-spectroscopy, photoluminescence peaks from the nanocrystals were observed.

The selective deposition of nanoparticles need not be achieved only under vacuum conditions. To demonstrate it, we used a colloidal solution of gold nanoparticles representing technological building blocks of defined shapes and dimensions. First, the silicon substrate covered by native oxide was exposed to a charged particle beam (ions or electrons) in a dual beam microscope (SEM and FIB) and then immersed in a HF modified solution of colloidal nanoparticles (Fig. 1). The irradiation of the native oxide layer by a low-fluence charged particle beam caused changes in the type of surface terminating groups. Large fluencies of the beams caused even more profound modification of surface composition, most likely due to formation of carbon layers under high vacuum conditions. As a result, by a proper selection of the initial substrate termination, pH solution and beam fluence either positive or negative deposition of the colloidal nanoparticles was achieved [4].

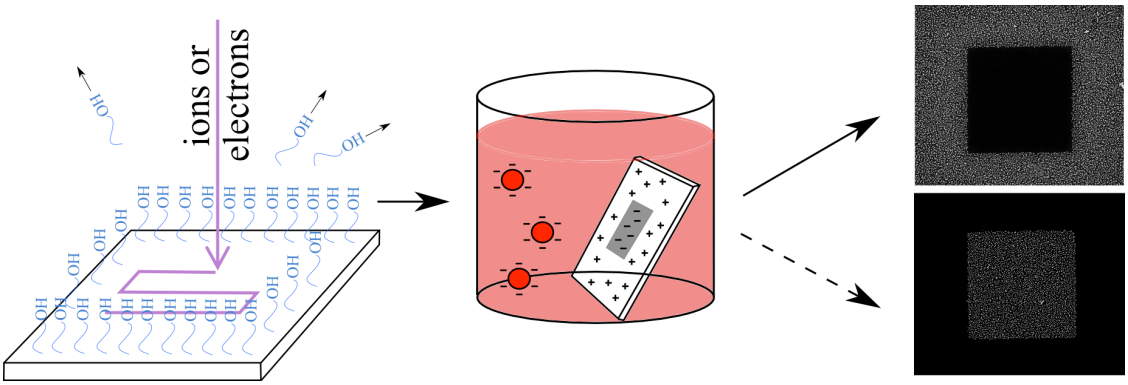


Fig. 1 Schematic of the selective deposition of Au nanoparticles from the coloidal solution.

[1] M. Bartošík, M. Kolíbal, J. Čechal, J. Mach, T. Šikola, J. Nanosci. Nanotechnology 9 (2009), 5887.

[2] J. Čechal, O. Tomanec, D. Škoda, K. Koňáková, T. Hrnčíř, J. Mach, M. Kolíbal, T. Šikola: J. Appl. Phys. 105 (2009), 084314.

[3] J. Mach, T. Šamořil, S. Voborný, M. Kolíbal, J. Zlámal, J. Spousta, L. Dittrichová, T. Šikola, Review of Scientific Instruments, 2011, 82, Vol. 8, 083302.

[4] M. Kolíbal, M. Konečný, F. Ligmajer, D. Škoda, T. Vystavěl, J. Zlámal, P. Varga, T. Šikola, ACS Nano 6(11), 2012, 10098.

# Pathways to surface-confined complex networks

*D. Écija, J.I. Urgel, A.C. Papageorgiou, S. Joshi, W. Auwärter, S. Klyatskaya, M. Ruben, A.P. Seitsonen, S. Fischer, S. Vijarayaraghavan, J. Reichert, K. Seufert, M.C. Aurisicchio, D. Bonifazi & J. V. Barth*

*Physik Department E20, Technische Universität München, 85748 Garching, Germany*

A major objective in modern surface science is the study of complex interfaces and the development protocols for their control, both in the static and dynamic regime. Fascinating examples regarding self-assembled networks on solid surfaces include hierarchical assemblies, pentagon tilings, or glassy 2D architectures. Related intricate chiral order phenomena have been elucidated and, in addition, quasicrystalline order has been observed in epitaxial and soft-matter self-assembled systems or polymers.

Herein we report advances towards surface-confined complex networks using metal-directed assembly on surfaces. This approach constitutes a versatile paradigm to design low-dimensional nanoarchitectures, frequently affording a favorable balance between robustness and spatial regularity. Specifically, we realized on-surface nanostructures and tesselations comprising (i) rare-earth metal centers and (ii) flexible molecular units. In both cases intriguing ordering phenomena unfold.

Following the first approach, by taking advantage of lanthanide centers for the engineering of surface coordination nanostructures and layers, we achieved a 2-D pattern known as the "semiregular snub square tiling", representing a molecular-level demonstration of one of the canonical tessellation patterns Johannes Kepler described more than 400 years ago (cf. Fig. 1). This becomes possible by fivefold Ce– (or Gd)-ligand CN-coordination motifs, which are planar and flexible, such that vertices connecting simultaneously trigonal and square polygons can be expressed. With the right concentration and stoichiometric ratio of rare-earth metal centers to ligands fully reticulated layers are expressed providing large domains of the prevailing snub square tiling. In addition minority tessellations occur related to motifs found for quasicrystalline surfaces.

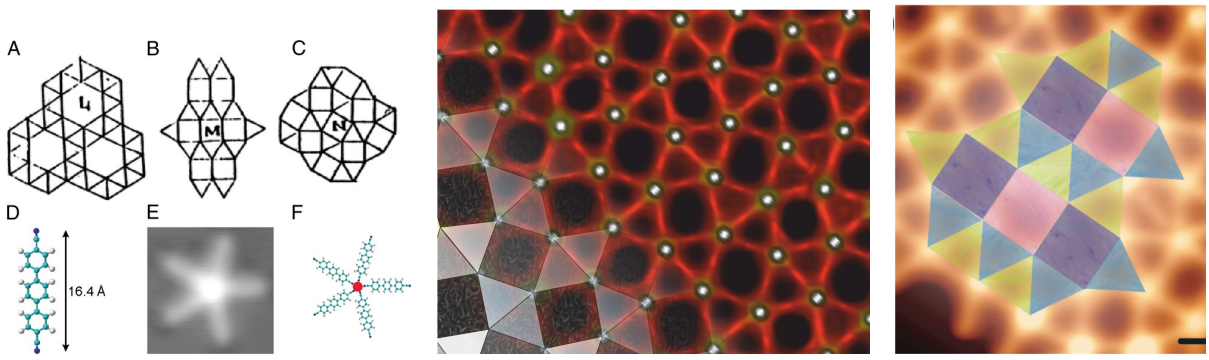


Fig. 1: Left panel: (A–C) Five-vertex Archimedean tilings of the plane as sketched by Johannes Kepler in *Harmonices Mundi*. (A) Snub hexagonal tiling, (B) elongated triangular tiling, and (C) snub square tiling. (D–F) Fivefold coordination node of cerium and carbonitrile linkers on Ag(111). (D) Paraterphenyl-dicarbonitrile; C (H, N) atoms in green (white, blue). (E and F) STM image and model of isolated pentameric Ce–carbonitrile coordination unit. Central and right panel : Five-vertex Archimedean surface tessellation by fully reticulated rare-earth-organic networks. The lanthanide-directed molecular self-assembly affords a semiregular snub square tiling (designated 3.3.4.3.4 with three triangles and two squares at each vertex) and a minority 3.3.3.4.4 scheme (Proc. Nat. Acad. Sci. 110,6678 (2013) and Urgel et al., subm.).

Regarding (ii) we notably investigated a 1,3,5-tris(pyridin-4-ylethynyl)benzene linker with three pyridyl groups connected to a central aryl ring through ethynyl moieties. The molecule is specifically equipped with pyridyl functional groups to steer a simultaneous expression of lateral pyri-dyl–pyridyl interactions and Cu–pyridyl coordination bonds. Carefully developed assembly protocols yield a new class of porous open assemblies, the formation of which is driven by multiple interactions, as illustrated in fig. 2.

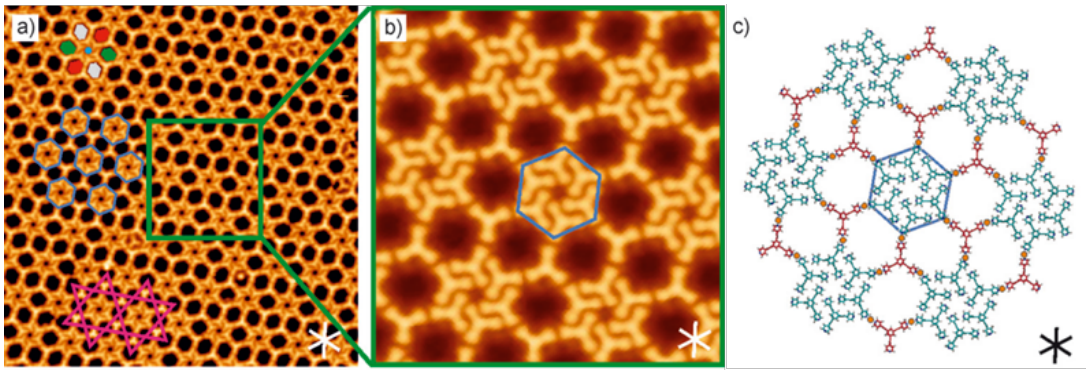


Fig. 2 Hierarchic molecular porous assembly based on multiple interactions. This commensurate network was obtained by the deposition of a tripod linker with three pyridyl groups and Cu atoms on Ag(111) for a local stoichiometric ratio of 0.75:1 (Cu/molecule). (Chem. Eur. J. 19 (2013) 14143)

The crucial influence of the underlying surface in the network formations is evidenced by using the same linker on Cu(111). Here we identified superlattice fromations interpreted in terms of 2D short-range disordered crystalline networks (cf. Fig. 3, left panel), i.e., sheet materials that displays a discrete diffraction diagram and present any of the following ordering characteristics: (1) the constituents are positioned following a crystalline lattice, but at the same time disordered with respect to their orientational or distortional degrees of freedom, or (2) the intermolecular links span a crystalline lattice, but the molecular building blocks present distortional or orientational short-range disorder. The STM data and detailed models in Fig. 3 (right panel) reveal the intruiging nature and complexity of such systems featuring in addition interesting dynamic properties where the flexibility comes into play.

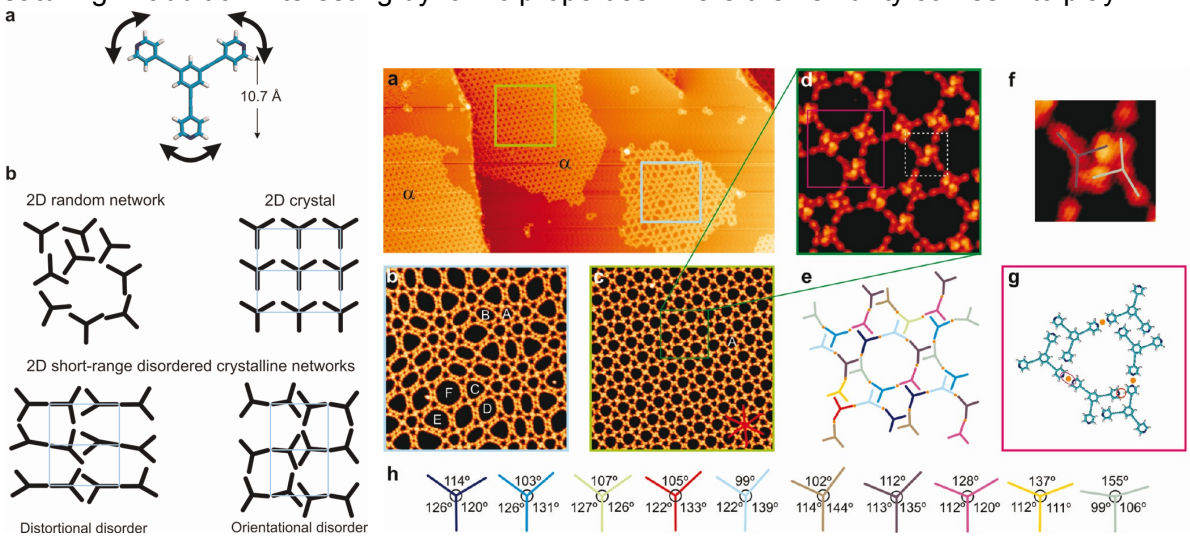


Fig. 3 Left: Types of assembly of a 2D supramolecular structure with different short- and long-range order characteristics for a tecton with 3-fold symmetry and geometrical flexibility; blue grid represents a crystalline lattice. Right: Metallosupramolecular 2D short-range distortional disordered crystalline networks on Cu(111) coexisting with a random phase. Molecular units exhibiting the same apparent opening angles are depicted with the same colors. Cu adatoms are represented by an orange circle. (ACS Nano. 6 (2012) 4258)

# Molecular Self-Assembly on Ag and Cu modified Au Surfaces: Intermolecular vs. Molecule-Substrate Interactions

H. Aitchison[1], H. Lu[2], S. Hogan[1], H. Früchtl[1], I. Cebula[3], M. Zharnikov[2], M. Buck[1]

[1]*EaStCHEM School of Chemistry, University of St Andrews, North Haugh, St Andrews KY16 9ST, United Kingdom*
[2]*Angewandte Physikalische Chemie, Universität Heidelberg, Im Neuenheimer Feld 253, 69120 Heidelberg, Germany*
[3]*Institute of Experimental Physics, University of Wroclaw, Pl. M. Borna 9, 50-204 Wroclaw, Poland,*

Aromatic carboxylic acids represent a versatile class of molecules for the self-assembly at interfaces as flexibility in the design of molecular structures combines favourably with the ability of carboxyl moieties to interact via hydrogen or metal-organic coordination bonding. This has been extensively exploited for the generation of two-dimensional supramolecular networks on surfaces both in a UHV environment and at the solid-liquid interface [1,2]. In contrast to these studies where molecules lie flat on the surface, reports on the self-assembly of aromatic carboxylic acids in a non-flat adsorption geometry are very scarce which is surprising as this opens up the third dimension [3]. One of the very few examples is the assembly of isophthalic acid (IPA, see Scheme 1, left) and trimesic acid (TMA) at the liquid/solid interface [4]. Involving coordination bonding of the carboxylate moiety to the substrate highly ordered monolayers are obtained. The film structures are crucially dependent on the strength of the molecule-substrate interaction which can be altered by electrochemical deposition of a mono/bilayer of Cu or Ag onto a Au(111)/mica substrate. This renders the inert Au surface reactive with Cu representing a more strongly interacting surface than Ag. The difference between the two metals is revealed by the striking difference in the structure of a TMA monolayer which yields a bipodal adsorption geometry in the case of Cu whereas on Ag a monopodal configuration is observed [5]. Reason is the substantial change in the relative strength of the intermolecular and molecule-substrate interactions. On Cu it is the latter which dominates whereas on Ag it is the former.

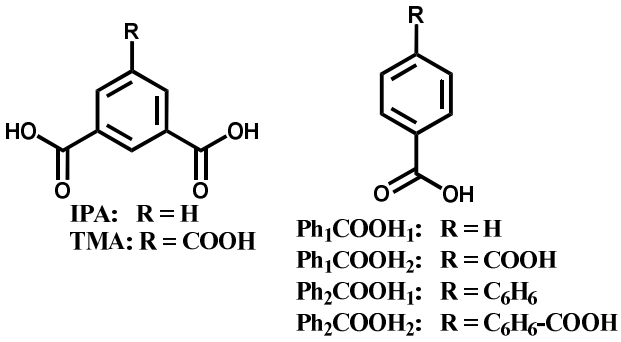


**Scheme 1**

Along our efforts to develop design strategies for coordination bonded monolayers of carboxylic acids a series of aromatic carboxylic acids was investigated by microscopy (STM),

spectroscopy (XPS, NEXAFS) and DFT calculations. The molecules studied differ in the number of COOH groups and phenyl rings (Scheme 1, right). Surprisingly, on Cu no ordered layers are formed whereas on Ag all molecules form highly organised layers as exemplified by Figure 1 which shows terephthalic acid.

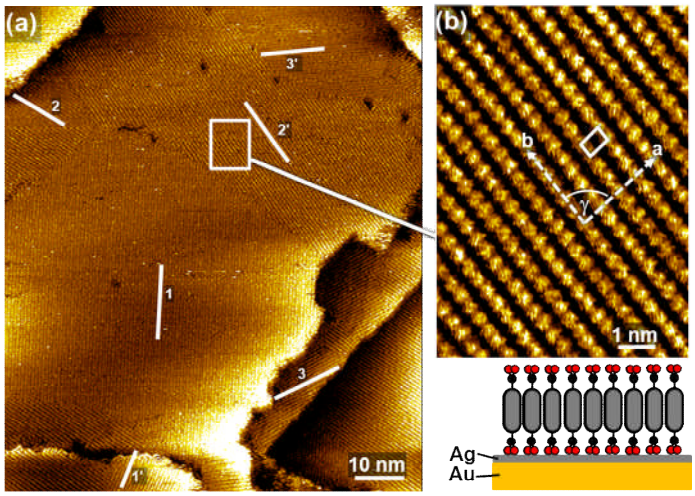


**Fig. 1:** STM image of terephthalic acid ($Ph_1COOH_2$) on Ag/Au(111)/mica. a) large scale image showing six domains which are related by rotational (1-3) and mirror symmetry (1'- 3'). Lines mark the directions of the rows of molecules. b) molecularly resolved image with the unit cell of the molecular lattice shown. Directions a and b are off the <11-2> direction by 95° and 10°, the angle γ is 85°.

For Cu with a strong coordination bonding the mismatch between lattice defined by the intermolecular interactions and the periodicity of the substrate-molecule interaction potential is too large to yield a long range order. In contrast, on Ag the intermolecular interactions dominate. This, on the one hand, enables the formation of highly crystalline layers rather independent of the details of the molecular structure. On the other hand, variations in the intermolecular interactions have a pronounced influence on the film structure. Comparison of the mono and dicarboxylic acids reveals substantial differences in the packing density and conformation of the molecules.

The results suggest that for Cu the molecular structures have to be carefully designed in order to obtain well defined layers. For Ag the design rules are much less restrictive which might be interesting for the use of aromatic carboxylic acids as templating layers for the epitaxial growth of supramolecular systems such as metal organic frameworks.

Support by the Leverhulme Trust and EPSRC is gratefully acknowledged.

[1] J. V. Barth, Annu. Rev. Phys. Chem., 58, 375 (2007).
[2] A. G. Slater, P. H. Beton and N. R. Champness, Chem. Sci., 2, 1440 (2011).
[3] I. Cebula, C. Shen and M. Buck, Angew. Chem. Int. Ed., 49, 6220 (2010).
[4] C. Shen, I. Cebula, C. Brown, J. Zhao, M. Zharnikov and M. Buck, Chem. Sci., 3, 1858 (2012).
[5] I. Cebula, H. Lu, M. Zharnikov and M. Buck, Chem. Sci., 4, 4455 (2013).

# New aspects of the nucleation of organic thin films

A. Winkler[1], L. Tumbek[1], A. Pimpinelli[2]

[1]*Institute of Solid State Physics, Graz University of Technology, Graz, Austria*
[2]*Rice Quantum Institute, Rice University, Houston, Texas , USA*
*(corresponding author: A.Winkler, a.winkler@tugraz.at)*

Organic thin films have recently attracted considerable interest due to their potential applicability for flexible organic electronics. In particular, the understanding of the initial steps of film formation, adsorption, diffusion, desorption and nucleation, is of utmost importance for a proper tailoring of organic films. The question arises whether large, anisotropic organic molecules behave in the nucleation process similarly as point-like atoms. Although this has been frequently assumed to describe organic film growth, some recent experimental results required a rethinking on this issue. In this contribution we summarize some recent results on the nucleation of rod-like molecules (pentacene (5A) and para-hexaphenyl(6P)) on amorphous mica and draw some general conclusions on this subject.

The organic molecules were deposited on sputter amorphized mica by physical vapor deposition in ultra-high vacuum (UHV). A quartz microbalance was used to quantify the deposited amount. Thermal desorption spectroscopy (TDS) was applied to obtain information on the energetics and kinetics of adsorption, nucleation and desorption. Ex-situ atomic force microscopy (AFM) was used to determine the morphology, island density and island size distribution of the sub-monolayer films. Both types of molecules formed islands, composed of standing molecules, on the sputter amorphized mica surface [1,2]. (Fig. 1) This is typical for organic film growth on weakly interacting substrates, e.g. on silicon dioxide, as frequently used in fundamental and application studies.

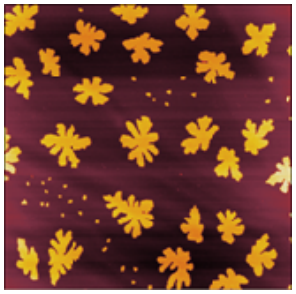

Fig. 1: 6P on amorphous mica

The first issue concerns the adsorption process. It is usually assumed in the literature that organic molecules, at sufficiently low temperature, adsorb with a probability of one. We could unequivocally demonstrate that this is not generally the case. The sticking coefficient for 5A at low, sub-monolayer coverage is clearly smaller than for higher coverage. Assuming a sticking of 1 for high coverage, the initial sticking coefficient $s_0$ calculates to be 0.6 [3]. An even smaller sticking coefficient of $s_0 = 0.2$ has been derived for rubicene on $SiO_2$ [4].

Another important issue is the nucleation process itself. It is nearly exclusively assumed that film growth can be described by diffusion-limited aggregation (DLA). According to the seminal paper by Venables et al. [5] the island density $N$ can be described by a power-law function of the deposition rate $R$, $N \sim R^{\alpha}$ , with $\alpha = i/(i+2)$, $i$ being the critical island size.

Thus, one can in principle determine $i$ by preparing sub-monolayer films at different deposition rates, counting the island density in the AFM image and plotting ln$N$ vs ln$R$. The slope of this line, which is predicted to be between 0.33 and 1, allows the calculation of $i$. However, it turns out that for both, pentacene and hexaphenyl on amorphous mica, these lines are bent and change from $\alpha = 0.7$ to $\alpha = 1.3$. The latter slope is inconsistent with DLA, however, can be explained by so-called attachment-limited aggregation (ALA) [6,7,8]. In this case $\alpha = 2i/(i+3)$. One can easily understand why this is a reasonable assumption for large organic molecules. On the one hand the diffusion coefficient is very high, due to low diffusion barriers, but on the other hand it can be argued that the incorporation of the molecules at the rim of the islands is sterically hindered because of the necessary reorientation.

A further aspect is the accommodation of the molecules upon adsorption and prior to nucleation. In the Venables model it is assumed that the molecules are instantaneously equilibrated and perform random hops before nucleation. We could recently show that the molecules may exist in a hot-precursor state after adsorption and move ballistically for some time before full accommodation [2]. This process has been modeled through an effective molecular temperature higher than the substrate temperature, which leads to a bend in the plot of ln$N$ vs $1/T$. This explains some puzzling results of the literature [1,11,12].

Finally, the scaling of the island size distribution (ISD) and/or the capture zone distribution (CZD) can be used to determine $i$, but so far analytic functions for ISD [9] and CZD [10] exist only for DLA. For CZD the scaling function is $P_\beta(s) = a_\beta \cdot s^\beta \cdot \exp(-b_\beta s^2)$, with $\beta = i+2$. We have extended the CZD also to attachment-limited aggregation; for this case we obtain $\beta = (i+3)/2$. Furthermore, we could prove that for compact islands the "exponent equality" $\alpha \cdot \beta = i$ holds, independent of the aggregation mechanism [13]. This important finding should help experimenters to better characterize nucleation and growth of thin films.

Supported by the Fonds zur Förderung der Wissenschaftlichen Forschung (Project #P23530).

[1] T. Potocar, S. Lorbek, D. Nabok, Q. Shen, L. Tumbek, G. Hlawacek, P. Puschnig, C. Ambrosch-Draxl, C. Teichert, and A. Winkler, Phys. Rev. B 83, 075423 (2011).
[2] A. Winkler and L. Tumbek, J. Phys. Chem. Lett. 4, 4080 (2013).
[3] L. Tumbek and A. Winkler, Surface Sci. submitted.
[4] B. Scherwitzl, W. Lukesch, A. Hirzer, J. Albering, G. Leising, R. Resel, and A. Winkler, J. Phys. Chem. C 117, 4115 (2013).
[5] J.A. Venables, G.D.T. Spiller, and M. Hanbücken, Rep. Prog. Phys. 47, 399 (1984).
[6] D. Kandel, Phys. Rev. Lett. 78, 499 (1997).
[7] J.A. Venables and H. Brune, Phys. Rev. B 66, 195404 (2002).
[8] L. Tumbek and A. Winkler, Surface Sci. 606, L55 (2012).
[9] J.G. Amar and F. Family, Phys. Rev. Lett. 74, 2066 (1995).
[10] A. Pimpinelli and T.L. Einstein, Phys. Rev. Lett. 99, 226102 (2007).
[11] G. Berlanda et al., Phys. Rev. B 69, 085409 (2004).
[12] J. Yang et al., J. Phys. Chem. 112, 7816 (2008).
[13] A. Pimpinelli, L. Tumbek, and A. Winkler, Phys. Rev. Lett. submitted.

# Insights Involving the Catalytically Active $Au/TiO_2$ Interfacial Sites for Oxidation Reactions Using Infrared Spectroscopy

M. McEntee, W. Tang[1], M. Neurock[1], and J. T. Yates, Jr.

*Department of Chemistry, University of Virginia, Charlottesville, VA 22904*
*(corresponding author: M. McEntee, e-mail: mlm4gf@virginia.edu)*

[1] *Department of Chemical Engineering, University of Virginia, Charlottesville, VA 22904*

Both bulk Au and metal oxides including (but not exclusively) $TiO_2$, $Fe_2O_3$, $Co_3O_4$ are poor catalysts separately for oxidation reactions. However, Haruta and his colleagues [1] discovered that Au nanoparticles (~3 nm in diameter) supported on these metal oxides strongly enhance catalytic activity for CO oxidation at temperatures even below 273K. Since this discovery, further studies have been done to investigate the nature of the catalytically active sites on $Au/TiO_2$. Behm et al. [2] found catalytic activity for CO oxidation to be proportional to the perimeter length of the $Au/TiO_2$ interface. Rodriguez et al. [3] studied the water gas shift reaction on an inverted catalyst with $TiO_2$ nanoparticles supported on a Au(111) single crystal and reasoned that the $TiO_2$-Au interface played a dominant role in the catalysis. These studies and others demonstrate that both the support and the Au nanoparticles are necessary for catalytic activity, and that the active sites are, surprisingly, at the Au particle perimeter.

The first step in the oxidation process is $O_2$ dissociation. In previous in situ Fourier transform transmission infrared spectroscopy (FTIR) experiments and density functional theory (DFT) calculations [4-7], we proposed a new dual catalytic site where in the $O_2$ molecule, an O atom attaches to Au and the other O atom attaches to a $Ti^{4+}$ site. This dual site generates low energy barriers for $O_2$ dissociation in the range 0.16-0.6 eV as a result of direct charge transfer from Au to the Ti site with subsequent charge transfer from the Ti to the $2\pi^*$ anti-bonding state of the $O_2$ molecule as shown in Figure 1 [7]. Electron density back

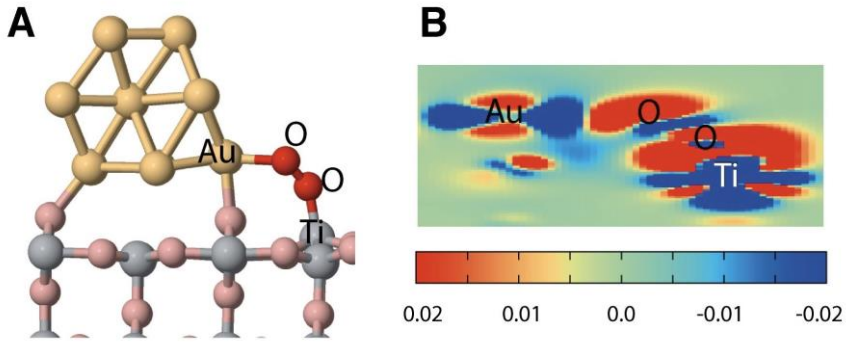


Figure 1. (A) The adsorption of $O_2$ to the Au-$Ti^{4+}$ dual catalytic site on a $Au/TiO_2$ catalyst. (B) Charge transfer from Au to Ti and backdonation into antibonding states of $O_2$ upon adsorption.

donation into the anti-bonding state of the $O_2$ increases the bonding energy of the $O_2$ molecule to the $Ti^{4+}$ site assisting in activation. Once $O_2$ dissociates, the active atomically bound O* can easily oxidize carbon- and oxygen-containing reactants. These low energy barriers allow us to study the sites not only for C-H bond activation but also C-C and C-O bond scission in a variety of important oxidation reactions.

Here we show one example using FTIR and DFT where Au supported on $TiO_2$ is highly selective in activating the C-H bonds at the $C_2$ and $C_3$ positions by basic O* and OH* species bound to Au for a linear carboxylic acid, propionic acid ($CH_3CH_2COOH$), to form intermediate unsaturated carboxylate surface species and then in breaking both C-O and C-C bonds to form an exotic species, ketenylidene ($Au_2C=C=O$), as depicted in Figure 2 below. The unique selectivity of $Au/TiO_2$ suggests that the sites and mechanism for the activation of C-H, C-C and C-O bonds are different than those that are active over supported Pd [8]. These differences provide novel ideas for future dual-site catalysts that are both highly active and selective.

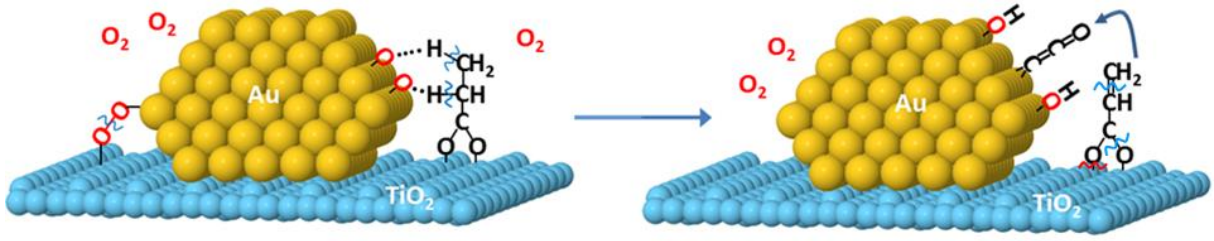


Figure 2. Schematic of the propionic acid oxidation mechanism on $Au/TiO_2$

We gratefully thank the DOE-Office of Basic Energy Sciences under grant number DE-SC0002365, as well as the FIRST Center for partial support for Wenjie Tang. We also acknowledge a fellowship for Monica McEntee from the AES Corporation through the AES Graduate Fellowships in Energy Research Program at the University of Virginia.

[1] H. Masatake, K. Tetsuhiko, S. Hiroshi, Y. Nobumasa, Chem. Lett. 2, 405-408 (1987)
[2] M. Kotobuki, R. Leppelt, D.A. Hansgen, D. Widmann, R.J. Behm, J. Catal. 264, 67-76 (2009)
[3] J. A. Rodriguez, S. Ma, P. Liu, J. Hrbek, J. Evans, M. Perez, Science 318, 1757-1760 (2007)
[4] I. X. Green, W. Tang, M. Neurock, J. T. Yates, Jr., Science 333, 736-739 (2011)
[5] I. X. Green, W. Tang, M. Neurock, J. T. Yates, Jr., Angew. Chem. Int. Ed. 50, 10186-10189 (2011)
[6] I. X. Green, M. McEntee, W. Tang, M. Neurock, J. T. Yates, Jr., Top. Catal. 56, 1512-1524 (2013)
[7] I. X. Green, W. Tang, M. Neurock, J. T. Yates, Jr., Submitted to Acc. Chem. Res. (2013)
[8] H. Bernas, K. Eränen, I. Simakova, A-R. Leino, K. Kordás, J. Myllyoja, P. Mäki-Arvela, T. Salmi, D. Y. Murzin, Fuel. 89, 2033-2039 (2010)

# The growth of $TiO_x$ on Pd(111) and Pd(100) by Chemical Vapor Deposition

M. H. Farstad[1], D. Ragazzon[2], M. Strømsheim[3], J. Gustafson[4], A. Sandell[2], and A. Borg[1]

[1]Dept. of Physics, Norwegian University of Science and Technology, NO-7491 Trondheim, Norway. (corresponding author: M. H. Farstad, e-mail: mari.farstad@ntnu.no)
[2]Dept. of Physics and Astronomy, Uppsala University, P. O. Box 530, SE-75121 Uppsala, Sweden
[3]Dept. of Chem. Eng., Norwegian University of Science and Technology, NO-7491 Trondheim, Norway
[4]Dept. of Synchrotron Research, Lund University, SE-221 00 Lund, Sweden

The reverse water gas shift reaction (rWGS) is an important process in industry [1]. Palladium is known to have a high hydrogen affinity [2] and $TiO_2$ is known to exhibit catalytic properties when combined with metals [3] which makes the $Pd/TiO_2$ system a promising candidate as a catalyst for rWGS. We have extensive experience with growth of $TiO_x$ by chemical vapor deposition (CVD) using titanium tertaisopropoxide (TTIP) as precursor on Au(111)[4, 5] where CVD allows us to grow different structures dependent on deposition temperature and amount. In the present work, we have applied this approach to grow $TiO_x$ structures on Pd(111) and Pd(100).

We have used High Resolution Photoelectron Spectroscopy (HRPES), Scanning Tunneling Microscopy (STM) and Low Energy Electron Diffraction (LEED) to map out and study the structure and growth of $TiO_x$ thin films on Pd(111) and Pd(100). In addition to growth series at different temperatures, oxidation and reduction of selected preparations have been performed.

Ti 2p spectra from growth of $TiO_x$ at temperature 500°C on Pd(111) is presented in Fig. 1. Here the development of the oxidized

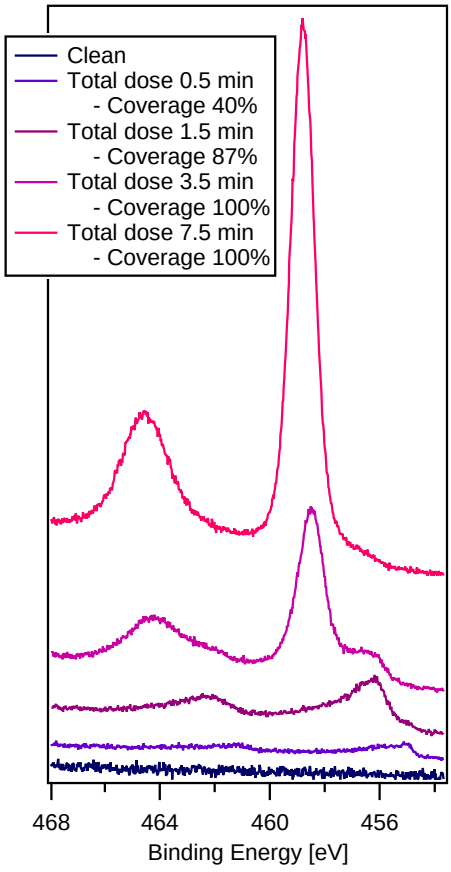


**Figure 1:** Ti 2p spectra from a growth series at 500°C on Pd(111). Coverages are calculated by CO titration. The spectra are shifted vertically for clarity.

$TiO_2$ phase can be followed. Initially, an alloy phase between Ti an Pd is formed, before partially oxidized $TiO_x$ starts growing. With increasing coverage the oxidation state of Ti increases until fully oxidized $TiO_2$ is reached at 100% coverage. Our data indicates that on Pd(111) $TiO_x$ grows as a reduced wetting layer until the substrate is completely covered, upon which fully oxidized $TiO_2$ forms.

When it comes to LEED patterns of $TiO_x$ on Pd(111) all doses and temperatures appear to exhibit the same type of pattern, this pattern is displayed in figure Fig. 2. The pattern indicates that the thin film consists of domains with different orientations. The fact that both the reduced thin films and the fully oxidized thin film has the same LEED pattern suggests that the interaction between the reduced layer and Pd(111) is determining the structure of the film. For Pd(100) we have observed several different LEED patterns dependent on the oxidation state of the $TiO_x$ thin film, pointing at weaker interaction with the Pd(100) substrate.

STM images confirm that $TiO_x$ grows as domains with different orientations on Pd(111). In figure Fig. 3 a STM image of a $TiO_x$ film grown at 500°C is displayed. Domain orientiations are indicated by lines. Another noteworthy feature is that the step edges, which on clean Pd(111) are straight lines, are here anything but straight. This disruption of the step edges start at very low $TiO_x$ coverages.

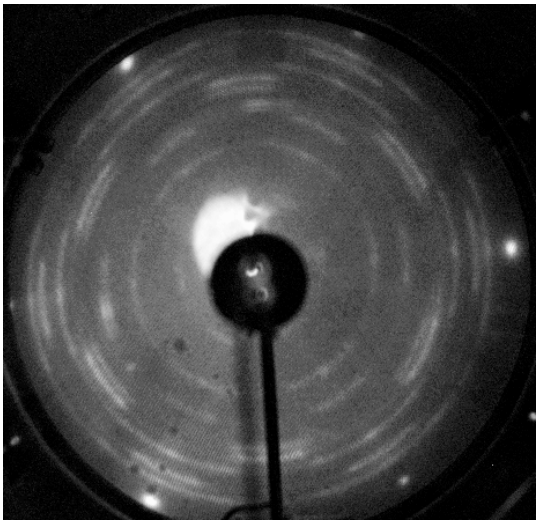

**Figure 2:** LEED pattern of Pd(111) with 86% coverage of $TiO_x$, grown at 500°C.

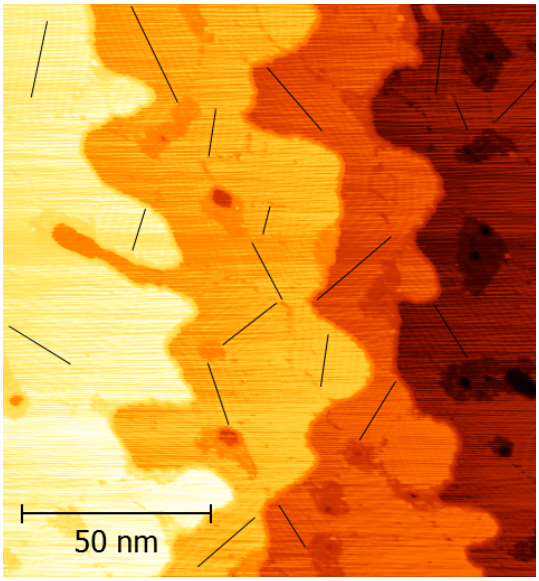


**Figure 3:** STM image of $TiO_x$ grown on Pd(111) at 500°C. Domains of different orientations are idicated by lines.

In summary, on both Pd(111) and Pd(100) the main growth steps are formation of a Ti-Pd alloy, followed by a reduced wetting layer of $TiO_x$ covering the entire sample, and finally fully oxidized $TiO_2$ starts to form. The main difference between the two substrate orientations appears to be the strength of the interaction between the $TiO_x$ thin film and Pd.

[1] P. Kaiser, R. B. Unde, C. Kern, A. Jess 85 (4), 489–499 (2013).

[2] T. Mitsui, M. Rose, E. Fomin, D. Ogletree, M. Salmeron, Surface Science 540, 5 – 11 (2003).

[3] J. A. Rodriguez, J. Evans, J. Graciani, J.-B. Park, P. Liu, J. Hrbek, J. F. Sanz, J. Phys. Chem. C 113, 7364–7370 (2009).

[4] D. Ragazzon, A. Schaefer, M. H. Farstad, L. E. Walle, P. Palmgren, A. Borg, P. Uvdal, A. Sandell, Surface Science 617, 211–217 (2013).

[5] A. Schaefer, D. Ragazzon, L. Walle, M. Farstad, A. Wichmann, M. Bâumer, A. Borg, A. Sandell, Applied Surface Science 282, 439–443 (2013).

# Intercalation in epitaxial graphene on SiC: From quasi-free standing graphene to superlattices

U. Starke[1], S. Forti[1], K.V. Emtsev[1], C. Coletti[1,2], and A.A. Zakharov[3]

[1]*Max-Planck-Institut für Festkörperforschung, Heisenbergstr. 1, D-70569 Stuttgart, Germany (corresponding author: U. Starke, e-mail: u.starke@fkf.mpg.de)*

[2]*present address: Center for Nanotechnology Innovation @NEST, Istituto Italiano di Tecnologia, Piazza San Silvestro 12, 56127 Pisa, Italy*

[3]*MAX-lab, Lund University, Lund, S-22100, Sweden*

Large scale epitaxial graphene (EG) grown on SiC single crystal wafers promises to be a suitable candidate for carbon based electronics [1]. However, the electronic and structural properties of EG are strongly influenced by the SiC substrate. Yet, these properties can be manipulated by functionalization of the graphene/SiC interface on an atomic scale. The $(6\sqrt{3}\times6\sqrt{3})R30°$-reconstructed first carbon layer on SiC(0001) has a graphene-like topology and atomic structure but has strong covalent bonds to the SiC substrate [2,3] – and thus exhibits no $\pi$-bands. This carbon layer can be turned into quasi-free standing monolayer graphene by intercalating foreign elements underneath. In this process of intercalation, the electronic properties of graphene are drastically affected by the interaction with the underlying substrate, and the results can be very different for different elements. In this work we demonstrate the wide range of effects arising from the modification of the interface layer by means of intercalation of elements of different types, namely hydrogen, germanium and cupper, under graphene layers, which were epitaxially grown on 6H-SiC(0001). These three very diverse elements, a monovalent atom well known for surface passivation in the Si-technology, a semiconductor and a metal, all intercalate under graphene and relieve the interaction between the graphene itself and the SiC substrate. The presence of this additional interface layer, however, has important consequences on the morphology and electronic structure of graphene.

The resulting atomic and electronic properties as well as the dynamics of the corresponding intercalation and desorption processes are characterized using various surface science techniques. The atomic structure and chemical bond configuration are studied using low-energy electron diffraction (LEED) and X-ray photoelectron spectroscopy (XPS), respectively. The electronic structure is analyzed using angle-resolved photoemission spectroscopy (ARPES), also in the home lab at MPI Stuttgart, as well as at the SIS-HRPES beamline of the Swiss light source (SLS) at the Paul-Scherrer-Institute (PSI), Villigen, Switzerland. The spatial formation of the graphene layers and areas of different doping is studied *in situ* by low energy electron microscopy (LEEM), $\mu$-LEED, photoelectron

microscopy (PEEM) and $\mu$-XPS using the ELMITEC III instrument at beamline I311 of the MAX-Lab synchrotron radiation facility in Lund, Sweden.

We show that while hydrogen [4,5] and Germanium [6] relieve the interaction between the substrate and the carbon layer without developing any ordered superstructure at the interface, the copper atoms arrange to form a superstructure with a long-range order which imposes a periodic potential strongly influencing the graphene's electronic properties [7]. The stability of the intercalation-decoupled graphene is investigated with particular attention to the effect of the temperature on the structure and the doping level. By annealing the Ge-intercalated graphene, *p*- and *n*-doped domains develop at the surface as a function of T, which can be prepared in coexistence on the surface leading to *p-n* junctions on a sub-100 nm scale. Quasi-free standing monolayer graphene obtained by hydrogen intercalation is initially *p*-doped and can be gradually modified towards charge neutrality by removal of individual hydrogen atoms. The Cu layer forms a coincidence superstructure together with the SiC surface, which induces periodic regions of different bond configuration for the carbon atoms in the graphene layer. As a result, a long range (3.2 nm) periodic potential is imposed onto the graphene layer, which leads to a profound modification of the electronic spectrum of the graphene layer. A surprisingly strong doping and the development of mini-Dirac cones are observed. The effects will be put into perspective by comparison to theoretical predictions.

This work was supported by the Deutsche Forschungsgemeinschaft (DFG) in the framework of the Priority program (SSP) 1459 *Graphene* within grant Sta315/8-1. C.C. acknowledges the Alexander von Humboldt Foundation for financial support. This research was partially funded by the European Community's Seventh Framework Programme (FP7/2007-2013) under grant agreement no. 226716. We are indebted to the staff at MAX-Lab (Lund, Sweden) and SLS (Villigen, Switzerland) for their advice and support.

[1] K.V. Emtsev et al., Nature Materials **8**, 203-207 (2009).
[2] K.V. Emtsev, F. Speck, Th. Seyller, L. Ley, and J.D. Riley, Phys. Rev. B **77**, 155303 (2008).
[3] C. Riedl, C. Coletti, and U. Starke, J. Phys. D **43**, 374009 (2010).
[4] C. Riedl, C. Coletti, T. Iwasaki, A.A. Zakharov, and U. Starke, Phys. Rev. Lett. **103**, 246804 (2009).
[5] S. Forti, K.V. Emtsev, C. Coletti, A.A. Zakharov, C. Riedl, and U. Starke, Phys. Rev. B **84**, 125449 (2011).
[6] K.V. Emtsev, A.A. Zakharov, C. Coletti, S. Forti, and U. Starke, Phys. Rev. B **84**, 125423 (2011).
[7] S. Forti, K.V. Emtsev, C. Coletti, A.A. Zakharov, and U. Starke, to be published.

# Low-energy plasmonic structure of doped free-standing graphene

V. M. Silkin, M. Pisarra,[1] A. Sindona,[1] P. Riccardi,[1] and J. M. Pitarke[2,3]

*Donostia International Physics Center, Paseo Manuel de Lardizabal 4, 20018 Donostia/San Sebastian, Basque Country, Spain,*
*Departamento de Fisica de Materiales, Facultad de Ciencias Químicas, Universidad del Pais Vasco/Euskal Herriko Unibertsitatea, Apdo. 1072, 20080 Donostia/San Sebastian, Basque Country, Spain*
*IKERBASQUE, Basque Foundation for Science, 48011 Bilbao, Spain*
*(corresponding author: V. M. Silkin, e-mail: waxslavas@sc.ehu.est)*

[1] *Dipartimento di Fisica, Universit della Calabria and INFN - Gruppo collegato di Cosenza, Via P. Bucci cubo 30 C, 87036 Arcavacata di Rende (CS), Italy*

[2] *Materia Kondentsatuaren Fisika Saila and Centro Fisica Materiales CSIC-UPV/EHU, 644 Posta Kutxatila, E-48080 Bilbo, Basque Country, Spain*

[3] *CIC nanoGUNE Consolider, Tolosa Hiribidea 76, E-20018 Donostia/San Sebastian, Basque Country, Spain*

Over the recent years, the interest in graphene [1] has impressively grown in both fundamental research and technological applications [2-4]. This is due to the fact that graphene exhibits a good number of interesting properties, related mainly to its *novel* electronic structure near the Fermi level represented by the so-called Dirac cone. A major issue is represented in this case by the variation of the charge carrier density, which is caused by several conditions. The appearance of a two-dimensional (2D) sheet plasmon in graphene adsorbed on a variety of supporting materials has been observed in several experiments [5-10], where the monolayer graphene happens to be doped by charge transfer to or from the substrate.

Here we present an *ab-initio* description of the energy-loss spectrum of doped free-standing monolayer graphene. We find that the strong anisotropy that is present in the graphene band structure near the Dirac point allows for the coexistence of a majority of electrons moving with two different velocities along the ΓK direction, thus leading to a remarkable realization of the old idea [11] that low-energy acoustic plasmons (whose energy exhibits a linear dependence on the wavenumber) should exist in the collective motion of a system of two types of electronic carriers.

A realization of an acoustic plasmon, in addition to a conventional two-dimensional (2D) plasmon, is predicted to occur for carriers in the very same 2D band of extrinsic (doped or gated) graphene. Whereas conventional 2D plasmon corresponds to the collective charge oscillations in which the two types of carriers oscillate in phase with one another [this plasmon at long wavelengths ($q \to 0$) has the same dispersion, $\sim q^{1/2}$, as the conventional 2D plasmon of a 2D free electron gas], the additional mode found here corresponds to a low-frequency acoustic oscillation [whose energy exhibits at long wavelengths a linear dependence on the 2D wave number q] in which two types of carriers in the very same energy band oscillate out of phase. Note, that the former mode was

predicted to exist in doped graphene theoretically some time ago [12-14] and observed in numerous experiments on different substrates [5-9]. On the other hand, if prediction of the latter mode is confirmed experimentally, it will represent the first realization of an acoustic plasmon originated in the collective motion of a system of two types of carriers exited within the very same energy band. The properties of this novel mode like strong in-plane anisotropy of its dispersion, variation of group velocity upon doping level and others will be discussed.

[1] K. S. Novoselov, A. Geim, S. V. Morozov, D. Jiang, Y. Zhang, S. V. Dubonos, I. V. Grigorieva, and A. A. Firsov, Science 306, 666 (2004)

[2] A. K. Geim and K. S. Novoselov, Nature Mater. 6, 183 (2007)

[3] A. H. Castro Neto, F. Guinea, N. M. R. Peres, K. S. Novoselov, and A. K. Geim, Rev. Mod. Phys. 81, 109 (2009)

[4] F. Bonaccorso, Z. Sun, T. Hasan, A. C. Ferrari, Nature Photon. 4, 611 (2010)

[5] Y. Liu, R. F. Willis, K. V. Emtsev, and T. Seyller, Phys. Rev. B **78**, 201403 (2008).

[5] C. Tegenkamp,H. Pfnür, T. Langer, J. Baringhaus, and H. W. Schumacher, J. Phys: Condens Matter 23, 012001 (2011).

[7] S. Y. Shin, C. G. Hwang, S. J. Sung, N. D. Kim, H. S. Kim, and J. W. Chung, Phys. Rev. B 63, 161403 (2011)

[8] J. Chen, *et al*, Nature 487, 77 (2012)

[9] Z. Fei, *et al*, Nature 487, 82 (2012)

[10] A. N. Grigorenko, M. Polini, K. S. Novoselov, Nature Photon. 6, 749 (2012)

[11] D. Pines, Can. J. Phys. 34, 1379 (1956)

[12] B. Wunsch, T. Stauber, F. Sols, and F. Guinea, New J. Phys. 8, 318 (2006)

[13] E. H. Hwang and S. Das Sarma, Phys. Rev. B 75, 205418 (2007)

[14] A. Hill, S. A. Mikhailov, and K. Ziegler, EPL 87, 27005 (2009)

# The electron band structure of multilayer graphene on C-face SiC studied by Angle Resolved Photoemission (ARPES).

L. I. Johansson, R. Armiento, J. Avila[1], C. Xia, S. Lorcy[1], I. A. Abrikosov, M. C. Asensio[1] and C. Virojanadara
(corresponding author: L. I. Johansson, email: lejoh@ifm.liu.se)

*Department of Physics, Chemistry and Biology, Linköping University, SE-58183 Linköping, Sweden*
*[1]Synchrotron SOLEIL, L'Orme des Merisiers, Saint Aubin-BP 48, 9192 Gif sur Yvette Cedex, France*

We have investigated graphene grown on C-face SiC substrates, using Low Energy Electron Microscopy (LEEM), X-ray Photo Electron Electron Microscopy (XPEEM), selected area Low Energy Electron Diffraction (micro-LEED) and also ARPES. The samples typically show [1,2] formation of fairly large (some μm) grains (crystallographic domains) of mono-and multi-layer graphene exhibiting sharp (1x1) spots in micro-LEED, but that adjacent grains have different azimuthal orientations. Selected area constant initial energy photoelectron angular distribution patterns, $E_i(k_x,k_y)$, collected, using XPEEM, indicate the same. When utilizing a small sampling area one Dirac cone, centered at each $\overline{K}$-point in the Brillouin zone, is clearly resolved. When using a large sampling area, several sets of such Dirac cones from differently oriented grains appear, giving rise to a ring-like pattern. Only one Dirac cone is, however, resolved at the $\overline{K}$-point using conventional ARPES (or XPEEM) although LEEM show multilayer graphene on most parts of the sample surface. This is illustrated by an ARPES spectrum in Fig. 1, recorded from an essentially bi-layer graphene sample [3]. One fairly broad π-band cone with the Dirac point located close to the Fermi energy is observed from the initial sample. After Na deposition on the sample the Dirac point is shifted down ca. 0.5 eV, due to electron doping. After subsequent heating the π-band cone is considerably broadened, which can be interpreted to indicate a splitting of π-bands due to Na intercalation in between the carbon layers and at the interface. Heating at higher temperatures results in de-intercalation of Na and at 950°C the initial band structure is essentially restored. In conventional ARPES the probing area is much larger than the typical grain size so a spectrum represents data averaged over many grains. In order to reveal the true/real electron band structure a study of individual graphene grains has to be made. This is possible using the nano-ARPES beamline ANTARES at SOLEIL and some results from such π-band mappings will also be presented and discussed.

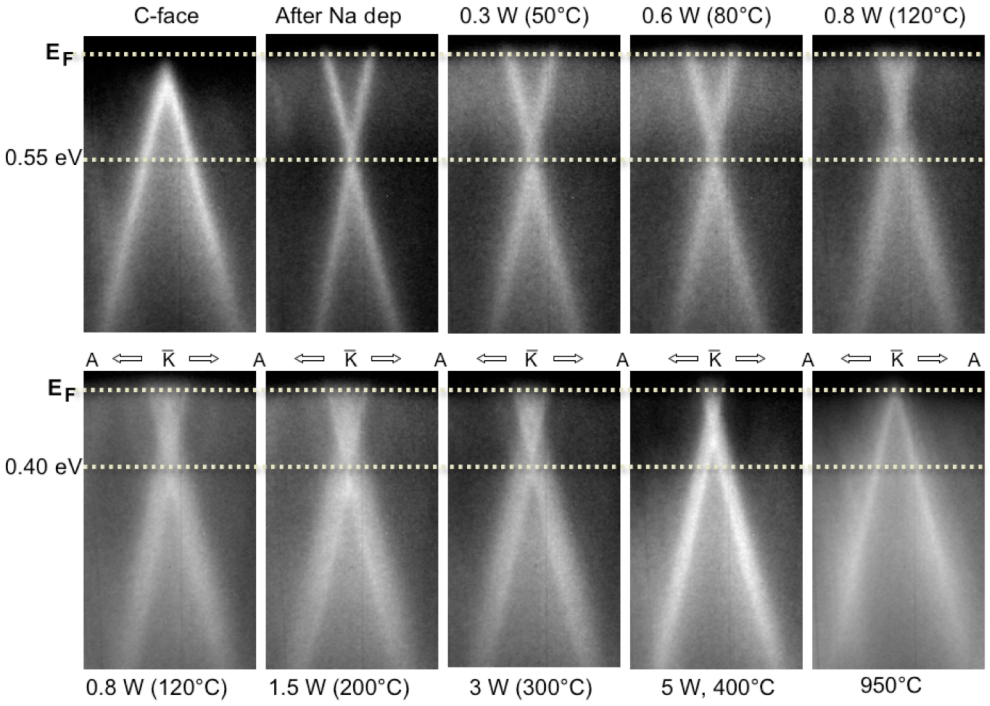


Fig. 1 The π-band structure recorded close to the $\overline{K}$ point before and after Na deposition and after heating at different temperatures, using a photon energy of 33 eV.

The authors gratefully acknowledge support from the European Science Foundation, within the EuroGRAPHENE (EPIGRAT) program and the Swedish Research Council (#621-2011-4252, #621-2011-4249, and Linnaeus Grant).

[1] L. I. Johansson, S. Watcharinyanon, A. A. Zakharov, T. Iakimov, R. Yakimova, and C. Virojanadara, Phys. Rev. B. **84**, 125405 (2011).
[2] L. I. Johansson, C. Xia, J. Ul Hassan, T. Iakimov, A. A. Zakharov, S. Watcharinyanon, R. Yakimova, E. Janzen, and C. Virojanadara, Crystals **3**, 1 (2013).
[3] L.I. Johansson, C. Xia, and C. Virojanadara, Graphene **2**, 1 (2013).

# Ultrafast charge transfer at graphene monolayers: hybridisation, final state dimensionality, and slow-down

D. Menzel[1], P. Lacovig[2], K.L. Kostov[3], R. Larciprete[4], and S. Lizzit[2]

*(corresponding author: D. Menzel, e-mail: dietrich.menzel@ph.tum.de)*

[1] *Physik-Department E20, Technische Universität München, 85748 München, Germany*
*Also at Fritz-Haber-Institut der MPG, Dept. CP, Faradayweg 4-6, 14195 Berlin, Germany*

[2] *Elettra Sincrotrone Trieste, S.S.14 km 163.5, 34149 Trieste, Italy*

[3] *Institute of General and Inorganic Chemistry, Bulgarian Academy of Sciences, 1113 Sofia, Bulgaria*

[4] *Institute of Complex Systems, 00133 Roma, Italy*

Despite the very large amount of work on graphene monolayers (Gr ML), the dynamics of excited states at its surfaces - which should be important for photochemistry on Gr and for contact formation to Gr in electrochemistry - have not been investigated much. We have used the core hole clock method [1, 2] with adsorbed argon to measure the transfer rate of a localized electron (the 4s electron on adsorbed, core-excited Ar) to the surfaces of Gr ML on different substrates with strongly varying Gr-substrate coupling [3]. We thus quantify the dynamics of charge transfer (with time constants, CTT, in the low *fs* region) and its dependence on the dimensionality of the final states and on the Gr-substrate bonding. Connections exist to STM intensities. Our first results have been presented at 3S'11 in Bacqeira [4]; part of our results have been published recently [5]. We have now measured additional systems, further extending the range of coupling. This larger range of systems leads to improved semiquantitative understanding and enables us to point out surprising effects and open questions.

We compare three examples of decoupled, quasi-freestanding Gr ML (on SiC, on O/Ru, and on $SiO_2$/Ru [6]) with strongly to weakly coupled Gr on metal surfaces [3] ((Ru(0001) with differently coupled "valleys" and "hills"; strongly coupled Ni(111) with well-matched geometry; very weakly coupled Pt(111)). We find strong variations of CTT between ~3 *fs* (Gr ML strongly coupled to substrate on Ru(0001) “valleys”) and ~ 16 *fs* (quasi-freestanding Gr ML, independent of the decoupling way). A ratio of 1.7 is found between the “hills” and “valleys” of the regularly corrugated Gr/Ru; surprisingly, Gr/Ni is close to the slower Ru "hills" region, and Gr/Pt is much slower than the latter, but still a factor of 2 faster than the decoupled layers. The very fast CT on Gr/Ru valleys is interpreted as due to Ru 4d-orbitals hybridized with Gr $\pi^*$-states "reaching through" the Gr layer; this effect changes with the

relative Gr/Ru alignment and distance. The slower CT for the stongly coupled and geometrically well-fitting Gr/Ni case is explainable by the fact that at the Ar*4s energy (~ 1.5 eV above $E_F$) only low density empty sp-orbitals are available for coupling with the Gr $\pi^*$-states. But also the Gr hills on Ru, and Gr on Pt, show rather fast CT and appear to be quite strongly coupled, contrary to current interpretations which describe these layers as purely van der Waals bound. Furthermore, the slow CT on the decoupled layers which are truly Van der Waals bound, with no available substrate states, is puzzling. We believe that this last difference is due to dimensionality - for the quasi-freestanding layers the final states are 2D states while for the Gr ML on metal surfaces, even for the weakly bound cases, CT leads eventually to transfer into 3D states. We will discuss effects which can lead to slowdown for the 2D case and to faster transfer for the weakly coupled Gr-metal cases.

We believe that our results shed light on the paths of CT in 2D/3D cases and also have bearing on the detailed understanding of tunneling microscopies and spectroscopies in an energy range potentially important for photochemistry on Gr.

Support by Elettra through beamtime allocation, and by the EC through travelling funds supporting these beamtimes are gratefully acknowledged.

[1] For an extensive review, see P.A. Brühwiler, O. Karis, and N. Martensson, Rev. Mod. Phys. **74**, 703 (2002)

[2] For a recent survey, see D. Menzel, Chem. Soc. Rev. 37, 2212 (2008)

[3] M. Batzill, Surf. Sci. Rep. 67, 83 (2012)

[4] S. Lizzit et al., Proc. Internat. Symposium on Surface Science 3S'11, Bacqueira 2011, p.25

[5] S. Lizzit et al., ACS Nano 5, 4359 (2013), DOI: 10.1021/nn-4008862

[6] S. Lizzit et al., Nano Lett. 12, 4503 (2012).

# *Friday*

# Surface Science and Model Catalytic Studies of Liquid Organic Hydrogen Carriers

M. Amende[1], C. Gleichweit[1], S. Schernich[1], O. Höfert[1], M.P.A. Lorenz[1], W. Zhao[1], K. Werner[1], M. Sobota[1], I. Nikiforidis[2], H.-J. Drescher[1], M. Koch[3], N. Brückner[3], D. Assenbaum[3], W. Hieringer[2], M. Laurin[1], A. Görling[2], C. Papp[1], P. Wasserscheid[3], H.-P. Steinrück[1], J. Libuda[1]

[1]*Lehrstuhl für Physikalische Chemie II, Friedrich-Alexander-Universität Erlangen-Nürnberg, Egerlandstr. 3, D-91058 Erlangen,Germany*

*(corresponding author: J. Libuda, e-mail: joerg.libuda@fau.de)*

[2] *Lehrstuhl für Theoretische Chemie, Friedrich-Alexander-Universität Erlangen-Nürnberg*

[3] *Lehrstuhl für Chemische Reaktionstechnik, Friedrich-Alexander-Universität Erlangen-Nürnberg*

Conventional storage methods for hydrogen require cryogenic temperature or high pressure. One promising concept to circumvent these drawbacks are so-called "liquid organic hydrogen carriers" (LOHCs).[1-3] LOHCs are organic compounds which can be catalytically converted from an energy-lean to an energy-rich state through reversible hydrogenation and dehydrogenation. Since LOHCs can be transported and stored without loss, they may help decoupling energy production and consumption with respect to both space and time, a key challenge in the transition to renewable energies. Being liquids with physicochemical properties similar to diesel, transportation and storage is simple and cost efficient, even at large scale. These properties qualify them as alternative energy carriers both for stationary and mobile applications.[1,3]

The most prominent LOHC is N-ethylcarbazole (NEC), which is capable of storing 5.8 wt% $H_2$ upon hydrogenation to dodecahydro-N-ethylcarbazole ($H_{12}$-NEC). We have explored the reaction mechanism of $H_{12}$-NEC both on single crystal surfaces (Pd(111) [2], Pt(111) [3,4]) and nanoparticles (Pd [1], Pt [5]) supported on $Al_2O_3$/NiAl(110), combining infrared reflection absorption spectroscopy (IRAS), high-resolution x-ray photoelectron spectroscopy (HR-XPS), and density functional theory (DFT), and molecular beam (MB) techniques. Activation

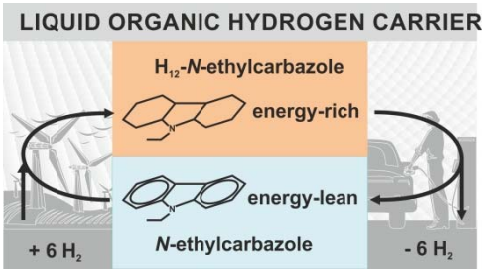


Fig. 1: $H_2$ storage via LOHCs, figure from [7].

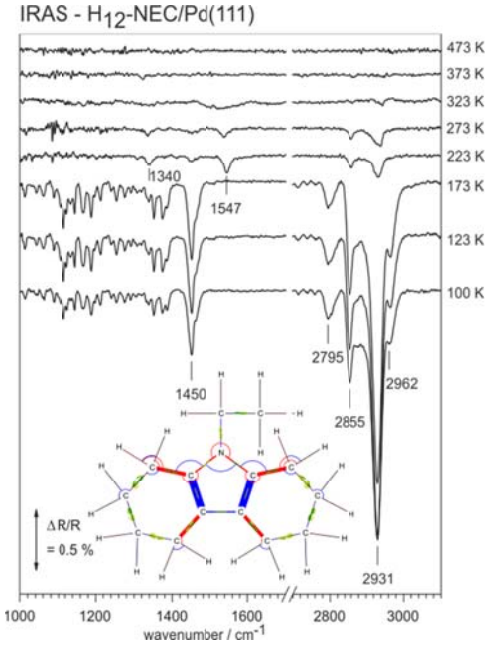


Fig. 2: IR spectra during $H_{12}$-NEC dehydrogenation on Pd(111). $H_8$-NEC is identified as the first stable intermediate by comparison with DFT calculations; inset: schematic representation of the vibrational mode around 1540 $cm^{-1}$, from [5].

of the molecule is found to occur via the H at the α-C position next to N. Subsequently, the inner 5-membered ring is dehydrogenated, leading to $H_8$-NEC as the first stable intermediate. Further dehydrogenation involves the 6-membered rings and competes with C-N bond scission. The latter is an undesired side reaction which leads do deterioration of the LOHC and to poisoning of the catalyst. Similar reaction mechanisms are identified on Pd and Pt, but with different kinetics. For example, Pd shows a substantially lower activation barrier for C-N bond scission. The latter reaction also shows pronounced structure dependencies, suggesting that low coordinated sites are more active for LOHC decomposition. Under continuous supply of reactants, the product spectrum changes, for example $H_8$-species are identified as the primarily gas phase products, even at high temperature where further dehydrogenation is possible. These phenomena are rationalized by ensemble effects that originate from coadsorbed species. The results highlight the importance of coadsorbed molecular fragments and atomic species that originate from decomposition and control the selectivity under reaction conditions.

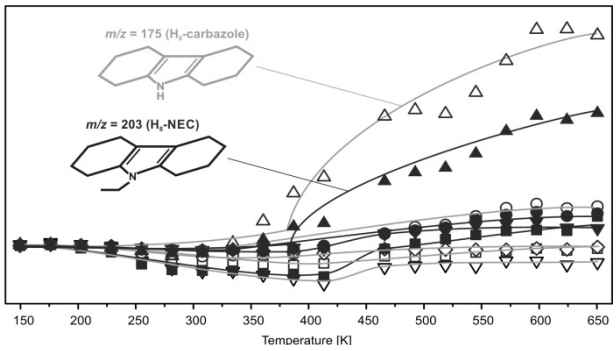


Fig. 3: Identification of primary gas phase products of $H_{12}$-NEC on Pt(111) using molecular beam techniques, from [7].

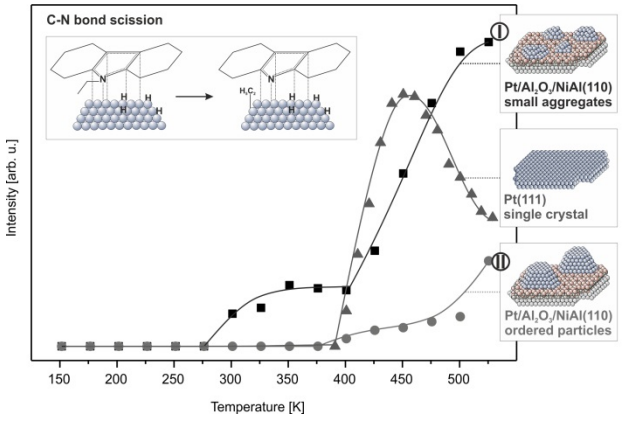


Fig. 4: Particle size and structure dependent C-N bond scission of $H_{12}$-NEC on Pt nanoparticles and Pt(111), from [8].

The authors acknowledge financial support by the Deutsche Forschungsgemeinschaft (DFG) within the Excellence Cluster "Engineering of Advanced Materials" in the framework of the excellence initiative. The present work was supported by BMW Forschung und Technik GmbH. P. W. acknowledge support by the ERC through their Advanced Investigator Grant (No. 267376). The authors thank BESSY II and the Helmholtzzentrum Berlin (HBZ).

[1] D. Teichmann, W. Arlt, P. Wasserscheid and R. Freymann, *Energy & Environ. Sci.* 4, 2767 (2011)

[2] D. Teichmann, W. Arlt and P. Wasserscheid, *International Journal of Hydrogen Energy* 37, 18118 (2012)

[3] D. Teichmann, K. Stark, K. Mueller, G. Zoettl, P. Wasserscheid, W. Arlt, *Energy & Environ. Sci.* 5, 9044 (2012)

[4] M. Sobota, I.Nikiforidis, M.Amende, B.S. Zanon, T.Staudt, O.Hoefert, Y.Lykhach, C.Papp, W.Hieringer, M.Laurin, D.Assenbaum, P.Wasserscheid, H.-P.Steinrueck, A.Goerling J.Libuda, *Chem. Eur. J.* 17,11542 (2011)

[5] M. Amende, S. Schernich, M. Sobota, I. Nikiforidis, W. Hieringer, D. Assenbaum, C. Gleichweit, H.-J. Drescher, C. Papp, H.-P. Steinrueck, A. Goerling, P. Wasserscheid, M. Laurin, J. Libuda, *Chem. Eur.* ***J.*** **19**, 10854 (2013)

[6] C. Gleichweit, M. Amende, S. Schernich, W. Zhao, M. P. A. Lorenz, O. Hoefert, N. Brueckner, P. Wasserscheid, J. Libuda, H.-P. Steinrueck, C. Papp, *ChemSusChem* **6**, 974 (2013)

[7] M. Amende, C. Gleichweit, S. Schernich, O. Höfert, M. P. A. Lorenz, W. Zhao, M. Koch, C. Papp, P. Wasserscheid, H.-P. Steinrück, J. Libuda, *ACS Catalysis*, in press

[8] M. Amende, C. Gleichweit, K. Werner, S. Schernich, W. Zhao, M. P. A. Lorenz, O. Höfert, C. Papp, M. Kock, P. Wasserscheid, M. Laurin, H.-P. Steinrück, J. Libuda, submitted.

# Model studies of Ni(Pd)-$ZrO_2$-$Pt_3$($Pd_3$)Zr solid oxide fuel cell (SOFC) anodes: preparation, stability, water and CO adsorption

Hao Li [1], Jake (Joong-Il) Choi [2], Wernfried Mayr-Schmölzer [2,3], Christian Weilach [1], Christoph Rameshan [1], Florian Mittendorfer [2,3], Josef Redinger [2,3], Michael Schmid [2] and Günther Rupprechter [1]

[1] *Institute of Materials Chemistry, Vienna University of Technology, 1060 Vienna, Austria*
*(corresponding author: G. Rupprechter, e-mail:* grupp@imc.tuwien.ac.at

[2] *Institute of Applied Physics, Vienna University of Technology, 1040 Vienna, Austria*

[3] *Center for Computational Materials Science, Vienna University of Technology, 1040 Vienna, Austria*

Solid Oxide Fuel Cells (SOFCs) are promising devices for effective energy generation. Nevertheless, improvements of their performance rely on a fundamental understanding of their components, such as the anode, the electrolyte and the cathode. The FWF SFB FOXSI, which is hosted at TU Wien, aims at elucidating the involved processes on a molecular level.

In order to model SOFC anodes well-ordered ultrathin films of $ZrO_2$ were grown in ultrahigh vacuum (UHV) by oxidation and annealing of $Pt_3Zr$ or $Pd_3Zr$ single crystals [1]. Ni or Pd was then deposited by physical vapor deposition. Ni particles supported by $ZrO_2$ are also widely used in the field of heterogeneous catalysis, such as for reforming reactions.

The chemical composition of the $ZrO_2$ model system was examined by high resolution X-ray Photoelectron Spectroscopy (XPS), the structure was characterized by Scanning Tunneling Microscopy (STM). Water and CO were used to probe the chemical properties of the $ZrO_2$-film and the metal nanoparticles, studied at near ambient pressure by AP-XPS and polarization modulation infrared reflection-adsorption spectroscopy (PM-IRAS).

A previously described route was followed to obtain a well-ordered and ultra-thin trilayer $ZrO_2$ film [1]: A cleaned $Pt_3Zr$ (0001) alloy substrate was oxidized at 673 K, followed by post-annealing at 1023 K. Apart from a signal characteristic of metallic zirconium resulting from the substrate ($Zr_{m,s}$), (synchrotron) XPS showed two distinctive oxidic species ($Zr_{1,o}$ and $Zr_{2,o}$). Depth profiling indicated that $Zr_{2,o}$ extended to deeper layers than $Zr_{1,o}$. After post-annealing of the oxide at 923 K, STM detected many small clusters with a height of about 1 nm. Increasing the annealing temperature to 1023 K led to the disappearance of most of the

small clusters, accompanied by a significant decrease of the intensity of $Zr_{2,o}$ in XPS. Thus, $Zr_{1,o}$ and $Zr_{2,o}$ were assigned to Zr oxide species within the trilayer zirconia film and a Zr oxide species in the zirconia clusters, respectively. Density Functional Theory (DFT) calculations corroborated and explained these assignments. Thermal Desorption Spectroscopy (TDS) using CO as probe molecule was then utilized to demonstrate that the entire substrate was covered by the zironia thin film.

The interaction of $ZrO_2$ with water was examined by synchrotron XPS (Lund). Surface defects, likely oxygen vacancies, created by soft sputtering, induced water dissociation, which was also enhanced at higher water pressures (low mbar range).

Ni and Pd nanoparticles grown on $ZrO_2$ were characterized via CO adsorption, monitored by TDS, XPS and PM-IRAS. At 200 K CO adsorbed on Ni particles in on-top adsorption geometry but at increasing temperature CO dissociation was observed that led to catalyst deactivation. Corresponding experiments with Pd- $ZrO_2$ did not show CO dissociation but likely encapsulation of the Pd nanoparticles.

Support by the Austrian Science Fund (FWF SFB-F45 FOXSI; projects 01/02/05/11) is gratefully acknowledged.

---

[1] M. Antlanger, et al., Phys. Rev. B., **86**, 03451, (2012).

# Structure of adsorption phases of oxygen on Ir(100)

L. Hammer, P. Ferstl, M.A. Schneider, A. Michl [1], S. Müller [1],
M.A. Arman [2], J. Knudsen [2], E. Lundgren [2], and F. Mittendorfer [3]

*Lehrstuhl für Festkörperphysik, Universität Erlangen-Nürnberg, Germany*
*(corresponding author: L. Hammer, e-mail: lutz.hammer@fau.de)*

[1] *Institute of Advanced Ceramics, Hamburg University of Technology, Germany*

[2] *Division of Synchrotron Radiation Research, Lund University, Sweden*

[3] *Institut für Angewandte Physik, Technische Universität Wien, Austria*

The adsorption of oxygen on the *unreconstructed* Ir(100) surface has been controversially discussed in the past. From experimental side there is only one ordered structure reported in literature so far, which is a 2×1-O phase at θ = 0.5 ML [1-4]. Another observed phase with "10×2" periodicity [2] was recently shown to be a shifted-row reconstruction of the iridium substrate [5]. In the 2×1 phase, oxygen atoms are found to assume bridge sites not sharing common Ir substrate atoms. This was proved by a LEED intensity analysis [3] and corroborated by all performed DFT studies [3-7]. A more recent XRD study [4] claimed that some additional oxygen (≈0.15 ML) randomly occupies hollow sites in between the double-spaced rows of regular bridge-bound oxygen atoms. Since an oxygen coverage exceeding 0.5 ML is usually inaccessible in experiment when dosing with molecular oxygen due to a vanishing dissociation probability, this finding was traced back to atomic oxygen adsorption produced by a glowing tungsten filament in the vicinity of the sample during gas dosing [4]. Consistently, an accompanying DFT study found that extra oxygen atoms (>0.5 ML) will prefer such hollow sites, however, only within an intermediate coverage range θ = 0.56 - 0.75 ML, while for higher coverages again exclusively bridge sites shall be assumed [4]. The partial hollow site occupation of oxygen at θ = 0.75 ML is also claimed by another DFT study [7], while our own extended DFT ground state analysis exclusively finds bridge site adsorption for all coverages [5].

In order to reach an unambiguous decision on the adsorption site we have performed further experiments by means of LEED, STM, TDS and HRXPS on this system. Oxygen coverages beyond θ = 0.5 ML were achieved either by the application of an atomic oxygen source, whereby $O_2$ is cracked within a hot Ir tube, or via exposing the surface to $NO_2$ at elevated temperatures, where these molecules decompose into O and NO with the latter desorbing from the surface. Both procedures result in a 1×1 phase containing almost twice the amount of oxygen compared to the 2×1-O structure (i.e. $\theta_{1\times1} \approx 1.0$ ML) as revealed from TDS spectra. Only negligible traces of CO or NO were detected either by XPS or TDS, and LEED I(E) spectra for both preparations were virtually identical. Lower coverages in the regime 0.5 ML < θ < 1.0 ML could then be achieved via partial desorption of oxygen from this 1×1-O phase.

In total we found four ordered phases of oxygen on the unreconstructed Ir(100) surface, the corresponding LEED pattern are displayed in Fig. 1. Additional to the already mentioned 2×1-O and 1×1-O phases two more phases were found, which are a 3×1-O for θ = 0.33 ML and 2×2-3O for θ = 0.75 ML. They undergo reversible order-disorder transitions at temperatures well below room temperature, which might be the reason that they remained undetected so far. Moreover, the 2×2-3O phase is only visible in a very narrow coverage range, while outside of this range a 2×1 LEED pattern is observed, i.e. the extra oxygen atoms beyond 0.5 ML disorder in between an ordered 2×1-O structure.

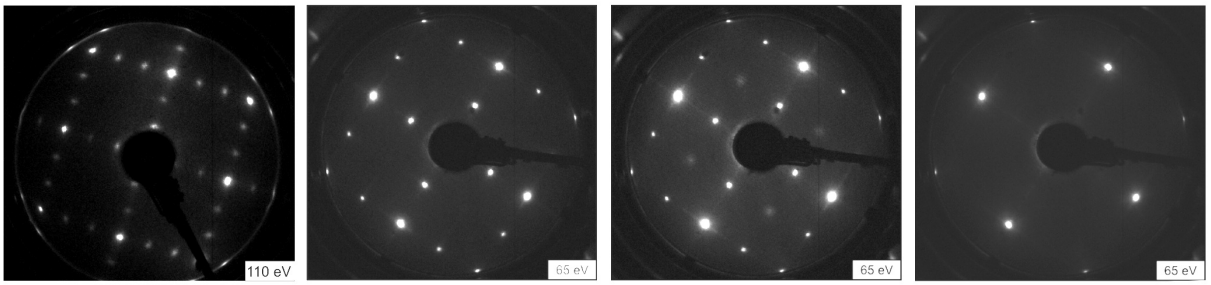


*Fig. 1: LEED pattern of the 3×1-O, 2×1-O, 2×2-3O and 1×1-O phases (from left to right).*

We have performed full-dynamical LEED intensity analyses for all ordered phases based on large intensity data sets taken at ≈100 K (total energy widths: 10215 eV for 3×1-O, 9938 eV for 2×1-O, 8270 eV for 2×2-3O and 4075 eV for 1×1-O phase). In all cases a very convincing agreement between calculated and experimental data could be achieved expressed by Pendry R-factors of $R_{P,3\times1} = 0.124$, $R_{P,2\times1} = 0.096$, $R_{P,2\times2} = 0.136$, and $R_{P,1\times1} = 0.077$. Moreover, in all cases the resulting structures coincided almost quantitatively with the predictions made by our DFT calculations for the respective phases. This holds not only for the position of the oxygen atoms, but also - in case of the superstructures - for the extended local relaxation patterns of the substrate. It should, however, be mentioned that according to our DFT calculations the 2×2-3O phase is not a ground state for the given coverage, instead a 4×1-3O phase is predicted to be significantly lower in energy. So far it is unclear, why our calculations obviously fail to produce the right energetic hierarchy of phases in this case.

The most prominent and surprising finding, however, is that the 2×2-3O phase indeed exhibits a mixed bridge and hollow site adsorption of oxygen, while for the neighbouring 2×1-O and 1×1-O phases all oxygen is exclusively adsorbed on bridge sites just as predicted by Sander et al. [4]. However, the structural parameters derived for the 2×2-3O phase by our LEED analysis deviate substantially from those given in Ref. 4.

Another approach to reveal the local adsorption structure of oxygen independent of long-range order is high resolution XPS. For that we have measured the Ir 4f and O 1s core levels as a function of oxygen coverage on Ir(100), cf. Fig.2. In order to avoid contamination by residual gas adsorption the surface was held at elevated temperatures during the measurements. Thus, the 3×1-O and 2×2-3O phases could not develop here as ordered phases. According to our DFT calculations remarkable Ir 4f core level shifts (≈0.35 eV) are expected both as a function of coverage and between hollow and bridge sites. The evaluation of data turns out to be rather time-consuming and is not yet completed to date.

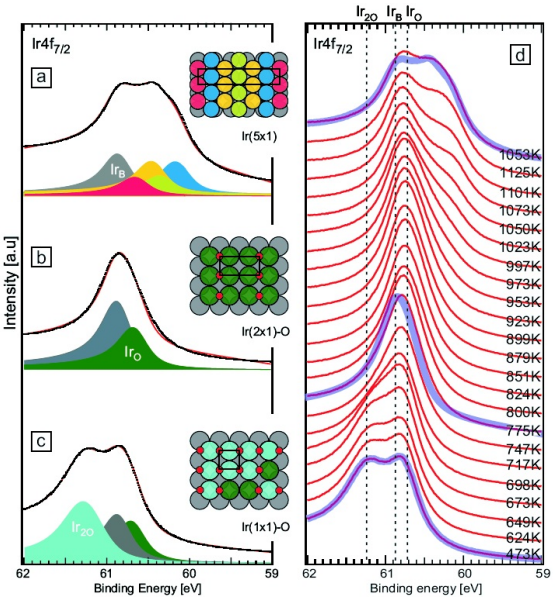


*Fig.2: Series of Ir4f$_{7/2}$ lines taken for increasing desorption temperatures (right), line fits for limiting phases (left).*

[1] J.T. Grant, Surf. Sci. 18 (1969) 228; [2] J. Küppers and H. Michel, Appl. Surf. Sci. 3 (1979) 179;
[3] K. Johnson et al., JCP 112 (2000) 10460; [4] D. Sander et al., PRB 81 (2010) 153403;
[5] M.A. Schneider et al., 3S13 Conf., Åre, Sweden, http://3s13.sljus.lu.se/3s13_bookofabstracts.pdf;
[6] I.A. Erikat et al., Eur. Phys. J. B 67 (2009) 35; [7] S.H. Ma et al., Eur. Phys. J. B 85 (2012) 216.

# Role of strain in the stability of hetero-epitaxial island on a nanopillar

M. Ignacio, O. Pierre-Louis, Y. Saito[1], P. Smereka[2]

*Institut Lumière Matière, Université Lyon 1, 43 Bd du 11 novembre 1918, 69622 Villeurbanne, France*
*(corresponding author: M. Ignacio, e-mail: maxime.ignacio@univ-lyon1.fr)*

[1] *Department of Physics, Keio University, 3-14-1 Hiyoshi, Hohoku-ku, Yokohma 223-8522, Japan*

[2] *Department of Mathematics, University of Michigan, Ann Arbor, MI 48109, USA*

Optoelectronics and microelectronics call for new techniques aiming at producing even smaller crystalline components of higher quality. Hetero-epitaxial growth on nanopatterned substrates such as nanopillar forests, is a promising direction to reduce mismatch strain and to obtain higher quality crystals. Indeed, 3D islands are grown on top of the pillars in a configuration which is similar to that of superhydrophobic liquid drops. However, as opposed to the case of liquids, elastic strain plays a major role in hetero-epitaxy. Using Kinetic Monte Carlo Simulations including elastic effects, we have studied in details the stability of a solid hetero-epitaxial island at the top of a nanopillar. We show that mismatch strain strain induces novel states for the island, including spontaneous symmetry-breaking and partial impalement of the islands in the nanopillars. Our results also suggest a non-trivial behavior and possible instabilities for solid-state catalytic particles governing nanowire growth.

[1] M. Ignacio, Y. Saito, P. Smereka, O. Pierre-Louis, preprint (2014)
[2] M. Ignacio, O. Pierre-Louis, Phys Rev. B 86 23410 (2012)
[3] P. Gaillard, Y. Saito, O. Pierre-Louis Phys Rev Lett 106 195501 (2011)
[4] K. Takano, Y. Saito, O. Pierre-Louis, Phys Rev B 82 075410 (2010)

# Surface diffusion of reactive solid nano-islands

F.Leroy*, Y.Saito**, F. Cheynis*, E. Bussmann***, O. Pierre-Louis****, P. Müller*

* Aix Marseille Université, CNRS CINaM UMR 7325, case 913 campus de Luminy, F-13288 Marseille cedex France

** Department of Physics, Keio university, 3-4 Hiyoshi, Kohoku, Yokohama, japan

***Sandia national laboratories, Albuquerque, NM 97185 USA

**** Institut Lumière Matière, UMR 5306, Université Lyon1-CNRS, 69622 Villeurbanne, France

Mass transport on surfaces is crucial to understand many processes at the basis of self-organization. It is in particular the case of spontaneous thermal migration of crystalline islands on a foreign substrate. Such motion of non reactive 3D crystallites has been reported long time ago [1, 2]. Usually, 3D islands migration obeys to Brownian motion with a size-dependent diffusion coefficient $D(R)$. Simple dimensional arguments have been proposed [3] to justify a $D = D_o R^{-n}$ behaviour with $n = d + 1$ when the limiting mass transport mechanism is surface diffusion, $n = d$ when the limited mass transport mechanism is surface attachment/detachment with $d = 3$ for 3D islands or $d = 2$ for 2D islands.

More recently the migration of reactive islands has been reported for 3D running droplets of Ga on GaAs [4], for copper-tin alloy bronze formation [5] and for Si liquid droplets on $SiO_2$ substrate [6, 7]. In the two first cases the island motion originates from a force gradient due to a modification of the interfacial energy induced by the reaction between the deposit and its underlying substrate leading to a non-brownian motion. In the case of Si liquid droplets it is the reactivity at the triple line that seems to be at the origin of the droplet motion but a complete statistical analysis of the mean square displacement is lacking.

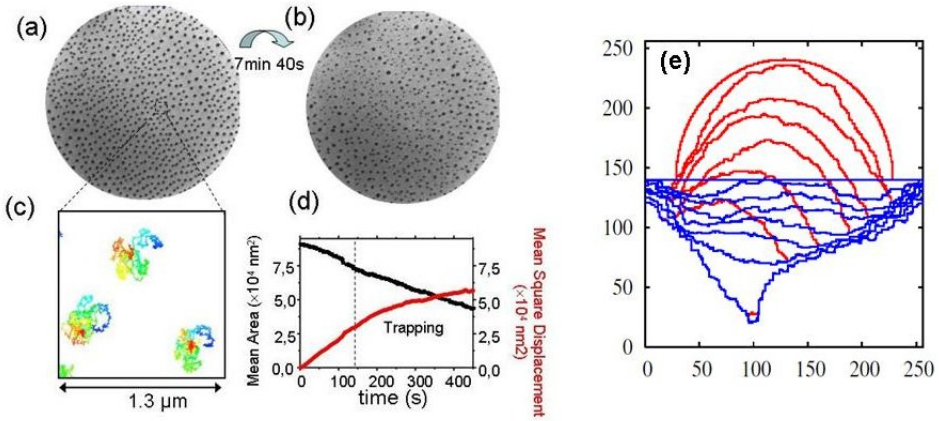


Figure 1: *(a) LEEM picture of $Si/SiO_2$ crystallites heated at $\sim 1000^{\circ}C$ , (b) the same after 7 min 40s, (c) Examples of trajectories of mass centers of nano-islands, (d) time-evolutions of the mean square displacements and mean projected area of Si nanoislands under reaction, (e) superimposed snapshots calculated by KMC showing the evolution of the island shape and of the underlying substrate.*

Here we report on the combined effects of reactivity, wetting and shape changes on the random motion of crystalline Si nano-islands on amorphous $SiO_2$ substrate observed during annealing. For this purpose, Si islands have been obtained by dewetting of a Silicon-on-insulator (SOI) ultra thin film [8] and their motion has been followed in-situ and in real time by means of low Energy Electron Microscopy (LEEM). Three diffusion regimes have been observed: (i)

in the early stages the nano-islands exhibit usual Brownian motion with $n \approx 3$ (ii) for longer time, the diffusion coefficient roughly does not depend on the island size so that the mean square displacement of the island varies linearly with time, (iii) for later times, the mean square displacement saturates until the Si islands shrink an disappear. The shape of the islands as well as the morphology of the $Si/SiO_2$ interface have been studied by ex-situ Atomic Force Microscopy within the three regimes. In the first regime trenches form in the vicinity of the triple line, whereas in the second and last regimes the chemical reaction $Si + Si_{O_2} \rightarrow 2SiO$ between the nano-islands and their underlying substrate leads to local etch pits.

Kinetic Monte Carlo (KMC) simulations have been performed by considering 2D hetero epitaxial Solid-on-Solid system on a square lattice. Surface diffusion and chemical reactions have been implemented in the KMC scheme. The KMC results allow to recover the three regimes experimentally observed with a good agreement in terms of surface diffusion behaviour and island morphology change.

In conclusion reactive Si islands on $SiO_2$ substrates annealed at high temperature exhibit a non-trivial diffusion behaviour. At short times equilibrium diffusion is observed. At intermediate times non-equilibrium diffusion associated to an increase of the effective diffusion coefficient is induced by a pinning/depinning mechanism of the triple line leading to time-variations of the wetting angle and thus to shape variations of the Si nano-islands. At later times the islands are trapped in the pits they have formed. The substrate profiles experimentally observed under the islands are consistent with the interfacial morphology obtained from KMC simulations due to interfacial reaction.

Finally this local etching mechanism can be at the origin of a technical process to make well ordered nanoholes in a Si membrane .

# References

[1] H. Reiss, J. Appl. Phys. 39 (1968) 5045.

[2] A. Masson, J. Metois, R. Kern, Surf. Sci. 27 (1971) 463.

[3] S. .Khare, T. Einstein, Phys. Rev. B. 54 (1996) 11752.

[4] J. Tersoff, D. Jesson, W. Tang, Science 324.

[5] A. Schmid, N. Bartelt, R. Hwang, Science 290 (2000) 1561.

[6] H. Kanai, S. Sugihara, H. Yamaguchi, T. Uchimaru, N. Obata, T. Kikuchi, F. Kimura, M. Ichinokura, J. Mat. Sci. 42 (2007) 9529.

[7] K. Sudoh, M. Naito, J. Appl. Phys. 108 (2010) 083520.

[8] F. Cheynis, E. Bussmann, F. Leroy, T. Passanante, Muller, Phys. Rev. B. 84 (2011) 245439.

# Morphology and Electronic Properties of Cu-Phthalocyanine:$C_{60}$ Bulk Heterojunction Blends for Photovoltaic Applications

F. Roth,[1] C. Lupulescu,[2] T. Arion,[1, 3] E. Darlatt,[4] A. Gottwald,[4] and W. Eberhardt[1,2]

[1)] Center for Free-Electron Laser Science / DESY, Notkestraße 85, D-22607 Hamburg,Germany

[2)] Inst. of Optics and Atomic Physics, TU Berlin, Straße des 17. Juni 135, D-10623 Berlin, Germany

[3)] Institut für Experimentalphysik, Universität Hamburg, Luruper Chaussee 149, D-22761 Hamburg, Germany

[4)] Physikalisch-Technische Bundesanstalt (PTB), Abbestraße 2-12, D-10587 Berlin, Germany

Phthalocyanines (PC) in combination with $C_{60}$ are benchmark materials for organic solar cells. Here we have studied the morphology and electronic properties of co-deposited mixtures (blends) of these materials forming a bulk heterojunction as a function of the concentration of the two constituents. In these materials the PC acts as the chromophore, while $C_{60}$, because of it's high electron affinity, is very efficient in dissociating the excitons created in the photoabsorption process, separating the charges and thus suppressing recombination.

Most of the basic science studies devoted to characterizing the electronic properties and the charge separation process (for a recent review see 1,2 and references therein) have been carried out on layered systems, so called planar heterojunctions. This limits the useable film thickness to the exciton diffusion length. For real devices however a film thickness about an order of magnitude larger is required for efficient light absorption. Consequently the attention has recently been transferred to mixed blends of organic molecules and $C_{60}$ (3,4). In previous experiments it was found that a well mixed phase separated blend exhibits the best device performance (5). This means that small crystalline domains, especially of $C_{60}$, well embedded into a PC matrix is the preferred configuration for bulk heterojunction solar cell applications. The individual regions/domains should be sufficiently small to enable efficient exciton diffusion and separation, while the crystallinity improves the charge carrier mobility, at least for the electrons within the $C_{60}$ crystallites. However from these studies a very puzzling question arises: the performance varies only very little over quite large changes in concentration of $C_{60}$ in the blends (5).

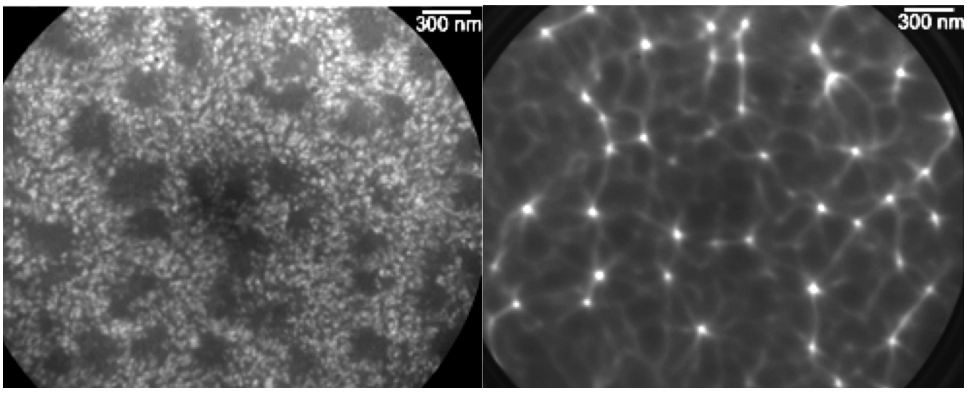


Fig. 1a (left). LEEM images of the surface of a CuPC :$C_{60}$ (1:1) mixture deposited on a Si wafer substrate. Fig. 1b (right) LEEM images of the surface of a CuPC:$C_{60}$ (10:1) mixture. The exposure time for each image was 5 s.

We have chosen a Si(100) 2x1 reconstructed wafer as substrate and deposited mixed films of $C_{60}$ and CuPC of about 15 nm thickness by thermal evaporation. The mixing ratio was determined by calibrating the evaporation rate of each evaporator individually using a quartz microbalance and confirmed by photoemission. The sample morphology was investigated using a commercial LEEM/PEEM instrument SPECS FE-LEEM P90 (6). The LEEM images of two different blends of CuPC:$C_{60}$ after deposition onto the (2x1) reconstructed Si(100)

surface are shown in Figs. 1a and b. First of all, the substrate reconstruction is not visible anymore. However the blends exhibit distinct differences in the morphology. While for the 1:1 mixed film (Fig. 1a) a phase separation into domains of 50 to 200 nm size is observed, the image (Fig. 1b) of the low $C_{60}$ content blend (10:1 CuPC:$C_{60}$) shows many bright spots connected by some faint lines. This is interpreted as a growth mode of CuPC in domains while the domain boundaries are decorated by $C_{60}$. Such a growth mode conveniently also explains the relatively unchanged performance concerning exciton separation in mixed films of low $C_{60}$ content. Regions of $C_{60}$ are accessible within the exciton diffusion length, even for low concentration blends.

The electronic properties of the blends were characterized by photoelectron spectroscopy recorded with a SCIENTA R4000 hemispherical electron spectrometer in the IDEEA apparatus (7) installed at the metrology light source MLS of the PTB (8). From these spectra it is obvious that the level alignment changes from the pure films to the mixtures/blends. In order to quantify these observations we have taken the spectra of the mixed films at various photon energies and fitted these using the spectra of the pure compounds allowing for an energy shift and overall intensity variation. The fitted intensities confirm the mixing ratio as determined by the quartz microbalance. The CuPC shifts in the 1:1 mixture are slightly larger (-360±35 meV) than in the 10:1 blend (-240±60 meV), while the shifts in the $C_{60}$ component are in the opposite direction but slightly smaller for the 1:1 blend (150±50meV) compared to 260±100 meV for the 10:1 blend. It is remarkeable that the relative alignment of the two constituents of this bulk heterojunction remains identical at about 500 meV shift measured relative to the electronic states of the separate systems. Analogous to the results for layer systems (9,10), we attribute this to the formation of an interface dipole, which already forms at monolayer coverage (11). This important result shows that the energetics of the exciton dissociation process are identical, independent of the mixing ratio, thus explaining why the performance hardly changes at all over large variations of the $C_{60}$ content in the bulk heterojunction.

References

[1] M. Fahlman, P. Sehati, W. Osikowicz, S. Braun, M. P.de Jong, and G. Brocks, J. Electron. Spectrosc. Relat. Phenom. **190** (2013), http://dx.doi.org/10.1016/j.elspec.2013.02.001, and references therein

[2] A. Opitz, J. Frisch, R. Schlesinger, A. Wilke, and N. Koch, J. Electron. Spectrosc. Relat. Phenom. **190** (2013), http://dx.doi.org/10.1016/j.elspec.2012.11.008, and references therein

[3] M. Riede, T. Mueller, W. Tress, R. Schueppel, and K. Leo, Nanotechnology **19**, 424001 (2008)

[4] P. Heremans, D. Cheyns, and B. P. Rand, Acc. Chem. Res. **42**, 1740 (2009)

[5] C. Schünemann, D. Wynands, L. Wilde, M. P. Hein, S. Pfützner, C. Elschner, K.-J. Eichhorn, K. Leo, and M. Riede, Phys. Rev. **B85**, 245314 (2012)

[6] R. Tromp, J. Hannon, A. Ellis, W. Wan, A. Berghaus, and O. Schaff, Ultramicroscopy **110**, 852 (2010)

[7] C. Lupulescu, T. Arion, U. Hergenhahn, R. Ovsyannikov, M. Förstel, G. Gavrila, and W. Eberhardt, J. Electron. Spectrosc. Relat. Phenom. (2013), http://dx.doi.org/10.1016/j.elspec.2013.09.002.

[8] A. Gottwald, R. Klein, R. Müller, M. Richter, F. Scholze, R. Thornagel, and G. Ulm, Metrologia **49**, S146 (2012).

[9] O. V. Molodtsova and M. Knupfer, J. Appl. Phys. **99**, 053704 (2006).

[10] M. Grobosch, V. Y. Aristov, O. V. Molodtsova, C. Schmidt, B. P. Doyle, S. Nannarone, and M. Knupfer, J. Phys. Chem. C **113**, 13219 (2009).

[11] N. Sai, R. Gearba, A. Dolocan, J. R. Tritsch, W.-L. Chan, J. R. Chelikowsky, K. Leung, and X. Zhu, J. Phys. Chem. Lett. **3**, 2173 (2012).

# Dynamics of steps at the sidewalls of nanowires

S.N. Filimonov, Yu.Yu. Hervieu

*Department of Physics, Tomsk State University, 634050 Tomsk, Russia*
*(corresponding author: S.N. Filimonov, e-mail: filimon@phys.tsu.ru)*

Radial growth of nanowires involves formation and propagation of monoatomic steps at atomically smooth nanowire sidewalls. These processes determine not only the radial growth rate of nanowires, but also stability of nanowires against shape transformations [1]. Here we study the step dynamics with a simple diffusion model taking into account the presence of a strong sink for adatoms at top of the nanowire and adatom exchange between the nanowire sidewall and surrounding substrate surface.

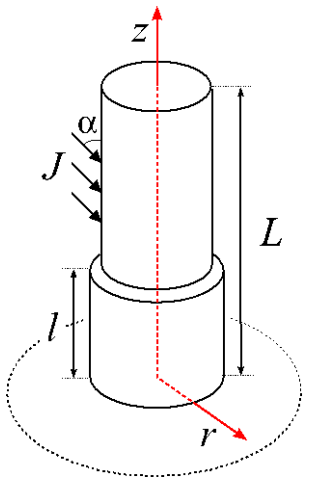


Fig.1. Cylindrical nanowire growing within a circular "feeding" area.

We consider a single cylindrical nanowire growing within a circular "feeding" area (Fig. 1). Atoms are deposited on the surface with a flux $J$ at an angle $\alpha$ to the nanowire growth axis. Since the sidewall and the surrounding substrate surface represent different crystal faces, the adsorption energies and diffusion barriers for adatoms on the sidewall and on the substrate are assumed to be different. Adatom concentration on the substrate surface ($n_s$) and on the sidewall ($n_f$) obey the following continuity equations [2]

$$\frac{D_s}{\mathrm{r}}\frac{d}{dr}\left(r\frac{dn_s}{dr}\right)+J\cos\alpha-\frac{n_s}{\tau_s}=0, \qquad D_f\frac{d^2n_f}{dz^2}+J\sin\alpha-\frac{n_f}{\tau_f}=0,$$

where $D$ and $\tau$ are the surface diffusion coefficient and the life time of an adatom on the surface before desorption, respectively. As the boundary conditions we use the balance conditions for the surface diffusion fluxes and the fluxes of adatoms from the substrate surface to the sidewall facet, to the step edge from the upper and lower terraces, and from the sidewall to the top facet of the nanowire. The adatom flux through the boundary of the surface cell was put to zero. From the solution of this boundary problem we found analytical expressions for the adatom fluxes into the step and to the nanowire top facet and expressed the step propagation velocity and the rate of the nanowire elongation as linear combinations of the supersaturations in the adsorption layer at the substrate ($\sigma_s$), at the sidewall ($\sigma_f$), and at top of the nanowire ($\sigma_t$):

$$\sigma_s=\frac{J\tau_s\xi\cos\alpha}{\tilde{n}}-1, \qquad \sigma_f=\frac{J\tau_f\xi\sin\alpha}{\tilde{n}}-1, \qquad \sigma_t=1-\frac{\tilde{n}_t}{\tilde{n}}.$$

Here $\tilde{n}$ and $\tilde{n}_t$ are the concentrations of adatoms at the sidewall in equilibrium with the step

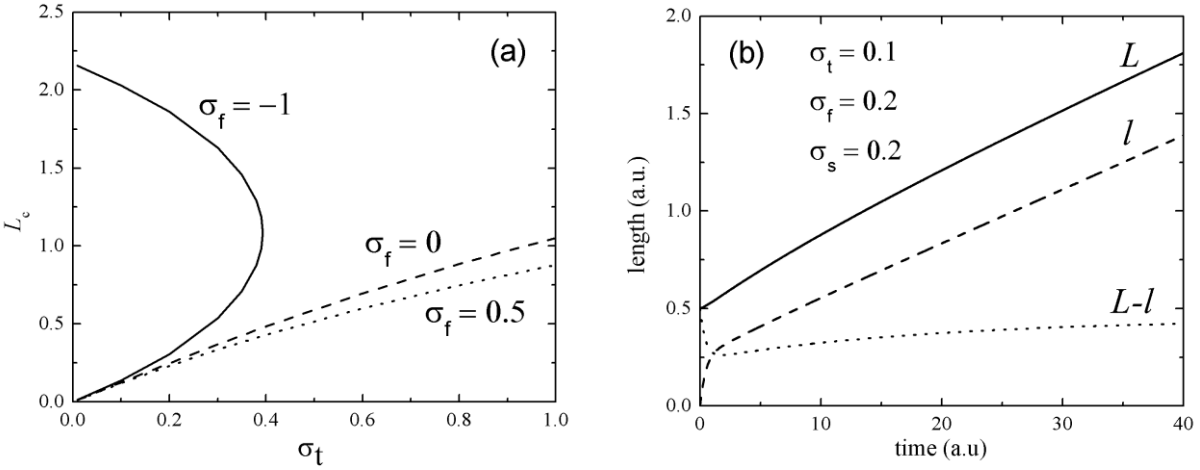


Fig. 2. (a) Critical nanowire length (see text for details); (b) nanowire length (solid), step position (dashed), and upper terrace width (dotted) as function of deposition time. All the lengths are shown in the units of the diffusion length of an adatom on the sidewall before desorption, time in the dimensionless units ($t\tilde{n}/\tau_f$).

and the nanowire top facet, respectively; $\xi = \exp(\Delta E_{sf}/k_B T)$ where $\Delta E_{sf}$ is the difference between the adatom adsorption energy on the substrate surface and that on the sidewall of the nanowire.

Analysis of the obtained expressions shows that survival of a step formed at the nanowire base depends strongly on the nanowire length. Under certain conditions the step velocity becomes zero. This happens at a critical nanowire length $L_c$, which depends strongly on $\sigma_s$, $\sigma_f$ and $\sigma_t$, as shown in Fig. 2(a). If the nanowire top is a strong sink for adatoms ($\sigma_t > 0$), the step propagation is suppressed when the step is approaching the top. If the nanowire is too short, the step is forced to decay from the very beginning and cannot survive. On the other hand the step formed at the base of a long nanowire might dissolve when direct adsorption at the sidewall is small as compared to desorption ($\sigma_f = -1$). At certain conditions a non-trivial re-entrant step behavior is expected.

In Fig. 2(b) results of self-consistent modeling of the step propagation and nanowire growth are shown. At the early stage of the nanowire growth the step velocity is high, but the step velocity slows down approaching top of the nanowire which serves as the strong sink for adatoms. Accordingly the width of the upper terrace initially decreases rapidly, then gradually increases saturating at long times (not shown) at $L - l \approx 0.45\lambda_f$. This effect may trigger bunching of steps propagating from the nanowire base. As a consequence a pensil-like shape of the nanowire will develop.

Support by the Russian Foundation for Basic Research (project # 13-02-12160) is gratefully acknowledged.

[1] M.C. Plante and R.R. LaPierre, J. Cryst. Growth 310, 356 (2008)
[2] V. G. Dubrovskii et al., Semiconductors 40, 1075 (2006)

# Surface Science differently: What holds paper fibers together

C. Teichert[1,2], F.J. Schmied[1,2,3], C. Ganser[1,2], L. Kappel[2,4], W. Fischer[2,4], U. Hirn[2,4], W. Bauer[2,4], and R. Schennach[2,5]

[1] *Institute of Physics, Montanuniversität Leoben, A-8700 Leoben, Austria (corresponding author: C. Teichert, e-mail: teichert@uniloeoben.ac.at)*

[2] *CD-Laboratory for Surface Chemical and Physical Fundamentals of Paper Strength, Graz University of Technology, A- 8010 Graz, Austria*

[3] *Mondi Uncoated Fine & Kraft Paper GmbH, A-1030 Vienna, Austria*

[4] *Institute for Paper, Pulp and Fiber Technology, Graz University of Technology, A-8010 Graz, Austria*

[5] *Institute of Solid State Physics, Graz University of Technology, A-8010 Graz, Austria*

Paper is one of the most versatile materials used by mankind. Although it is already known for centuries, the process of bonding two fibers together is still under discussion. During fabrication of paper, single pulp fibers approach each other and form bonds during the drying process. The formation of bonds between the surfaces of two single fibers is up to now a speculative issue. There have been several mechanisms suggested which play a significant role in forming fiber-fiber bonds that lead to a fiber network which is called paper. Among these mechanisms are hydrogen bonds, electrostatic interactions, interdiffusion of cellulose molecules, induced dipoles, and mechanical interlocking. More recently, also micro-compressions and capillary bridges are considered to contribute significantly to the bond strength.

Here, we employed a novel method to measure fiber joint strength, which is based on conventional atomic force microscopy (AFM) [1]. With this technique, single fiber-fiber bonds of unrefined as well as refined pulp fibers have been tested dynamically and statically. Besides yielding the joint strength, AFM is used to inspect the formerly bonded surface (see figure 1). This allows not only to determine the bond area but to correlate discontinuities in the force-versus-distance plots prior to the bond breaking with surface features. For refined pulp, we could demonstrate that interlocking of dangling fibrils and fibril bundles result in a doubling of joint strength compared to unrefined fibers [2]. Inspection of the fibers' hardness and reduced modulus by AFM based nanoindentation [3] and the evaluation of surface roughness as a function of humidity could reveal the role of capillary forces in fiber bonding [4].

In conclusion, surface characterization of cellulose fibers using modern scanning probe techniques helps to gain new insights into the mechanisms of fiber-fiber bonding and their contribution to the fiber-fiber bond strength. With this knowledge, new fabrication routes can be deduced by packaging paper industries to increase the strength of an ancient natural and bio-degradable product that becomes more and more a high-tech material.

Support by Mondi and the Federal Ministry of Economy, Family and Youth and the National Foundation for Research, Technology and Development, Austria, is gratefully acknowledged.

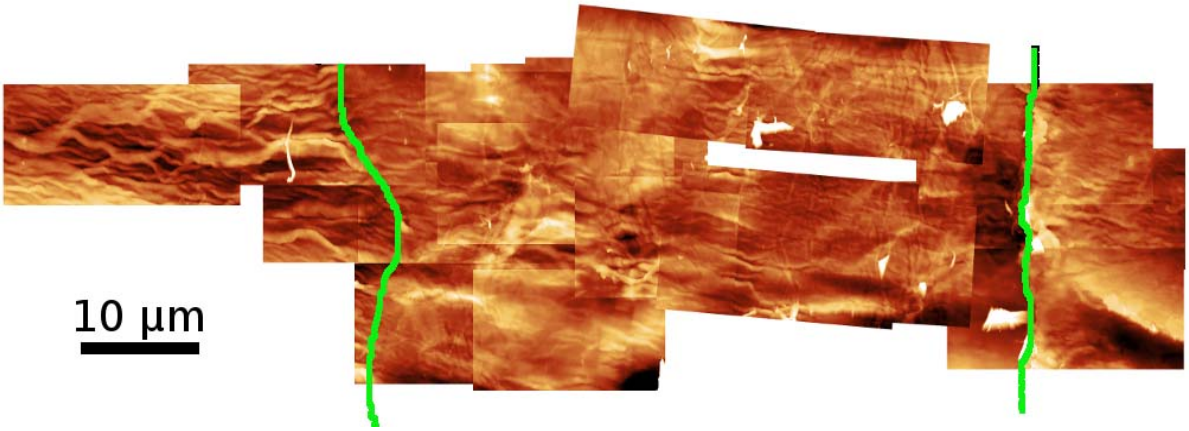


Figure 1. Stitched AFM images of the formerly bonded area of a paper fiber. The green lines mark the border between the formerly bonded and unbonded areas. The bright features inside the bonded area are dangling fibrils which previously worked as bridging elements.

[1] F.J. Schmied, C. Teichert, L. Kappel, U. Hirn, R. Schennach, Rev. Sci. Instrum. 83, 073902 (2012)

[2] F.J. Schmied, C. Teichert, L. Kappel, U. Hirn, W. Bauer, R. Schennach, Sci. Rep. 3, 2432 (2013)

[3] C. Ganser, U. Hirn, S. Rohm, R. Schennach, C. Teichert, Holzforschung, 2013, doi:10.1515/hf-2013-0014

[4] B.N.J. Persson, C. Ganser, F. Schmied, C. Teichert, R. Schennach, E. Gilli, U. Hirn, J. Phys.-Cond. Mat. 25, (2013) 045002

# Determination of nanoparticle surface area for improved nanotoxicology studies

M. E. Messing, C. R. Svensson[1], L. Ludvigsson[2], J. Pagels[1], B. O. Meuller[2], K. Deppert[2], and J. Rissler[1]

*Synchrotron Radiation Research, Lund University, 221 00 Lund, Sweden*
*(corresponding author: M. E. Messing, e-mail: maria.messing@sljus.lu.se)*

[1] *Ergonomics and Aerosol Technology, Lund University, 221 00 Lund, Sweden*

[2] *Solid State Physics, Lund University, 221 00 Lund, Sweden*

With the increasing amount of products and applications found in our everyday life based on engineered nanoparticles [1] the concerns about possible adverse health effects of nanoparticles are being discussed intensively [2]. Not only should the final product be safe to use for consumers, but also the exposure of the product to the environment (e.g. when consumers wash off sunscreens or cosmetics containing nanoparticles) should preferably be harmless. Moreover, the handling of particles during fabrication of the products should be carried out in a safe way. A potential risk during product fabrication and handling is inhalation of the nanoparticles and hence a number of both *in vivo* and *in vitro* studies to investigate nanoparticle toxicity for this exposure route have been performed.

For nanotoxicology investigations of air-borne particles to provide relevant results and to enable categorical studies of nanotoxicity it is ever so important that the particle exposure of, for example cells, closely resembles the "real" exposure situation, that the dosimetry is well defined, and that the characteristics of the deposited nanoparticles are known in detail [3]. By synthesizing the particles in the gas-phase and directly depositing them onto lung cells, the particle deposition conditions in the lung is closely mimicked. In the present work we present a setup for generation of gas-borne nanoparticles of a variety of different materials [4] with highly controlled and tunable particle characteristics, and demonstrate the method by both *in vitro* and *in vivo* depositions of gold particles.

The particle characteristics identified to play the most important roll for the toxicological response include shape, mass, number concentration, solubility, surface chemistry and surface area [5, 6]. In our setup the number and mass concentrations are measured on-line, the shape is determined by electron microscopy and the surface area is determined using three different models. The mass and surface area dose is, furthermore, calculated and from these calculations accurate deposition times to cause an inflammatory response during exposure, according to literature, are determined [7]. The generated particles are then deposited onto

primary lung cells using an air-liquid-interface (ALI) chamber as well as directly inhaled by living mice.

The first major advantage of the setup used is that it allows for a comparison of the dependence of the toxicological response on surface area, when using particles of the same mass and number concentration. The second major advantage is the simplicity by which particles of different materials are produced that provides the possibility to directly compare the effect of nanoparticle material on toxicology, when all other size related parameters are chosen to be the same.

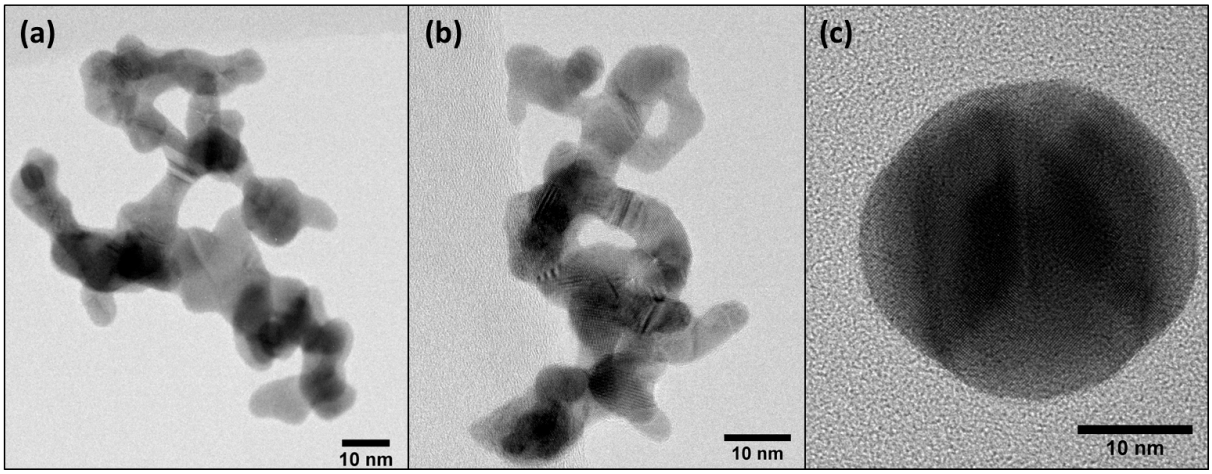


**Figure 1:** TEM images of (a) an evaporation/condensation generated agglomerate gold particle with a mobility diameter of 60 nm, (b) a spark discharge generated agglomerate particle with a mobility diameter of 60 nm and (c) a spark discharge generated particle with an original mobility diameter of 60 nm (compare to b) that has been sintered at 700C which reduced the mobility diameter to 31 nm and the surface area by about a factor of 6.

This work was performed within the Nanometer Structure Consortium at Lund University (nm@LU) and supported by the Swedish Council for Working Life and Social Research (FAS) through project 2009-1291, FORMAS through projects 216-2009-1294 and 2008-1467, the Swedish Governmental Agency for Innovation Systems VINNOVA through project 2009-01117, and the FAS-centre METALUND.

[1] M. Geiser and W. G. Kreyling Part. Fibre Toxicol. 7, 2 (2010)

[2] G. Oberdorster, E. Oberdorster and J. Oberdorster, Environ Health Perspect. 113, 829 (2005)

[3] R. N. Grass, L. K. Limbach, E. K. Athanassiou and W. J. Stark, J. Aerosol Sci. 41, 1123 (2010)

[4] M. E. Messing, K. A. Dick, L. R. Wallenberg and K. Deppert, Gold Bull. 42, 20 (2009)

[5] A. D. Maynard and E. D. Kuempel, J Nanopart. Res. 7, 587 (2005)

[6] C. R. Svensson, M. E. Messing, M. Lundqvist, A. Schollin, K. Deppert, J. H. Pagels, J. Rissler and T. Cedervall, Plos One 8, e74702 (2013)

[7] M. E. Messing, C. R. Svensson, J. Pagels, B. O. Meuller, K. Deppert and J. Rissler, Nanotoxicol. 7, 1052 (2013)

# Author Index

**POST-DEADLINE ABSTRACT**

# Measuring the profile of a molecular beam source on the Machine for Reactivity Studies

J. Pavelec, J. Hulva[1], D. Halwidl, M. Bickel, F. Brunbauer, M. Schmid, G. Parkinson, and U. Diebold

*Institut für Allgemeine Physik, Technische Universität Wien, A-1040 Wien, Austria*
*(Corresponding author: J. Pavelec, e-mail: pavelec@iap.tuwien.ac.at)*

[1] *Institute of Physical Engineering, Brno University of Technology, Brno, Czech Republic*

The Machine for Reactivity Studies (The Mrs.) is a newly constructed UHV setup designed to investigate surface chemistry of bulk metal oxide samples. Temperature Programmed Desorption (TPD) will be combined with Ultra Violet Photoemission Spectroscopy, Photoemission Spectroscopy with monochromatic X-ray source, Low Energy Electron Diffraction, and Ion Scattering Spectroscopy, allowing the reaction intermediates to be determined as a function of temperature. These high resolution spectroscopies will complement existing scanning tunneling microscopy studies in the group.

TPD requires the adsorption of atoms or molecules on sample surfaces at low temperature. However, to ensure good thermal contact between the metal oxide single crystal and sample holder, it is necessary to clamp the sample with a retiring frame. For high quality TPD spectra the direct dose to the retaining frame should be as low as possible. Therefore, a Molecular Beam (MB) will be used to evenly adsorb molecules on a well-defined area of the sample surface *only* [1, 2]. Ideally, the MB should possess a top hat distribution with a diameter at the sample of 3.5 mm.

The Molecular Beam Monitor (MBM) was developed to measure the profile of our MB. Here, we describe the working principle of the MB and the MBM, as well as design improvements to the previously published MBM [1].

The MBM can be characterized as an accumulation detector [2]. It consists of an orifice through which a closed volume containing an ion gauge can be accessed. Gas particles from the source accumulate inside the volume of the detector causing a pressure change. When the pressure in the closed volume is stabilized, it corresponds to the pressure inside the molecular beam. By recording the pressure whilst scanning the orifice through the beam in two orthogonal axes, the profile and intensity can be determined. The MBM is designed to be able to move in two perpendicular directions to characterize whole beam profile. As the main improvement over other

designs of MBMs [1, 3] the ion gauge is placed inside the UHV chamber. This minimises the volume of the detector and leads to a shorter stabilisation time.

Support by the U.S. Department of Energy and Vienna University of Technology CATMAT project are gratefully acknowledged.

[1] J. Libuda, I. Meusel, J. Hartmann, and H. J. Freund. A molecular beam/surface spectroscopy apparatus for the study of reactions on complex model catalysts. Review of Scientic Instruments, 71(12):4395-4408, 2000.

[2] Chapter: H. Pauly, Other Low-Energy Beam Sources, book: Giacinto Scoles. Atomic and Molecular Beam Methodes, Volume 1, Oxford university Press, 1988.

[3] R. W. Bickes, K. R. Newton, J.M. Hermann, and R. B. Bernstein. Utilization of an arc-heated jet for production of supersonic seeded beams of atomic nitrogen. Journal of Chemical Physics, 64(9):3648-3657, 1976.

**POST-DEADLINE ABSTRACT**

# Observing molecules on catalyst surface during reaction

Violeta Navarro Paredes

Kamerlingh Onnes Laboratory, Leiden, The Netherlands.

Catalysts' surfaces have largely been studied with traditional surface science techniques down to the atomic level. Those techniques are typically used under vacuum conditions. However there is a difference of many orders of magnitude in pressure between those vacuum studies and the industrial conditions at which catalysts work. Even though the studies in vacuum can be very revealing [1], the "pressure gap" leads to dramatic differences between laboratory and industrial conditions. The reaction mechanisms and the changes on the catalyst surface during the reaction [2] can be intrinsically different under the fore mentioned pressures.

In our lab we follow catalysts at the atomic scale reproducing the conditions of pressure and temperature used in the industry. We do this using a scanning tunneling microscope (STM) which can work under high pressures and temperatures [2, 3]. The STM is inside a small gas flow reactor placed in a UHV chamber where traditional surface science techniques are used to prepare and characterize the samples, before exposing them to reaction conditions. We can visualize the structural changes on the surface of the catalyst during the reaction. Simultaneously we use mass spectrometry to detect the gaseous products of the reaction.

As a model catalyst, we have used a single crystal of cobalt, Co(0001), to study the Fischer-Tropsch synthesis (FTS). This reaction is the catalytic process that produces hydrocarbons of different chain lengths from a mixture of CO and $H_2$. Among others, desulphurised (therefore clean) fuel is one of the main products of the reaction. Although this reaction is of extreme industrial relevance, the fundamental mechanisms are still not completely understood [4]. We have observed several changes on the very dynamic cobalt surface during the reaction. For example, islands with internal periodic structures appear on the surface. We believe these are alkane molecules produced during the reaction, which self assemble on the surface depending on their length.

**References:**

1- G. Ertl. *Angewandte Chemie International Edition*, **52**, 1, 52–60, (2013).
Y.D.Yin, *et al*., Science, **304**, 5671. 711 (2004). R. Schaub, *et al*.. Phys. Rev. Let. **87**, 26 (2001).
2- B.L.M. Hendriksen, *et al*., *Topics in Catalysis*, **36**, 1–4 (2005).
3- C.T. Herbschleb. To be published.
4- J. Wilson *et al*., J. *Phys. Chem.* **99**, 7860 (1995)

A PASSION FOR PERFECTION

PFEIFFER VACUUM


# Vacuum solutions from a single source

Pfeiffer Vacuum stands for innovative and custom vacuum solutions worldwide, technological perfection, competent advice and reliable service. We are the only supplier of vacuum technology that provides a complete product portfolio:

- Pumps for vacuum generation up to $10^{-13}$ hPa
- Vacuum measurement and analysis equipment
- Leak detectors and leak testing systems
- System technology and contamination management solutions
- Chambers and components

**Are you looking for a perfect vacuum solution? Please contact us:**

**Pfeiffer Vacuum Austria GmbH**
T +43 1 8941704 · F +43 1 8941707 · office@pfeiffer-vacuum.at

**www.pfeiffer-vacuum.com**


# SYMPOSIUM ON SURFACE SCIENCE 2014
## St. Christoph am Arlberg, Austria
## March 9 - March 15, 2014

Friedrich Aumayr, Ulrike Diebold and Peter Varga, organizers
Institute of Applied Physics, Vienna University of Technology (TU Wien)

### Sunday, 9 March 2014

| | |
|---|---|
| 16:00 - 18:30 | REGISTRATION |
| 18:30 - 19:30 | DINNER |
| 20:00 - 20:20 | OPENING |

*chair:* ***VARGA***

| | |
|---|---|
| 20:25 - 20:45 | HEINZMANN |
| 20:45 - 21:05 | MICHELY |
| 21:05 - 21:25 | BRUNE |

### Monday, 10 March 2014

| | |
|---|---|
| 07:15 - 08:00 | BREAKFAST |

*chair:* ***DIEBOLD***

| | |
|---|---|
| 08:00 - 08:20 | SCHNEIDER |
| 08:20 - 08:40 | SETVIN |
| 09:15 - 12:00 | SKIING INSTRUCTIONS |
| 12:00 - 13:00 | LUNCH |
| 13:30 - 15:30 | SKIING INSTRUCTIONS |

*chair:* ***ALTMAN***

| | |
|---|---|
| 16:40 - 17:00 | IBACH |
| 17:00 - 17:20 | PFNÜR |
| 17:20 - 17:40 | DIL |
| 17:40 - 18:00 | PROTOGENOV |
| 18:00 - 18:20 | MÜLLER N. |
| 18:30 - 19:30 | DINNER |

*chair:* ***HENDRIKSEN***

| | |
|---|---|
| 19:30 - 19:50 | GIESSIBL |
| 19:50 - 20:10 | STEURER |
| 20:10 - 20:30 | VAN BAARLE |
| 20:30 - 20:50 | MÜLLER S. |

### Tuesday, 11 March 2014

| | |
|---|---|
| 07:15 - 08:00 | BREAKFAST |

*chair:* ***ERNST***

| | |
|---|---|
| 08:00 - 08:20 | REUTER |
| 08:20 - 08:40 | GUSTAFSON |
| 09:15 - 12:00 | SKIING INSTRUCTIONS |
| 12:00 - 13:00 | LUNCH |
| 13:30 - 15:30 | SKIING INSTRUCTIONS |

*chair:* ***TAGLAUER***

| | |
|---|---|
| 16:40 - 17:00 | ORTEGA |
| 17:00 - 17:20 | KOSHIKAWA |
| 17:20 - 17:40 | ÅHLUND |
| 17:40 - 18:00 | KAMPEN |
| 18:00 - 18:20 | MAIER |
| 18:30 - 19:30 | DINNER |

*chair:* ***THORNTON***

| | |
|---|---|
| 19:30 - 19:50 | FÖRSTER |
| 19:50 - 20:10 | MITTENDORFER |
| 20:10 - 20:30 | YUHARA |
| 20:30 - 20:50 | OBERHOFER |

### Wednesday, 12 March 2014

| | |
|---|---|
| 07:15 - 08:00 | BREAKFAST |

*chair:* ***AUMAYR***

| | |
|---|---|
| 08:00 - 08:20 | MORGENSTERN |
| 08:20 - 08:40 | GREBER |
| 09:15 - 12:00 | SKIING INSTRUCTIONS |
| 12:00 - 13:00 | LUNCH |
| 13:30 - 15:30 | SKIING INSTRUCTIONS |

*chair:* ***BAUER***

| | |
|---|---|
| 16:30 - 16:50 | SEIFERT |
| 16:50 - 17:10 | SCHUCH |

*chair:* ***SEITSONEN***

| | |
|---|---|
| 17:10 - 18:30 | POSTER INTRODUCTION |
| 18:30 - 19:30 | DINNER |
| 19:30 - 21:30 | POSTERSESSION |

### Thursday, 13 March 2014

| | |
|---|---|
| 07:15 - 08:00 | BREAKFAST |

*chair:* ***FASEL***

| | |
|---|---|
| 08:00 - 08:20 | MARBACH |
| 08:20 - 08:40 | ŠIKOLA |
| 09:15 - 12:00 | SKIING INSTRUCTIONS |
| 12:00 - 13:00 | LUNCH |
| 13:30 - 15:30 | SKIING INSTRUCTIONS |

*chair:* ***RENAUD***

| | |
|---|---|
| 16:40 - 17:00 | BARTH |
| 17:00 - 17:20 | BUCK |
| 17:20 - 17:40 | WINKLER |
| 17:40 - 18:00 | Mc ENTEE |
| 18:00 - 18:20 | FARSTAD |
| 18:30 - 19:30 | DINNER |

*chair:* ***ECHENIQUE***

| | |
|---|---|
| 19:30 - 19:50 | STARKE |
| 19:50 - 20:10 | SILKIN |
| 20:10 - 20:30 | JOHANSSON |
| 20:30 - 20:50 | MENZEL |

### Friday, 14 March 2014

| | |
|---|---|
| 07:15 - 08:00 | BREAKFAST |

*chair:* ***LEMELL***

| | |
|---|---|
| 08:00 - 08:20 | LIBUDA |
| 08:20 - 08:40 | RUPPRECHTER |
| 09:15 - 12:00 | GIANT SLALOM RACE |
| 12:00 - 13:00 | LUNCH |
| 13:30 - 15:30 | SKIING INSTRUCTIONS |

*chair:* ***SUCHORSKI***

| | |
|---|---|
| 16:30 - 16:50 | HAMMER |
| 16:50 - 17:10 | IGNACIO |
| 17:10 - 17:30 | CHEYNIS |
| 17:30 - 17:50 | EBERHARDT |
| 17:50 - 18:10 | FILIMONOV |

*chair:* ***MÜLLER P.***

| | |
|---|---|
| 18:30 - 18:50 | TEICHERT |
| 18:50 - 19:10 | MESSING |
| 19:10 - 19:35 | GIANT SLALOM RACE AWARD CEREMONY |
| 20:00 | CONFERENCE DINNER |